Optic axon guidance during development and regeneration in the zebrafish

Cameron Wyatt

PhD Thesis

Submitted in accordance with the regulations for the degree of PhD

Centre for Neuroregeneration

The University of Edinburgh

December 2010

Abstract

Directed regeneration of axons in the CNS has potential for the treatment of CNS disorders and injuries. In contrast to mammals, following optic nerve lesion zebrafish regenerate axons that navigate to their correct targets and form new synapses leading to functional recovery. Correct pathfinding is thought to rely on a range of molecular cues in the CNS which the growing axon expresses receptors for. However, the specific guidance cues are not well elucidated. It is likely that a proportion of them will be the same as during development, while some may be specific to regeneration. Alternatively, axons may simply retrace former trajectories guided by the molecular environment or mechanical constraints of degenerating tracts, as demonstrated in the mammalian PNS.

To elucidate this, we investigated regeneration in the *astray/robo2* knockout mutant which exhibits misprojection of optic axons during development leading to the establishment of ectopic tracts. We show that degenerating tracts do not provide a strong guidance cue for regenerating axons in the CNS as ectopic tracts in the *astray* mutant are not repopulated following lesion despite presenting a similar environment to entopic degenerating tracts. We also find that as *astray* mutant (knockout) and *robo2* morphant (transient knockdown) projection and termination errors persist in the adult, it is clear that there is not an efficient correction mechanism for large-scale pathfinding errors of optic axons during development. In addition, we find a reduced importance of the axon guidance receptor Robo2 and its repellent ligand Slit2 for pathfinding during regeneration as specific developmental pathfinding errors of optic axons in *astray* mutants are corrected during adult optic nerve regeneration and global overexpression of Slit2 elicits pathfinding defects during development but not regeneration.

To address regeneration-associated gene regulation in axotomised retinal ganglion cells, we carried out a microarray analysis. We found that many genes detected as a gradient in the adult retina during regeneration are not differentially expressed in the embryonic eye, despite having distinct expression patterns in other embryonic tissues. Of the genes which exhibit strong differential expression in the retina of both regenerating adults and developing embryos, *foxI1* is one of the most interesting candidates as other *fox* genes have been implicated in axon guidance and due to its highly restricted retinal expression pattern. Surprisingly, further investigation has revealed that *foxI1* knockout mutant embryos have retinotectal projections which appear normal in terms of axon pathfinding and mapping.

Another family of genes indicated by the array, which are cytosolic phosphoproteins known to be involved in the signal transduction cascade of multiple inhibitory guidance cues during axon growth, are the *crmps*. Knocking down *crmp2* with morpholinos during development resulted in a sparser innervation of the tectum with individual axons which trend towards having less complex arbors with shorter branches and reduced overall axon length.

As a whole this work adds to our current knowledge of optic axon guidance during development and regeneration and the relative importance and effect of selected potential guidance cues, which may help toward informing future mammalian CNS regeneration research.

Table of contents

Acknowledgements

I would like to thank everyone who made it possible for me to be where I am today, in my scientific career and in my life. Whether that help came in the form of scientific advice, friendship, support, unconditional love, back rubs, jam filled baked goods or their unceasing efforts to keep me completely sane through the gift of improv musical numbers.

So thank you to:

Drs. Catherina G. Becker and Thomas Becker.

The members of the Becker lab (Benedicte Autin, Tatyana Dias, Anselm Ebert, Veronika Kuscha, Jolanda Münzel, Anneliese Norris, Jochen Ohnmacht, Michell Reimer, Sudeh Riahi, Angela Scott, Zhen "Jane" Zhong).

My parents, Sheila and Robert Wyatt. My sister, Kirsty Wyatt.

My long-suffering partner, Chelsie Boyd.

My gran, Sylvia Brockett.

And Steve the invisible, pink, jazz pianist unicorn who only I can see.

Statement of original contribution

The work in this thesis has been performed by the candidate, Cameron Wyatt, unless specifically stated otherwise.

Cameron Wyatt

04/12/2010

Co-authorship statement

The work presented in chapter two of this thesis has been previously published.

Wyatt C, Ebert A, Reimer MM, Rasband K, Hardy M, Chien CB, Becker T, Becker CG. Analysis of the *astray/robo2* zebrafish mutant reveals that degenerating tracts do not provide strong guidance cues for regenerating optic axons. J Neurosci. 2010 Oct 13;30(41):13838-49.

The thesis author, Cameron Wyatt, was the primary researcher for results presented in chapter two under the guidance of Dr. CG Becker and Dr. T Becker. Further experimental work was contributed by A Ebert, MM Reimer, Dr. K Rasband, M Hardy, Dr. CB Chien, Dr. T Becker and Dr. CG Becker.

1. Introduction

1.1 Zebrafish as a model organism

Kingdom: Animalia
Phylum: Chordata
Class: Actinopterygii (Infraclass: Teleostei)
Order: Cypriniformes
Family: Cyprinidae
Genus: Danio
Species: Danio rerio

The zebrafish is a tropical freshwater minnow native to streams of the southeastern Himalayan region. In captivity they can live for up to 5 years and grow to an adult size of 2 to 4cm, continuing to grow throughout life. They are popular aquarium fish due to their ease of raising and maintenance which is also a key factor in their success as a model organism in scientific research, where they are mainly used in studies of development and genetics. Sequencing of the complete zebrafish genome by the Sanger Institute began in 2001 and is ongoing (http://www.sanger.ac.uk/Projects/D_rerio). So far over 1.4Gigabases have been sequenced, containing over 24,000 known protein coding genes. Annotations are constantly updated and sequences are freely accessible using the Ensembl genome browser (http://www.ensembl.org/Danio_rerio/Info/Index). This facilitates the design of primers and morpholinos (antisense-oligonucleotides) and the generation of transgenic lines, of which there is a growing resource bank. Microarrays of the entire known zebrafish genome are also available. Comprehensive information resources are available through The Zebrafish Model Organism Database (http://www.zfin.org). Material resources, including transgenic fish and well characterised mutant lines, are available to the zebrafish community through the Zebrafish International Resource Centre (http://www.zebrafish.org/zirc/home/guide.php). The transgenic tools available include conditional gene activation systems such as the Cre/lox system (Langenau et al., 2005) and heat shock-inducible GAL4/UAS expression system (Scheer et al., 2002).

Zebrafish are an ideal model system for studying development in vivo. They breed daily, reliably and all year round when kept on a 14 hour light cycle. They have a large clutch size of around 160 eggs per female under optimum conditions which is convenient for obtaining robust numbers of experimental embryos (Spence and Smith, 2006). The large, transparent and sturdy

nature of the externally fertilised eggs lends them well to microinjection of a variety of substances, such as morpholino oligonucleotides, RNA or plasmid constructs, allowing the knockdown or overexpression of chosen genes with relative ease during development (Nasevicius and Ekker, 2000; Malicki et al., 2002).

Morpholinos are oligonucleotides with nucleic acid bases bound to morpholine rings which interfere with expression of a target gene when injected into the fertilised egg. There are two distinct classes of morpholino. Start codon directed morpholinos prevent translation of mRNA by interfering with the progression of the ribosomal initiation complex in the region of the start codon which causes a reduction in protein expression. Splice site directed morpholinos prevent normal processing of mRNA by spliceosomes by steric blocking of target pre-mRNA which results in alternatively spliced mRNA which is translated into an altered protein. Morphants (morpholino injected embryos) can be generated on demand, far more easily than generating a mutant knockout line, as morpholinos can be easily and rapidly designed for any gene of interest. Morpholinos also provide a means to study transient gene knockdown during development as, depending on the specific morpholino and concentration injected, they have an effective period of 2 to 18 days following injection (unpublished observations). Splice site directed morpholinos have the further advantage that their efficiency of knockdown can be assessed by comparing the ratio of wild type mRNA and aberrant mRNA for the target gene through RT-PCR. These same properties that lend the zebrafish embryo to morpholino use also make it an ideal candidate for zinc-finger nucleases, the latest powerful molecular method for making targeted gene knockouts (Ekker, 2008).

Zebrafish development is well characterised and a variety of transgenic reporter lines that express fluorescent proteins in retinal ganglion cells (RGCs) are available, allowing live imaging e.g Tg(*pou4f3:gap43-GFP*)^{s356t} (*POU domain, class 4, transcription factor 3*, formerly known as *brn3c*) (Xiao et al., 2005) and *sonic hedgehog a* Tg(*shha:gfp*) (Shkumatava et al., 2004). Rapid development from fertilised egg to free-swimming, feeding animal in 5 to 6 days allows rapid turnaround for developmental experiments. The embryos are largely transparent which allows the expression of fluorescent transgenes expressed within the nervous system to be observed in live embryos. Mutant lines almost completely lacking pigment, such as *casper*, are also available to enhance this potential for live viewing further (Henion et al., 1996). Their near constant size during early development also facilitates the use of techniques such as time lapse microscopy of

the live embryo without the complications of rapid size increase. In both the embryonic and adult situation, compounds can be introduced into the organism by adding them directly to the water.

Finally, one of the most distinguishing features of the zebrafish is its capacity for regeneration. A high capacity for regeneration has been shown during development and during adulthood in various tissues and organs, including regeneration of the blood vessels, lymph system, epithelium, peripheral nervous system, sensory cells of the lateral line and the heart. (LeClair and Topczewski, 2010; O'Brien et al., 2009; Ma et al., 2008; Poss et al., 2002). However the most remarkable and relevant property of zebrafish for our work, when compared to other traditional model organisms, is their high capacity for regeneration of the CNS (Becker and Becker., 2008).

1.2 Regeneration following CNS injury in zebrafish in comparison to other classes

Following injury to the CNS mammals lack functionally significant regeneration, resulting in permanent deficits (Chaudhry and Filbin, 2007). This is in contrast to adult zebrafish which are capable of regenerating axons that can navigate through the site of injury to reach their correct targets and form new synapses leading to functional recovery (Becker et al., 2004a; Tanaka and Ferretti, 2009). In adult zebrafish robust regrowth of severed brainstem neuron axons in the spinal cord and severed RGC axons in the optic tract has been demonstrated (Becker et al., 2004a; Becker and Becker, 2007). Damage to the CNS of mammals, including humans, whether through injury or disease, often causes irreversible loss of motor and sensory function (Dijkers, 2005). Due to its relevance to the most common cause of permanent severe disability in humans, axon regeneration and its failure in mammals has been extensively studied. The failure of axonal regeneration in mammals appears to be largely due to a low intrinsic capacity of mature CNS neurons for axon regrowth and an inhibitory CNS environment which expresses inhibitory myelin-associated molecules such as *nogo*-A (Spencer et al., 2003; Schwab, 2004) and extracellular matrix molecules such as the chondroitin sulfate proteoglycans found in the glial scar (Carulli et al., 2005; Fawcett, 2006). While zebrafish also express *nogo*-A, the zebrafish homolog lacks one of its inhibitory domains (Diekmann et al., 2005). Furthermore, zebrafish express the transcript *nogo*-66 which is 70% identical to mammalian *Nogo*-66. However, while *Nogo*-66 inhibits regeneration in mammals, *nogo*-66 signalling does not impair regeneration in zebrafish (Abdesselem et al., 2009). In contrast to mammalian myelin, myelin and

oligodendrocytes isolated from goldfish, do not inhibit the growth of goldfish RGC axons or rat dorsal root ganglion neurons in vitro (Wanner et al., 1995). While fish myelin appears to be less inhibitory of axon growth than mammalian myelin, it is not growth promoting as the majority of regenerating axons from the brainstem avoid myelin debris, to grow through the central grey matter of the spinal cord (Becker and Becker., 2001). In addition to the relative paucity of inhibitory molecules following a lesion in the teleost CNS, there is also the presence of axon growth promoting molecules including L1 homologues (Becker et al., 2004a), P0 (Schweitzer et al., 2003), and *contactin1a* (Schweitzer et al., 2007). In mammals the growth promoting Schwann cells of the PNS, but not oligodendrocytes of the inhibitory CNS, express L1 and P0 (Oudega and Xu, 2006), suggesting some similarity between teleost oligodendrocytes and mammalian Schwann cells. Thus, fish oligodendrocytes might contribute to a CNS environment supportive of axon growth. The glial scar, which forms at the site of injury in mammals and is associated with chondroitin sulfate upregulation, is a potent obstacle to regeneration (Silver and Miller, 2004). In contrast to mammals, there is no evidence for major astrocytic scarring in fish CNS (Schweitzer et al., 2007). Interestingly while increased immunoreactivity for chondroitin sulfates has been demonstrated in the lesioned goldfish optic nerve (Battisti et al., 1992), it has not been found in zebrafish (Becker and Becker, 2002). However the properties of the glial environment are not the sole determinants of regeneration through the lesion site, as cell intrinsic properties play an important role as CNS axons of adult teleosts, lampreys and lizards can regenerate through a glial environment which is inhibitory to the regeneration of rodent axons (Yamada et al., 1995; Lurie and Selzer, 1991; Lang et al., 1998).

Regeneration of the CNS in fish has received extensive study and revealed a remarkable capacity for regeneration which far exceeds the functional but imperfect regeneration in the CNS of larval Anurans and reptiles (Egar et al., 1970; Iten and Bryant, 1976; Anderson and Waxman, 1981; Filoni and Bosco, 1982; Géraudie et al., 1988; Zupanc et al., 1998). However, to add further complexity, regenerative capacity varies between species within an order (Rehermann et al., 2009; Russo et al., 2004; Egar et al., 1970; Filoni and Bosco, 1981; Lin et al., 2007) and between populations of neurones within a species. Spinal cord regeneration in lizard tail amputation is quite limited, lacking neurogenesis. This is in contrast to regeneration following neurotoxic insult to the brain which involves robust neurogenesis (Font et al., 1991). As with the zebrafish, the salamander is capable of CNS regeneration throughout life but for most classes

regeneration is highly influenced by life-stage. Birds and mammals, while capable of limited regeneration during embryogenesis, lose this ability as they mature (Beattie et al., 1990; Filoni and Gibertini, 1969; Mizell, 1968; Nicholls and Saunders, 1996). The same is true of frogs which are capable of a wide range of CNS and non-CNS regeneration in their larval form but not in their adult form. In contrast, highly regenerative salamanders such as the neotenous axolotl maintain throughout life the combinatorial expression of transcription factors which is necessary for neural tube formation during development (McHedlishvili et al., 2007) and maintain the sonic hedgehog secreting floorplate, which is associated with neural tube development in all vertebrates (Schnapp et al., 2005). Hedgehog family genes are expressed in the embryonic floor plate which gives rise to the ventrolateral motor neuron progenitor (pMN) domain which in turn expresses *nkx6.1*, *pax6*, and *olig2* in all vertebrates (Jessell, 2000; Cheesman et al., 2004; Park et al., 2004; Fuccillo et al., 2006). Sonic hedgehog-a expressing and pMN-like ependymoradial glial cells (which express *Tg(olig2:egfp)*, Nkx6.1, and Pax6) have been shown in the unlesioned adult zebrafish spinal cord (Reimer, Kuscha, Wyatt et al., 2009). During regeneration following a spinal cord lesion, numbers of pMN-like ependymoradial glial cells and expression levels of these factors greatly increase. This may indicate the importance of access to embryonic gene activity patterns and transcriptional programmes in regeneration. The ependymoradial glial cells themselves are further examples of such holdovers from development which are associated with highly regenerative species. Radial glia are cells with radial processes that line the central canal of the neural tube in developing amniotes and are necessary for neurogenesis. Radial glia, or radial glia-like cells, are retained in the adult CNS of highly regenerative classes such as fish and salamanders but are lost through neural differentiation in amniotes (Zamora, 1978; Sims et al., 1991; García-Verdugo et al., 2002). However they are present in specific niches in the adult CNS which undergo neurogenesis in amniotes (Alvarez-Buylla et al., 1987; García-Verdugo et al., 2002). The ongoing neurogenesis in amniotes that has so far been discovered may not be of relevance to standard regeneration paradigms, such as spinal cord lesion induced paralysis, which is a major model for mammalian CNS regeneration, as neurogenesis has not been found in the rat spinal cord (Horner et al., 2000).

Following an optic nerve lesion in mammals, up to 90% of RGCs die off, possibly due to removal of trophic support originating from their targets (Fawcett, 2006). Zebrafish do not show this marked cell death, with less than 20% of RGCs apoptosing following lesion (Zhou and

Wang, 2002). Frogs, which can be thought to be an intermediate evolutionary step between fish and mammals, show around 50% RGC survival (Beazley et al., 1986). The reduced regenerative capacity of the CNS of higher vertebrates may be viewed, perhaps simplistically, as a natural consequence of increases in CNS complexity through evolution (Northcutt, 2001). However it may be that specific adaptations have left some species more capable of intrinsic CNS regeneration than others. Some lizards are capable of adult spinal cord axonogenesis, whereas frogs, with arguably less complex nervous systems, are not. A potential explanation lies in the specialised escape mechanism of these lizards; the ability to shed and regrow the tail (see Table 1 for comparison). Tail regeneration is accomplished by the recapitulation of some developmental programs in concert with mechanisms specific to regeneration (Clause and Capaldi, 2006). While this regeneration is imperfect, e.g. spinal column bone partially replaced by cartilage (Barber, 1944) and innervation by one instead of three spinal nerves (Bellairs and Bryant, 1985), it is sufficient to regrow a functioning, innervated tail (Duffy et al., 1992). This reinnervation follows extensive sprouting from spinal and supraspinal neurones (Duffy et al., 1992). It may be that this survival strategy has primed the lizard nervous system, to a limited extent, for regeneration. The mechanism of growth in teleosts is an adaption which may contribute to their remarkable capacity for regeneration. Teleosts, unlike mammals, grow continuously throughout life. This process involves not only the enlargement of existing cells but also proliferation, including neurogenesis and axonogenesis which has been demonstrated in the brain and sensory systems (detailed below for the optic system) (Easter and Stuermer, 1984; Marcus et al., 1999; Zupanc, 2008). It has also been speculated that the same is true of the motor system as, unlike in mammals where muscle tissue growth is accomplished by increasing the size of existing cells, fish continue to produce new muscle cells throughout their life, which may require continued neurogenesis to supply matching efferent innervation (Zupanc, 2008). However ongoing neurogenesis in the uninjured adult zebrafish has not been found in the spinal cord (Reimer, Kuscha, Wyatt et al., 2009).

Animal	Embryo or larva regeneration	Adult regeneration	Axonogenesis	Ependymal tube formation	Successful neurogenesis
Lamprey	+	+	+	(+)/?	(+)/?
Fish	+	+	+	+	+
Salamander	+	+	+	+	+
Frog	+	–	+	+/–	+/–
Lizard	?	+	+	+	–
Bird	+	–	+/–	+/–	+/–
Mammal	+	–	+/–	+/–	?/–

Table 1.1. Summarised comparison of spinal cord regeneration across classes following lesion.

Capability for regeneration loosely ties with the evolutionary period since the class diverged from the common ancestor, with more recently diverged classes exhibiting the lowest capacity for regeneration. While fish undergo spontaneous functional regeneration, larval Anurans will regenerate but lose this ability in the spinal cord as they mature, lizards show limited regeneration without neurogenesis and birds and mammals are capable of limited spinal cord regeneration only during a narrow embryonic window.

Modified from Tanaka and Ferretti, 2009.

1.3 Regeneration in the optic system

1.3.1 Cellular regeneration of the retina

The high regenerative capacity of the zebrafish also extends to the optic system. Regeneration of the retina is accomplished by a variety of vertebrate classes employing different methods but regeneration of the teleost optic system is arguably the most successful and complete in terms of restoration of structure and function. In teleosts, radial glia-like cells, the Mueller glia, give rise to progenitors cells which regenerate the retina, whereas newts and larval frogs recapitulate development by forming a new retinal neuroepithelium with cells derived from the retinal pigment epithelium (Hitchcock and Raymond, 1992; Mitashov, 1996; Lamba and Reh, 2008; Tsonis and Del Rio-Tsonis, 2004). In the adult situation, the frog retains the capacity for ongoing neurogenesis in the retina but loses the capacity for complete regeneration of the retina (Mitashov, 1996). Retinal regeneration can be induced in bird and mammal embryos only during a brief window with the application of ectopic growth factors. This process does not recapitulate development as the retinal pigment epithelium (RPE) is converted to retina without RPE renewal and results in a retina with abnormal apical–basolateral polarity (Park and Hollenberg, 1991).
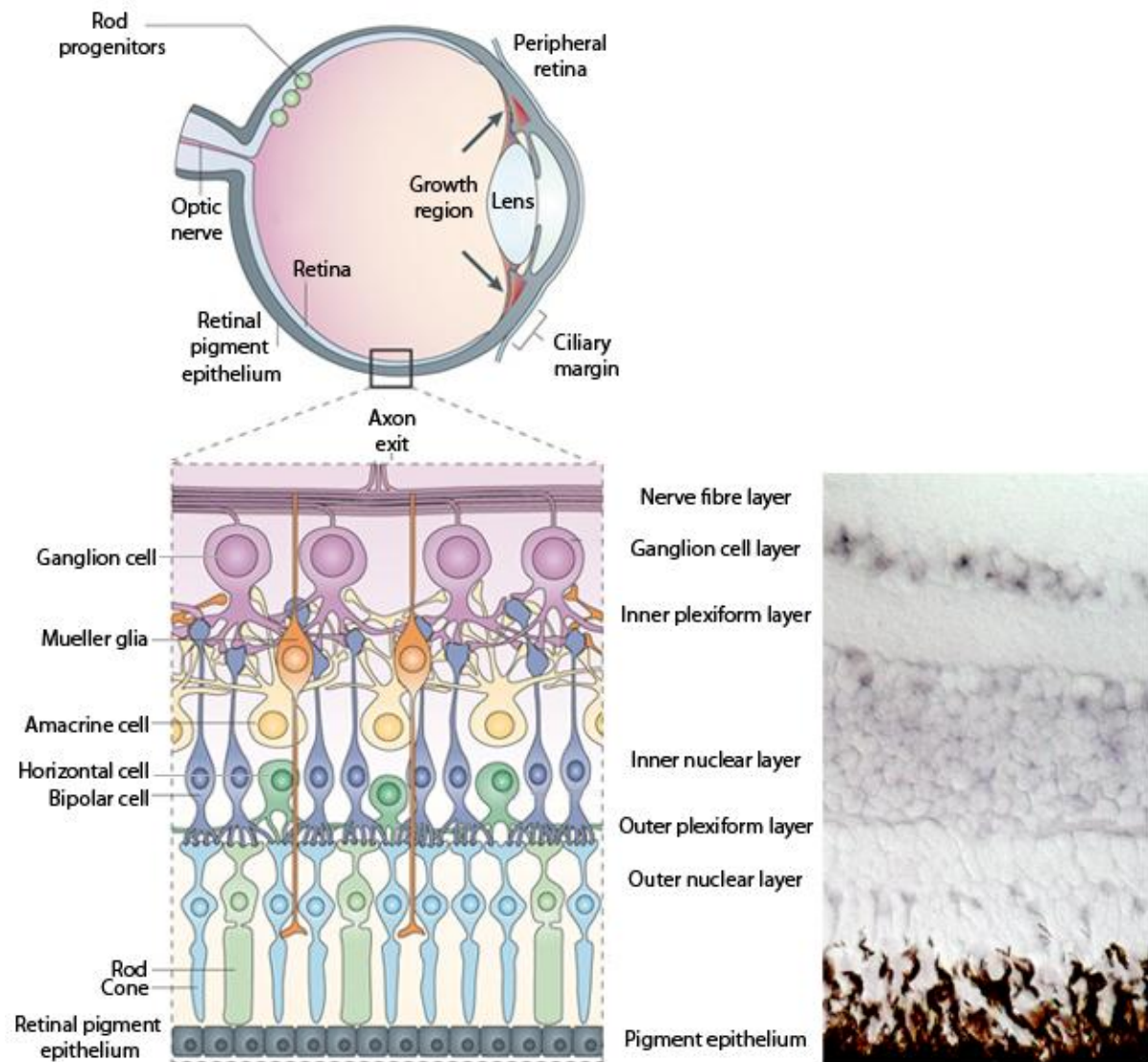
Fig. 1.1. Structure of the eye and retina.

The right hand image is an in situ hybridisation on retinal cryosection showing expression of *roundabout2* in the retinal ganglion cell layer of an adult zebrafish following optic nerve crush.

Adapted from Tanaka and Ferretti, 2009.

1.3.2 Ongoing neurogenesis and axonogenesis

Zebrafish, unlike mammals, grow continuously throughout life. This process involves not only the enlargement of existing cells but also proliferation, including neurogenesis (Zupanc, 2008). In teleosts both the retina and tectum grow throughout life. Neurogenesis occurs in the periphery

of the retina in an area called the ciliary margin, in a process common to fish and amphibians. These newborn RGCs in the retinal margin extend axons which exit the eye via the optic nerve head and navigate along the existing optic tract, within a specific bundle, to terminate onto the tectum and pretectal targets (Easter and Stuermer, 1984; Marcus et al., 1999). This clearly shows that the adult zebrafish CNS is capable of supporting the growth and navigation of axons from the retina to the tectum. The continuously generated RGCs in adult growth have axons which express developmental antigens such as the cell recognition molecules polysialylated NCAM and L1 (Bernhardt, 1999).

1.3.3 Retinal ganglion cell axon regeneration

RGCs with regenerating axons following axotomy present similar characteristics to newly generated RGCs. RGCs with regenerating axons reenter a growth state in which they reexpress various development associated genes which include cytoskeletal proteins, membrane bound recognition molecules of the immunoglobulin family, including *neural cell adhesion molecule* (*ncam*) and L1 homologues, and *growth associated protein 43* (*gap43*), an indicator of axon growth (Bernhardt,1999). These genes are very likely to play a role in axon regrowth. Reduced L1 expression has been shown to impair axon regrowth (Becker et al., 2004a). However regeneration associated growth does not appear to be a complete recapitulation of development as regulation of the growth associated genes differs between the two processes. During development, but not regeneration, *ncam* is present on axons in its highly polysialylated form, embryonic-*ncam* (*encam*) (Harman et al., 2003). Other regeneration associated molecules, including the actin-interacting protein Gelsolin (Roth et al., 1999), the recognition molecules zfNLRR (Bormann et al., 1999) and Contactin1a (Schweitzer et al., 2007) are expressed at much higher levels during axon regrowth than during development. This would suggest that growth of axons during development and during regeneration relies on a similar but distinct pattern of gene regulation. Other cell types also contribute to the growth promoting environment following lesion. Photoreceptors secret Purpurin which promotes axon growth in RGCs (Matsukawa et al., 2004) and other growth promoting molecules such as Axogenesis Factors-1 and -2, are secreted by optic nerve glia into the surrounding environment (Petrausch et al., 2000a).
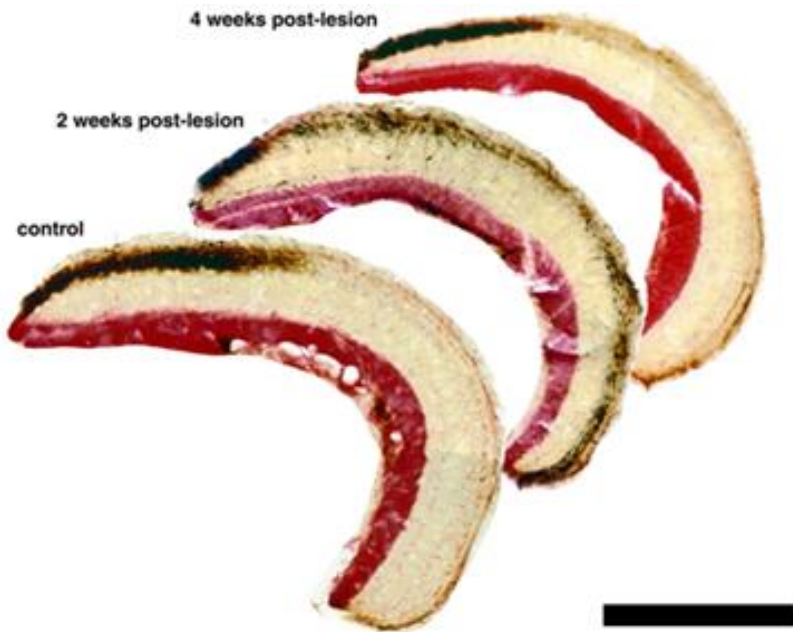
Fig. 1.2. Regeneration of the optic projection onto the tectum is precise in zebrafish.

Four weeks after an optic nerve crush, RGC axons have regenerated to the tectum and terminated in a spatially restricted manner similar to unlesioned controls.

Coronal sections. Medial is left, dorsal is up. Bar is 200µm.

Figure used with the kind permission of Dr. T Becker.

1.3.4 Restoration of function

The teleost optic system is capable of robust regeneration with spontaneous restoration of function, in contrast to the lack of regeneration in mammals, and functional but less robust regeneration in reptiles and Anurans. These regenerating RGC axons reach their appropriate targets leading to arborisation and a restoration of vision (McDowell et al., 2004; Bernhardt, 1999). This is a very important distinction as, although most anamniotes have the capacity for some optic nerve regeneration, the extent and functionality of the regeneration varies and regrowth of axons does not necessarily lead to functional connections. While lizards may undergo spontaneous axon regeneration following an optic nerve lesion, they do not exhibit spontaneous restoration of vision and require visual conditioning to achieve it (Beazley et al., 2003; Dunlop et al., 2004; Rodger et al., 2006). While zebrafish RGC axon regeneration is relatively precise with the vast majority of axons reaching their correct targets, it is not perfect.

In zebrafish and goldfish, an increase in misprojecting axons, relative to the unlesioned projection, has been observed following lesion induced regeneration, such as ipsilaterally projecting axons not typically found in teleosts (Springer,1981; Becker et al., 2000a). Zebrafish RGC axons can regenerate regardless of whether the nerve fibre layer and ensheathing oligodendrocytes tubes remain intact. This is in contrast to the peripheral nervous system of mice in which regenerating axons rely on the mechanical support provided by intact Schwann cell tubes (Nguyen et al., 2002).

1.3.5 Axon navigation

The regenerating optic axons must navigate a complex environment in the adult CNS which has undergone many changes and increased in complexity since the optic tract was established during the first days of development, including a difference in scale of over tenfold. The average length of an RGC axon's primary branch at 3 days post fertilisation (dpf) is 330 microns compared to the approximately 4mm length of the adult optic tract (unpublished observations). Furthermore, regenerating axons cannot navigate by fasciculation with existing axons, as is the case for developing axons (Pittman et al., 2008). The regenerating axons must make many directional choices to navigate through critical intermediate and final targets so re-establishing the correct route for the optic nerve which crosses at the optic chiasm and enters the anterior tectum in a tight fasicle, travelling along the roof of the tectum and then terminating in the correct area and layer of the tectum. The pattern of RGCs on the retina is mirrored onto the tectum with temporal retina RGCs projecting axons to anterior tectum and nasal retina RGCs projecting axons to the posterior tectum (Fig. 1.3) (Udin and Fawcett, 1988). This retinotopic map is highly precise. When this map is first established during development the axons grow precisely to their intended targets without excessive overshooting and do not undergo the extensive pruning which occurs in mammals during retinotopic map formation. Establishment of the retinotopic map during development is brought about by gradients of guidance cues in the tectum and complementary receptor gradients in the retina (Inatani, 2005). For most of this process the distances involved make it impossible for a growing axon to home in on its specific target directly so pathfinding, along cues in the vicinity of the axon, is likely to be the dominant influence.

1.3.5.1 Molecular determinants of axon pathfinding and retinotopic map formation

The idea that neural maps are determined by gradients of signals in the projecting and target areas was first suggested by Roger Sperry in 1945 with his chemo affinity theory which was informed by his work in the retina (Sperry, 1945). It is now evident that correct pathfinding relies on a range of, often overlapping, molecular gradients in the CNS which the growing axon expresses receptors for. These chemotaxis-linked molecules can induce inhibition of growth, repel axons or promote growth and be diffusible or substrate bound (Tessier-Lavigne and Goodman, 1996). To navigate through the extracellular environment the axon must be able to detect and respond to these cues. This is achieved by asymmetric alterations to the cytoskeleton at the growth cone.

1.3.5.2 Growth cone dynamics in axon pathfinding

The growth cone is a highly motile structure at the growing tip of the axon. The growth cone is a swelling with many finger-like projections called filopodia which possess a largely actin based cytoskeleton, with the actin being formed into densely packed bundles. Whereas the lamellipodia, located between the filopodia, are filled with randomly oriented networks of actin filaments (Letoumeau, 1983; Bridgman and Dailey, 1989; Okabe and Hirokawa, 1991). While the filopodia and lamellipodia cytoskeletons are dominated by actin, the cytoskeleton of the central domain of the growth cone is mostly composed of microtubules. As there is constant turnover and rearrangement of these actin and microtubule components, which generate mechanical forces and influence the cell shape, the growth cone is highly dynamic (Goshima et al., 1997; Diefenbach et al., 1999; Fournier et al., 2000; Mack et al., 2000; Kamiguchi and Lemmon, 2000; Buck and Zheng, 2002). Thus molecules which can influence the dynamics of the growth cone cytoskeleton can influence the direction and rate of growth of axons (Tessier-Lavigne and Goodman, 1996; Arimura et al., 2005; also see chapter 4). To facilitate this the membrane of the filopodia contains receptors and cell adhesion molecules which play a role in detecting guidance cues and responding to them. The growth cone is dense with organelles to allow for rapid response to environmental cues, including such processes as local translation, obviating the significant delay which would be required for transporting proteins along the length of an axon to the growth cone (Jung and Holt, 2011). Due to these properties the growth cone can rapidly respond to extracellular cues by turning, changing rate of growth, branching or

collapsing. Such rapid response may be vital to the correct behaviour of a growth cone as blocking local translation has been shown to inhibit the turning but not the growth of axons (Campbell and Holt, 2001). However that is not to say growth cones advance uniformly, as they have been found to slow or become more complex when reaching choice points in their pathways (Mason and Erskine, 2000). Extracellular signals are transduced through various second messengers such as kinases, GTPases, calcium and cyclic nucleotides (See Fig. 4.1 for an example) to promote or inhibit the assembly of actin filaments or microtubules (Gallo and Letourneau, 2004). Attractant cues, such as NGF, stabilise the cytoskeleton thus the side of the growth cone which receives the greatest attractant input will be preferentially stabilised leading to the growth cone turning towards the source of the gradient (Gundersen and Barrett, 1979; Gallo and Letourneau, 1998). In a similar manner repellent cues, such as Sema3A, destabilise the cytoskeleton leading to the growth cone turning away from the source of the cue or collapsing (Dontchev and Letourneau, 2002).

1.3.5.3 Modulation of intra-axonal signalling pathways

The effects of guidance molecules on axon growth are generally not direct as they act through varied intermediate transduction pathways, where the signal can be modified by other inputs to the pathway. Cytoskeletal-associated proteins perform a variety of roles which are integral to correct axon growth and pathfinding, such as actin bundling (Fascin and Filamin), vesicle transport (Myosin), and tubulin binding (Crmp2). Thus modifiers of growth and guidance have many potential targets which are often intricately linked. This results in the same guidance cue having different effects depending on the balance of the pathways within a specific growth cone. Netrin-1 acts as an attractant when signalling via the DCC receptor but a repellent via the Unc-5 receptor (Kennedy, 2000; Shekarabi et al., 2005). The balance of these pathways is dynamic and the response of the same growth cone to a specific guidance cue may change over time. Furthermore, the response of the growth cone to guidance cues can vary depending on the levels of intracellular molecules and their possible modifications. An increase in the levels of certain cyclic nucleotides such as cAMP, can switch the growth cone response to the Netrin-1 guidance cue from repulsion to attraction, while lowering levels of cAMP will switch attraction to repulsion (Song et al., 1997; Ming et al., 1997). This is also the case for cGMP and Sema3A guidance (Song et al., 1998). Further modulation is introduced by modifications to proteins in the

growth cone which can alter their properties and so affect the growth cone's response to signalling molecules. Phosphorylation of the intracellular molecule Crmp2 is required for Sema3A induced growth cone collapse to occur (Brown et al., 2004; Arimura et al., 2005). Therefore, without the phosphorylation of Crmp2 by kinases such as Rho-kinase, the downstream effects of Sema3A would be reduced or blocked (see chapter 4).

1.3.5.4 Axon guidance is highly specific and efficient

Such a finely controlled and dynamic guidance system is necessary due to the need for axons to navigate to their correct targets through a complex nervous system which consists of many tracts and targets. Each growth cone must be able to detect and respond to the guidance signals which direct it to its correct target, while navigating through tissues which may express guidance molecules for different subsets of axons and may contain the targets of other axons. Therefore the growth cone must be able to modulate its responsiveness over time and depending on the environment it must navigate. The use of overlapping gradients to direct axon growth is an extremely efficient method as the number of neurones in the human brain, which must project axons to their correct targets, is several orders of magnitude greater than the total number of genes in the genome (Schmucker and Flanagan, 2004). This means that different axons must respond differently to the same guidance cues which are re-used throughout the nervous system. While it is widely agreed that overlapping gradients are key determinants of axon guidance, which specific combinations of molecules influence these choices and are required for correct axon navigation is not well understood in vivo during development and even less so during regeneration. However several of the molecules which play a role in the establishment of the retinotectal projection have been identified due to extensive study of the optic system owing to its simplicity and accessibility; a selection are introduced in section 1.3.5.7.

1.3.5.5 Molecular guidance gradients define relative maps

Molecular gradients are not the sole determinant of axon guidance and targeting. Another factor which influences the final target of an axon is axon-axon competition. When a portion of the retina is ablated, the remaining RGC axons will spread out across the tectum to occupy the available space (Goodhill and Richards, 1999). Thus removing competing axons leads to the remaining axons interpreting the guidance cues in a similar but altered manner. Conversely,

when the tectum is partially ablated, the axons bunch together. If axon targeting was absolutely governed by molecular gradients it is unlikely that they would exhibit this adaption to the altered environment. It has been shown that axon guidance molecules, such as the Ephrins, define relative, not absolute, maps as overexpressing EphA receptors in a subset of axons leads to a shift in mapping for not only the overexpressing axons but also their wild type neighbours (Brown et al., 2000; Reber et al., 2004).

1.3.5.6 Axon guidance in development and regeneration
The ability of zebrafish RGC axons to navigate to the tectum and restore the retinotopic map following a lesion of the optic nerve is an apparent recapitulation of their developmental pathfinding and targeting ability (Becker et al., 2000a). If this is the case then regenerating optic axons must actively read specific molecular cues which are similar to those that guide developing pioneer axons to their targets (Becker and Becker, 2007). The identities of many developmental guidance cues and potential regenerative guidance cues have been indicated by RGC axon pathfinding mutants from zebrafish mutagenesis screens (Xiao et al., 2005; Gulati-Leekha and Goldman, 2006). If such re-establishment of the axon guidance molecular gradients found in development occurs, it would require coordinated gene regulation. At present the genes responsible for this are unknown but it is expected that a proportion of them will be the same genes responsible for the initial establishment of the axon guidance gradients found during development. As zebrafish generate RGCs, which project axons to the tectum, throughout life it can be expected that environmental cues might be present for navigation by these newly generated axons. Therefore it is possible that these pre-existing cues are used by regenerating axons also. However it is possible that regenerating axons are guided by a set of molecules distinct from those expressed during development or for the guidance of newly generated axons in the adult. Other influences on axon navigation could potentially come from mechanical or molecular interactions with the denervated brain tracts. For example, in the regenerating peripheral nervous system of mice, denervated Schwann cell tubes provide mechanical guidance for regenerating axons (Nguyen et al., 2002). At the same time, Schwann cells up-regulate a number of axon growth promoting molecules (Oudega and Xu, 2006), which is also true for oligodendrocytes in the fish CNS (Stuermer et al., 1992). Which mechanism, or perhaps combination of mechanisms, are required for axon regeneration is currently one of the most

important questions in neuroscience as the answers will guide future strategies for directed axon regeneration in the treatment of CNS disorders. We can now begin to address this complex question as in the last 15 years, several axon guidance cues have been discovered, in part due to studies in the zebrafish optic system, as well as many more potential axon guidance cues, some of which regenerating RGC axons are known to express receptors for.

1.3.5.7 Guidance molecules

1.3.5.7.1 Tenascin-R

Tenascin-R is an extracellular matrix molecule that acts as a repellent guidance molecule for optic axons during development (Becker et al., 2003) and is a potential inhibitor of axonal regeneration in the adult mammalian CNS (Becker et al., 2000b). Such repellent or inhibitory activity can guide axons by defining boundaries and thus confining the trajectories of the growing axons towards their correct targets and preventing axon branches growing beyond their appropriate areas. Tenascin-R has been shown to border the pathway of newly generated RGC axons in the adult zebrafish (Becker et al., 2004b). During regeneration RGCs upregulate expression of the Tenascin-R receptor, Contactin1a (Pesheva et al., 1993; and unpublished observations). Therefore Tenascin-R may be involved in axon guidance in the adult zebrafish as its expression is retained in the adult situation and during regeneration.

1.3.5.7.2 Chondroitin Sulfates

Chondroitin sulfate proteoglycans (CSPGs) are extracellular matrix molecules which play important roles for axon guidance during development (Faissner and Steindler, 1995; Fukuda et al., 1997) and limit plasticity in the adult CNS (Hockfield et al., 1990; Corvetti and Rossi, 2005). The CSPGs exhibit varied fine structure alterations, which contribute to protein interaction, due to the action of modifying enzymes. One class of CSPG modifying enzyme is the chondroitin sulfotransferases which add sulfate groups to specific sugar residue positions. Increased immunoreactivity for chondroitin sulfates is associated with the glial scar in mammals, in which the scar exhibits mostly inhibitory effects on axon regeneration (Silver and Miller, 2004). In contrast, the lesioned optic nerve of zebrafish has not shown an increase in chondroitin sulfate immunoreactivity (Becker and Becker, 2002). Chondroitin sulfate immunoreactivity

persists in the adult zebrafish in nonretinorecipient pretectal nuclei. These nuclei, which are embedded in the optic tract, must not be targeted by regenerating RGC axons if they are to reach their correct targets. Chondrotin sulfates repel regenerating zebrafish RGC axons in vitro and digestion of chondroitin sulfates with chondroitinase leads to an increase in misrouting of regenerating axons in vivo (Becker and Becker, 2002).

1.3.5.7.3 Netrin-1

Netrin-1 is a secreted guidance signal for developing axons, expressed in the optic nerve head. In the rat, the expression of netrin-1 is developmentally downregulated and its receptors are downregulated following lesioning of the optic nerve. In marked contrast, adult goldfish retain expression of *netrin-1* and its receptors are expressed in newly generated RGCs and upregulated in regenerating axotomised RGCs. The increased expression of *netrin-1* in the highly regenerative adult goldfish RGCs and decreased expression in the regeneration impaired adult rat RGCs, may indicate a potential role for *netrin-1* in teleost axon guidance during regeneration (Petrausch et al., 2000b).

1.3.5.7.4 Ephrins

The establishment of the retinotopic map of RGC axons onto the tectum is guided by gradients of guidance cues in the tectum and corresponding receptor gradients in the retina (See Figure 3.1) (Inatani, 2005). The Ephrin-As and their Eph receptors are important inhibitory molecules involved in this process. Rostrocaudal gradients of Ephrin-A2 and Ephrin-A5 persist in both the unlesioned and lesioned adult zebrafish tectum (Becker et al., 2000a). In adult goldfish, Ephrin signalling has been shown to be required for the correct reestablishment of the topographic map following lesion (Rodger et al., 2004).

1.3.5.7.5 Heparan Sulfates

Heparan sulfate proteoglycans (HSPGs) are expressed extensively in the developing brain and are involved in RGC axon navigation. HSPGs are important for growth cone navigation (Lee and Chien, 2004) and, in mice, a lack of HSPGs has been shown to increase retinoretinal projection of RGCs (Inatani et al., 2003). HSPGs are extracellular matrix molecules with varied fine structure alterations, which contribute to protein interaction, due to the action of modifying

enzymes (Esko and Selleck, 2002). These modifications of the sugar residues of the HSPGs include epimerization, de-acetylation and sulfation. Sulfation is carried out by heparan sulfate transferases (HST) which add sulfate groups to specific sugar residue positions of the heparan sulfate sugars (Lee and Chien, 2004). HS6ST1 sulfates the 6-O position of glucosamine and has been shown to affect retinal axon guidance in the chiasm of developing mice (Pratt et al., 2006).

1.3.5.7.6 Sulfatases

Sulfatases (sulfs) remove sulfate groups from specific sugar residues of HSPGs. Sulf1 and Sulf2 are secreted 6-O-endosulfatases involved in the processing of the 6-O position of glucosamine of HSPGs. They have an opposing activity to HS6ST1 which adds sulfate groups to the same target residue. The roles of Sulf1 and Sulf2 during normal development are not well understood but it has been shown in the mouse that they have overlapping yet essential functions (Holst et al., 2007).

1.3.5.7.7 Semaphorins

Semaphorins are a family of secreted or transmembrane glycoproteins, many of which signal through Plexins (Kruger et al, 2005). The majority of semaphorins are associated with areas of exclusion for Plexin and Neuropilin co-receptor expressing neurons in the developing nervous system (Fiore and Püschel, 2003; Huber et al., 2003). Repulsive Semaphorin signalling has been shown in various developing nervous systems including in RGCs of zebrafish (Liu et al., 2004; Becker and Becker, 2007) and class 3 Semaphorins have been implicated in the inhibition of mammalian CNS regeneration (Niclou et al., 2006). As with chondroitin sulfate, the homologues of Semaphorin3A continue to be expressed in a nonretinorecipient pretectal nuclei in the adult zebrafish. Furthermore, regenerating RGCs re-express the receptor Neuropilin-1Aa and so may be able to detect repellent Semaphorin cues (unpublished observations).

1.3.5.7.8 Collapsin response mediator proteins

Collapsin response mediator proteins (Crmps) are a family of phosphoproteins which are highly expressed in the nervous system (Liu and Strittmatter, 2001). While not guidance cues themselves, the Crmps are involved in the signal transduction cascade of multiple inhibitory guidance cues, including Semaphorins, during axon growth (Liu and Strittmatter, 2001). The

crmps exhibit a high level of cross species homology (Quinn et al., 1999). This high level of evolutionary conservation highlights the functional importance of the Crmps. The expression pattern of Crmp2 in the embryonic brain is also consistent across the major model organisms, indicating its functional importance; mouse (Byk et al., 1996), cat (Cnops et al., 2004), zebrafish (Schweitzer et al., 2005; Christie et al., 2006), *Xenopus* (Kamata et al., 1998) and chick (Goshima et al., 1995). Interest in *crmp2* first arose due to a *crmp2* mutant in *C.elegans* which has severely uncoordinated movement which is due to abnormal axon guidance and outgrowth including premature axon termination, abnormal branching, aberrant pathfinding and a superabundance of microtubules in neurons (Hedgecock et al., 1985; Desai et al., 1988; Siddiqui and Culotti, 1991; Li et al., 1992). The *crmps* play a role in growth cone morphology and it has been shown that Crmp2 enhances the advance of growth cones by regulating microtubule assembly (Arimura et al., 2005).
(See chapter 4).

1.3.5.7.9 Roundabouts

In the zebrafish, Roundabout *2* (Robo2) is a receptor for repellent extracellular matrix cues of the *slit* class (Dickson and Gilestro, 2006) and is known to be expressed in RGCs (Challa et al. 2001; Lee et al. 2001). Robo was first identified as the gene responsible for CNS axon pathway defects in a *Drosophila* mutant (Seeger et al., 1993).

1.3.5.7.9.1 Robos are repellent guidance cues for developing axons

Robo was shown to encode an immunoglobulin superfamily transmembrane receptor protein which carries out signal transduction via its cytoplasmic domain and is highly expressed in growth cones (Kidd et al., 1998a; Bashaw and Goodman, 1999). Robo expression is necessary for correct crossing at the midline by commissural axons as without Robo expression these axons recross the midline multiple times instead of only once and ipsilateral axons aberrantly cross (Seeger et al., 1993; Kidd et al., 1998b). Based on evidence from *Drosophila* it was shown that Slit, expressed by cells near the midline, repels axons from the midline via Robo mediated repulsion (Kidd et al. 1999; Brose et al. 1999). Axons which project ipsilaterally express Robo receptors and are repelled by Slit, while commissural axons have lower levels of Robo expression before crossing the midline which allows any attractant cues to overcome the Slit

repulsion. Following crossing, upregulation of Robo leads to the repulsive cues overcoming the attractants and the axon is repelled from the midline (Kidd et al., 1998a; Sun et al., 2000). Interestingly, in zebrafish Robo2 plays an important role in pathfinding of RGC axons even prior to approaching the midline as shown by errors in the *astray* mutant (Hutson and Chien, 2002) which may suggest that the precise function of *robo2* is not completely conserved between invertebrates and vertebrates. In vertebrates, in vitro experiments have shown that Slit proteins can repel various axons which express Robos including chick olfactory bulb axons, rat spinal motor axons, mouse hippocampal axons, and rodent RGC axons (Brose et al., 1999; Li et al., 1999; Nguyen Ba-Charvet et al., 1999; Niclou et al., 2000; Erskine et al., 2000; Ringstedt et al., 2000). Other functions of Robo/Slit signalling include effects on cell migration (Wu et al., 1999; Zhu et al.,1999).

1.3.5.7.9.2 Robos are highly conserved in vertebrates

The four known mammalian *robos* (Kidd et al., 1998a; Yuan et al., 1999a; Huminiecki et al., 2002) are orthologues of the four known zebrafish *robos*; *robo1-4* (Lee et al., 2001; Bedell et al., 2005). However, unlike *Drosophila robo1*, *Drosophila robo2* and *robo3* are not orthologues of their vertebrate namesakes and appear to have arisen due to independent genome duplication events (Dickson and Gilestro, 2006). The zebrafish Robos have high interspecies homology and high intrafamily homology, with the exception of Robo4 which is smaller than the other Robos with only around half of the conserved Robo family domains (Lee et al., 2001; Bedell et al., 2005). Similarly in mice, Robo4 is the least homologous member of the *robo* family (Park et al., 2003). The functional properties of Slits and Robos are also preserved across species as Slit and Robo proteins from different species can successfully interact (Brose et al., 1999). As with *Drosophila*, mammals have 3 slit genes which are expressed by midline cells (Holmes et al. 1998; Itoh et al. 1998; Nakayama et al.1998; Brose et al. 1999; Li et al. 1999; Yuan et al. 1999b). Zebrafish have 4 *slit* genes due to the teleost genome duplication resulting in a *slit1a* and *slit1b* (Hutson et al., 2003), which are also expressed at the midline and guide the optic pathway in a largely repellent manner (Barresi et al., 2005).

1.3.5.7.9.3 Expression patterns

1.3.5.7.9.3.1 Robos

The four known zebrafish *robo* genes (*robo1* to *4*) are highly expressed in the developing nervous system in overlapping but distinct patterns. As well as being expressed in the visual system, olfactory system, cranial ganglia, hindbrain and spinal cord, they are also expressed in other tissues such as the somites and fin buds (Lee et al., 2001). Both the timing of expression and spatial patterning suggest a role in axon guidance. The *robo* family is differentially expressed in the zebrafish optic system during development in a manner which supports a role for these proteins in retinal axon guidance. By 36hpf, during early optic system formation, *robo2* is strongly expressed throughout the RGC layer (Lee et al., 2001), at a time when axons are navigating from the retina to the tectum and are beginning to reach the optic chiasm (Stuermer, 1988; Burrill and Easter, 1995). By 48hpf, *robo2* expression is restricted to the peripheral retina where later born RGCs are being added in an annular fashion and are extending axons towards the tectum. *Robo1* and *robo3* do not appear to be expressed in the developing retina. However they are expressed in the tectum. While *robo3* expression in the tectum is confined to only a subset of superficial cells, *robo1* and *robo2* are widely expressed in the tectum, with *robo2* exhibiting the strongest expression (Lee et al., 2001). *Robo2* and, at a much reduced level, *robo1* and *robo3* are expressed dorsal to the optic chiasm in the ventral diencephalon (Lee et al., 2001). By 76hpf, when axons are reaching the tectum and arborising, the pattern of *robo* expression from early development has largely persisted with *robo2* still highly expressed throughout the tectum and RGCs (Campbell et al., 2007). Of the *robos*, *robo2* expression is most widespread in the retinotectal system and surrounding areas where axons must make navigation choices, which may suggest its importance in this system. This was confirmed in the zebrafish mutant Astray, which expresses a truncated form of Robo2 which lacks the domains required to function as a receptor due to a point, nonsense mutation (Fricke et al., 2001). Zebrafish *robo2* expression in the developing RGC layer is comparable to that of mammalian *robo2* (Erskine et al., 2000; Niclou et al., 2000; Ringstedt et al., 2000). Whereas *robo1* does not appear to be expressed in the zebrafish while it is expressed in the mammalian RGC layer in scattered cells (Erskine et al., 2000; Niclou et al., 2000; Ringstedt et al., 2000). However it has been shown that Robo2 but not Robo1 is required for slit mediated intraretinal guidance in the mouse (Thompson et al., 2009).

In mice it has been shown that Robo3 suppresses the influence of Robo1 and 2 on commissural axons, while *robo1* knockout has shown to be a weak phenocopy of *robo2* knockout (Long et al., 2004). In the zebrafish it has been shown through transplantation that *robo2* is required eye-autonomously for correct retinal axon pathfinding (Fricke et al., 2001).

1.3.5.7.9.3.2 Slits

How precisely Robos and Slits interact on the structural level is poorly understood and the affinity of one Robo family member for any particular Slit family member is unclear. Although in *Drosophila* it has been demonstrated that the Robos bind with similar affinity to Slit domains (Howitt et al. 2004). There is some evidence that Slits may have other receptors than Robos from knockout work in mice which revealed a more severe pathfinding phenotype when the *slits* were knocked out compared to knockout of the *robos* (Jaworski et al., 2010). Regional specificity of Slits in mouse intraretinal axon guidance may also indicate redundancy with other guidance signals (Thompson et al., 2009). From expression patterns of *slits* and *robos*, it can be inferred that Slit2 is likely to be an important ligand for Robo2 in the retinotectal system. In zebrafish Slit2 is expressed in the optic stalk where it may be involved in optic nerve fasciculation (Niclou et al., 2000) as it has been shown in rodent models (Erskine et al., 2000; Ringstedt et al., 2000). In zebrafish the expression patterns of *slit2* and *slit3* in the forebrain, rostral and caudal to the optic tract respectively, define a corridor through which RGC axons pass (Hutson and Chien, 2002). Whereas in the rodent the pathway is bounded by *slit1* and *slit2* (Erskine et al., 2000; Niclou et al., 2000; Ringstedt et al., 2000). This suggests that while the *slits* are expressed in a manner consistent with influencing RGC guidance across classes, the specific *slits* involved may differ between classes. While zebrafish *slit1a* expression may not define the optic tract boundary as with mammalian *slit1*, it is expressed throughout the tectum and weakly in the RGCs during development. *Slit1b* and *slit2* are not detectably expressed in the tectum but are expressed in the retina, but not in the RGCs. *Slit3* is expressed in neither the tectum nor the retina (Campbell et al., 2007).

1.3.5.7.9.4 Astray mutant

A functional null mutant for *robo2* (*Astray*[ti272z]) exhibits various targeting errors of optic axons during development, including pathfinding errors (rostro-caudal pathfinding errors, ectopic midline crossing), and termination errors (increased terminal arbor sizes) of optic axons during development (Fricke et al., 2001; Campbell et al., 2007). Similar pathfinding defects are observed in *slit* or *robo* deficient mice (Plump et al., 2002; Plachez et al., 2008). Mutant growth cones are larger and more complex than wild-type and time-lapse analysis indicates that, unlike wild type optic axons, optic axons in *astray* mutants do not correct errors during growth across the chiasm (Hutson and Chien, 2002).

(See chapter 2).
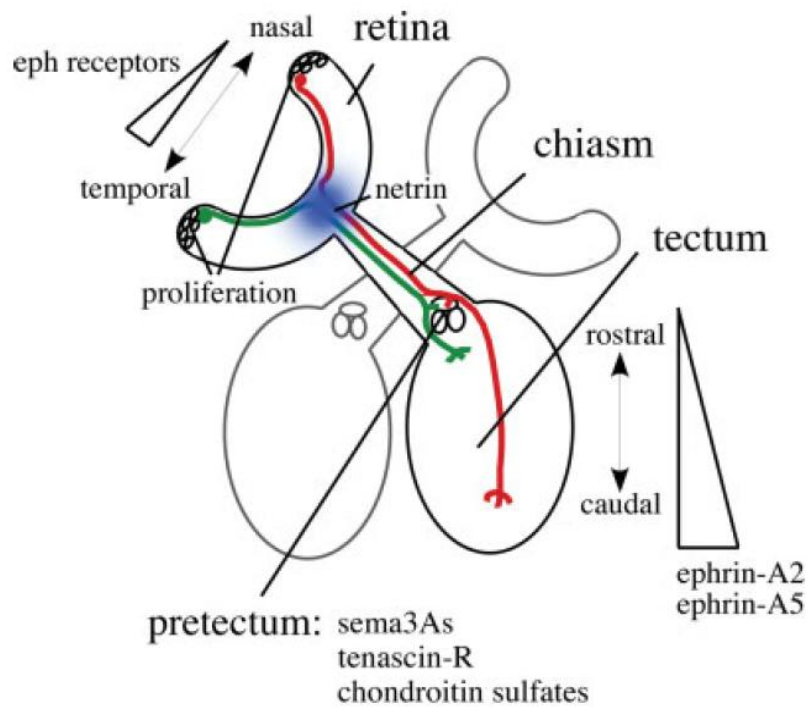
Fig. 1.3. Guidance cues are present in the optic pathway of adult fish.

Diagram of the optic system (dorsal view) indicating expression of potential guidance molecules at the optic nerve head (Netrin), the pretectum (Sema3As, Tenascin-R, Chondroitin sulfates), and the tectum (Ephrin-A2 and A5). RGCs are continuously generated in the retinal margin (proliferation). Typical trajectories of temporal (green) and nasal (red) optic axons are indicated.

Modified from Becker and Becker, 2007.

1.5 Summary

In summary, zebrafish are capable of a high degree of spontaneous CNS regeneration and possess a CNS that is both rich in growth promoting molecules and low in inhibitory molecules. The optic nerve lesion paradigm in zebrafish offers an anatomically discrete and highly accessible extension of the CNS which undergoes full regeneration within four weeks and has a 100% survival rate in our hands. The retinotectal system in particular has been well studied. Following axotomy, RGCs upregulate expression of a specific set of molecules associated with axon growth and pathfinding. These cues contribute to the ability of the RGC axons to regrow and navigate to their appropriate targets, leading to functional connections and the restoration of vision. The precise array of molecular determinants which are necessary for this process are currently not well elucidated. Such knowledge would greatly inform future research towards directed axon regeneration in mammals and humans for the treatment of CNS disorders and injuries. Towards this end, we have set out to uncover the molecular determinants of axon regeneration and guidance through a molecular analysis of the zebrafish retinotectal system. The availability of whole-genome microarrays for the zebrafish (Agilent) make it possible to obtain an overview of regeneration related gene regulation in order to identify novel guidance related genes. The identities of several guidance cues have been indicated by the study of RGC pathfinding mutants (Xiao et al., 2005; Gulati-Leekha and Goldman, 2006). Potential guidance molecules can be readily knocked down with morpholinos and any resultant pathfinding errors can be relatively easily studied in the semi-transparent embryos. The heatshock inducible GAL4/UAS system also offers the potential to perturb putative guidance molecules in both the embryonic and adult situation. Investigating how such embryonic pathfinding errors compare to possible pathfinding errors in adult regeneration will offer insight into the question of to what extent regeneration is a recapitulation of development. Furthermore the pathfinding mutant, *astray* (Karlstrom et al., 1996), offers the opportunity to disentangle the source of guidance cues in regeneration by studying how degenerating ectopic projections influence regeneration.

1.6 Bibliography

Abdesselem H, Shypitsyna A, Solis GP, Bodrikov V, Stuermer CA. No Nogo66- and NgR-mediated inhibition of regenerating axons in the zebrafish optic nerve. J Neurosci. 2009 Dec 9;29(49):15489-98. PubMed PMID: 20007473.

Arimura N, Ménager C, Kawano Y, Yoshimura T, Kawabata S, Hattori A, Fukata Y, Amano M, Goshima Y, Inagaki M, Morone N, Usukura J, Kaibuchi K. Phosphorylation by Rho kinase regulates CRMP-2 activity in growth cones. Mol Cell Biol. 2005 Nov;25(22):9973-84. PubMed PMID: 16260611; PubMed Central PMCID: PMC1280267.

Alvarez-Buylla A, Buskirk DR, Nottebohm F. Monoclonal antibody reveals radial glia in adult avian brain. J Comp Neurol. 1987 Oct 8;264(2):159-70. PubMed PMID: 2445794.

Anderson MJ, Waxman SG. Morphology of regenerated spinal cord in Sternarchus albifrons. Cell Tissue Res. 1981;219(1):1-8. PubMed PMID: 7285088.

Barber LW. Correlations between wound healing and regeneration in fore-limbs and tails of lizards. The Anatomical Record. 1944 Aug;89(4):441-453.

Barresi MJ, Hutson LD, Chien CB, Karlstrom RO. Hedgehog regulated Slit expression determines commissure and glial cell position in the zebrafish forebrain. Development. 2005 Aug;132(16):3643-56. Epub 2005 Jul 20. PubMed PMID: 16033800.

Bashaw GJ, Goodman CS. Chimeric axon guidance receptors: the cytoplasmic domains of slit and netrin receptors specify attraction versus repulsion. Cell. 1999 Jun 25;97(7):917-26. PubMed PMID: 10399919.

Battisti WP, Shinar Y, Schwartz M, Levitt P, Murray M. Temporal and spatial patterns of expression of laminin, chondroitin sulphate proteoglycan and HNK-1 immunoreactivity during regeneration in the goldfish optic nerve. J Neurocytol. 1992 Aug;21(8):557-73. PubMed PMID: 1380544.

Beattie MS, Bresnahan JC, Lopate G. Metamorphosis alters the response to spinal cord transection in Xenopus laevis frogs. J Neurobiol. 1990 Oct;21(7):1108-22. PubMed PMID: 2258724.

Beazley LD, Darby JE, Perry VH. Cell death in the retinal ganglion cell layer during optic nerve regeneration for the frog Rana pipiens. Vision Res. 1986;26(4):543-56. PubMed PMID: 3488614.

Beazley LD, Rodger J, Chen P, Tee LB, Stirling RV, Taylor AL, Dunlop SA. Training on a visual task improves the outcome of optic nerve regeneration. J Neurotrauma. 2003 Nov;20(11):1263-70. PubMed PMID: 14651812.

Becker CG, Becker T. Repellent guidance of regenerating optic axons by chondroitin sulfate glycosaminoglycans in zebrafish. J Neurosci. 2002 Feb 1;22(3):842-53. PubMed PMID: 11826114.

Becker CG, Becker T. Growth and pathfinding of regenerating axons in the optic projection of adult fish. J Neurosci Res. 2007 Sep;85(12):2793-9. Review. PubMed PMID: 17131420.

Becker CG, Becker T. Adult zebrafish as a model for successful central nervous system regeneration. Restor Neurol Neurosci. 2008;26(2-3):71-80. Review. PubMed PMID: 18820403.

Becker CG, Lieberoth BC, Morellini F, Feldner J, Becker T, Schachner M. L1.1 is involved in spinal cord regeneration in adult zebrafish. J Neurosci. 2004a Sep 8;24(36):7837-42. PubMed PMID: 15356195.

Becker CG, Meyer RL, Becker T. Gradients of ephrin-A2 and ephrin-A5b mRNA during retinotopic regeneration of the optic projection in adult zebrafish. J Comp Neurol. 2000 Nov 20;427(3):469-83. Erratum in: J Comp Neurol 2001 Sep 17;438(2):252. PubMed PMID: 11054707.

Becker CG, Schweitzer J, Feldner J, Becker T, Schachner M. Tenascin-R as a repellent guidance molecule for developing optic axons in zebrafish. J Neurosci. 2003 Jul 16;23(15):6232-7. PubMed PMID: 12867507.

Becker CG, Schweitzer J, Feldner J, Schachner M, Becker T. Tenascin-R as a repellent guidance molecule for newly growing and regenerating optic axons in adult zebrafish. Mol Cell Neurosci. 2004b Jul;26(3):376-89. PubMed PMID: 15234343.

Becker T, Anliker B, Becker CG, Taylor J, Schachner M, Meyer RL, Bartsch U. Tenascin-R inhibits regrowth of optic fibers in vitro and persists in the optic nerve of mice after injury. Glia. 2000b Feb 15;29(4):330-46. PubMed PMID: 10652443.

Becker T, Becker CG. Regenerating descending axons preferentially reroute to the gray matter in the presence of a general macrophage/microglial reaction caudal to a spinal transection in adult zebrafish. J Comp Neurol. 2001 Apr 23;433(1):131-47. PubMed PMID: 11283955.

Becker T, Wullimann MF, Becker CG, Bernhardt RR, Schachner M. Axonal regrowth after spinal cord transection in adult zebrafish. J Comp Neurol. 1997 Jan 27;377(4):577-95. PubMed PMID: 9007194.

Bedell VM, Yeo SY, Park KW, Chung J, Seth P, Shivalingappa V, Zhao J, Obara T, Sukhatme VP, Drummond IA, Li DY, Ramchandran R. roundabout4 is essential for angiogenesis in vivo. Proc Natl Acad Sci U S A. 2005 May 3;102(18):6373-8. Epub 2005 Apr 22. PubMed PMID: 15849270; PubMed Central PMCID: PMC1088354.

Bellairs AA, Bryant SV. Effects of amputation of limbs and digits of lacertid lizards. Anat Rec. 1968 Aug;161(4):489-95. PubMed PMID: 5696192.

Bernhardt RR. Cellular and molecular bases of axonal regeneration in the fish central nervous system. Exp Neurol. 1999 Jun;157(2):223-40. Review. PubMed PMID: 10364435.

Bormann P, Roth LW, Andel D, Ackermann M, Reinhard E. zfNLRR, a novel leucine-rich repeat protein is preferentially expressed during regeneration in zebrafish. Mol Cell Neurosci. 1999 Mar;13(3):167-79. PubMed PMID: 10328879.

Bridgman PC, Dailey ME. The organization of myosin and actin in rapid frozen nerve growth cones. J Cell Biol. 1989 Jan;108(1):95-109. PubMed PMID: 2642912; PubMed Central PMCID: PMC2115362.

Brose K, Bland KS, Wang KH, Arnott D, Henzel W, Goodman CS, Tessier-Lavigne M, Kidd T.Slit proteins bind Robo receptors and have an evolutionarily conserved role in repulsive axon guidance. Cell. 1999 Mar 19;96(6):795-806. PubMed PMID: 10102268.

Brown A, Yates PA, Burrola P, Ortuño D, Vaidya A, Jessell TM, Pfaff SL, O'Leary DD, Lemke G. Topographic mapping from the retina to the midbrain is controlled by relative but not absolute levels of EphA receptor signaling. Cell. 2000 Jul 7;102(1):77-88. PubMed PMID: 10929715.

Brown M, Jacobs T, Eickholt B, Ferrari G, Teo M, Monfries C, Qi RZ, Leung T, Lim L, Hall C.Alpha2-chimaerin, cyclin-dependent Kinase 5/p35, and its target collapsin response mediator protein-2 are essential components in semaphorin 3A-induced growth-cone collapse. J Neurosci. 2004 Oct 13;24(41):8994-9004. PubMed PMID: 15483118.

Buck KB, Zheng JQ. Growth cone turning induced by direct local modification of microtubule dynamics. J Neurosci. 2002 Nov 1;22(21):9358-67. PubMed PMID: 12417661.

Burrill JD, Easter SS Jr. The first retinal axons and their microenvironment in zebrafish: cryptic pioneers and the pretract. J Neurosci. 1995 Apr;15(4):2935-47. PubMed PMID: 7722638.
Byk T, Dobransky T, Cifuentes-Diaz C, Sobel A. Identification and molecular characterization of Unc-33-like phosphoprotein (Ulip), a putative mammalian homolog of the axonal guidance-associated unc-33 gene product. J Neurosci. 1996 Jan 15;16(2):688-701. PubMed PMID: 8551352.

Campbell DS, Holt CE. Chemotropic responses of retinal growth cones mediated by rapid local protein synthesis and degradation. Neuron. 2001 Dec 20;32(6):1013-26. PubMed PMID: 11754834.

Campbell DS, Stringham SA, Timm A, Xiao T, Law MY, Baier H, Nonet ML, Chien CB. Slit1a inhibits retinal ganglion cell arborization and synaptogenesis via Robo2-dependent and -independent pathways. Neuron. 2007 Jul 19;55(2):231-45. PubMed PMID: 17640525.

Carulli D, Laabs T, Geller HM, Fawcett JW. Chondroitin sulfate proteoglycans in neural development and regeneration. Curr Opin Neurobiol. 2005 Feb;15(1):116-20. Review. Erratum in: Curr Opin Neurobiol. 2005 Apr;15(2):252. PubMed PMID: 15721753.

Challa AK, Beattie CE, Seeger MA. Identification and characterization of roundabout orthologs in zebrafish. Mech Dev. 2001 Mar;101(1-2):249-53. PubMed PMID: 11231085.

Chaudhry N, Filbin MT. Myelin-associated inhibitory signaling and strategies to overcome inhibition. J Cereb Blood Flow Metab. 2007 Jun;27(6):1096-107. Epub 2006 Oct 11. Review. PubMed PMID: 17033690.

Cheesman SE, Layden MJ, Von Ohlen T, Doe CQ, Eisen JS. Zebrafish and fly Nkx6 proteins have similar CNS expression patterns and regulate motoneuron formation. Development. 2004 Nov;131(21):5221-32. Epub 2004 Sep 29. PubMed PMID: 15456722.

Christie TL, Starovic-Subota O, Childs S. Zebrafish collapsin response mediator protein (CRMP)-2 is expressed in developing neurons. Gene Expr Patterns. 2006 Jan;6(2):193-200. Epub 2005 Sep 15. PubMed PMID: 16168718.

Clause AR, Capaldi EA. Caudal autotomy and regeneration in lizards. J Exp Zool A Comp Exp Biol. 2006 Dec 1;305(12):965-73. Review. PubMed PMID: 17068798.

Corvetti L, Rossi F. Degradation of chondroitin sulfate proteoglycans induces sprouting of intact purkinje axons in the cerebellum of the adult rat. J Neurosci. 2005 Aug 3;25(31):7150-8. PubMed PMID: 16079397.

Cnops L, Van de Plas B, Arckens L. Age-dependent expression of collapsin response mediator proteins (CRMPs) in cat visual cortex. Eur J Neurosci. 2004 Apr;19(8):2345-51. PubMed PMID: 15090061.

Desai C, Garriga G, McIntire SL, Horvitz HR. A genetic pathway for the development of the Caenorhabditis elegans HSN motor neurons. Nature. 1988 Dec 15;336(6200):638-46. PubMed PMID: 3200316.

Dickson BJ, Gilestro GF. Regulation of commissural axon pathfinding by slit and its Robo receptors. Annu Rev Cell Dev Biol. 2006;22:651-75. Review. PubMed PMID: 17029581.

Diefenbach TJ, Guthrie PB, Stier H, Billups B, Kater SB. Membrane recycling in the neuronal growth cone revealed by FM1-43 labeling. J Neurosci. 1999 Nov 1;19(21):9436-44. PubMed PMID: 10531447.

Diekmann H, Klinger M, Oertle T, Heinz D, Pogoda HM, Schwab ME, Stuermer CA. Analysis of the reticulon gene family demonstrates the absence of the neurite growth inhibitor Nogo-A in fish. Mol Biol Evol. 2005 Aug;22(8):1635-48. Epub 2005 Apr 27. PubMed PMID: 15858203.

Dijkers MP. Quality of life of individuals with spinal cord injury: a review of conceptualization, measurement, and research findings. J Rehabil Res Dev. 2005 May-Jun;42(3 Suppl 1):87-110. Review. PubMed PMID: 16195966.

Dontchev VD, Letourneau PC. Nerve growth factor and semaphorin 3A signaling pathways interact in regulating sensory neuronal growth cone motility. J Neurosci. 2002 Aug 1;22(15):6659-69. PubMed PMID: 12151545.

Duffy MT, Liebich DR, Garner LK, Hawrych A, Simpson SB Jr, Davis BM. Axonal sprouting and frank regeneration in the lizard tail spinal cord: correlation between changes in synaptic circuitry and axonal growth. J Comp Neurol. 1992 Feb 15;316(3):363-74. PubMed PMID: 1577990.
Dunlop SA, Tee LB, Stirling RV, Taylor AL, Runham PB, Barber AB, Kuchling G, Rodger J, Roberts JD, Harvey AR, Beazley LD. Failure to restore vision after optic nerve regeneration in reptiles: interspecies variation in response to axotomy. J Comp Neurol. 2004 Oct 18;478(3):292-305. PubMed PMID: 15368531.

Easter SS Jr, Stuermer CA. An evaluation of the hypothesis of shifting terminals in goldfish optic tectum. J Neurosci. 1984 Apr;4(4):1052-63. PubMed PMID: 6325603.

Egar M, Simpson SB, Singer M. The growth and differentiation of the regenerating spinal cord of the lizard, Anolis carolinensis. J Morphol. 1970 Jun;131(2):131-51. PubMed PMID: 5425076.

Ekker SC. Zinc finger-based knockout punches for zebrafish genes. Zebrafish. 2008 Summer;5(2):121-3. Review. PubMed PMID: 18554175; PubMed Central PMCID: PMC2849655.

Erskine L, Williams SE, Brose K, Kidd T, Rachel RA, Goodman CS, Tessier-Lavigne M, Mason CA. Retinal ganglion cell axon guidance in the mouse optic chiasm: expression and function of robos and slits. J Neurosci. 2000 Jul 1;20(13):4975-82. PubMed PMID: 10864955.

Esko JD, Selleck SB. Order out of chaos: assembly of ligand binding sites in heparan sulfate.Annu Rev Biochem. 2002;71:435-71. Epub 2001 Nov 9. Review. PubMed PMID: 12045103.

Faissner A, Steindler D. Boundaries and inhibitory molecules in developing neural tissues. Glia. 1995 Apr;13(4):233-54. Review. PubMed PMID: 7615335.

Fawcett JW. The glial response to injury and its role in the inhibition of CNS repair. Adv Exp Med Biol. 2006;557:11-24. Review. PubMed PMID: 16955702.

Filoni S, Bosco L. Comparative analysis of the regenerative capacity of caudal spinal cord in larvae of serveral Anuran amphibian species. Acta Embryol Morphol Exp. 1981 Dec-1982 Jan;2(3):199-226. PubMed PMID: 6983200.

Filoni S, Gibertini G. A study of the regenerative capacity of the central nervous system of anuran amphibia in relation to their stage of development. I. Observations on the regeneration of the optic lobe of Xenopus laevis (Daudin) in the larval stages. Arch Biol (Liege). 1969;80(4):369-411. PubMed PMID: 5401735.

Fiore R, Püschel AW. The function of semaphorins during nervous system development. Front Biosci. 2003 May 1;8:s484-99. Review. PubMed PMID: 12700098.

Font E, García-Verdugo JM, Alcántara S, López-García C. Neuron regeneration reverses 3-acetylpyridine-induced cell loss in the cerebral cortex of adult lizards. Brain Res. 1991 Jun 14;551(1-2):230-5. PubMed PMID: 1717105.

Fournier AE, Nakamura F, Kawamoto S, Goshima Y, Kalb RG, Strittmatter SM. Semaphorin3A enhances endocytosis at sites of receptor-F-actin colocalization during growth cone collapse. J Cell Biol. 2000 Apr 17;149(2):411-22. PubMed PMID: 10769032; PubMed Central PMCID: PMC2175148.

Fricke C, Lee JS, Geiger-Rudolph S, Bonhoeffer F, Chien CB. astray, a zebrafish roundabout homolog required for retinal axon guidance. Science. 2001 Apr 20;292(5516):507-10. PubMed PMID: 11313496.

Fuccillo M, Joyner AL, Fishell G. Morphogen to mitogen: the multiple roles of hedgehog signalling in vertebrate neural development. Nat Rev Neurosci. 2006 Oct;7(10):772-83. Review. Erratum in: Nat Rev Neurosci. 2006 Nov;7(11):902. PubMed PMID: 16988653.

Fukuda T, Kawano H, Ohyama K, Li HP, Takeda Y, Oohira A, Kawamura K.Immunohistochemical localization of neurocan and L1 in the formation of thalamocortical pathway of developing rats. J Comp Neurol. 1997 Jun 2;382(2):141-52. PubMed PMID: 9183685.

Gallo G, Letourneau PC. Localized sources of neurotrophins initiate axon collateral sprouting. J Neurosci. 1998 Jul 15;18(14):5403-14. PubMed PMID: 9651222.

Gallo G, Letourneau PC. Regulation of growth cone actin filaments by guidance cues. J Neurobiol. 2004 Jan;58(1):92-102. Review. PubMed PMID: 14598373.

García-Verdugo JM, Ferrón S, Flames N, Collado L, Desfilis E, Font E. The proliferative ventricular zone in adult vertebrates: a comparative study using reptiles, birds, and mammals.Brain Res Bull. 2002 Apr;57(6):765-75. Review. PubMed PMID: 12031273.

Géraudie J, Nordlander R, Singer M, Singer J. Early stages of spinal ganglion formation during tail regeneration in the newt, Notophthalmus viridescens. Am J Anat. 1988 Dec;183(4):359-70. PubMed PMID: 3218623.

Goodhill GJ, Richards LJ. Retinotectal maps: molecules, models and misplaced data. Trends Neurosci. 1999 Dec;22(12):529-34. Review. PubMed PMID: 10542427.

Goshima Y, Kawakami T, Hori H, Sugiyama Y, Takasawa S, Hashimoto Y, Kagoshima-Maezono M, Takenaka T, Misu Y, Strittmatter SM. A novel action of collapsin: collapsin-1 increases antero- and retrograde axoplasmic transport independently of growth cone collapse. J Neurobiol. 1997 Sep;33(3):316-28. PubMed PMID: 9298768.

Goshima Y, Nakamura F, Strittmatter P, Strittmatter SM. Collapsin-induced growth cone collapse mediated by an intracellular protein related to UNC-33. Nature. 1995 Aug 10;376(6540):509-14. PubMed PMID: 7637782.

Gulati-Leekha A, Goldman D. A reporter-assisted mutagenesis screen using alpha 1-tubulin-GFP transgenic zebrafish uncovers missteps during neuronal development and axonogenesis.Dev Biol. 2006 Aug 1;296(1):29-47. Epub 2006 Jun 19. PubMed PMID: 16784739.

Gundersen RW, Barrett JN. Neuronal chemotaxis: chick dorsal-root axons turn toward high concentrations of nerve growth factor. Science. 1979 Nov 30;206(4422):1079-80. PubMed PMID: 493992.

Harman AM, Rodger J, Ahmat A, Thomas C, Bartlett C, Chen P, Dunlop SA, Beazley LD. PSA-NCAM is up-regulated during optic nerve regeneration in lizard but not in goldfish. Exp Neurol. 2003 Jul;182(1):180-5. PubMed PMID: 12821388.

Hedgecock EM, Culotti JG, Thomson JN, Perkins LA. Axonal guidance mutants of Caenorhabditis elegans identified by filling sensory neurons with fluorescein dyes. Dev Biol. 1985 Sep;111(1):158-70. PubMed PMID: 3928418.

Henion PD, Raible DW, Beattie CE, Stoesser KL, Weston JA, Eisen JS. Screen for mutations affecting development of Zebrafish neural crest. Dev Genet. 1996;18(1):11-7. PubMed PMID: 8742830.

Hitchcock PF, Raymond PA. Retinal regeneration. Trends Neurosci. 1992 Mar;15(3):103-8. Review. PubMed PMID: 1373917.

Hockfield S, Kalb RG, Zaremba S, Fryer H. Expression of neural proteoglycans correlates with the acquisition of mature neuronal properties in the mammalian brain. Cold Spring Harb Symp Quant Biol. 1990;55:505-14. PubMed PMID: 2132834.

Holmes GP, Negus K, Burridge L, Raman S, Algar E, Yamada T, Little MH. Distinct but overlapping expression patterns of two vertebrate slit homologs implies functional roles in CNS development and organogenesis. Mech Dev. 1998 Dec;79(1-2):57-72. PubMed PMID: 10349621.

Holst CR, Bou-Reslan H, Gore BB, Wong K, Grant D, Chalasani S, Carano RA, Frantz GD, Tessier-Lavigne M, Bolon B, French DM, Ashkenazi A. Secreted sulfatases Sulf1 and Sulf2 have overlapping yet essential roles in mouse neonatal survival. PLoS One. 2007 Jun 27;2(6):e575. PubMed PMID: 17593974; PubMed Central PMCID: PMC1892809.

Horner PJ, Gage FH. Regenerating the damaged central nervous system. Nature. 2000 Oct 26;407(6807):963-70. PubMed PMID: 11069169.

Howitt JA, Clout NJ, Hohenester E. Binding site for Robo receptors revealed by dissection of the leucine-rich repeat region of Slit. EMBO J. 2004 Nov 10;23(22):4406-12. Epub 2004 Oct 21. PubMed PMID: 15496984; PubMed Central PMCID: PMC526463.

Huber AB, Kolodkin AL, Ginty DD, Cloutier JF. Signaling at the growth cone: ligand-receptor complexes and the control of axon growth and guidance. Annu Rev Neurosci. 2003;26:509-63. Epub 2003 Mar 28. Review. PubMed PMID: 12677003.

Huminiecki L, Gorn M, Suchting S, Poulsom R, Bicknell R. Magic roundabout is a new member of the roundabout receptor family that is endothelial specific and expressed at sites of active angiogenesis. Genomics. 2002 Apr;79(4):547-52. PubMed PMID: 11944987.

Hutson LD, Chien CB. Pathfinding and error correction by retinal axons: the role of astray/robo2.Neuron. 2002 Jan 17;33(2):205-17. PubMed PMID: 11804569.

Hutson LD, Jurynec MJ, Yeo SY, Okamoto H, Chien CB. Two divergent slit1 genes in zebrafish. Dev Dyn. 2003 Nov;228(3):358-69. PubMed PMID: 14579375.

Inatani M. Molecular mechanisms of optic axon guidance. Naturwissenschaften. 2005 Dec;92(12):549-61. Epub 2005 Oct 12. Review. PubMed PMID: 16220285.

Inatani M, Yamaguchi Y. Gene expression of EXT1 and EXT2 during mouse brain development.Brain Res Dev Brain Res. 2003 Mar 14;141(1-2):129-36. PubMed PMID: 12644256.

Iten LE, Bryant SV. Stages of tail regeneration in the adult newt, Notophthalmus viridescens. J Exp Zool. 1976 Jun;196(3):283-92. PubMed PMID: 932660.

Itoh A, Miyabayashi T, Ohno M, Sakano S. Cloning and expressions of three mammalian homologues of Drosophila slit suggest possible roles for Slit in the formation and maintenance of the nervous system. Brain Res Mol Brain Res. 1998 Nov 20;62(2):175-86. PubMed PMID: 9813312.

Jessell TM. Neuronal specification in the spinal cord: inductive signals and transcriptional codes.Nat Rev Genet. 2000 Oct;1(1):20-9. PubMed PMID: 11262869.

Jung H, Holt CE. Local translation of mRNAs in neural development. WIREs RNA 2011 2; 153–165

Kamata T, Daar IO, Subleski M, Copeland T, Kung HF, Xu RH. Xenopus CRMP-2 is an early response gene to neural induction. Brain Res Mol Brain Res. 1998 Jun 15;57(2):201-10. PubMed PMID: 9675418.

Kamiguchi H, Lemmon V. Recycling of the cell adhesion molecule L1 in axonal growth cones. J Neurosci. 2000 May 15;20(10):3676-86. PubMed PMID: 10804209; PubMed Central PMCID: PMC1237010.

Karlstrom RO, Trowe T, Klostermann S, Baier H, Brand M, Crawford AD, Grunewald B, Haffter P, Hoffmann H, Meyer SU, Müller BK, Richter S, van Eeden FJ, Nüsslein-Volhard C, Bonhoeffer F. Zebrafish mutations affecting retinotectal axon pathfinding. Development. 1996 Dec;123:427-38. PubMed PMID: 9007260.

Kennedy TE. Cellular mechanisms of netrin function: long-range and short-range actions. Biochem Cell Biol. 2000;78(5):569-75. Review. PubMed PMID: 11103947.

Kidd T, Bland KS, Goodman CS. Slit is the midline repellent for the robo receptor in Drosophila. Cell. 1999 Mar 19;96(6):785-94. PubMed PMID: 10102267.

Kidd T, Brose K, Mitchell KJ, Fetter RD, Tessier-Lavigne M, Goodman CS, Tear G. Roundabout controls axon crossing of the CNS midline and defines a novel subfamily of evolutionarily conserved guidance receptors. Cell. 1998a Jan 23;92(2):205-15. PubMed PMID: 9458045.

Kidd T, Russell C, Goodman CS, Tear G. Dosage-sensitive and complementary functions of roundabout and commissureless control axon crossing of the CNS midline. Neuron. 1998b Jan;20(1):25-33. PubMed PMID: 9459439.

Kruger RP, Aurandt J, Guan KL. Semaphorins command cells to move. Nat Rev Mol Cell Biol. 2005 Oct;6(10):789-800. Review. PubMed PMID: 16314868.

Lamba D, Karl M, Reh T. Neural regeneration and cell replacement: a view from the eye. Cell Stem Cell. 2008 Jun 5;2(6):538-49. Review. PubMed PMID: 18522847; PubMed Central PMCID: PMC2692223.

Lang DM, Monzón-Mayor M, Bandtlow CE, Stuermer CA. Retinal axon regeneration in the lizard Gallotia galloti in the presence of CNS myelin and oligodendrocytes. Glia. 1998 May;23(1):61-74. PubMed PMID: 9562185.

Langenau DM, Feng H, Berghmans S, Kanki JP, Kutok JL, Look AT. Cre/lox-regulated transgenic zebrafish model with conditional myc-induced T cell acute lymphoblastic leukemia. Proc Natl Acad Sci U S A. 2005 Apr 26;102(17):6068-73. Epub 2005 Apr 12. PubMed PMID: 15827121; PubMed Central PMCID: PMC1087915.

LeClair EE, Topczewski J. Development and regeneration of the zebrafish maxillary barbel: a novel study system for vertebrate tissue growth and repair. PLoS One. 2010 Jan 15;5(1):e8737. PubMed PMID: 20090899; PubMed Central PMCID: PMC2806924

Lee JS, Chien CB. When sugars guide axons: insights from heparan sulphate proteoglycan mutants. Nat Rev Genet. 2004 Dec;5(12):923-35. Review. PubMed PMID: 15573124.

Lee JS, Ray R, Chien CB. Cloning and expression of three zebrafish roundabout homologs suggest roles in axon guidance and cell migration. Dev Dyn. 2001 Jun;221(2):216-30. PubMed PMID: 11376489.

Letourneau PC. Differences in the organization of actin in the growth cones compared with the neurites of cultured neurons from chick embryos. J Cell Biol. 1983 Oct;97(4):963-73. PubMed PMID: 6352712; PubMed Central PMCID: PMC2112607.

Li HS, Chen JH, Wu W, Fagaly T, Zhou L, Yuan W, Dupuis S, Jiang ZH, Nash W, Gick C, Ornitz DM, Wu JY, Rao Y. Vertebrate slit, a secreted ligand for the transmembrane protein roundabout, is a repellent for olfactory bulb axons. Cell. 1999 Mar 19;96(6):807-18. PubMed PMID: 10102269.

Li W, Herman RK, Shaw JE. Analysis of the Caenorhabditis elegans axonal guidance and outgrowth gene unc-33. Genetics. 1992 Nov;132(3):675-89. PubMed PMID: 1468626; PubMed Central PMCID: PMC1205206.

Lin G, Chen Y, Slack JM. Regeneration of neural crest derivatives in the Xenopus tadpole tail.BMC Dev Biol. 2007 May 24;7:56. PubMed PMID: 17521450; PubMed Central PMCID: PMC1890292.

Liu BP, Strittmatter SM. Semaphorin-mediated axonal guidance via Rho-related G proteins. Curr Opin Cell Biol. 2001 Oct;13(5):619-26. Review. PubMed PMID: 11544032.

Liu Y, Berndt J, Su F, Tawarayama H, Shoji W, Kuwada JY, Halloran MC. Semaphorin3D guides retinal axons along the dorsoventral axis of the tectum. J Neurosci. 2004 Jan 14;24(2):310-8. PubMed PMID: 14724229.

Long H, Sabatier C, Ma L, Plump A, Yuan W, Ornitz DM, Tamada A, Murakami F, Goodman CS, Tessier-Lavigne M. Conserved roles for Slit and Robo proteins in midline commissural axon guidance. Neuron. 2004 Apr 22;42(2):213-23. PubMed PMID: 15091338.

Lurie DI, Selzer ME. Preferential regeneration of spinal axons through the scar in hemisected lamprey spinal cord. J Comp Neurol. 1991 Nov 22;313(4):669-79. PubMed PMID: 1783686.

Ma EY, Rubel EW, Raible DW. Notch signaling regulates the extent of hair cell regeneration in the zebrafish lateral line. J Neurosci. 2008 Feb 27;28(9):2261-73. PubMed PMID: 18305259.

Mack TG, Koester MP, Pollerberg GE. The microtubule-associated protein MAP1B is involved in local stabilization of turning growth cones. Mol Cell Neurosci. 2000 Jan;15(1):51-65. PubMed PMID: 10662505.

Malicki JJ, Pujic Z, Thisse C, Thisse B, Wei X. Forward and reverse genetic approaches to the analysis of eye development in zebrafish. Vision Res. 2002 Feb;42(4):527-33. Review. PubMed PMID: 11853769.

Marcus RC, Shimamura K, Sretavan D, Lai E, Rubenstein JL, Mason CA. Domains of regulatory gene expression and the developing optic chiasm: correspondence with retinal axon paths and candidate signaling cells. J Comp Neurol. 1999 Jan 18;403(3):346-58. PubMed PMID: 9886035.

Mason C, Erskine L. Growth cone form, behavior, and interactions in vivo: retinal axon pathfinding as a model. J Neurobiol. 2000 Aug;44(2):260-70. Review. Erratum in: J Neurobiol 2000 Nov 5;45(2):134. PubMed PMID: 10934327.

Matsukawa T, Sugitani K, Mawatari K, Koriyama Y, Liu Z, Tanaka M, Kato S. Role of purpurin as a retinol-binding protein in goldfish retina during the early stage of optic nerve regeneration: its priming action on neurite outgrowth. J Neurosci. 2004 Sep 22;24(38):8346-53. PubMed PMID: 15385617.

McDowell AL, Dixon LJ, Houchins JD, Bilotta J. Visual processing of the zebrafish optic tectum before and after optic nerve damage. Vis Neurosci. 2004 Mar-Apr;21(2):97-106. PubMed PMID: 15259561.

McHedlishvili L, Epperlein HH, Telzerow A, Tanaka EM. A clonal analysis of neural progenitors during axolotl spinal cord regeneration reveals evidence for both spatially restricted and multipotent progenitors. Development. 2007 Jun;134(11):2083-93. PubMed PMID: 17507409.

Ming GL, Song HJ, Berninger B, Holt CE, Tessier-Lavigne M, Poo MM. cAMP-dependent growth cone guidance by netrin-1. Neuron. 1997 Dec;19(6):1225-35. PubMed PMID: 9427246.

Mitashov VI. Mechanisms of retina regeneration in urodeles. Int J Dev Biol. 1996 Aug;40(4):833-44. Review. PubMed PMID: 8877458.

Mizell M. Limb regeneration: induction in the newborn opossum. Science. 1968 Jul 19;161(838):283-6. PubMed PMID: 5657335.

Nakayama M, Nakajima D, Nagase T, Nomura N, Seki N, Ohara O. Identification of high-molecular-weight proteins with multiple EGF-like motifs by motif-trap screening. Genomics. 1998 Jul 1;51(1):27-34. PubMed PMID: 9693030.

Nasevicius A, Ekker SC. Effective targeted gene 'knockdown' in zebrafish. Nat Genet. 2000 Oct;26(2):216-20. PubMed PMID: 11017081.

Nguyen Ba-Charvet KT, Brose K, Marillat V, Kidd T, Goodman CS, Tessier-Lavigne M, Sotelo C, Chédotal A. Slit2-Mediated chemorepulsion and collapse of developing forebrain axons. Neuron. 1999 Mar;22(3):463-73. PubMed PMID: 10197527.

Nguyen QT, Sanes JR, Lichtman JW. Pre-existing pathways promote precise projection patterns. Nat Neurosci. 2002 Sep;5(9):861-7. PubMed PMID: 12172551.

Nicholls J, Saunders N. Regeneration of immature mammalian spinal cord after injury. Trends Neurosci. 1996 Jun;19(6):229-34. Review. PubMed PMID: 8761958.

Niclou SP, Ehlert EM, Verhaagen J. Chemorepellent axon guidance molecules in spinal cord injury. J Neurotrauma. 2006 Mar-Apr;23(3-4):409-21. Review. PubMed PMID: 16629626.

Niclou SP, Jia L, Raper JA. Slit2 is a repellent for retinal ganglion cell axons. J Neurosci. 2000 Jul 1;20(13):4962-74. PubMed PMID: 10864954.

Northcutt RG. Changing views of brain evolution. Brain Res Bull. 2001 Aug;55(6):663-74. Review. PubMed PMID: 11595351.

O'Brien GS, Martin SM, Söllner C, Wright GJ, Becker CG, Portera-Cailliau C, Sagasti A.Developmentally regulated impediments to skin reinnervation by injured peripheral sensory axon terminals. Curr Biol. 2009 Dec 29;19(24):2086-90. Epub 2009 Dec 3. PubMed PMID: 19962310; PubMed Central PMCID: PMC2805760.

Okabe S, Hirokawa N. Actin dynamics in growth cones. J Neurosci. 1991 Jul;11(7):1918-29. PubMed PMID: 1712377.

Oudega M, Xu XM. Schwann cell transplantation for repair of the adult spinal cord. J Neurotrauma. 2006 Mar-Apr;23(3-4):453-67. Review. PubMed PMID: 16629629.

Park CM, Hollenberg MJ. Induction of retinal regeneration in vivo by growth factors. Dev Biol. 1991 Nov;148(1):322-33. PubMed PMID: 1936569.

Park HC, Shin J, Appel B. Spatial and temporal regulation of ventral spinal cord precursor specification by Hedgehog signaling. Development. 2004 Dec;131(23):5959-69. PubMed PMID: 15539490.

Park KW, Morrison CM, Sorensen LK, Jones CA, Rao Y, Chien CB, Wu JY, Urness LD, Li DY. Robo4 is a vascular-specific receptor that inhibits endothelial migration. Dev Biol. 2003 Sep 1;261(1):251-67. PubMed PMID: 12941633.

Pesheva P, Gennarini G, Goridis C, Schachner M. The F3/11 cell adhesion molecule mediates the repulsion of neurons by the extracellular matrix glycoprotein J1-160/180. Neuron. 1993 Jan;10(1):69-82. PubMed PMID: 7678967.

Petrausch B, Jung M, Leppert CA, Stuermer CA. Lesion-induced regulation of netrin receptors and modification of netrin-1 expression in the retina of fish and grafted rats. Mol Cell Neurosci. 2000b Oct;16(4):350-64. PubMed PMID: 11085873.

Petrausch B, Tabibiazar R, Roser T, Jing Y, Goldman D, Stuermer CA, Irwin N, Benowitz LI. A purine-sensitive pathway regulates multiple genes involved in axon regeneration in goldfish retinal ganglion cells. J Neurosci. 2000a Nov 1;20(21):8031-41. PubMed PMID: 11050124.

Pittman AJ, Law MY, Chien CB. Pathfinding in a large vertebrate axon tract: isotypic interactions guide retinotectal axons at multiple choice points. Development. 2008 Sep;135(17):2865-71. Epub 2008 Jul 24. PubMed PMID: 18653554; PubMed Central PMCID: PMC2562560.

Plachez C, Andrews W, Liapi A, Knoell B, Drescher U, Mankoo B, Zhe L, Mambetisaeva E, Annan A, Bannister L, Parnavelas JG, Richards LJ, Sundaresan V. Robos are required for the correct targeting of retinal ganglion cell axons in the visual pathway of the brain. Mol Cell Neurosci. 2008 Apr;37(4):719-30. Epub 2007 Dec 23. PubMed PMID: 18272390.

Plump AS, Erskine L, Sabatier C, Brose K, Epstein CJ, Goodman CS, Mason CA, Tessier-Lavigne M. Slit1 and Slit2 cooperate to prevent premature midline crossing of retinal axons in the mouse visual system. Neuron. 2002 Jan 17;33(2):219-32. PubMed PMID: 11804570.

Poss KD, Wilson LG, Keating MT. Heart regeneration in zebrafish. Science. 2002 Dec 13;298(5601):2188-90. PubMed PMID: 12481136.

Pratt T, Conway CD, Tian NM, Price DJ, Mason JO. Heparan sulphation patterns generated by specific heparan sulfotransferase enzymes direct distinct aspects of retinal axon guidance at the optic chiasm. J Neurosci. 2006 Jun 28;26(26):6911-23. PubMed PMID: 16807321.

Quinn CC, Gray GE, Hockfield S. A family of proteins implicated in axon guidance and outgrowth. J Neurobiol. 1999 Oct;41(1):158-64. Review. PubMed PMID: 10504203.

Reber M, Burrola P, Lemke G. A relative signalling model for the formation of a topographic neural map. Nature. 2004 Oct 14;431(7010):847-53. PubMed PMID: 15483613.

Rehermann MI, Marichal N, Russo RE, Trujillo-Cenóz O. Neural reconnection in the transected spinal cord of the freshwater turtle Trachemys dorbignyi. J Comp Neurol. 2009 Jul 10;515(2):197-214. PubMed PMID: 19418545; PubMed Central PMCID: PMC2697850.

Reimer MM, Kuscha V, Wyatt C, Sörensen I, Frank RE, Knüwer M, Becker T, Becker CG.Sonic hedgehog is a polarized signal for motor neuron regeneration in adult zebrafish. J Neurosci. 2009 Dec 2;29(48):15073-82. PubMed PMID: 19955358; PubMed Central PMCID: PMC2841428.

Ringstedt T, Braisted JE, Brose K, Kidd T, Goodman C, Tessier-Lavigne M, O'Leary DD. Slit inhibition of retinal axon growth and its role in retinal axon pathfinding and innervation patterns in the diencephalon. J Neurosci. 2000 Jul 1;20(13):4983-91. PubMed PMID: 10864956.

Rodger J, King CE, Lukehurst S, Chen PB, Dunlop SA, Beazley LD, Ziman MR. Changing Pax6 expression correlates with axon outgrowth and restoration of topography during optic nerve

regeneration. Neuroscience. 2006 Nov 3;142(4):1043-54. Epub 2006 Sep 14. PubMed PMID: 16973301.

Rodger J, Vitale PN, Tee LB, King CE, Bartlett CA, Fall A, Brennan C, O'Shea JE, Dunlop SA, Beazley LD. EphA/ephrin-A interactions during optic nerve regeneration: restoration of topography and regulation of ephrin-A2 expression. Mol Cell Neurosci. 2004 Jan;25(1):56-68. PubMed PMID: 14962740.

Roth LW, Bormann P, Wiederkehr C, Reinhard E. Beta-thymosin, a modulator of the actin cytoskeleton is increased in regenerating retinal ganglion cells. Eur J Neurosci. 1999 Oct;11(10):3488-98. PubMed PMID: 10564357.

Russo RE, Fernández A, Reali C, Radmilovich M, Trujillo-Cenóz O. Functional and molecular clues reveal precursor-like cells and immature neurones in the turtle spinal cord. J Physiol. 2004 Nov 1;560(Pt 3):831-8. Epub 2004 Aug 26. PubMed PMID: 15331672; PubMed Central PMCID: PMC1665269.

Scheer N, Riedl I, Warren JT, Kuwada JY, Campos-Ortega JA. A quantitative analysis of the kinetics of Gal4 activator and effector gene expression in the zebrafish. Mech Dev. 2002 Mar;112(1-2):9-14. PubMed PMID: 11850174.

Schmucker D, Flanagan JG. Generation of recognition diversity in the nervous system. Neuron. 2004 Oct 14;44(2):219-22. Review. PubMed PMID: 15473961.

Schnapp E, Kragl M, Rubin L, Tanaka EM. Hedgehog signaling controls dorsoventral patterning, blastema cell proliferation and cartilage induction during axolotl tail regeneration. Development. 2005 Jul;132(14):3243-53. PubMed PMID: 15983402.

Schwab ME. Nogo and axon regeneration. Curr Opin Neurobiol. 2004 Feb;14(1):118-24. Review. PubMed PMID: 15018947.

Schweitzer J, Becker CG, Schachner M, Becker T. Expression of collapsin response mediator proteins in the nervous system of embryonic zebrafish. Gene Expr Patterns. 2005 Aug;5(6):809-16. PubMed PMID: 15922676.

Schweitzer J, Becker T, Becker CG, Schachner M. Expression of protein zero is increased in lesioned axon pathways in the central nervous system of adult zebrafish. Glia. 2003 Feb;41(3):301-17. PubMed PMID: 12528184.

Schweitzer J, Gimnopoulos D, Lieberoth BC, Pogoda HM, Feldner J, Ebert A, Schachner M, Becker T, Becker CG. Contactin1a expression is associated with oligodendrocyte differentiation and axonal regeneration in the central nervous system of zebrafish. Mol Cell Neurosci. 2007 Jun;35(2):194-207. Epub 2007 Mar 3. PubMed PMID: 17425960.

Seeger M, Tear G, Ferres-Marco D, Goodman CS. Mutations affecting growth cone guidance in Drosophila: genes necessary for guidance toward or away from the midline. Neuron. 1993 Mar;10(3):409-26. PubMed PMID: 8461134.

Shekarabi M, Moore SW, Tritsch NX, Morris SJ, Bouchard JF, Kennedy TE. Deleted in colorectal cancer binding netrin-1 mediates cell substrate adhesion and recruits Cdc42, Rac1, Pak1, and N-WASP into an intracellular signaling complex that promotes growth cone expansion. J Neurosci. 2005 Mar 23;25(12):3132-41. PubMed PMID: 15788770.

Shkumatava A, Fischer S, Müller F, Strahle U, Neumann CJ. Sonic hedgehog, secreted by amacrine cells, acts as a short-range signal to direct differentiation and lamination in the zebrafish retina. Development. 2004 Aug;131(16):3849-58. Epub 2004 Jul 14. PubMed PMID: 15253932.

Siddiqui SS, Culotti JG. Examination of neurons in wild type and mutants of Caenorhabditis elegans using antibodies to horseradish peroxidase. J Neurogenet. 1991;7(4):193-211. PubMed PMID: 1886035.

Silver J, Miller JH. Regeneration beyond the glial scar. Nat Rev Neurosci. 2004 Feb;5(2):146-56. Review. PubMed PMID: 14735117.

Sims TJ, Gilmore SA, Waxman SG. Radial glia give rise to perinodal processes. Brain Res. 1991 May 17;549(1):25-35. PubMed PMID: 1893250.

Song H, Ming G, He Z, Lehmann M, McKerracher L, Tessier-Lavigne M, Poo M. Conversion of neuronal growth cone responses from repulsion to attraction by cyclic nucleotides. Science. 1998 Sep 4;281(5382):1515-8. PubMed PMID: 9727979.

Song HJ, Ming GL, Poo MM. cAMP-induced switching in turning direction of nerve growth cones. Nature. 1997 Jul 17;388(6639):275-9. Erratum in: Nature 1997 Sep 25;389(6649):412. PubMed PMID: 9230436.

Spence R, Jordan WC, Smith C. Genetic analysis of male reproductive success in relation to density in the zebrafish, Danio rerio. Front Zool. 2006 Apr 5;3:5. PubMed PMID: 16597325; PubMed Central PMCID: PMC1501009.

Spencer T, Domeniconi M, Cao Z, Filbin MT. New roles for old proteins in adult CNS axonal regeneration. Curr Opin Neurobiol. 2003 Feb;13(1):133-9. Review. PubMed PMID: 12593992.

Sperry RW. Restoration of vision after crossing of optic nerves and after contralateral transplantation of eye. J Neurophysiol 1945 8: 15–28

Springer AD. Normal and abnormal retinal projections following the crush of one optic nerve in goldfish (Carassius auratus). J Comp Neurol. 1981 Jun 10;199(1):87-95. PubMed PMID: 7263949.

Stuermer CA. Retinotopic organization of the developing retinotectal projection in the zebrafish embryo. J Neurosci. 1988 Dec;8(12):4513-30. PubMed PMID: 2848935.

Stuermer CA, Bastmeyer M, Bähr M, Strobel G, Paschke K. Trying to understand axonal regeneration in the CNS of fish. J Neurobiol. 1992 Jul;23(5):537-50. Review. PubMed PMID: 1431836.

Sun Q, Bahri S, Schmid A, Chia W, Zinn K. Receptor tyrosine phosphatases regulate axon guidance across the midline of the Drosophila embryo. Development. 2000 Feb;127(4):801-12. PubMed PMID: 10648238.

Tanaka EM, Ferretti P. Considering the evolution of regeneration in the central nervous system.Nat Rev Neurosci. 2009 Oct;10(10):713-23. Review. PubMed PMID: 19763104.

Tessier-Lavigne M, Goodman CS. The molecular biology of axon guidance. Science. 1996 Nov 15;274(5290):1123-33. Review. PubMed PMID: 8895455.

Thompson H, Andrews W, Parnavelas JG, Erskine L. Robo2 is required for Slit-mediated intraretinal axon guidance. Dev Biol. 2009 Nov 15;335(2):418-26. Epub 2009 Sep 25. PubMed PMID: 19782674; PubMed Central PMCID: PMC2814049.

Tsonis PA, Del Rio-Tsonis K. Lens and retina regeneration: transdifferentiation, stem cells and clinical applications. Exp Eye Res. 2004 Feb;78(2):161-72. Review. PubMed PMID: 14729349.

Udin SB, Fawcett JW. Formation of topographic maps. Annu Rev Neurosci. 1988;11:289-327. Review. PubMed PMID: 3284443.

Wanner M, Lang DM, Bandtlow CE, Schwab ME, Bastmeyer M, Stuermer CA. Reevaluation of the growth-permissive substrate properties of goldfish optic nerve myelin and myelin proteins. J Neurosci. 1995 Nov;15(11):7500-8. PubMed PMID: 7472501.

Wu W, Wong K, Chen J, Jiang Z, Dupuis S, Wu JY, Rao Y. Directional guidance of neuronal migration in the olfactory system by the protein Slit. Nature. 1999 Jul 22;400(6742):331-6. PubMed PMID: 10432110; PubMed Central PMCID: PMC2041931.

Xiao T, Roeser T, Staub W, Baier H. A GFP-based genetic screen reveals mutations that disrupt the architecture of the zebrafish retinotectal projection. Development. 2005 Jul;132(13):2955-67. Epub 2005 Jun 1. PubMed PMID: 15930106.

Yamada H, Miyake T, Kitamura T. Regeneration of axons in transection of the carp spinal cord.Zoolog Sci. 1995 Jun;12(3):325-32. PubMed PMID: 7580813.

Yuan SS, Cox LA, Dasika GK, Lee EY. Cloning and functional studies of a novel gene aberrantly expressed in RB-deficient embryos. Dev Biol. 1999a Mar 1;207(1):62-75. PubMed PMID: 10049565.

Yuan W, Zhou L, Chen JH, Wu JY, Rao Y, Ornitz DM. The mouse SLIT family: secreted ligands for ROBO expressed in patterns that suggest a role in morphogenesis and axon guidance. Dev Biol. 1999b Aug 15;212(2):290-306. PubMed PMID: 10433822.

Zamora AJ. The ependymal and glial configuration in the spinal cord of urodeles. Anat Embryol (Berl). 1978 Jul 17;154(1):67-82. PubMed PMID: 677484.

Zhou LX, Wang ZR. [Changes in number and distribution of retinal ganglion cells after optic nerve crush in zebrafish]. Shi Yan Sheng Wu Xue Bao. 2002 Jun;35(2):159-62. Chinese. PubMed PMID: 15344337.

Zhu Y, Li H, Zhou L, Wu JY, Rao Y. Cellular and molecular guidance of GABAergic neuronal migration from an extracortical origin to the neocortex. Neuron. 1999 Jul;23(3):473-85. PubMed PMID: 10433260.

Zupanc GK. Adult neurogenesis and neuronal regeneration in the brain of teleost fish. J Physiol Paris. 2008 Jul-Nov;102(4-6):357-73. Epub 2008 Oct 17. Review. PubMed PMID: 18984045.

Zupanc GK, Kompass KS, Horschke I, Ott R, Schwarz H. Apoptosis after injuries in the cerebellum of adult teleost fish. Exp Neurol. 1998 Aug;152(2):221-30. PubMed PMID: 9710521.

2. Analysis of the *astray/robo2* zebrafish mutant reveals that degenerating tracts do not provide strong guidance cues for regenerating optic axons

2.1 Summary

During formation of the optic projection in *astray*/*robo2* mutant zebrafish, optic axons exhibit rostro-caudal pathfinding errors, ectopic midline crossing and increased terminal arbor size. Here we show that these errors persist into adulthood, even when *robo2* function is conditionally reduced only during initial formation of the optic projection. Adult errors include massive ectopic optic tracts in the telencephalon. During optic nerve regeneration in *astray*/*robo2* animals, these tracts are not re-populated and ectopic midline crossing is reduced compared to unlesioned mutants. This is despite a comparable macrophage/microglial response and upregulation of *contactin1a* in oligodendrocytes of entopic and ectopic tracts. However, other errors, such as expanded termination areas and ectopic growth into the tectum, were frequently re-committed by regenerating optic axons. Retinal ganglion cells with regenerating axons re-express *robo2* and expression of *slit* ligands is maintained in some areas of the adult optic pathway. However, *slit* expression is reduced rostral and caudal to the chiasm, compared to development and ubiquitous overexpression of Slit2 did not elicit major pathfinding phenotypes. This shows that (1) there is not an efficient correction mechanism for large-scale pathfinding errors of optic axons during development; (2) degenerating tracts do not provide a strong guidance cue for regenerating optic axons in the adult CNS, unlike the PNS; and (3) *robo2* is less important for pathfinding of optic axons during regeneration than during development.

2.2 Introduction

In adult fish and amphibians, severed optic axons are capable of correctly growing through their original pathways and of functional target re-innervation (Becker and Becker, 2007). Given that the distances regenerating axons cover are much greater than during development and that regenerating axons cannot navigate by fasciculation with existing axons, as is the case for developing axons (Pittman et al., 2008), the question arises how precise navigation and target re-innervation is accomplished. Answering this question may have wider consequences in the context of achieving directional axonal regeneration in the CNS of mammals, in which axon regrowth is currently difficult to induce (Chaudhry and Filbin, 2007).

Mechanical or molecular interactions with the denervated brain tracts could guide regenerating axons. For example, in the regenerating peripheral nervous system of mice, denervated Schwann cell tubes provide mechanical guidance for regenerating axons (Nguyen et al., 2002). At the same time, Schwann cells up-regulate a number of axon growth promoting molecules (Oudega and Xu, 2006), which is also true for oligodendrocytes in the fish CNS (Stuermer et al., 1992). Alternatively, regenerating optic axons may actively read specific molecular cues, similar to those that guide developing pioneer axons to their targets (Becker and Becker, 2007). It is difficult to distinguish between these mechanisms in vivo, because degenerating tracts always overlap with the appropriate trajectories of regenerating axons. We decided to address this problem using the zebrafish *astray* mutant (Karlstrom et al., 1996). In this mutant, ectopic optic tracts are formed in a stochastic manner during development. If these tracts acted as non-specific guidance cues for regenerating axons they would divert some of the regenerating optic axons from their correct trajectories.

Astray^{ti272z} is a functional null mutation for *robo2* (Fricke et al., 2001), a receptor for repellent extracellular matrix (ECM) cues of the Slit class (Dickson and Gilestro, 2006). These mutants show pathfinding (rostro-caudal pathfinding errors, ectopic midline crossing) and termination errors (increased terminal arbor sizes) of optic axons during development (Fricke et al., 2001; Campbell et al., 2007), which are similar to those in *slit* or *robo* deficient mice (Plump et al., 2002; Plachez et al., 2008). Time-lapse analysis indicates that optic axons in *astray* mutants, in contrast to wild type axons, do not correct errors during growth across the chiasm (Hutson and Chien, 2002). However, the long-term fate of aberrantly growing axons in *astray* mutants has not been determined. Moreover, similar to other ECM molecules (Becker and Becker, 2002; Becker et al., 2004), Robo/Slit guidance could be important for regenerating optic axons.

Our analysis shows that ectopic tracts are not a preferred guidance cue for regenerating optic axons, despite a comparable cellular and molecular reaction to deafferentation in entopic and ectopic optic tracts. Dramatic pathfinding errors found in optic axons of adult *astray (robo2)* mutants are strongly reduced after regeneration. There are fewer expression domains of *slits* in adults than in embryos and over-expression of Slit2 does not affect axon regrowth. This indicates that Slit/Robo2 interactions are less important during regeneration than during development.

2.3 Materials and methods

2.3.1 Animals

All fish are kept and bred in our laboratory fish facility according to standard methods (Westerfield, 1989) and all experiments have been approved by the British Home Office. We used homozygous *astray*^{ti272z} mutants (Karlstrom et al., 1996; Fricke et al., 2001), which are adult viable, crossed with Tg*(pou4f3:gap43-GFP)*^{s356t} (Xiao et al., 2005) transgenic fish to visualize the optic projection in living larvae. Tg*(pou4f3:gap43-GFP)*^{s356t} line was kindly provided by Dr. Herwig Baier. We also used the Tg*(hsp70l:slit2-EGFP)*^{rw015d} line for Slit2-GFP fusion protein overexpression (Yeo et al., 2004) and Tg*(hsp70l:mcherry)*^{zc62} control; both transgenes use the 1.5 kb hsp70l promoter (Halloran et al., 2000).

2.3.2 Analysis of living larvae

To assess the presence of an ectopic projection to the telencephalon, 5-day-old larvae were anesthetized in 0.01% aminobenzoic acid ethylmethylester (MS222, Sigma, St. Louis, MO) and the presence of axons in the telencephalon was assessed under a stereo-microscope equipped with fluorescence detection (SV8, Zeiss, Oberkochen, Germany). Subsequently, larvae were returned to tank water and raised to adulthood (older than 3 months of age).

2.3.3 Analysis of heat-shocked larvae

Hsp70l:mCherry or *hsp70l:slit2-EGFP* embryos were heat shocked for 1 hour in a 38°C water bath at 32 hpf, allowed to recover at 28.5°C, then fixed at 48 hpf. Embryos were mounted in agarose, and the right eye was injected with DiO or DiI, respectively (Hutson et al., 2004). Embryos were imaged laterally using a 488 or 568 nm laser for excitation and a 20x air or 40x water objective to capture a z-stack of axon labelling and a differential interference contrast image of the embryo.

2.3.4 Adult optic nerve lesion and heat-shocks

Optic nerve crush lesion was performed as described (Becker et al., 2000). Briefly, fish were deeply anesthetized by immersion in 0.033% MS222. The left eye was gently rotated out of its socket and the exposed opaque optic nerve was crushed with a pair of watchmaker's forceps. A

clear stripe across the nerve indicated successful crush. Fish were revived in tank water and allowed to survive for up to 4 weeks post-lesion. For heat shock application, lesioned animals underwent daily heat shocks beginning at 3 days post-lesion until 21 days post-lesion, when optic nerve tracing took place. Tank water was heated from 25°C to 39°C, remained at this elevated temperature for at least one hour and was allowed to cool down again. This procedure has previously been shown to elicit gene expression from the hsp70l promoter in adult fish (own unpublished observations and Lee et al., 2005).

2.3.5 Immunohistochemistry

Antibodies for Tenascin-R (Becker et al., 2004), Tyrosine Hydroxylase (mab318, Millipore, Livingston, UK), GFP (A 11122, Invitrogen) and serotonin (S5545, Sigma) were used for immunofluorescent detection on 50 µm floating sections as described (Reimer et al., 2008) and analyzed by confocal microscopy. Labelling intensity was measured by calculating the mean pixel brightness for a defined area of the dorsal tectum for wild type and *astray* animals using ImageJ (http://rsbweb.nih.gov/ij/).

2.3.6 In situ hybridisation and combination with immunohistochemistry

Probes for *robo2*, *slit1a* (Campbell et al., 2007), *slit1b* (Hutson et al., 2003), *slit2, slit3* (Yeo et al., 2001) and *contactin1a* (Schweitzer et al., 2007) have been described. Non-radioactive in situ hybridisation was carried out on cryosections (14 µm in thickness) from fresh frozen eyes and brains with digoxigenin-labelled probes as described (Becker et al., 2000). Combination of *contactin1a* in situ hybridisation with immunohistochemistry for macrophages/microglial cells with the 4C4 antibody (Becker and Becker, 2001) was carried out sequentially as described (Schweitzer et al., 2007).

2.3.7 Analysis of the adult optic projection

Labelling of the optic projection with biocytin (Sigma) has been described (Becker et al., 2000). Briefly, fish were deeply anesthetized and the entire optic nerve was cut followed by immediate application of a piece of gelatine foam soaked with the tracer. The tracer was allowed to be transported in the axons for 2.5 hours. Fish were transcardially perfused with 2% glutaraldehyde/2% paraformaldehyde and brains were cross-sectioned on a vibrating blade

microtome (Microm, Volketswil, Switzerland) at a thickness of 50 µm. Biocytin was detected with the ABC-kit (Vectastain, Burlingame, CA) and sections were counterstained with Neutral Red (Sigma). Ectopic tracts were scored when bundles of straight parallel axons were detected. Commissures and tracts were scored as containing optic axons, when at least two (posterior commissure) or three (optic chiasm) axonal profiles per section were detectable, to discount low levels of spontaneous misrouting in wild type animals. Variability of measurements is given as SEM.

2.3.8 Morpholino experiments

We used a splice blocking morpholino for *robo2* (5'-TAAAAAGTAGCGCAACTCACCATCC-3') that targets the exon1-intron1 splice donor site, injecting 1 nl/embryo of a 1 mM morpholino solution (Becker et al., 2003). For comparison, a non-active control morpholino was injected (GCTCCGCCACATCACAACACGCGC, Becker et al., 2003). For PCR analysis of aberrant splicing, RNA was extracted from pooled tissue of 15 larvae per time point using the RNeasy Mini Kit (Qiagen, UK). Reverse transcription, using random primers (Promega, Madison, WI, USA), was performed with the SuperScript III kit (Invitrogen, UK). The following primers were used to amplify the appropriately and aberrantly spliced sequence in PCR: *robo2*ex1 forward (AAACGTGTTCTGGGGTTGAG), binding in exon 1, 31 bp upstream of the start codon; and *robo2*ex2 reverse (CAGATCGGAGGGGTGTTCTA), binding in exon 2. To determine whether the morpholino phenocopies the *astray* mutant during early development of the optic projection, DiI was applied to the whole optic nerve of 3- to 4-day-old *robo2* morpholino-injected larvae as described (Becker et al., 2003).

2.4 Results

Using adult *astray* mutants we aimed to answer the following questions: (1) Is there a mechanism to correct developmental pathfinding errors of optic axons in the long term? (2) Are degenerating tracts used as a non-specific guidance cue for regenerating optic axons in the adult brain? (3) Does *robo2* play a role for guidance of regenerating optic axons?
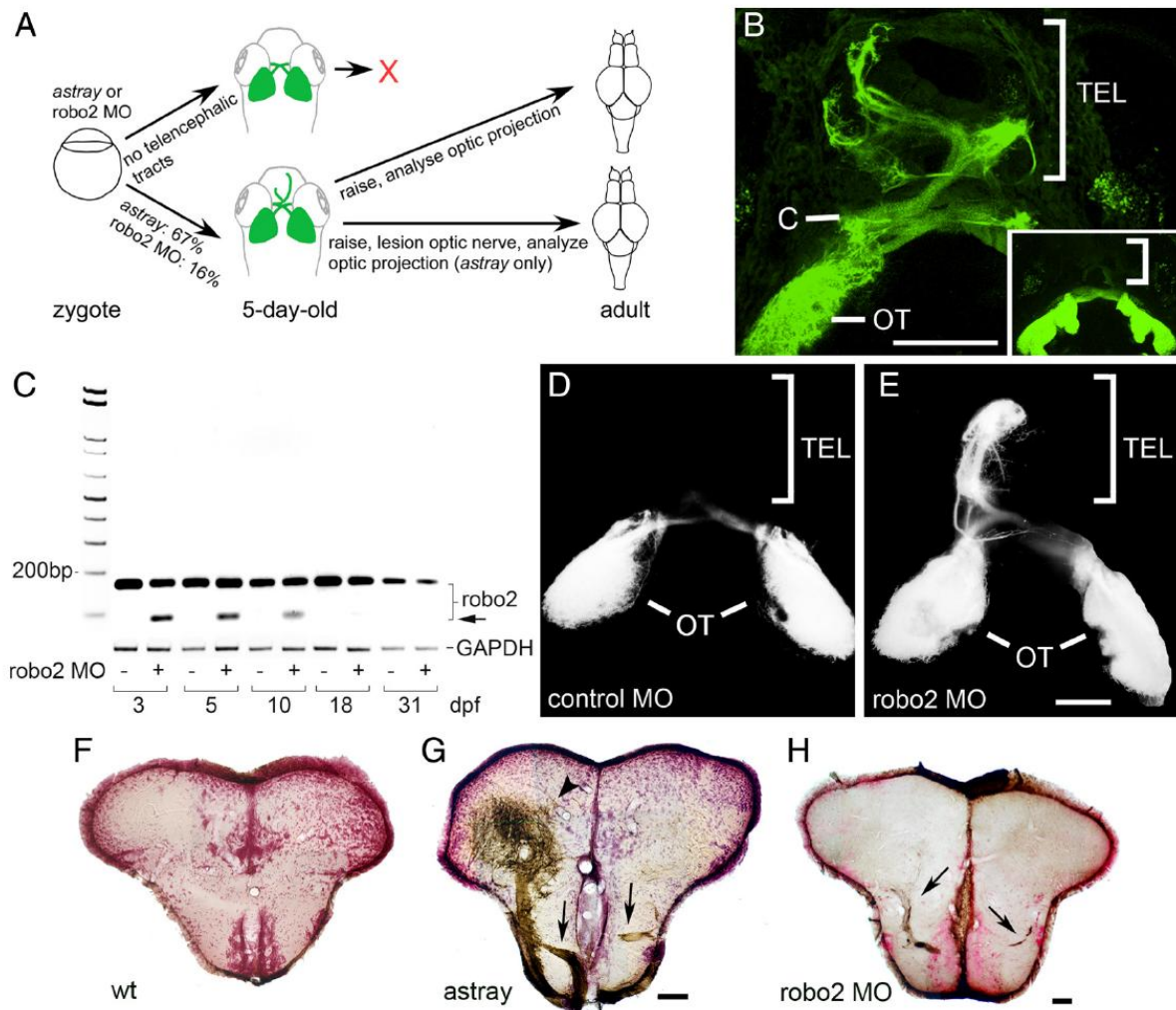
Fig. 2.1 Pathfinding errors in the optic projection are retained in adults in *astray* mutants and in *robo2* morphants. A: Experimental paradigm. Living 5-day-old larvae were pre-selected for the presence of aberrant telencephalic optic tracts and raised for adult experiments as indicated. **B:** Dorsal views are shown (rostral is up). Living *astray* larvae were selected according to the presence of GFP positive optic axons in the telencephalon (TEL). Inset shows a wild type projection without telencephalic tracts. (C = chiasm; OT= optic tectum). Brightly-labelled neuromasts have been removed from the projection for clarity. **C:** PCR analysis of *robo2* mRNA expression with and without *robo2* splice-blocking morpholino (MO). The morpholino reduces the abundance of the wild type transcript and an erroneous transcript (arrow) becomes detectable through at least 10 dpf. GAPDH is used as an

internal standard. **D,E:** Dorsal views of DiI-traced optic projections (rostral is up) indicate *astray*-like pathfinding errors in *robo2* morpholino-injected (E), but not in control morpholino-injected (D) 5-day-old larvae. The ectopic projection to the telencephalon is mainly unilateral. **F-H:** Photomicrographs show optic axons (brown) in cross sections of the adult telencephalon (counterstained in red); dorsal is up. Ectopic tracts of optic axons (arrows in G,H) are present in the telencephalon of *astray* (G) and *robo2* morphant (MO) animals (H), but not in wild type (F). The arrowhead in G indicates a dense termination area of ectopic optic axons in the dorsal telencephalon. Scale bars: B = 100 μm (250 μm for inset); D,E = 100 μm; F,G = 200 μm; H = 100 μm.

Part of this figure was kindly contributed by Dr. Thomas Becker (A and F-H) and Dr. Ken Rasband (B).

2.4.1 Developmental targeting errors persist in adult *astray* mutants

To determine whether there is an efficient mechanism for correcting developmental targeting errors of optic axons, we analyzed whether developmental misprojections are retained in adult *astray* mutants. *Astray* embryos show variability in the penetrance of the axon misrouting phenotype. To enrich our sample for animals with clear developmental misprojections, *astray* mutants were crossed into a *pou4f3:GFP* (previously, *brn3c:GFP*) background, which labels optic axons in living larvae. Thus, we were able to select larvae for raising that had a strong phenotype. This was judged based on the presence of ectopic telencephalic projections, which were detected in 66.9% ± 7.10% (n = 92 larvae) of the larvae (Fig. 2.1A, B). (Larvae were sorted by Dr. Thomas Becker and the image for Fig. 2.1B was taken by Dr. Ken Rasband). The fact that a third of the mutants did not have a telencephalic projection suggests that tract formation in the telencephalon is a stochastic event, and not because of optic axons consistently following secondary cues in the absence of Robo2 signaling.
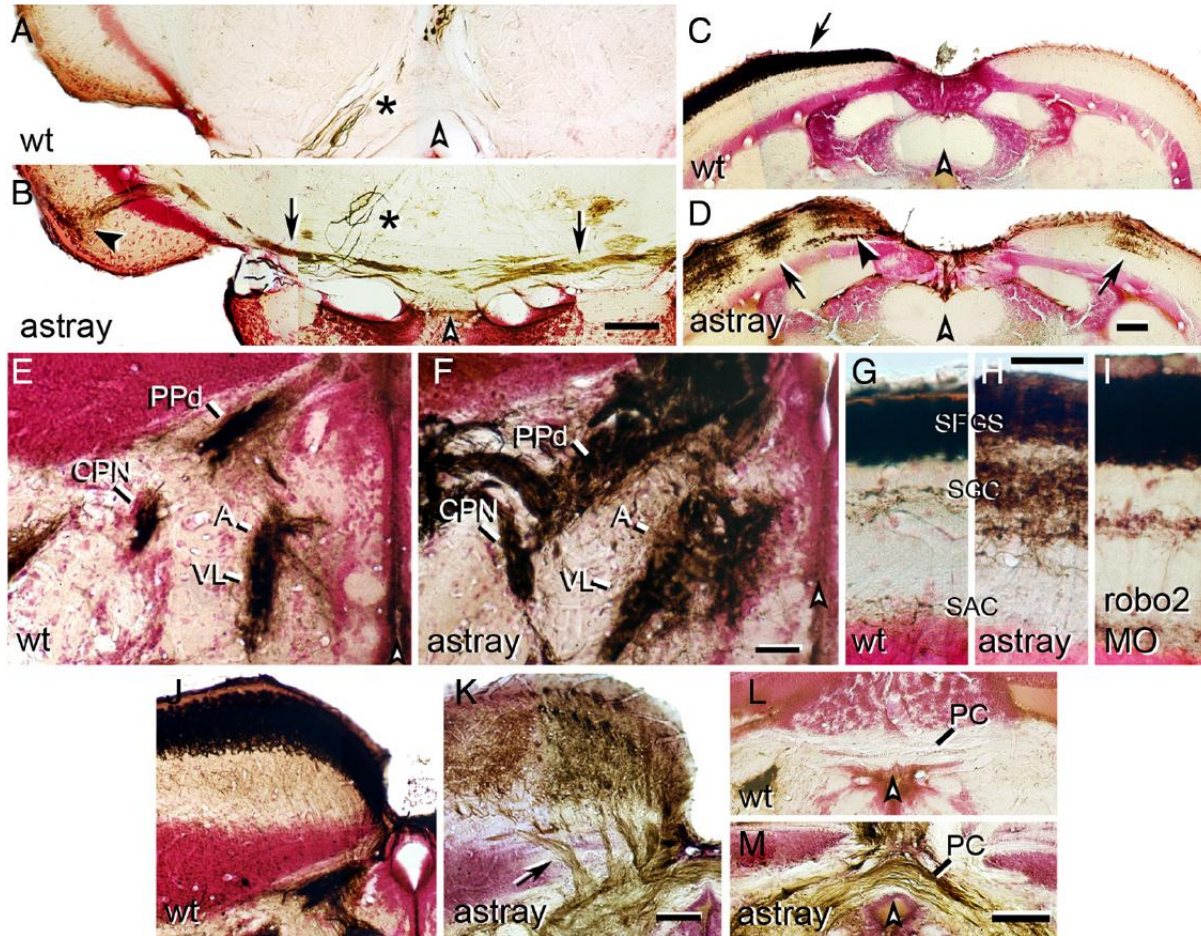
Fig. 2.2 Aberrations of the optic projection in adult *astray* mutants and *robo2* morphants. Photomicrographs show optic axons (brown) in cross sections of the adult brain (counterstained in red); dorsal is up. White arrowheads indicate brain midline. **A,B:** Ectopic optic tracts (arrows in B) in the tegmentum of *astray* mutants cross the midline and terminate in the ipsilateral tectum (black arrowhead). No ectopic tracts are present in wild type animals (A). Asterisks (A,B) indicate large diameter axons of the oculomotor nucleus that are always inadvertently retrogradely traced from the eye muscles. **C,D:** In wild type fish (C), optic axons cover the entire contralateral tectum only (arrow in C). In *astray* mutants (D) the contralateral and ipsilateral tectal halves are innervated in ocular dominance column-like patches (arrows in D). Note deep axons growing into the tectum in *astray* mutants (black arrowhead in D). **E,F:** Innervation of the central pretectal nucleus (CPN), the anterior (A) and ventro-lateral thalamus (VL), as well as the dorsal part of the periventricular pretectal nucleus (PPd) is expanded in *astray* (F) compared to wild type (E). **G-I:** Innervation of tectal layers is expanded in *astray* mutants (H), but not in *robo2* morpholino treated animals (I) compared to wild type (G) (SFGS = stratum fibrosum et griseum superficiale; SGC = stratum griseum centrale; SAC = stratum album centrale). **J,K:** In *astray* mutants (K), but not in wild type animals (J), optic axons enter the tectum in several individual deep fascicles (arrow in K). **L,M:** Optic axons cross in the posterior commissure (PC) in *astray* (M), but not in wild type fish (L). Scale bars: A,B,E-I = 50 µm; C,D,J-M = 100 µm.

This figure was kindly contributed by Anselm Ebert.

50

2.4.2 Errors in rostro-caudal pathfinding

Optic projections of adults were traced unilaterally to reveal midline crossing of optic axons (Adult optic projection tracing in Fig. 2.1 was performed by Dr. Thomas Becker). Wild type animals never showed any axons in the telencephalon (n = 12 animals) (Fig. 2.1F). In 14 of 15 *astray* mutants with a confirmed ectopic larval telencephalic projection, such a projection was also found at the adult stage (Fig. 2.1G). In these fish, ectopic tracts entered the telencephalon ventrally, rostral to the chiasm. Fascicles of optic axons often re-crossed the midline in the ventral telencephalon. Some tracts projected all the way to the olfactory bulb. At the end of fascicles, dense arborisation fields were found, particularly in the dorsal telencephalon. In the one fish without optic axons in the adult telencephalon, telencephalic tracts detected at the larval stage could have either originated exclusively from the unlabelled eye or been reduced during later development.

Caudally misprojecting ectopic tracts of optic axons, often seen in *astray* larvae (Fricke et al., 2001), were never observed in wild type adults (Fig. 2.2A), but were present in the tegmentum at the level of the caudal tectum in *astray* adults (4 of 15 animals; Fig. 2.2B) (The optic projection tracing in Fig. 2.2 was performed by Anselm Ebert). These tracts crossed the mid-line in the tegmentum and axons grew dorsally to terminate in superficial layers of the tectum. Overall, the observations that 14 of 15 larvae pre-selected for the presence of ectopic optic tracts in the telencephalon retained these as adults and that several of these animals displayed other ectopic tracts suggest that *astray* mutants that had ectopic tracts as larvae usually retained them into adulthood.

2.4.3 Aberrant midline crossing

In addition to midline crossing of ectopic telencephalic and tegmental tracts, we observed ectopic midline crossing of optic axons in the posterior commissure in *astray* adults (12 of 15 animals), but never in wild type (n = 12 animals; Fig. 2.2L,M). Ectopic crossing in the posterior commissure is extremely common in *astray* larvae (Fricke et al., 2001; KR and CBC, in preparation). The tectum is innervated exclusively contralaterally as a continuous layer in all wild type animals (Fig. 2.2C). In contrast, we observed blocks of innervation in the ipsilateral tectum of all *astray* mutants (15 of 15 animals; Fig. 2.2D). In the contralateral tectum of *astray*, gaps in the innervation were observed (13 of 15 animals), presumably resulting from ectopic

ipsilateral innervation by the unlabelled eye. Ipsilateral tectum innervation is probably a consequence of axons re-crossing the midline caudal to the chiasm, because ipsilateral growth of axons at the chiasm was rare and indistinguishable from wild type (data not shown and Becker et al., 2000).

Discrete blocks of tectal innervation probably represent eye-specific segregation of optic axons into ocular dominance columns. Ocular dominance columns are induced in the tectum of frogs (Constantine-Paton and Law, 1978) and fish (Meyer, 1982) in an activity dependent manner, whenever more than one eye innervates one tectal half. Moreover, tracing the larval optic projection from the left and right eyes with two different lipophilic tracers in *astray* mutants often labels segregated patches of innervation on the tectum, directly showing the presence of ocular dominance columns in larval *astrays* (CBC, data not shown). This suggests that *robo2* is not required for activity dependent axon/axon interactions.

2.4.4 Aberrant growth of optic axons into the tectum

The dorsal brachium of the optic tract is tightly fasciculated in wild type animals (n = 12, Fig. 2.2J). In all adult *astray* mutants, it enters the tectum in an abnormally broad front of individual fascicles (15 of 15 animals, Fig. 2.2K), indicating defasciculation of the optic tract in *astray* mutants. Within the tectum, close to the dorsal midline, fascicles of optic axons run deep, giving off axons dorsally to terminate in the superficial retinorecipient layers (13 of 15 animals, Fig. 2.2D). This never occurs in wild type (Fig. 2.2C). Optic axon fascicles deep within the tectum are most likely a consequence of defasciculated growth into the tectum, since individual fascicles can be seen to enter the rostral tectum ventral to the retinorecipient zone (Fig. 2.2K).

2.4.5 Expanded target innervation

Larval *astray* mutants exhibit larger terminal arbors than wild type animals (Campbell et al., 2007). In adult wild type animals, terminal fields are small, dense and sharply delineated. In the adult *astray* mutants retino-recipient pretectal nuclei, including the central pretectal nucleus (CPN), anterior thalamus (A), ventro-lateral thalamus (VL) and the dorsal part of the periventricular pretectal nucleus (PPd), showed expanded innervation fields with more diffuse borders (15 of 15) compared to wild type (Fig. 2.2E,F). We were able to quantify the lateral extent of the A/VL terminal field at the level of the CPN, which was significantly enlarged in

astray mutants (203. 2 ± 18.4 µm SEM) compared to wild type animals (124.7 ± 6.7 µm; Mann-Whitney U-test, P = 0.0005). However, the cytoarchitecture of the pretectal area, visualized by neutral red counter-stain, was indistinguishable in wild type and *astray* animals. For example the distance between the CPN and the dorsal aspect of the ventricle was comparable between *astray* (333.5 ± 13.4 µm) and wild type animals (323.3 ± 14.1; P = 0.6). This suggests that optic axons terminated beyond their normal boundaries.

In the tectum of wild type animals, most optic axons terminate in the stratum fibrosum et griseum superficiale (SFGS). In contrast, in *astray* mutants terminations of axons were more dispersed. A substantial proportion of optic axons innervated layers that were deeper than the SFGS (15 of 15 animals, Fig. 2.2G,H), resulting in a doubling in the depth of densely innervated tectal layers. The total depth of the termination zone in *astray* mutants was 92.4 ± 3.7 µm compared to 48.8 ± 1.7 µm in wild type animals (ANOVA, P < 0.0001), whereas the total thickness of the tectum was unchanged in *astray* mutants (185.1 ± 4.3 µm), compared to wild type animals (198.3 ± 10.2 µm, Mann-Whitney U-test, P = 0.4). This suggests that optic axons terminated beyond their normal target layers. Overall, developmental pathfinding and termination errors of optic axons in *astray* mutants are mostly retained in adults. Thus long-term error correction of the optic projection is inefficient in *astray* mutants.

2.4.6 Robo2 deficiency is not the reason for inefficient correction of pathfinding errors of optic axons

Is the failure to correct pathfinding errors a consequence of the lack of Robo2? It is possible that *robo2* function is not only needed for correct pathfinding and terminal branching of optic axons, but also for error correction once ectopic tracts are present. Alternatively, a lack of error correction could be a general property of optic axons in zebrafish. To distinguish between these alternatives, we conditionally knocked down *robo2* expression during early development to induce targeting errors, but allowed *robo2* expression levels to recover during subsequent development, so as not to interfere with a possible *robo2*-dependent correction mechanism.

To this end, we injected a splice-blocking morpholino against *robo2* into embryos. Our PCR analysis of mRNA extracts from injected larvae indicated a reduction in correctly spliced *robo2* mRNA at 3 dpf (days post-fertilization; Fig. 2.1C). At this time point the optic projection first forms a retinotopic projection on the tectum (Kaethner and Stuermer, 1994). However,

significant amounts of correctly spliced mRNA were still detectable, indicating only a partial knockdown. Importantly, a shorter aberrant band was detected by RT-PCR. We cloned and sequenced this band and found that it lacked a large part of exon 1, including 57 bp of coding sequence (spanning the start codon) and 24 bp of the 5' UTR, indicating usage of a cryptic upstream splice donor. While the predicted first ATG in the aberrantly spliced RNA is in frame, it lies 197 bp downstream of the usual start codon, well past the signal sequence and halfway through the first Ig domain of Robo2. It is thus very likely that no functional protein is translated from this RNA. As expected, at 5 dpf levels of correctly spliced *robo2* mRNA were close to normal and expression of the aberrantly spliced mRNA was reduced. The aberrant band was nearly undetectable by 18 dpf. Thus, the morpholino partially knocks down *robo2* expression and becomes ineffective by 18 days post-fertilization.

Analysis of the optic projection at 5 dpf by DiI tracing in wild type larvae and live observation of GFP fluorescence in *pou4f3:GFP* transgenic larvae after morpholino injection showed a partial phenocopy of the *astray* mutant. Out of 12 DiI traced larvae, 2 showed aberrant growth of the optic projection, with ectopic projections to the telencephalon, although these projections appeared unilateral—unlike most *astray* mutants—perhaps reflecting an incomplete knockdown of *robo2* function (Fig. 2.1D,E). A few of the ectopic axons appeared to re-cross the midline in the posterior commissure, but no other *astray*-like errors were observed. The telencephalic pathfinding errors seen in *robo2* morphants (morpholino-injected animals) are a definitive phenotype, very specifically associated with *astray* mutants and never observed in thousands of wild type larvae or after injecting scores of other morpholinos (CBC, unpublished data). Combined with the RT-PCR data, this partial phenocopy of the *astray* phenotype therefore indicates a specific action of the morpholino (Nasevicius and Ekker, 2000).

To determine whether ectopic tracts in the telencephalon are retained in adulthood, we sorted live *pou4f3:GFP* transgenic *robo2* morphants and raised those that had these tracts. The frequency of ectopic telencephalic tracts was 16.4% ± 4.4% (n = 243 larvae), which was lower than in *astray* mutants (67%), likely because of incomplete knockdown of *robo2* (Fig. 2.1A,D,E). In adult *robo2* morphants that had been presorted as larvae for an ectopic telencephalic projection, tracing from both optic nerves showed a retained ectopic projection (n=5). Ectopic tracts were not as massive as those observed in *astray* mutants, probably because transient morpholino efficacy allowed later-developing optic axons to pathfind correctly.

Of 4 additional unilaterally traced animals, 1 showed axons in the telencephalon (Fig. 2.1H). In addition, two of the unilaterally traced animals showed ectopic tracts in the telencephalon that were not labelled by the tracer, but clearly discernable because of their whitish-appearing myelin and asymmetrical location in dissected brains (not shown). It is likely that these aberrant tracts consist of optic axons derived from the unlabelled eye, which would suggest that aberrant tracts in morpholino-injected animals often derive from only one eye. This would also be consistent with the unilateral telencephalic projection in morpholino-injected larvae (see above).

In addition to telencephalic projections, we observed ocular dominance column-like innervation of the ipsilateral tectum in 1 of 4 unilaterally traced animals, indicating that ectopic midline crossing occurred in morpholino-injected animals. Other errors of optic axons observed in *astray* mutants, such as caudal growth into the tegmentum, more dispersed terminations, and irregular growth into the tectum were not found in adult morpholino-injected animals. Specifically, the terminations of optic axons were not more dispersed in morpholino treated fish (n = 9 animals; mean thickness of termination zone: 47.8 ± 1.41 µm, ANOVA, P = 0.8) than in uninjected wild type animals (48.8 ± 1.7; Fig. 2.2I). This is consistent with the absence of these late phenotypes in morphant larvae.

Thus ectopic growth of optic axons, caused by partial knock down of *robo2* expression during early development, is not corrected during subsequent development when *robo2* expression levels have recovered. Overall, this suggests the general absence of an efficient correction mechanism for developmental pathfinding errors of optic axons in zebrafish.
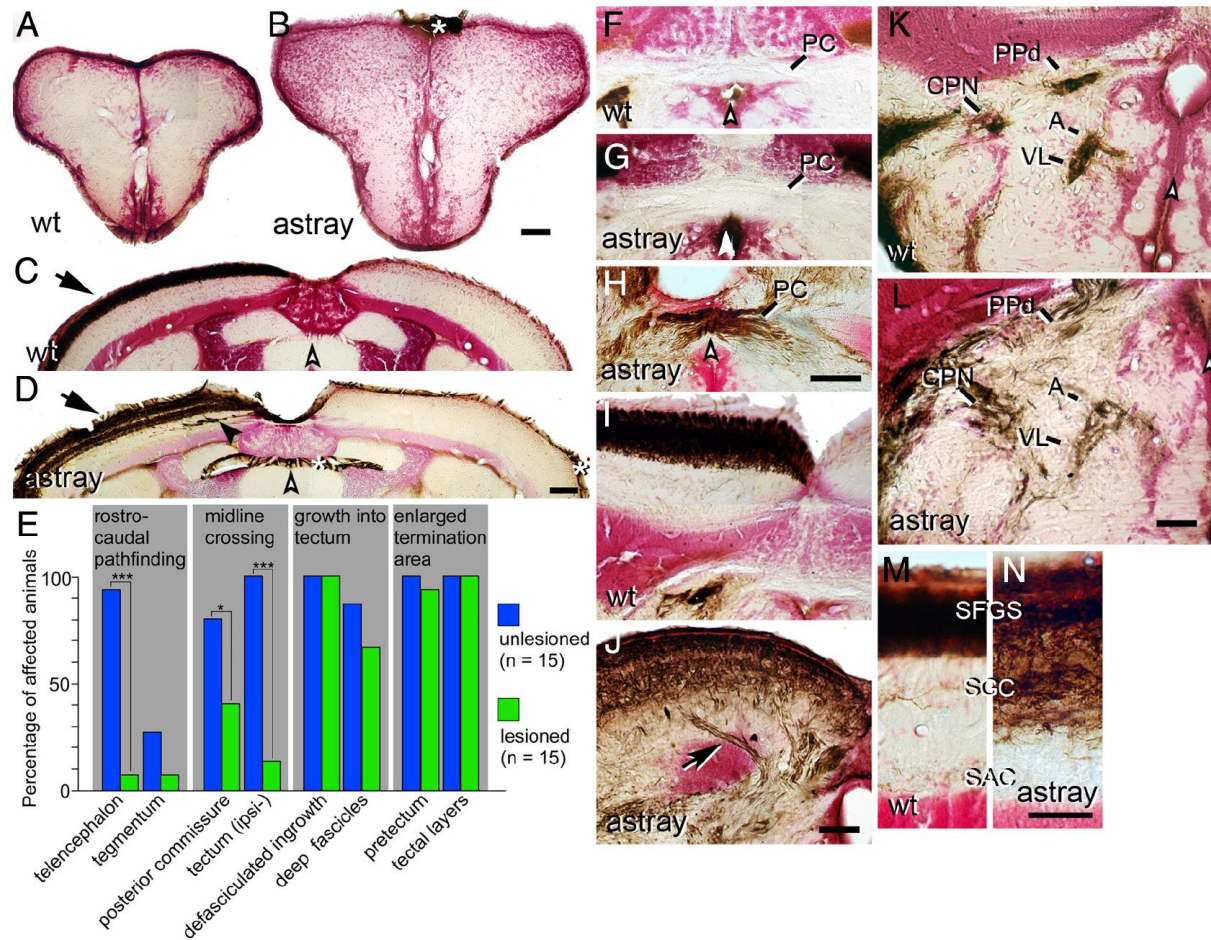
Fig. 2.3 Correction and recurrence of errors by regenerating optic axons in adult *astray* mutants. Optic axons are stained brown in cross sections of the adult brain (counterstained in red); dorsal is up. White arrowheads indicate the brain midline. Asterisks indicate non-specific labelling of the meninges. **A,B:** No regenerated optic axons are present in wild type (A) or *astray* (B) telencephalon. **C,D:** The regenerated optic projection in the tectum is exclusively contralateral (arrow) in wild type (C) and *astray* (D), but erroneous growth of deep fascicles (black arrowhead in D) recurs in *astray*. **E:** Frequencies of different *astray* phenotypes before and after regeneration of the optic projection in animals pre-selected for the presence of telencephalic tracts in larvae. * = P <0.05, *** = P < 0.0001. **F-H:** Regenerating optic axons do not cross the posterior commissure (PC) in wild type fish (F). Regenerated optic axons show ectopic crossing in the posterior commissure in some *astray* animals (H), but not in others (G). **I,J:** Regenerated axons enter the tectum in separate fascicles in *astray* (arrow in J), but not in wild type (I). **K,L:** Termination areas of regenerated optic axons in the pretectum are expanded in *astray* animals (L), compared to wild type animals (K). **M,N:** In *astray* (N), reinnervation of tectal layers is expanded compared to wild type (M) after regeneration. For abbreviations see Fig. 2.2. Scale bars: A,B = 200 µm; C,D,F-L =100µm; M,N = 50 µm.

This figure was kindly contributed by Dr. Thomas Becker and Anselm Ebert.

2.4.7 Degenerating tracts are not a strong guidance cue for regenerating optic axons

Next we asked whether degenerating optic tracts are a non-specific guidance cue for regenerating optic axons. If this was the case, regenerating optic axons in *astray* should faithfully re-populate not only the entopic tracts found in wild type animals but also ectopic tracts, such that the regenerated projection looks similar to the unlesioned projection in *astray*. Alternatively, if regenerating axons can only use specific pathfinding cues, they should rarely follow ectopic tracts, which lack such cues. To distinguish between these scenarios, we determined whether regenerating optic axons projected to the telencephalon in *astray* mutants.

A regenerated optic projection in adult zebrafish is indistinguishable from an unlesioned projection, except for a slight increase in the occurrence of ipsilateral optic axons in the optic tract (Becker et al., 2000). Adult *astray* mutants with a confirmed larval optic projection to the telencephalon received an optic nerve lesion and the regenerated projection was traced unilaterally at 4 weeks post-lesion. Rostro-caudal pathfinding errors were strongly reduced in the regenerated projection: Ectopic tracts in the telencephalon were observed in none of the wild type fish with a regenerated optic projection (Fig. 2.3A) and in only 1 of 15 *astray* animals (Fig. 2.3B) (The optic projection tracing in Fig. 2.3 was performed by Dr. Thomas Becker and Anselm Ebert). This is significantly different from unlesioned *astray* animals (14 of 15, see above; Fisher's Exact test, $p < 0.0001$). In the tegmentum, optic axons were present in no wild type animals and in only 1 of 15 *astray* mutants with a regenerated optic projection, compared to 4 of 15 unlesioned *astray* animals, showing the same tendency to correct developmental pathfinding errors during regeneration.

2.4.8 Cellular and molecular changes after deafferentation are similar in ectopic and entopic optic tracts

Regeneration of optic axons into ectopic tracts could have been prevented by a degeneration that was too quick, such that the tracts had disappeared by the time axons arrived in the brain, or delayed, such that entry was blocked for regenerating axons. Ectopic tracts could also differ from entopic tracts in the expression of growth promoting molecules they contain. Therefore, we decided to observe degeneration of ectopic and entopic tracts and gene expression at a time point when entopic tracts are about to be re-populated.

To determine when axons regenerate we performed anterograde tracing experiments of the optic projection. At 8 days after an optic nerve cut lesion, 11 of 13 wild type animals had regenerating axons in the diencephalic optic tract and in 8 of 13 animals axons had reached the rostral tectum. By 16 days post-lesion, all animals (n = 4) had optic axons reaching the caudal tectum and 3 of 4 animals exhibited complete coverage of the tectum by optic axons (data not shown). This indicates that at about 1 week post-lesion, axons have regrown to an extent that they could have entered ectopic telencephalic tracts.

As an indicator of tract degeneration, we decided to observe macrophage/microglial cell invasion of ectopic telencephalic tracts at 1 week post-lesion by immunohistochemistry. Tracts were identified by their dark appearance in differential interference contrast microscopy, their typical asymmetrical dorso-ventral extent, and dense immunolabelling for macrophages/microglial cells. We found a massive macrophage/microglial cell reaction that was comparable between ectopic and entopic tracts in all *astray* mutants (n = 4 animals; Fig. 2.4). The macrophage/microglial cell reaction in *astray* was not different from lesioned wild type animals (n = 4) (Schweitzer et al., 2003; Schweitzer et al., 2007). This suggests a similar timing of degeneration in ectopic and entopic tracts in *astray* animals.

To determine whether oligodendrocytes might have failed to increase expression of axon growth-promoting molecules (Becker and Becker, 2007) in ectopic tracts of *astray* animals, we double-labelled sections for *contactin1a* mRNA by in situ hybridisation. *Contactin1a* mRNA is upregulated by oligodendrocytes of the optic tract after a lesion and may promote axon growth (Schweitzer et al., 2007). We found a similar increase in expression of *contactin1a* mRNA in ectopic and entopic tracts in *astray* animals at seven days post-lesion. This matched increased expression observed in lesioned wild type animals (n = 4; data not shown and Schweitzer et al., 2007). This suggests that ectopic tracts contain oligodendrocytes that display a typical lesion response. Thus, at least some aspects of the cellular and molecular composition of ectopic and entopic tracts are comparable at a time when regenerating axons choose their path.
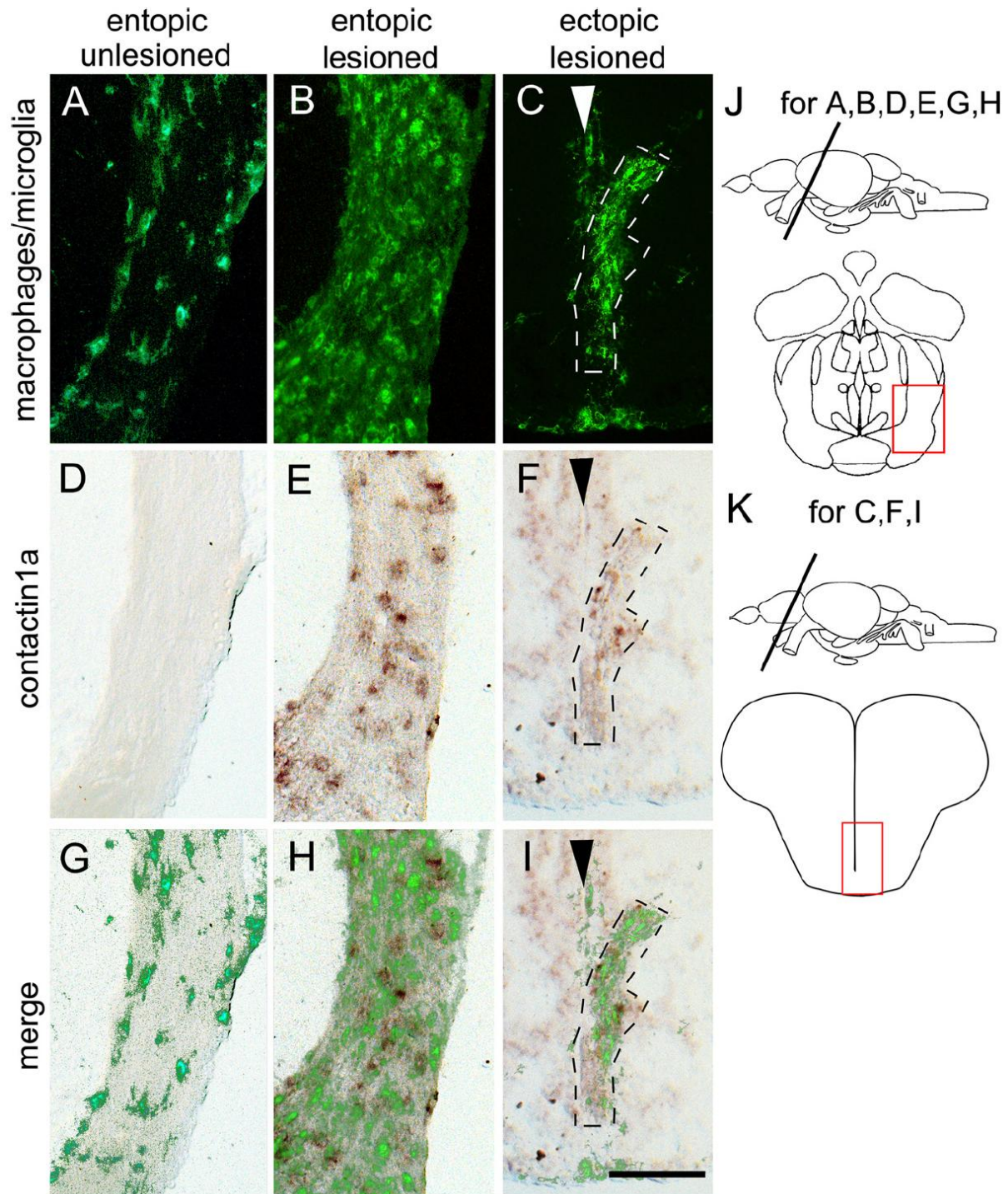
Fig. 2.4. De-afferented ectopic optic tracts in the telencephalon of *astray* mutants display macrophage/microglial cell activation and increased *contactin1a* mRNA expression comparable to entopic tracts. Cross sections through the adult brain are shown as indicated in J,K. Macrophage/microglial cell immunolabelling (A-C) and *contactin1a* mRNA labelling (D-F) is comparable between de-afferented entopic (B, E, H) and ectopic *astray* optic tracts (C,F,I). Both signals are increased compared to unlesioned entopic tracts (A,D,G). Arrowheads in C,F,I indicate telencephalic midline. G, H, I shows superimposition of macrophage/ microglial cell and *contactin1a* mRNA labelling. Scale bar = 200 µm.

2.4.9 Pathfinding errors but not termination errors of optic axons are reduced in the regenerated optic projection of *astray* mutants

To test the hypothesis that *robo2* deficiency impairs correct regeneration of optic axons, we analyzed the entire trajectories of regenerated optic axons in *astray* mutants. In the following we describe errors committed by regenerating optic axons in *astray* mutants, which were never observed in wild type animals, unless stated otherwise (13 animals). Error frequencies are compared with those in unlesioned *astray* mutants (Fig. 2.3E).

Robo2 deficiency does not influence the frequency of erroneous ipsilateral axon growth in the chiasm during optic nerve regeneration. Even though ipsilateral axons were observed in regenerated *astray* mutants (8 of 15 animals) at a higher frequency than in unlesioned *astray* mutants (1 of 15, Fisher's Exact test, P = 0.014), this proportion still matched that of regenerated wild type animals (6 out of 13, not significant, data not shown). This confirms our earlier observation that regenerating optic axons show an elevated rate of ipsilateral growth during regeneration even in wild type animals (Becker et al., 2000).

In the posterior commissure, ectopic midline crossing was reduced compared to unlesioned *astray* mutants. Optic axons crossing in the posterior commissure were present in the regenerated projection in only 6 of 15 animals, compared to 12 of 15 in unlesioned *astray* animals (one-sided Fisher's Exact test, P = 0.03; Fig. 2.3F-H).

In the tectum ipsilateral innervation was also strongly reduced. Two of 15 *astray* animals with a regenerated optic projection showed ipsilateral tectal innervation, which was significantly less than in unlesioned *astray* mutants (15 of 15; Fisher's Exact test, P <0.00001; Fig. 2.3C,D). Reduced ipsilateral innervation is probably a consequence of reduced midline crossing in the posterior commissure.

Defasciculation of the dorsal optic tract as it enters the tectum (15 of 15 animals; Fig. 2.3I,J) and ectopic fascicles of optic axons in deep tectal layers (10 of 15 animals; 3C,D) were observed in *astray* mutants with a regenerated optic projection. This was not statistically different from frequencies of phenotypes found in unlesioned *astray* mutants (15 of 15 animals for defasciculation of the dorsal optic tract and 13 of 15 animals for the presence of ectopic fascicles in deep tectal layers; Fig. 2.3E).

Termination patterns of regenerating *astray* axons were indistinguishable from unlesioned *astray* mutants. Reinnervated terminal fields in pretectal nuclei were expanded in 14

of 15 animals, whereas the regenerated innervation of pretectal nuclei was highly precise in all wild type fish (n = 13 animals; Fig. 2.3K,L). Tectal innervation was also expanded in all *astray* mutants with a regenerated projection (mean depth of termination zone: 89.6 ± 2.6 µm) matching that of unlesioned *astray* mutants (92.4 ± 3.7 µm, see above) and significantly thicker than in wild type animals with a regenerated optic projection (depth of termination zone: 48.5 ± 1.9 µm; ANOVA, P < 0.0001; Fig. 2.3M,N).

Thus, many pathfinding errors of optic axons occur much less frequently (rostro-caudal errors, ectopic midline crossing) in *astray* fish with a regenerated optic projection than in unlesioned mutants. However, irregular growth into the tectum and termination errors in the pretectum and tectum are repeated. The simplest explanation for these repeated errors is that *robo2* is required for certain pathfinding decisions and for correct termination of regenerating axons.

2.4.10 *Robo2* and *slits* are expressed during optic nerve regeneration

Next we asked whether *robo2* and *slit* ligands are expressed at the right time and place to be involved in targeting of regenerating optic axons in adult fish. We performed in situ hybridisation for *robo2* in the retina, as well as the potential ligands *slit1a, slit1b, slit2* and *slit3* in the optic pathway and in the brain, before and after optic nerve crush of wild type animals (In situ hybridisations for *robo2* and *slit2* expression in Fig. 2.5 were performed by Dr. Thomas Becker). The retina of adult teleost fish grows continuously in an annular fashion, i.e. central retina is older than peripheral retina (Easter and Stuermer, 1984). In the juvenile zebrafish retina (4 weeks post-fertilization), *robo2* is expressed in the peripheral growth zone of the retina, next to the undifferentiated ciliary margin zone (Fig. 2.5A). In more central, older parts of the retina the retinal ganglion cells did not show detectable levels of *robo2* mRNA expression. This is typical for genes involved in axonal growth of newly formed retinal ganglion cells (Bernhardt et al., 1996; Laessing and Stuermer, 1996).

In the unlesioned adult retina (Fig. 2.5B), no *robo2* mRNA expression was detected in the retinal ganglion cell layer. At 1 week after a lesion of the optic nerve in adult animals, when most axons have passed the chiasm/optic tract region, *robo2* mRNA expression was not detectably up-regulated in the retina by in situ hybridisation and PCR (data not shown). However

at 2 weeks post-lesion, when axons navigate close to their targets, upregulation in the retinal ganglion cell layer of the entire retina was detectable by in situ hybridisation (Fig. 2.5C).

Slits showed mRNA expression in the brain that was unchanged between unlesioned animals and animals at 2 weeks post-lesion and is described here as it pertains to the optic projection. *Slit1a* mRNA showed the most widespread expression in the brain, including the ventral diencephalon and the tectum. In the tectum, expression was strongest in large neurons in the SFGS. The mRNA was also detectable in the outer aspect of the cell dense stratum periventriculare (SPV), but not in the ventricular layer of ependymo-radial glial cells (Fig. 2.5E). *Slit1b* mRNA expression was mostly restricted to specific brain midline zones, such as at the medial aspect of the habenula and at the level of the posterior commissure (Fig. 2.5F,G). Low levels of expression were detected in the ventral telencephalon, rostral to the chiasm. *Slit2* showed strong and highly localized mRNA expression throughout the habenula and in the ventral diencephalon at the level of the chiasm (Fig. 2.5D). *Slit3* mRNA showed low levels of expression in the A/VL and PPd region of the diencephalon (Fig. 2.5H). A strong *slit3* mRNA signal was found in the tegmental midline, which did not coincide with the trajectories of optic axons (data not shown). Thus, retinal ganglion cells with regenerating axons express *robo2* mRNA, while their axons navigate a brain that expresses *slit* ligands close to the optic pathway.
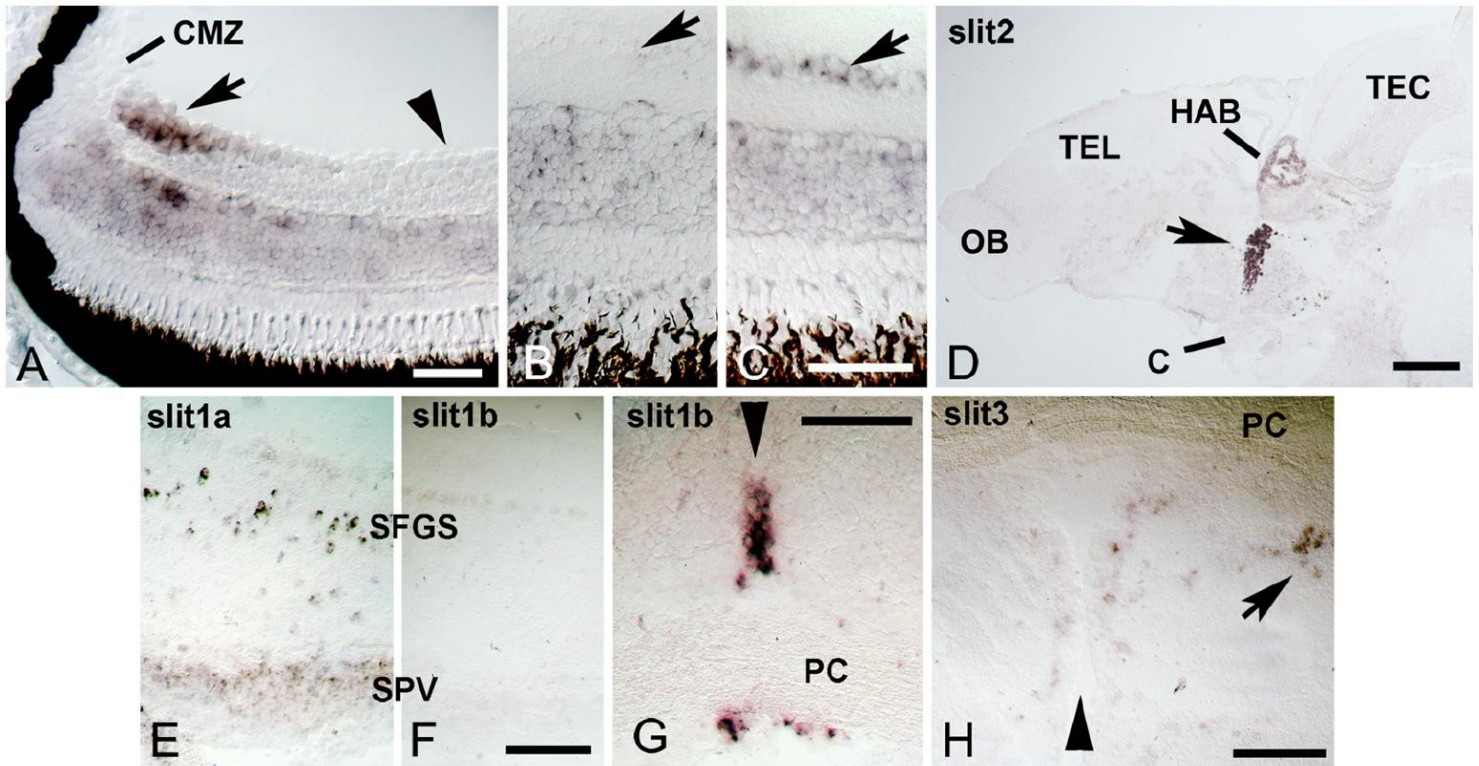
Fig. 2.5. *Robo2* **and** *slits* **are expressed during regeneration of the adult optic projection.** Cross sections are shown, except for D. **A:** In the retina of unlesioned juvenile, 4-week-old animals, *robo2* mRNA is expressed in recently differentiated retinal ganglion cells in the peripheral growth zone of the retina (arrow) next to the ciliary margin zone (CMZ). Older, more central retinal ganglion cells (arrowhead) do not express detectable levels of *robo2* mRNA. **B,C:** In the adult (> 3 months of age) central retina, *robo2* mRNA is re-expressed in the retinal ganglion cell layer at 2 weeks post-lesion (arrow in C) compared to the retinal ganglion cell layer in unlesioned controls (arrow in B). **D:** A sagittal section of the brain is shown (rostral left, dorsal up). Conspicuous expression of *slit2* mRNA is found in the habenula (HAB) and in the ventral diencephalon (arrow) at the level of the optic chiasm (C) (OB = olfactory bulb, TEL = telenencephalon, TEC = tectum mesencephali). **E,F:** *Slit1a* (E), but not *slit1b* (F), is expressed in the deafferented tectum at one week post-lesion. (SPV = stratum periventriculare, SFGS = stratum fibrosum et griseum superficiale) **G:** Strong local expression of *slit1b* mRNA is found at the level of the posterior commissure (PC) in cross sections of the brain. **H:** Low levels of *slit3* mRNA expression are found in the pretectum, including the PPd area (arrow). Arrowheads in G,H indicate the brain midline. Scale bars in A,C,G = 50 µm; D = 200 µm; E,F,H = 100 µm.

Part of this figure was kindly contributed by Dr. Thomas Becker (A-D).

63

2.4.11 Tectal cytoarchitecture is comparable between *astray* and wild type animals

Expansion of optic axon terminations beyond wild type retinorecipient layers is consistently found in all *astray* mutants with a regenerated optic projection. To estimate the potential contribution of developmentally altered brain morphology to these targeting errors, we analyzed the laminated architecture of the denervated tectum. We found that the layered expression of Tenascin-R (Becker et al., 2004), another extracellular matrix protein, as well as Tyrosine Hydroxylase and serotonin immuno-positive afferents (Kaslin and Panula, 2001) was comparable between *astray* mutants and wild type animals in the tectum at 1 week post-lesion (Fig. 2.6) (Immunhistochemistry in Fig. 2.6 was performed by Dr. Thomas Becker). At this time, the tectum is denervated and the first regenerating optic axons have just begun to reach it (see above). However, the intensity of Tenascin-R immunoreactivity increased by 41% (n = 3 animals, mean pixel brightness was 96.2 ± 6.7 in *astray* and 68.0 ± 5.5 in wild type, Mann-Whitney U-test, $P < 0.05$). Intensity of Tyrosine Hydroxylase immunopositive axons increased by 94% (n = 3, brightness was 48.0 ± 3.1 in *astray* and 24.8 ± 2.0 in wild type, Mann-Whitney U-test, $P < 0.05$). Serotonergic innervation was unchanged (brightness was 37.4 ± 12.0 in *astray* and 37.0 ± 12.0 in wild type). As the basic layering of extracellular matrix and afferent systems is retained in *astray* mutants, it is unlikely that the massive laminar termination errors of regenerating optic axons are solely caused by developmentally altered tectal cytoarchitecture.
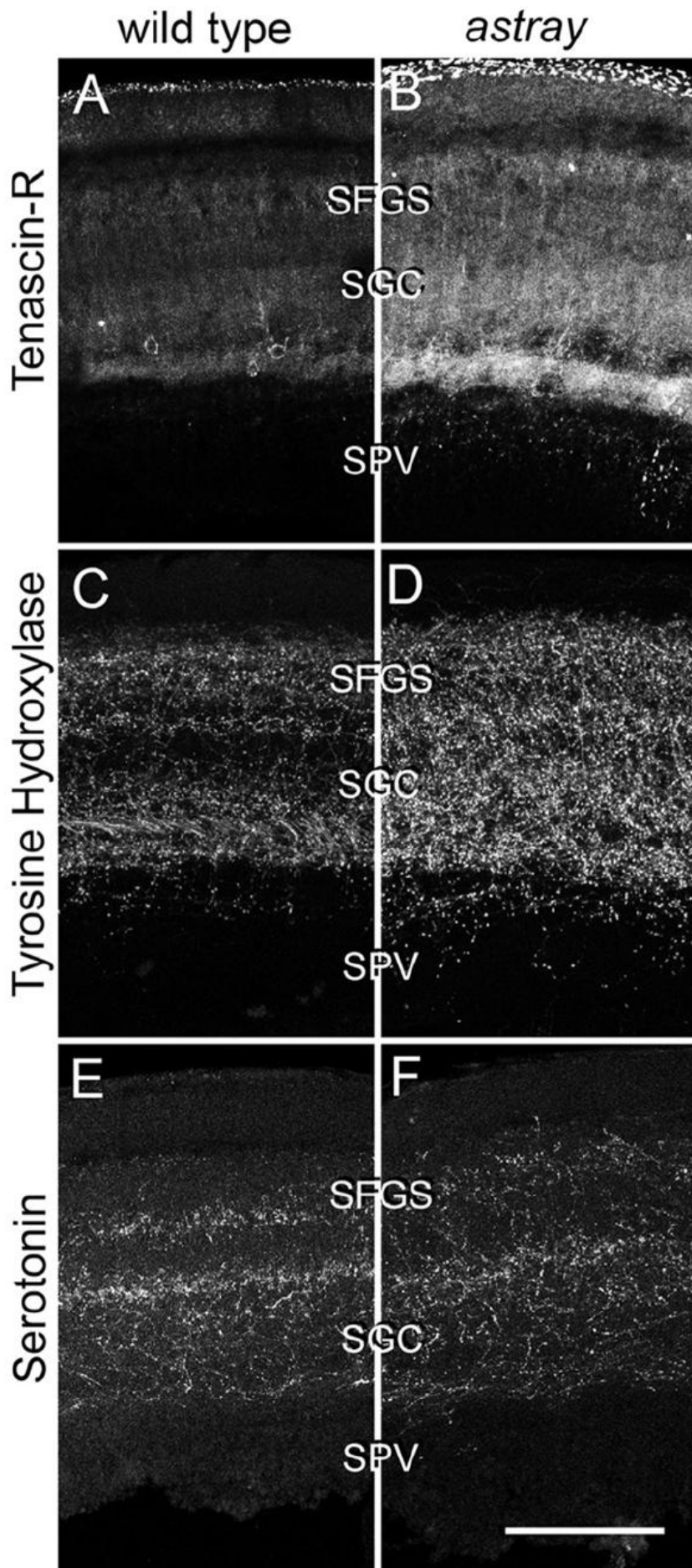
Fig. 2.6. Comparison of laminar distribution of different markers in the denervated tectum at 1 week post-lesion. Cross sections through the dorsal tectum are shown (dorsal is up). Tenascin-R (A,B), Tyrosine Hydroxylase (C,D), and serotonin (E,F) immunoreactivities show comparable distribution in wild type and *astray* animals. However, labelling intensity of Tenascin-R and Tyrosine Hydroxylase was increased in *astray* mutants relative to wild type animals. For anatomical abbreviations see previous figures. Scale bar = 100 µm. This figure was kindly contributed by Dr. Thomas Becker.

2.4.12 Ubiquitous overexpression of Slit2-GFP during regeneration of the optic projection does not lead to major pathfinding errors

To determine the effect of acutely compromising Robo/Slit signaling during regeneration we ubiquitously overexpressed a Robo ligand to mask endogenous *slit* expression patterns. We used a fish line (*hsp70l:slit2-GFP*) in which Slit2-GFP fusion protein overexpression can be induced by heat shock (Yeo et al., 2004). In all heat-shocked embryos, the optic tract is severely disrupted after a single heat-shock, including *astray*-like rostral and caudal pathfinding errors; such profound disruption is never seen in *hsp70l:mcherry* controls (Fig. 2.7A,B) (Embryo heatshocks and scans in Fig. 2.7A and B were performed by Melissa Hardy). Daily heat-shocks of adults led to a homogeneous 82% increase in immunodetectability of GFP in sections of the adult brain (non-heatshock: 9.8 ± 2.30, n=6 animals; heatshock: 17.9 ± 2.70, n=8 animals; $p = 0.01$), indicating successful overexpression of Slit2 (Fig. 2.7C-F). Applying this treatment to animals with optic nerve lesions did not lead to ectopic telencephalic (Fig. 2.7G,H) or tegmental projections, nor crossing of axons in the posterior commissure (Fig. 2.7K,L), presence of ipsilateral axons in the tectum or increased termination layer depth of optic axons during regeneration (n = 4 animals). We detected deep running fascicles of optic axons in the rostro-medial tectum of all animals (n = 4), not found in wild type. However, this was also observed in all unlesioned *hsp70l:slit2-GFP* fish (n = 12), which possessed an otherwise wild type-like optic projection. Thus, ubiquitous overexpression of *slit2* during optic nerve regeneration did not induce *astray*-like pathfinding phenotypes. This is consistent with a reduced importance of Robo/Slit interactions for pathfinding of adult regenerating optic axons.
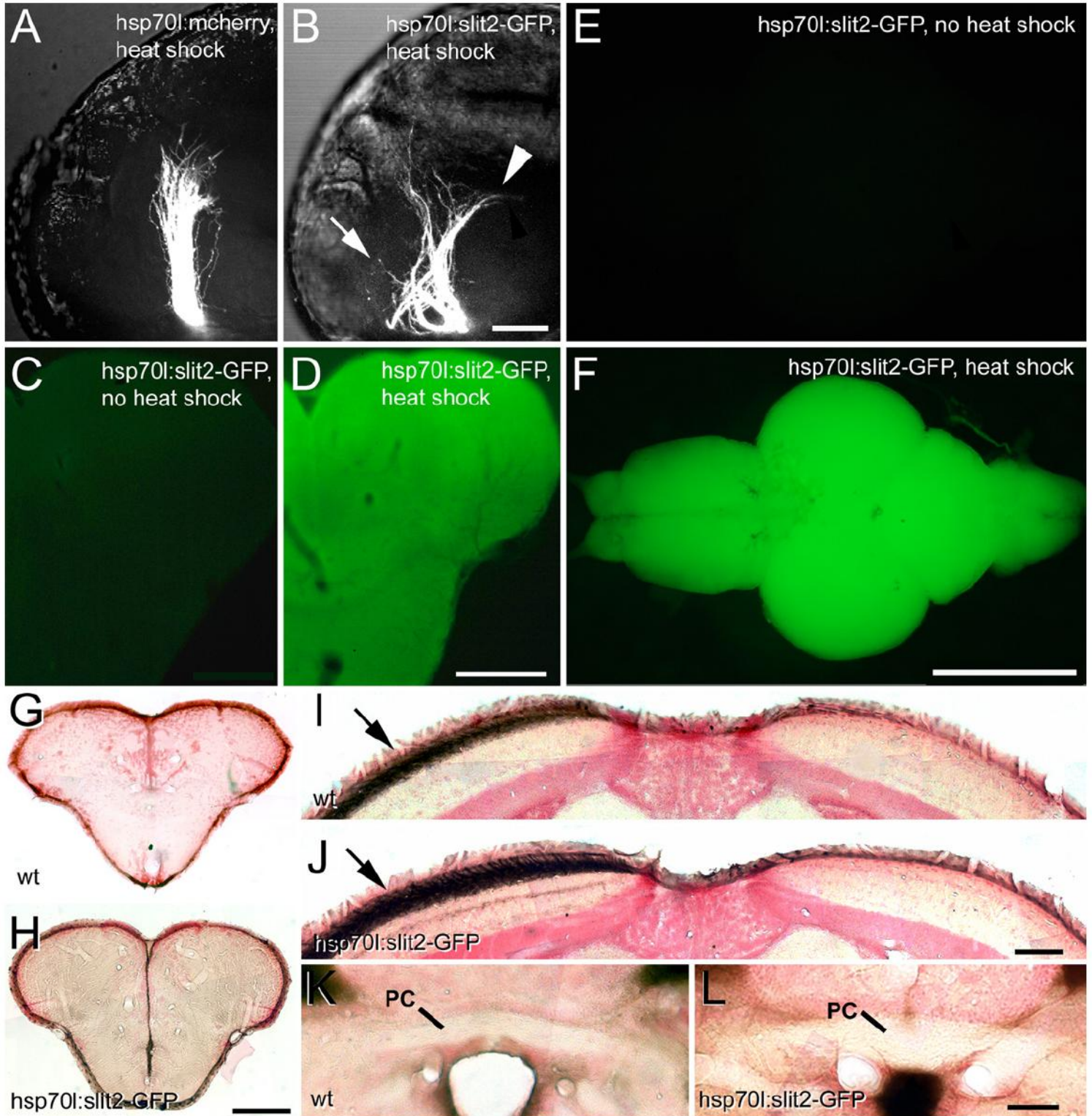
Fig. 2.7. Ubiquitous over-expression of Slit2-GFP causes *astray*-like phenotypes in the developing, but not the regenerating optic projection. A,B: Lateral views (maximal-intensity projections) of optic axons in heat-shocked embryos at 48 hpf show an essentially wild type projection in *hsp70l:mcherry* control embryos, but in *hsp70l:slit2-GFP* embryos the tract is severely disorganized with anterior (arrow) and posterior (arrowhead) misprojections.

C-F: After repeated heat-shocks the entire brain of *hsp70l:slit2-GFP* animals (F) shows intense GFP fluorescence, compared to non-heat shocked controls (E). Similarly, immuno-detection of GFP in sections of the telencephalon shows homogeneous immunoreactivity after heat shock (D), but not in non-heat-shocked controls (C). **G-L:** Regenerating optic axons in heat shocked wild type (wt) and *hsp70l:slit2-GFP* transgenic fish do not grow into the telencephalon (G,H) or the posterior commissure (PC in K,L) and exclusively populate the contralateral tectum (arrows in I,J). Scale bars A,B = 50 µm; C,D = 200 µm; E,F = 1 mm; G,H = 200 µm; I,J = 100 µm; K,L = 50 µm. Part of this figure was kindly contributed by Melissa Hardy (A and B).

2.5 Discussion

We show here for the first time that degenerating tracts are not a strong guidance cue for regenerating CNS axons, that *robo2* may contribute to correct pathfinding and termination of regenerating optic axons, and that correction of large-scale developmental pathfinding errors of optic axons is inefficient in zebrafish.

2.5.1 Degenerating tracts in the CNS are not an attractive guidance cue

The adult *astray* mutant uniquely enabled us to test whether degenerating CNS tracts are a strong guidance cue for regenerating axons. This is because the mutant contains ectopic optic tracts that develop stochastically in two thirds of the animals and are mostly retained in adults. Thus, regenerating axons are confronted with degenerating tracts that do not overlap with the correct trajectory to their targets.

If degenerating tracts were an attractive guidance cue, we would expect regenerating optic axons to re-enter these tracts in almost all cases. However, growth of regenerating optic axons into the telencephalon was extremely rare (1 of 15 animals) following an optic nerve crush in *astray* mutants that had been pre-selected for the presence of a telencephalic projection at the larval stage. Ectopic tracts were clearly present at 1 week post-lesion and underwent degeneration that was indistinguishable from entopic and wild type tracts, as judged by the macrophage/microglial cell response. This was the time point when regenerating optic axons repopulated tracts in the brain. Moreover, evidence from previous enucleation experiments (Schweitzer et al., 2003; Schweitzer et al., 2007) indicates that optic tracts are unchanged in diameter through at least 4 weeks post-lesion, when regeneration is complete (Becker et al., 2000). This strongly suggests that degenerating ectopic tracts are available to regenerating axons, but are not re-entered. This differs from observations in the peripheral nervous system in mice, where repeated imaging of regenerating motor axons suggested that they retraced their former trajectories within remaining Schwann cell tubes because of mechanical constraints and possibly by interacting with Schwann cell and basal lamina derived growth-promoting molecules (Nguyen et al., 2002). Similarly, it has been suggested from electron-microscopic observations of the optic nerve of salamanders that regenerating optic axons use degenerating fibers as guidance cues (Turner and Singer, 1974).

Regenerating optic axons do not enter ectopic tracts despite the presence of growth-promoting molecules. We show here that the axon growth-promoting *contactin1a* is upregulated by oligodendrocytes in the lesioned ectopic tracts in a fashion similar to lesioned entopic optic tracts. This suggests that ectopic tracts are not avoided because they may lack growth promoting molecules expressed in lesioned entopic tracts. In fact, fish oligodendrocytes re-express a number of growth promoting molecules after an optic nerve lesion, such as L1-related proteins (Bernhardt et al., 1996; Ankerhold et al., 1998) and P0 (Brösamle and Halpern, 2002; Schweitzer et al., 2003). In mammals, oligodendrocytes survive an optic nerve lesion (Ludwin, 1990), but expression of L1 and P0 is restricted to peripheral Schwann cells (Martini, 1994). Overall, this suggests that regenerating optic axons show active, target-oriented navigation during regeneration.

2.5.2 Robo2 may contribute to correct distal targeting of regenerating optic axons

The frequencies of specific errors committed by regenerating *robo2* deficient axons (Fig. 2.3E) suggest that *robo2* is less important for correct rostro-caudal pathfinding and avoidance of ectopic midline crossing than during development, but may be necessary for fasciculated growth of regenerating optic axons into the tectum and for precise target zone termination of optic axons.

Spatio-temporal expression patterns of *robo2* and *slit* ligands correlate with these differences: *Robo2* is not detectably re-expressed in any retinal ganglion cells after optic nerve crush at 1 week post-lesion, when regenerating optic axons have to make pathway choices in the chiasm/tract region. Rostro-caudal pathfinding errors originate in this region in unlesioned *astray* mutants. Thus, the slow upregulation of *robo2* suggests that even in wild type animals optic axons may not rely on Robo/Slit guidance during early regrowth. Use of alternate guidance systems may explain why in *astray* mutants, despite the strong expression domain of *slit2* in the diencephalon, few pathfinding errors are found close to the chiasm in the regenerated optic projection. In addition, specific *slit* expression domains seen near the developing chiasm are not detectable at the adult stage: In developing animals, *slit3* mRNA borders the chiasm rostrally and caudally and *slit2* mRNA borders it rostrally, which channels developing optic axons into the chiasm and prevents them from forming ectopic tracts (Hutson and Chien, 2002). Moreover, we found here that conditional overexpression of *slit2* during regeneration did not induce ectopic

regrowth of optic axons, which is consistent with a reduced importance of Robo/Slit signaling. However, we cannot exclude that significantly increased levels of Slit2 were insufficient to fully mask endogenous *slit* expression domains. Taken together, these observations suggest that early pathway decisions of regenerating optic axons are not decisively determined by Robo/Slit interactions. Thus, other guidance cues may prevent regenerating optic axons from forming ectopic tracts during regeneration. Candidates for such cues are chondroitin sulfates (Becker and Becker, 2002), Tenascin-R (Becker et al., 2004) and Semaphorins (Becker and Becker, 2007), which are present along the adult optic pathway and may guide regenerating optic axons in a combinatorial manner.

In contrast to early pathway decisions, in more distal parts of the optic pathway, reached when *robo2* re-expression is detectable in retinal ganglion cells, *slit* expression patterns correlate with targeting errors: The posterior commissure, through which regenerating axons aberrantly cross, is bisected by midline *slit1b* mRNA expression. Aberrantly large terminal fields in the pretectum correlate with *slit1a* and *slit3* mRNA expression there. The rostral tectum, in which defasciculated growth of regenerating axons occurs and abnormal deep innervation of the tectum originates in *astray* mutants, is bordered by *slit2* and *slit1b* mRNA expression in the habenula. Expanded termination zones of optic axons in the tectum of *astray* mutants correlate with *slit1a* expression in the SFGS, the main optic axon receiving layer. In the developing tectum, Slit1a/Robo2 interactions negatively regulate branch tip numbers and size of terminal arbors of optic axons (Campbell et al., 2007). However, it remains to be seen whether less inhibited arbor growth in *astray* mutants also leads to targeting to inappropriate tectal layers of developing or regenerating optic axons.

We cannot exclude that a developmentally altered morphology of the adult *astray* brain may contribute to some aspects of targeting errors of regenerating *astray* optic axons. However, massive tectal termination errors are found in all *astray* animals with a regenerated optic projection, while our analysis of tectal cytoarchitecture suggests that any alterations in *astray* mutants are subtle. Therefore, it is likely that re-expression of *robo2* in retinal ganglion cells contributes to correct distal targeting of regenerating optic axons.

2.5.3 Correction of developmental pathfinding errors of optic axons is inefficient

The pathfinding errors observed in the unlesioned adult projection of *astray* mutants are similar to those in larvae, which show rostro-caudal pathfinding errors and aberrant midline crossing (Fricke et al., 2001). Enlarged termination zones in the pretectal targets and tectum of *astray* adults are also reminiscent of the enlarged terminal arbors observed for single optic axons in larval *astray* mutants (Campbell et al., 2007). Thus, we have no evidence that developmental errors made by retinal axons in *astray* larvae are corrected later; in the case of pathfinding, it is clear that larval errors can persist through adulthood.

The lack of *robo2* function is probably not responsible for the inability of *astray* mutants to correct errors, since rostral pathfinding errors caused by the temporary knock down of *robo2* during early development of *robo2* morphants are not corrected at later stages, when Robo2 expression has recovered.

In other axon guidance mutants, the extent of error correction for axonal pathfinding varies. In contrast to optic axons in *astray*, severe projection errors of peripheral nerves in Sema3A deficient mice are corrected during development by an unknown mechanism (White and Behar, 2000). However, EphA4 deficient mice retain developmental miswiring of the corticospinal projection in adults, leading to a severely abnormal gait (Kullander et al., 2003). In contrast to our observations in the CNS of *astray*, a naturally-occurring transient ("erroneous") ipsilateral optic projection in amniotes appears to be eliminated by cell death because of limited trophic factor availability (Isenmann et al., 1999) and by activity-dependent pruning mechanisms involving NMDA receptors (Ernst et al., 2000). However, activity-dependent mechanisms are unlikely to be wholly defective in *astray* mutants, because tecta innervated by both eyes show segregation of axons into ocular dominance column-like patches, a form of axon reorganization that depends on activity (Meyer, 1982) and likely involves NMDA function (Schmidt et al., 2000) in fish.

It is possible that the misprojections in adult *astray* mutants have been stabilized by target-derived trophic support. This could derive from the tectum, reached in all cases by caudally misprojecting axons, or from the extensive dorsal telencephalic arborisation field, reached by rostrally misprojecting axons. As the telencephalic termination field is ectopic, it is unclear which factors might stabilize optic axons that terminate here.

The functional consequences of mistargeting of optic axons in adult *astray* mutants are unknown. However, larval *astray* mutants exhibit surprisingly normal optokinetic and optomotor responses (Neuhauss et al., 1999).

2.6 Conclusion

Our findings suggest that regenerating optic axons of zebrafish show active navigation, which likely depends in part on *robo2* function, and are not efficiently guided by the degenerating original tracts. This implies that presenting axons in the non-regenerating CNS of mammals with growth-promoting glial cells (Barnett and Riddell, 2007) may not be sufficient to induce directed growth of axons, unless specific navigational cues are also provided.

2.7 Bibliography

Ankerhold R, Leppert CA, Bastmeyer M, Stuermer CA (1998) E587 antigen is upregulated by goldfish oligodendrocytes after optic nerve lesion and supports retinal axon regeneration. Glia 23:257-270.

Barnett SC, Riddell JS (2007) Olfactory ensheathing cell transplantation as a strategy for spinal cord repair--what can it achieve? Nat Clin Pract Neurol 3:152-161.

Becker CG, Becker T (2002) Repellent guidance of regenerating optic axons by chondroitin sulfate glycosaminoglycans in zebrafish. J Neurosci 22:854-862.

Becker CG, Becker T (2007) Growth and pathfinding of regenerating axons in the optic projection of adult fish. J Neurosci Res 85:2793-2799.

Becker CG, Meyer RL, Becker T (2000) Gradients of ephrin-A2 and ephrin-A5b mRNA during retinotopic regeneration of the optic projection in adult zebrafish. J Comp Neurol 427:469-483.

Becker CG, Schweitzer J, Feldner J, Becker T, Schachner M (2003) Tenascin-R as a repellent guidance molecule for developing optic axons in zebrafish. J Neurosci 23:6232-6237.

Becker CG, Schweitzer J, Feldner J, Schachner M, Becker T (2004) Tenascin-R as a repellent guidance molecule for newly growing and regenerating optic axons in adult zebrafish. Mol Cell Neurosci 26:376-389.

Becker T, Becker CG (2001) Regenerating descending axons preferentially reroute to the gray matter in the presence of a general macrophage/microglial reaction caudal to a spinal transection in adult zebrafish. J Comp Neurol 433:131-147.

Bernhardt RR, Tongiorgi E, Anzini P, Schachner M (1996) Increased expression of specific recognition molecules by retinal ganglion cells and by the optic pathway glia accompanies the successful regeneration of retinal axons in adult zebrafish. J Comp Neurol 376:253-264.

Brösamle C, Halpern ME (2002) Characterization of myelination in the developing zebrafish. Glia 39:47-57.

Campbell DS, Stringham SA, Timm A, Xiao T, Law MY, Baier H, Nonet ML, Chien CB (2007) Slit1a inhibits retinal ganglion cell arborization and synaptogenesis via robo2-dependent and -independent pathways. Neuron 55:231-245.

Chaudhry N, Filbin MT (2007) Myelin-associated inhibitory signaling and strategies to overcome inhibition. J Cereb Blood Flow Metab 27:1096-1107.

Constantine-Paton M, Law MI (1978) Eye-specific termination bands in tecta of three-eyed frogs. Science 202:639-641.

Dickson BJ, Gilestro GF (2006) Regulation of commissural axon pathfinding by slit and its robo receptors. Ann Rev Cell Dev Biol 22:651-675.

Easter SS, Stuermer CAO (1984) An evaluation of the hypothesis of shifting terminals in goldfish optic tectum. J Neurosci 4:1052-1063.

Ernst AF, Gallo G, Letourneau PC, McLoon SC (2000) Stabilization of growing retinal axons by the combined signaling of nitric oxide and brain-derived neurotrophic factor. J Neurosci 20:1458-1469.

Fricke C, Lee JS, Geiger-Rudolph S, Bonhoeffer F, Chien CB (2001) Astray, a zebrafish roundabout homolog required for retinal axon guidance. Science 292:507-510.

Halloran MC, Sato-Maeda M, Warren JT, Su F, Lele Z, Krone PH, Kuwada JY, Shoji W (2000) Laser-induced gene expression in specific cells of transgenic zebrafish. Development 127:1953-1960.

Hutson LD, Chien CB (2002) Pathfinding and error correction by retinal axons: the role of astray/robo2. Neuron 33:205-217.

Hutson LD, Jurynec MJ, Yeo SY, Okamoto H, Chien CB (2003) Two divergent slit1 genes in zebrafish. Dev Dyn 228:358-369.

Isenmann S, Cellerino A, Gravel C, Bähr M (1999) Excess target-derived brain-derived neurotrophic factor preserves the transient uncrossed retinal projection to the superior colliculus. Mol Cell Neurosci 14:52-65.

Kaethner RJ, Stuermer CAO (1994) Growth behavior of retinotectal axons in live zebrafish embryos under TTX-induced neural impulse blockade. J Neurobiol 25:781-796.

Karlstrom RO, Trowe T, Klostermann S, Baier H, Brand M, Crawford AD, Grunewald B, Haffter P, Hoffmann H, Meyer SU, Muller BK, Richter S, van Eeden FJ, Nusslein-Volhard C, Bonhoeffer F (1996) Zebrafish mutations affecting retinotectal axon pathfinding. Development 123:427-438.

Kaslin J, Panula P (2001) Comparative anatomy of the histaminergic and other aminergic systems in zebrafish (Danio rerio). J Comp Neurol 440:342-377.

Kullander K, Butt SJ, Lebret JM, Lundfald L, Restrepo CE, Rydstrom A, Klein R, Kiehn O (2003) Role of EphA4 and EphrinB3 in local neuronal circuits that control walking. Science 299:1889-1892.

Laessing U, Stuermer CAO (1996) Spatiotemporal pattern of retinal ganglion cell differentiation revealed by the expression of neurolin in embryonic zebrafish. J Neurobiol 29:65-74.

Lee Y, Grill S, Sanchez A, Murphy-Ryan M, Poss KD (2005) Fgf signaling instructs position-dependent growth rate during zebrafish fin regeneration. Development 132:5173-5183.

Ludwin SK (1990) Oligodendrocyte survival in Wallerian degeneration. Acta Neuropathol (Berl) 80:184-191.

Martini R (1994) Expression and functional roles of neural cell surface molecules and extracellular matrix components during development and regeneration of peripheral nerves. J Neurocytol 23:1-28.

Meyer RL (1982) Tetrodotoxin blocks the formation of ocular dominance columns in goldfish. Science 218:589-591.

Nasevicius A, Ekker SC (2000) Effective targeted gene 'knockdown' in zebrafish. Nat Genet 26:216-220.

Neuhauss SC, Biehlmaier O, Seeliger MW, Das T, Kohler K, Harris WA, Baier H (1999) Genetic disorders of vision revealed by a behavioral screen of 400 essential loci in zebrafish. J Neurosci 19:8603-8615.

Nguyen QT, Sanes JR, Lichtman JW (2002) Pre-existing pathways promote precise projection patterns. Nat Neurosci 5:861-867.

Oudega M, Xu XM (2006) Schwann cell transplantation for repair of the adult spinal cord. J Neurotrauma 23:453-467.

Pittman AJ, Law MY, Chien CB (2008) Pathfinding in a large vertebrate axon tract: isotypic interactions guide retinotectal axons at multiple choice points. Development 135:2865-2871.

Plachez C, Andrews W, Liapi A, Knoell B, Drescher U, Mankoo B, Zhe L, Mambetisaeva E, Annan A, Bannister L, Parnavelas JG, Richards LJ, Sundaresan V (2008) Robos are required for the correct targeting of retinal ganglion cell axons in the visual pathway of the brain. Mol Cell Neurosci 37:719-730.

Plump AS, Erskine L, Sabatier C, Brose K, Epstein CJ, Goodman CS, Mason CA, Tessier-Lavigne M (2002) Slit1 and Slit2 cooperate to prevent premature midline crossing of retinal axons in the mouse visual system. Neuron 33:219-232.

Reimer MM, Sörensen I, Kuscha V, Frank RE, Liu C, Becker CG, Becker T (2008) Motor neuron regeneration in adult zebrafish. J Neurosci 28:8510-8516.

Schmidt JT, Buzzard M, Borress R, Dhillon S (2000) MK801 increases retinotectal arbor size in developing zebrafish without affecting kinetics of branch elimination and addition. J Neurobiol 42:303-314.

Schweitzer J, Becker T, Becker CG, Schachner M (2003) Expression of protein zero is increased in lesioned axon pathways in the central nervous system of adult zebrafish. Glia 41:301-317.

Schweitzer J, Gimnopoulos D, Lieberoth BC, Pogoda HM, Feldner J, Ebert A, Schachner M, Becker T, Becker CG (2007) Contactin1a expression is associated with oligodendrocyte differentiation and axonal regeneration in the central nervous system of zebrafish. Mol Cell Neurosci 35:194-207.

Stuermer CA, Bastmeyer M, Bähr M, Strobel G, Paschke K (1992) Trying to understand axonal regeneration in the CNS of fish. J Neurobiol 23:537-550.

Turner JE, Singer M (1974) The ultrastructure of regeneration in the severed newt optic nerve. J Exp Zool 190:249-268.

Westerfield M (1989) The zebrafish book: a guide for the laboratory use of zebrafish (Brachydanio rerio). Eugene: University of Oregon Press.

White FA, Behar O (2000) The development and subsequent elimination of aberrant peripheral axon projections in semaphorin3A null mutant mice. Dev Biol 225:79-86.

Xiao T, Roeser T, Staub W, Baier H (2005) A GFP-based genetic screen reveals mutations that disrupt the architecture of the zebrafish retinotectal projection. Development 132:2955-2967.

Yeo SY, Little MH, Yamada T, Miyashita T, Halloran MC, Kuwada JY, Huh TL, Okamoto H (2001) Overexpression of a slit homologue impairs convergent extension of the mesoderm and causes cyclopia in embryonic zebrafish. Dev Biol 230:1-17.

Yeo SY, Miyashita T, Fricke C, Little MH, Yamada T, Kuwada JY, Huh TL, Chien CB, Okamoto H (2004) Involvement of Islet-2 in the Slit signaling for axonal branching and defasciculation of the sensory neurons in embryonic zebrafish. Mech Dev 121:315-324.

3. Putative axon guidance genes expressed as gradients in the RGC layer of the retina during optic nerve regeneration revealed by a microarray study

3.1 Introduction

As can be seen from the preceding chapter, while *robo2* and *slit2* play important roles for correct axon navigation during development, they are of reduced importance in regeneration. This leaves the question, what are the key genes required for successful regeneration? Such knowledge would greatly inform future research towards directed axon regeneration in mammals and humans for the treatment of CNS disorders and injuries. Currently the list of known developmental genes is much longer and well studied than known regeneration associated genes. All model organisms must go through development but only a select few exhibit adult CNS regeneration. As the zebrafish is one of the latter, we used this model to generate a list of regulation of regeneration associated genes in axotomised RGCs of the adult zebrafish using a single channel oligonucleotide microarray.

3.1.1 Optic nerve lesion paradigm in adult zebrafish

The optic nerve lesion paradigm in zebrafish offers an anatomically discrete and highly accessible extension of the CNS which undergoes full regeneration within four weeks and has an almost 100% survival rate in our hands. The retinotectal system in particular has been well studied. The cell bodies of the RGC neurones form the RGC layer in the retina, a discrete tissue which can be readily isolated from neighbouring tissues and the site of injury. This is in contrast to other regeneration models such as spinal cord where many different types of neurones are axotomized and some neurones of interest are difficult to separate from support cells and invading immune cells near the lesion site (Carmel et al., 2001; De Biase et al., 2005; Guo et al., 2010). Transcriptional changes in the regenerating dorsal root ganglia (DRG) have been extensively studied by microarray screens but suffer from similar drawbacks (Bonilla et al., 2002; Costigan et al., 2002; Nilsson et al 2005). Failure to separate out such cells may result in a list of general injury and repair associated genes rather than genes specifically associated with axon injury and regrowth as the other types of cells are contributing to wound response and repair. Furthermore, as the optic nerve is highly accessible and the eye remains intact following an optic nerve lesion, wound repair processes should be kept to a minimum in this paradigm.

3.1.2 Retinal ganglion cell gene regulation following axotomy

Following axotomy, RGCs regulate expression of a specific set of molecules associated with axon growth and pathfinding, including cell surface receptors and transcription factors (Veldman et al., 2007). This regulation includes both up and down regulation, as, for example, a reduction in receptors for inhibitory molecules can enhance regeneration. These cues contribute to the ability of the RGC axons to regrow and navigate to their appropriate targets, leading to functional connections and the restoration of vision. The precise array of molecular determinants which are necessary for this process is currently not well elucidated. The sequencing of the zebrafish genome and subsequent availability of whole-genome microarrays for the zebrafish make it possible to obtain an overview of regeneration related gene regulation in RGCs to identify novel guidance related genes by examining changes in gene expression following optic nerve lesion (Cameron et al., 2005; Veldman et al., 2007). This is a powerful technique for uncovering regeneration-associated genes in an unbiased way, particularly when combined with techniques to enrich the sample for RGCs, such as fluorescence activated cell sorting (FACS) or laser capture microdissection.

3.1.3 Microarray studies

The basic principle on which microarrays are based is that of complementary sequence binding and visualisation thereof. This is the same principle at work in many of the most common and basic laboratory techniques, such as visualising double stranded nucleotides on a gel. The greater the number of complementary base pairs in a nucleotide sequence, the more tightly the strands anneal. Following washing steps, only strongly paired strands will remain hybridised with labelled probe. Probe-target hybridisation can be detected and quantified through the detection of fluorophores, silver or chemiluminescence-labelled targets to determine relative abundance of nucleic acid sequences in the target (Fig. 3.1). The total intensity of signal from each spot of probe, called a feature, is dependent on the total number of probes bound by the target. The intensity of this feature can then be compared to the intensity of a duplicate feature (containing the same probe) under different conditions, allowing for relative quantitation. While this process is quite simple in principle, the key advantage of microarrays over other techniques based on similar principles, such as in situ hybridisation or PCR, is that they offer massively parallel detection of targets. Microarrays can contain tens of thousands of probes and so the use of

microarrays has greatly accelerated specific forms of investigation such as genetic screening. In addition to their uses in studying expression levels of genes, microarrays are also used to genotype, resequence mutant genomes and detect single nucleotide polymorphisms.

A microarray consists of thousands of microscopic spots, called features, each containing picomoles of a different DNA probe (oligonucleotides) designed to match the sequence of known or predicted open reading frames. In the case of Agilent arrays this is accomplished by depositing oligonucleotide monomers onto specially prepared glass slides using an industrial inkjet process. In this way oligonucleotide probes are synthesised via phosphoramidite chemistry directly onto the array (link to microarray technology overview on Agilent's website). The probes are assembled a nucleotide at a time using a masking process so only specified spots receive each addition of nucleotides. The incorporation of user-generated custom probes into a standard array is made possible by this flexible printing process. Probes tend to be produced as either 25 or 60mers. The longer the probe the greater the specificity to the target but the lower the density of spotting onto the array, hence increased costs. In standard microarrays, the probes are bound to a solid surface of glass or silicon, known as the chip, via covalent bonding to a chemical matrix. Non-chip based arrays are also available which make use of microscopic beads for each probe.

Microarrays can be either single-channel or two-channel. Two-channel arrays involve cDNA probes generated from two different samples and labelled with two different fluorophores being applied to the same feature. Single-channel arrays use only one fluorophore and apply only one sample per feature. Due to this, one feature is required per sample, meaning single-channel arrays require twice as many features as a comparable two-channel array. However single-channel arrays are more robust, as a single aberrant sample will not contaminate the results of other samples on separate features, and data can be more easily compared between different experiments. Single-channel microarrays indicate relative levels of hybridisation with the target. This does not indicate the absolute abundance of the target gene but the relative abundance in comparison to other samples run in duplicate features within the array. Comparisons between different genes run on the same array are uninformative as the reaction kinetics during amplification and probe production will vary between templates, distorting initial levels of transcript. Depending on the experimental design, two-channel arrays can be used for

determining absolute levels of expression, but such use of microarrays is uncommon as qPCR is more suited to this task.

Microarrays can be used to answer a wide range of questions, depending on the samples compared in the array. To study both spatial and temporal gene regulation in the retina following optic nerve lesion we are comparing four samples obtained from unilaterally lesioned zebrafish. By isolating mRNA from retina containing RGCs of the regenerating lesioned and unlesioned optic tract, within the same animals, we can compare fold change with the least biological variability possible. By isolating retina containing RGCs from opposing extents of the retina (nasal retina versus temporal retina) we can compare spatial gene expression. Spatial regulation across the retina of transcription factors or cell surface receptors gives a good indication of genes related to formation of the retinotectal map. Thus four samples can be compared within an array to provide a list of genes potentially involved in regeneration or pathfinding of RGCs. As potential players in the regenerative response, our main focus is on cell surface receptors, ligands and transcription factors. While the mRNA for these classes of proteins will be found in RGCs, the corresponding ligands for the receptors will be expressed in the tract and brain and so will not be targets for an RGC based microarray. We hypothesise that of the genes indicated by the array some will be known from development to be involved in RGC axon pathfinding while some may be unique to regeneration. Due to the teleost genome duplication (Amores et al., 2004; Chen et al., 2004), others may be homologues or paralogues, of known regeneration associated genes.
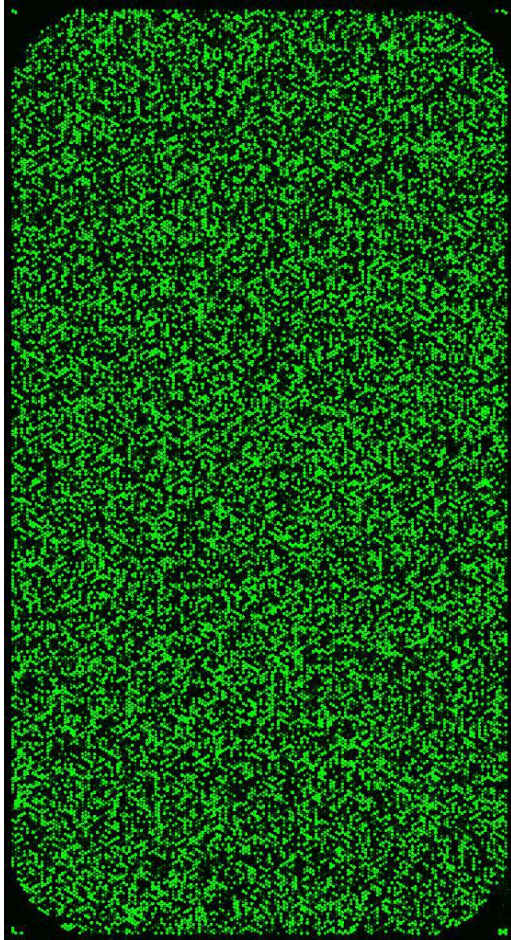
Fig. 3.1. Fluorescence signals of the Cy3-hybridised Agilent microarray from this project which were detected using Agilent's Microarray Scanner System (Agilent Technologies). Each dot in the image is an oligonucleotide containing spot. The more intense the signal, the more target is present, which gives an indication of the level of gene expression in the sample. This image was created by Miltenyi Biotec.

3.1.4 Exploiting microarray findings

Expression patterns in whole mount embryos and sections of adult retina and brain can be verified with in situ hybridisation and the fold changes qualitatively verified. qPCR can be used to quantitatively verify fold changes in retinal mRNA. Potential guidance molecules can be readily knocked down during development with morpholinos and any resultant pathfinding errors can be relatively easily studied in the semi-transparent embryos. Morpholinos can also be applied to transected axons to reveal the functional relevance of candidate genes during axon regeneration. In the adult zebrafish, morpholino knockdown in neurones following retrograde axonal transport of morpholino has been demonstrated in the spinal lesion model (Becker et al.,

2004) and is adaptable to the optic system for selective targeting of RGCs (Veldman et al., 2007; unpublished observations). This allows selective knockdown during regeneration without equivalent manipulation during development so allowing the study of altered regeneration in an animal which underwent unaltered development. The heatshock inducible GAL4/UAS system also offers the potential to perturb putative guidance molecules in both the embryonic and adult situation, and as with the morpholino paradigm, it allows selective manipulation during development and/or regeneration. There exists a wide range of zebrafish RGC pathfinding mutants due to multiple mutagenesis screens having been carried out with a focus on the retinotectal system (Muto et al., 2005; Xiao et al., 2005; Gulati-Leekha and Goldman, 2006). However many more mutagenesis screens have been carried out in the zebrafish with the focus on other tissues and processes (Mullins et al., 1994; Driever et al., 1996; Baraban et al., 2007). Candidate genes from the microarray would provide an indication of which pre-existing mutants may harbour an unstudied optic system phenotype. This offers opportunities for studying the effects of gene knockout during development and regeneration, if the mutants are viable. While this lacks the manipulative possibilities of morpholinos (the gene is constantly and permanently knocked out), the advantage is that of complete knockout, rather than partial knockdown, enhancing any putative phenotype. Investigating how such embryonic pathfinding errors compare to possible pathfinding errors in adult regeneration will offer insight into the question to what extent regeneration is a recapitulation of development.

3.2 Summary

Of the 21410 probes on the array 7092 demonstrated differential levels of binding to our samples, based on a single biological replicate. The expression patterns of the 32 most highly regulated genes, with particular focus on transcription factors, were investigated by RNA in situ hybridisation during development and regeneration. While differential expression patterns for 17 of these genes could be demonstrated during early and mid embryonic development (1dpf and 3dpf), none demonstrated expression patterns in the adult regenerating retina. The success of the in situ hybridisations was confirmed by multiple control probes which ran within the same batches and control embryos on the same slides as the adult retina. As the microarray data gives no indication of absolute expression, only relative levels, it may be that the in situ method is not sensitive enough to detect the expression gradients in the adult retina. One of the genes that exhibited the most pronounced expression pattern in the developing retina, *foxi1*, has a knockout mutant, *foxi1*$^{-hi3747}$, in which we could detect no obvious optic projection pathfinding errors.

3.3 Materials and methods

3.3.1 Animals

All fish are kept and bred in our laboratory fish facility according to standard methods (Westerfield, 1989) and all experiments have been approved by the British Home Office.

3.3.2 Optic nerve lesion

Optic nerve crush lesion was performed as described (Becker et al., 2000). Adult zebrafish (older than 6 months and ≥2cm in length) were deeply anesthetized by immersion in 0.02% aminobenzoic acid ethylmethylester (MS222; Sigma, St. Louis, MO) until swimming posture and startle response became absent. The animal was placed on a cooled surface of metal resting on water ice to slow its metabolism. The mucus membrane sealing the left eye was removed with watchmaker's forceps. The left eye was then gently lifted from its socket with two pairs of watchmaker's forceps (Fig. 3.2). The exposed optic nerve was crushed with forceps behind the eyeball at a distance at which the ophthalmic artery runs parallel to the nerve and was thus spared from the crush. A translucent stripe across the otherwise whitish optic nerve at the site where the forceps had been applied indicated a successful crush of the nerve. Fish were revived by gently pulling them through aquarium water. Fish were observed for 2 hours following the operation and checked daily until tissue extraction at 7 days post lesion. Survival rates approached 100%.
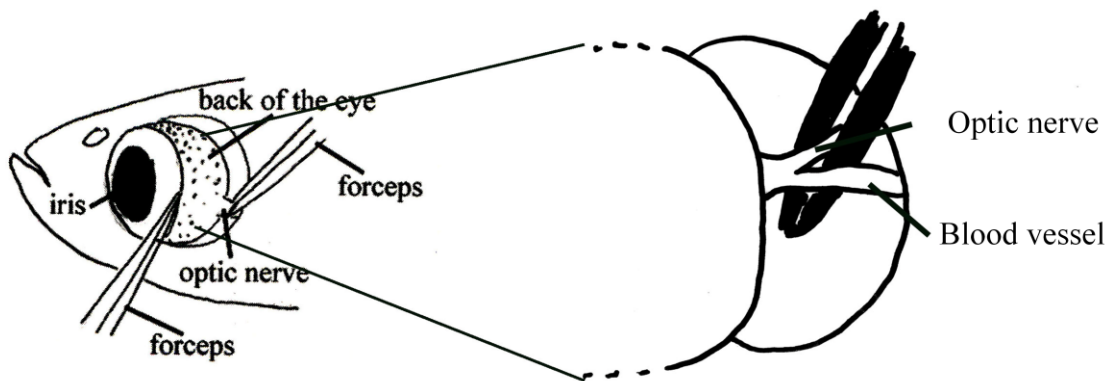
Fig. 3.2. Schematic of optic nerve crush.
Following removal of the mucus membrane, the eye is gently lifted from its socket with two pairs of watchmaker's forceps. The exposed optic nerve is crushed with forceps behind the eyeball at a distance at which the ophthalmic artery runs parallel to the nerve. Adapted from Liu and Londraville, 2003.

3.3.3 Tissue extraction

At 7 days post lesion the operated fish were terminally anaesthetised in 0.1% MS222. The left eye was lifted from its socket with watchmaker's forceps and the optic nerve severed with surgical scissors. The eye was then placed in a petri dish containing phosphate buffered saline (PBS). Using a razorblade and watchmaker's forceps the cornea was pierced to relieve internal pressure and then a window cut in the cornea. The lens was removed through this opening and the eye was then divided into thirds by cutting from dorsal to ventral. The orientation of the eye was judged by an area of dark pigment on the dorsal extent of the eye. The middle third was discarded to leave a nasal third and a temporal third. The nasal and temporal thirds were then carefully teased apart to separate the retina from the rest of the eye (Fig. 3.3). The amount of non-retinal tissue included in the sample was kept to a minimum but could not be completely eliminated. The retinal layers separated from the nasal and temporal eye thirds were then separately flash frozen in 1.5ml reaction tubes immersed in liquid nitrogen. The same procedure was then carried out for the right (control) eye, giving 4 samples: Nasal Lesioned, Temporal Lesioned, Nasal Control and Temporal Control (see Figure 3.3). The retinas of 10 fish were pooled for each sample which were then sent to Miltenyi Biotec for RNA extraction and running on a microarray.

Fig. 3.3. Schematic of retinal tissue sample isolation and sample pairings.
Following the post-mortem removal of the left (lesioned) eye from the fish and extraction of the lens from the eye, the eye was cut into (approximately) thirds as indicated. The central third was discarded. The remaining outer thirds were then carefully teased apart to separate the retina from the rest of the eye. The retinal layers separated from the nasal and temporal eye thirds were then separately flash frozen in 1.5ml reaction tubes immersed in liquid nitrogen. The same procedure was then carried out for the right (control) eye, giving 4 samples: Nasal Lesioned, Temporal Lesioned, Nasal Control and Temporal Control. The array data for these samples were compared pairwise as indicated. Nasal versus Temporal reveals spatial regulation (fold difference). Control versus Lesion reveals temporal regulation (fold change). Red dots on left optic nerve indicate approximate location of crush lesion.

3.3.4 Microarray

The microarray was a standard Agilent Whole Zebrafish Genome Oligo Microarray 4x44K oligonucleotide expression array. I designed 60 probes for 30 genes of interest from the literature, which were not already included, using the e-Array application. Two probes were designed per gene in non-overlapping stretches of sequence to provide robustness against sequence errors or unknown splice sites. The microarray consists of 44,000 features each containing picomoles of a different DNA probe (in this case 60 base long oligonucleotides). Probes are generally targeted to the last 900 bases of mRNA sequence, as these are the most faithfully amplified when producing cDNA with polyT primers. The single microarray consists of four chips which allow four separate biological samples to be run on 44,000 probes (or, in this case, 22,000 probes each performed in technical intra-microarray duplicate). This allows all four of our samples to be run on the same microarray. This type of array is a single channel array which uses a single fluorophore to provide an indication of relative levels of gene expression between different samples. It does not give an absolute readout of gene expression levels as each unique RNA sequence will not amplify at a uniform rate. Expression levels can be compared between the same RNA sequence in different samples but not different RNA sequences within the same sample. Thus allowing us to compare gene expression between our four samples. The microarray was processed by Miltenyi Biotec.

Seven days after unilateral optic nerve lesion, the retinas of ten adult wild type fish were surgically dissected and processed to give four pooled samples: left (lesioned) eye nasal retina, left (lesioned) temporal retina, right (control) eye nasal retina, right (control) eye temporal retina. RNA was isolated from our frozen tissue samples by Miltenyi Biotec using a standard RNA extraction protocol (Chomczynski and Sacchi, 1987). RNA quality and concentrations were then assessed by Miltenyi Biotec using the Agilent 2100 Bioanalyzer platform (Agilent Technologies) (Mueller et al, 2000). The RNA chips contain an interconnected set of microchannels that is used for separation of nucleic acid fragments based on their size as they are driven through it electrophoretically. These results are visualized in a gel image and an electropherogram. The Agilent 2100 Bioanalyzer expert software generates an RNA Integrity Number (RIN) as a measure of overall integrity quality of the total RNA samples. The RIN is calculated based on several parameters including 28S RNA/18S RNA peak area ratios and unexpected 5S RNA peaks. RINs range from 1 to 10, with 10 being the highest quality and anything greater than 6

being considered as sufficient quality for gene expression profiling experiments (Fleige et al, 2006). Cy3-labelled cRNA was then generated by Miltenyi Biotec from 1 µg of each total RNA sample using the Agilent Low RNA Input Linear Amp Kit (Agilent Technologies). cRNA yields and dye incorporation rates were measured by Miltenyi Biotec using the Nanodrop ND-1000 Spectrophotometer (Nanodrop Technologies). Each sample was hybridised on the standard Agilent zebrafish oligonucleotide expression array by Miltenyi Biotec. Hybridisation onto the Agilent 60mer oligo microarray was carried out according to the Agilent Gene Expression Hybridisation kit. 1.65 µg of Cy3-labelled fragmented cRNA in hybridisation buffer was hybridised for 17 hours at 65°C onto the array. The array was washed once with 6xSSPE buffer containing 0.005% N-lauroylsarcosamine for 1 minute at room temperature. This was followed by a wash with 0.06xSSPE buffer containing 0.005% N-lauroylsarcosine for 1 minute at 37°C, followed by a final wash with acetonitrile for 30 seconds.

The hybridised array was then scanned with an Agilent Microarray Scanner System (Agilent Technologies) by Miltenyi Biotec. The scanned images were then processed using Agilent Feature Extraction Software (FES) which determines feature intensities, rejects outliers and calculates statistical confidences. Differential gene expression data generated by FES was analysed using Rosetta Resolver gene expression data analysis system (Rosetta Biosoftware) by Miltenyi Biotec. This allowed the comparison of single intensity profiles against each other to generate gene regulation ratios between samples. The p-values generated by this process refer to the technical replicates and are not biologically significant. This is because, although 10 fish were pooled per sample, each sample is a single biological sample which was carried out on a single array in technical duplicate. The comparison of signal intensities in the 4 samples allows a comparison of fold change of gene expression following lesion and fold difference between opposing extents of the retina. Miltenyi Biotec then visualised the data in scatter plots of signal intensities for each sample comparison. The annotation of the array was incomplete and non-standardised so automated gene ontology software could not be used. The genes with the most pronounced fold changes (both positive and negative) following lesion were manually annotated. Indicator genes which had already been proven to have specific patterns of regulation in the adult retina during regeneration were selected from the literature. These indicator genes were used to gauge the array's biological validity by comparing their known regulation patterns to the fold changes obtained from the array for these specific genes. From the list of annotated genes,

candidate genes which are differentially regulated during regeneration were selected. Particular focus was given to genes for cell surface molecules which are likely to be receptors for axon guidance molecules, upstream transcription factors and downstream signalling molecules which may be involved in transduction guidance signals, and molecules related to those which have an axon guidance role in development.

3.3.5 In situ hybridisation

3.3.5.1 cDNA

RNA was extracted from pooled tissue of 15 larvae per time point using the RNeasy Mini Kit (Qiagen, UK). Reverse transcription, using random primers (Promega, Madison, WI, USA), was performed with the SuperScript III kit (Invitrogen, UK). The Nanodrop ND-1000 Spectrophotometer (Nanodrop Technologies, USA) was used to check concentrations and give an approximation of quality. For probe making templates, RNA was also extracted and processed from adult brain (1 brain) and adult retinas (2 whole retinas or 5 retinal thirds) in the same manner as for embryos.

3.3.5.2 Probe making

Primers for probe making were designed using Primer3 (http://frodo.wi.mit.edu/primer3/) and synthesized by VHBio (VHBio.co.uk). The sequences for primers used for in situ hybridisation probe making can be found in Table 3.1.

Gene	Direction	Sequence
FOXI1	Forward	5'- ACTGCGACTCCAACTTCAGC -3'
	Reverse	5'- GTGTTGAGATGGCCTGGTTC -3'
FGA	Forward	5'- CGTTGAAGGATGTGTTGGTG -3'
	Reverse	5'- AGCTCCACCCTCAGAAGAC -3'
FOXDI-Like	Forward	5'- TTCCGTGCCGACAGTAATCC -3'
	Reverse	5'- GTGGCAATGTTCACCATTCAGC -3'
PLXDC2-Like	Forward	5'- TGTTCACATCCAAGCCAGAG -3'
	Reverse	5'- TGTTCACATCCAAGCCAGAGG -3'
DLX2A	Forward	5'- TGGCTTACATCTGTCGTTGG -3'
	Reverse	5'- AGTGGCAGAGATGTTCATTC GG -3'
HOXC5A	Forward	5'- GTCCAATTACGCGTACGAAGG -3'
	Reverse	5'- ATACGTCTGCGACGTGTGAG -3'
HOXB1A	Forward	5'- AGGCTGGATACCACCACTTG -3'
	Reverse	5'- CTCGCGTCAGATACTTGCTG -3'
HOXA3A	Forward	5'- CGTGTCTTCTCTCACCGTAGG -3'
	Reverse	5'- GGAGTGGCTGTACCAGTTCC -3'
RGMB	Forward	5'- AGC AGG ATC TTA CTA CCC CGG -3'
	Reverse	5'- TGT CCC TCC TGG TCA ATG C -3'
RGMA	Forward	5'- AAA GGA GCA GGA CCA TCG G -3'
	Reverse	5'- CTC TGC TGC TCG TGC CTT AA -3'
FGF3	Forward	5'- GCTTCTTGGATCCGAGTTTGG -3'
	Reverse	5'- GGAAGAGGGAAGCTTTGTCC -3'
FGF4	Forward	5'- TGCGTGGCTAGGATACACAG -3'
	Reverse	5'- GTCTTCCACCTCGCAAAGAG -3'
PDX1	Forward	5'- CAAGGACTCTTGTGCCTTCC -3'
	Reverse	5'- TGATGTGTCTCTCGGTGAGG -3'
HSF2	Forward	5'- TGAAACACAGCTCGAACGTC -3'
	Reverse	5'- TCATCTCCAGGGACTCATCC -3'
FOXG1A	Forward	5'- CACAGAACGGTGCACGAAGA -3'
	Reverse	5'- CTGGGAGGTCATGGATGGG -3'
FOXD1	Forward	5'- AGACTGGACACGGAACGTGAG -3'
	Reverse	5'- GAAGGAAGGCCGACTTGGAC -3'
EPHA4B	Forward	5'- CCATCCCAACATCATCCGAC -3'
	Reverse	5'- ATAGGGACCGTGGTGGGAG -3'

Table 3.1. Sequences for primers used for in situ hybridisation probe making.

3.3.5.3 Reverse transcription polymerase chain reaction

Reverse Transcription Polymerase Chain Reaction (RT-PCR) was carried out on an MJ Mini, Personal thermal cycler (BioRad).

Reaction assembly, as optimised based on manufacturer's recommendations:

21.5µl H_2O

3 µl Thermo Polymerase buffer (NEB)

ThermoPol Buffer (20 mM Tris-HCl, 10 mM (NH4)2SO4, 10 mM KCl, 2 mM MgSO4, 0.1 % Triton X-100, pH 8.8)

2 µl dNTPs (10mM ATP, 10mM CTP, 10mM GTP and 10mM UTP in H_2O)

1 µl cDNA (50-100 ng/ µl)

0.5 µl Taq Polymerase enzyme (5 units per µl)

2 µl primer pair (10 µM forward and 10µM reverse primer in H_2O)

The program used was as follows:

Initial denaturation	95°C	5 minutes
Denaturation	95°C	30 seconds
Annealing	Varies°C	45 seconds
Elongation	72°C	90 seconds
Final elongation	72°C	5 minutes

The elongation step was increased for longer amplicons and decreased for shorter amplicons, based on the estimate of 60 seconds elongation required for every 1000 bases of amplicon. Following PCR, the amplicons were purified from the reaction mixture using the MinElute PCR Purification kit (Qiagen).

3.3.5.4 Ligation into vector

The purified amplicon was then ligated into the pGEM-T Easy vector using the pGEM-T Easy kit (Promega, Madison) as per manufacturer's instructions.

5 µl 2X Rapid ligation buffer, T4 DNA Ligase

1 µl pGEM-T Easy Vector (50ng)

3 µl PCR product (Varies depending on concentration and length of amplicon as per Promega optimisation calculation)

1 µl T4 DNA Ligase (3 Weiss units / µl)

10 µl H_2O

After mixing thoroughly, the mix was left at 4°C overnight.

Following ligation, an aliquot was directly used for transformation in *E.coli*.

3.3.5.5 Plasmid transformation into bacteria

The plasmids were then used to transform *E.coli* XL blue cells. 3µl of ligation mixture was added to 200µl of frozen XL blue suspension. After 30 minutes on ice, the mixture was heated to 42°C for precisely 30 seconds to induce uptake of the plasmid. After a further 5 minutes on ice, 250µl of LB medium (13 capsules per 500ml water, Fisher) was added to the bacteria suspension which was then shaken for 1 hour at 37°C. The bacteria were spread onto 0.1% ampicillin agar plates and incubated overnight at 37°C. Bacteria which did not contain vectors would lack ampicillin resistance and fail to multiply.

3.3.5.6 Colony PCR

To ascertain if any colonies which developed overnight contained the correct insert, colony PCR was used. This involved RT-PCR (as above) with the exception that a colony picked from a plate was used as the template in place of cDNA. The colony was briefly dipped into the PCR mix and then wiped into a grid square on a fresh 0.1% ampicillin agar plate. Each square of the grid corresponded to a separate PCR tube. The primers used to amplify the insert were the same ones used to generate the amplicon for the insert. Primers for the T7 and SP6 sites contained in the vector (flanking the multiple insertion site) could also be used. The reaction product was ran on a 1% agar gel with ethidium bromide (7µl per 100ml) to determine if the amplicon was of the

expected size before proceeding to create a midi preparation from colonies of the corresponding grid square. One colony was selected and incubated overnight at 37°C in 50ml of LB medium with 50µg/ml ampicillin whilst shaking. The midi preparation was then purified using the HiSpeed Plasmid Midi kit (Qiagen). After checking the concentration of the purified plasmid was in a suitable range (200 to 600 ng/µl) with the Nanodrop, a sample was sequenced by DNASeq at the University of Dundee. If a midi purification was found to have a concentration lower than 200ng/µl it was usually an indication of reduced quality and so advisable to repeat the midi step. Following verification of the sequence against the Ensembl sequence using DNAman software, a sample of the purified plasmid was linearised using a suitable restriction endonuclease (NEB) and following NEB guidelines. The number of units of enzyme used was calculated as the minimum number of units indicated in the NEB catalogue to digest the weight of plasmid during an overnight incubation plus an additional 50% to ensure complete linearisation. Enzymes with star activity were avoided. Linearised plasmid was then ran on a gel alongside a sample of unlinearised plasmid to verify complete linearisation. The linearisation mixture was then purified using QIAQuick kit (Qiagen). Using the MAXIscript kit (Ambion), the purified linearisation was used as template to synthesise a digoxygenin labelled RNA probe. Sense probes were also made to be used as controls.

3.3.5.7 In situ hybridisation on cryosections

For in situ hybridisation, the eyes and brain of 7 days post lesion (dpl) fish were removed intact and embedded in TissueTek (Fisher) in electron microscopy molds. They were then flash frozen by 30 second immersion in a 50ml plastic tube containing 2-methylbutane chilled by liquid nitrogen before transferring to –80°C for storage. The same process was carried out for the embedding of whole embryos (3 to 5 dpf). In situ hybridisation was performed on cryosections of whole embryos, adult eyes and adult brain. The frozen blocks of TissueTek containing the tissue were cut into 14µm sections on a Leica CM3050 cryostat. The embryos and brains were cut either coronally, parasagittally or horizontally. The eyes were mounted to give nasotemporal sections with each section containing both the lesion and control eye side by side. The cryosections were thawmounted onto Superfrost glass slides (VWR) and placed in a slide rack immersed in 4% paraformaldehyde (in PBS) overnight at 4°C to fix the tissue. Approximately 40 adult eye sections were mounted onto each slide, along with 10 whole embryo sections. This

protocol was carried out under RNase free conditions, including the use of filter pipette tips and nuclease free water. The next steps permeabilised the tissue. The slides were washed 3 times for 10 minutes in 1xPBS, then placed in 70% ethanol for 10 minutes. Followed by rinsing in deionised water for 10 minutes twice. They were then placed into 0.1M HCl for 10 minutes and washed in 1xPBS for 10 minutes twice. Racks were placed in 0.1M triethanolamine immediately after adding 0.25% acetic acid anhydride (0.5ml added to 200ml) for 20 minutes. Slides were then washed in 1xPBS for 5 minutes twice. Followed by dehydration in an ascending ethanol gradient; 5 minutes each in 70%, 80% and then 95% ethanol. Slides were removed from the racks and left until dry (30 to 60 minutes). The area of slide containing sections was encircled with PAP-Pen (VWR) and slides were placed into an incubation chamber lined with tissue paper soaked in a 1:1 formamide and PBS solution to reduce evaporation. 600μl of 1:1 formamide and hybridisation mix solution (see solutions) was pipetted onto each slide, covering all sections. Prehybridisation took place for 3 hours at 37°C. Following prehybridisation, the prehybridisation mix was pipetted off and quickly replaced with 200μl of hybridisation mix containing 1:500 DIG-labelled RNA probe. Incubation chamber was then sealed with Parafilm (Fisher) and sections were hybridised at 55°C overnight. After pouring off hybridisation mix, slides were put into racks in prewarmed 0.2x saline sodium citrate buffer (SSC) at 55°C for 30 minutes twice, followed by washing in prewarmed 0.1xSSC / formamide (1:1) at 55°C for 90 minutes thrice. Slides were then returned to room temperature and washed with 0.2xSSC for 10 minutes. Following a 10 minute equilibration in buffer 1, the slides were then blocked for 30-60 minutes in buffer 2. The borders of the slides were then dried using tissue paper and the PAP-Pen boundary was re-applied around the slides. The slides were then placed in an incubation chamber lined with tissue paper soaked in buffer 2. 500μl of anti-DIG-alkaline phosphatase coupled antibody diluted in buffer 2 (1:2000) was then quickly pipetted onto each slide before the sections dried. The chamber was sealed with parafilm and left at 4°C overnight to incubate. Following incubation, sections were washed in buffer 1 for 15 minutes twice and then placed into an incubation chamber lined with tissue paper soaked in buffer 1. 400μl of NBT/BCIP staining solution (Sigma) was then pipetted onto the slides for 5 minutes. The NBT/BCIP solution was then removed, having buffered the pH of the slides, and replaced by fresh NBT/BCIP solution which was left in the dark to develop the colour reaction. Length of development varied from 30 minutes to 3 days depending on the probe. After the signal was

sufficiently developed, the slides were washed in 1xPBS for 10 minutes twice. The slides were coverslipped with elvanol (Carl Roth).

3.3.5.7.1 Cryosection in situ hybridisation solutions

10 x PBS - Phosphate buffered saline
160g NaCl (MW: 58.44)
28.39g Na_2HPO_4 (MW: 141.96)
4g KCl (MW: 74.56)
4.8g KH_2PO_4 (MW: 136.09)
Make up to 2L with filtered H_2O water
For 1xPBS of pH7.4

20XSSC - Saline sodium citrate buffer
175.32g NaCl (MW: 58.44)
77.42g Trisodium citrate $Na_3C_6H_5O_7$ (MW: 258.06)
Make up to 1L with filtered H_2O

4 % PFA - Paraformaldehyde
16g PFA powder
80ml filtered H_2O
Stir while heating (keeping below 60°C)
Add 4 drops of 1M NaOH
Once clear add 40ml 10XPBS
Bring up to 400ml with filtered H_2O
Filter PFA
Adjust to pH7.4 if required

10 x Grundmix
2 ml 1 M Tris/HCl pH 7.5
200 Xl 0.5 M EDTA

2 ml 50X Denhardt´s solution (Sigma D 9905)

2 ml tRNA 25 mg/ml (Boehringer, Yeast tRNA 109525)

1 ml poly A RNA 10 mg/ml (Sigma P 9403)

2.8 ml nuclease free H_2O

Store at –20 °C

Hybridisation mix

25 ml deionized formamide

5 ml 10x Grundmix

3.3 ml 5M NaCl

2.5 ml 2M DTT

10 ml dextran sulfate

4.7 ml nuclease free H_2O

Buffer 1

100 mM Trizma Base

150 mM NaCl

Adjust to pH 7.5

Modified buffer 2

1 % Blocking Reagent (Roche Diagnostics, Mannheim, Germany)

0.5 % BSA, Fraction V

Heat to 60 °C while stirring until blocking reagent dissolves

Store at –20 °

Staining solution

BCIP / NBT Staining tablets (SigmaFast, B-5655) in 10ml ddH_2O

Blocking buffer

1% (weight/volume) Blocking Reagent

0.5% (weight/volume) BSA in Buffer 1

3.3.5.8 Whole mount embryo in situ hybridisation

For fixation of specimens, firstly 24hpf embryos were dechorionated with watchmaker forceps in PBS in a small petri dish. The PBS was replaced with 4% paraformaldehyde in PBS, pH7.2 and the dishes wrapped with parafilm and left overnight at 4°C. The following day embryos were transferred into 1.5ml eppendorf tubes and washed four times with PBS/0.1% Tween (PBST) for 5 minutes per wash at room temperature (RT). For each wash 1ml of solution is used unless specified otherwise. The PBST was replaced with 100% methanol for 5 minutes at RT and then 100% methanol again for a minimum incubation of 30 minutes at -20°C. Embryos were washed in 75%, 50% and then finally 25% methanol/PBST for 5 minutes at RT (all following steps are at RT unless specified otherwise). The embryos were then washed twice with PBST for 5 minutes. This was followed by digestion with proteinase K (0.7μl proteinase K / 1ml PBST) for 10 minutes (10 minutes for 24hpf embryos, with increased or decreased incubation for older or younger embryos respectively). Then washed twice briefly (~30 seconds) in glycine/PBST (2mg glycine / 1ml PBST). Followed by further fixation in 4% paraformaldehyde in PBS for 20 minutes. Filter pipette tips were used from this point onwards as any RNase introduced from this point on would destroy the probes. The PFA was thoroughly washed out with 4 washes in PBST for 5 minutes. Followed by a 5 minute wash in 300μl whole mount hybridisation buffer. Which was replaced with 400μl whole mount hybridisation buffer for prehybridisation for a minimum of 3 hours minimum at 55°C. Tubes were wrapped with parafilm to reduce evaporation (buffer contains formamide). Prehybridisation reduces non-specific binding of the probe. Towards the end of the prehybridisation step, digoxygenin labelled probes were diluted to 1:1000 in hybridisation buffer and heated to 80°C for 10 minutes to reduce secondary structures which might impair the action of the probe. Probes were then briefly centrifuged and chilled on ice. Prehybridisation solution was removed from the embryos and replaced by probe solution for an overnight hybridisation at 55°C, wrapped in parafilm. Following the overnight incubation, embryos were washed twice for 30 minutes at 55°C with 50% formamide / 50% 2XSSCT. Solutions were preheated to 55°C before adding them to the embryos. Embryos were then washed once in 1XSSCT for 15 minutes at 55°C and twice in 0.2XSSCT for 30 minutes at 55°C. Filter tips are no longer required as the following steps do not contain formamide or free RNA. Samples were then incubated with Boehringer/Roche blocking reagent at RT for 1 hour (400μl per eppendorf). The blocking reagent was then replaced with anti-DIG alkaline phosphatase fab

fragments, diluted to 1:2000 in fresh blocking reagent, and left overnight at 4°C. Before use the fab fragments were spun down to precipitate antibody clumps and only the supernatant used. This reduced non-specific labelling. Following the overnight incubation, the embryos were thoroughly washed with six PBST washes for 20 minutes each at RT. Embryos were then transferred to a 24 well plate to make subsequent development of the stain easier to monitor. An NBT/BCIP tablet was dissolved in 10ml of filtered H_2O and the embryos were equilibrated for 5 minutes in the dark in the resultant solution. This step buffered the pH of the embryos. The solution was then replaced with fresh solution and the embryos were then left in the dark to develop the signal for 30 minutes to 2 days. During this time the progress of development was observed until staining was optimum as judged by the quality of the specific signal compared to the background staining. This process could be slowed or accelerated by adjusting the temperature. Once staining was complete, the embryos were washed three times in PBS for 5 minutes and then cleared in an ascending gradient of glycerol with PBS (30% glycerol, 50% and 70%) for 5 minutes or longer. Embryos were then de-yolked using insect pins (to make them easier to mount successfully) and then mounted in 70% glycerol using vaseline spacers to prevent adhesion flattening the embryo.

3.3.5.8.1 Whole mount in situ hybridisation solutions
PBST
0.1% (by volume) Tween 20 in 1x PBS

SSCT
0.1% (by volume) Tween 20 in 1x SSC

Whole mount hybridisation buffer
5 ml deionized formamide
2.5 ml 20x SSC
10 μl Tween 20
100 μl 100 mg/ml yeast tRNA (109525, Boehringer)
2.38 ml nuclease free H_2O
10 μl 50 mg/ml heparin

All other solutions are the same as for in situ hybridisation on cryosections.

3.3.6 Tracing

Lipophilic tracers, DiI (1,1'-dioctadecyl-3,3,3',3'-tetramethylindocarbocyanine perchlorate, Invitrogen) and DiO (3,3'-dioctadecyloxacarbocyanine perchlorate, Invitrogen), were used to investigate possible errors of pathfinding and targeting in *foxi1*$^{-hi3747}$ mutant embryos (Nissen et al., 2003). 3dpf *foxi1*$^{-hi3747}$ mutant embryos were kindly supplied by Judy Peirce and Dr. Bernardo Blanco of the Westerfield laboratory, University of Oregon, immersed in 4% PFA. The embryos were the offspring of a heterozygous cross, as the mutation is homozygous lethal around 6dpf. The homozygous embryos were then sorted from the heterozygous and non-mutant embryos based on the "chinless" phenotype in which homozygous embryos have an underdeveloped hyomandibular and third and fourth branchial arches (Nissen et al., 2003). The heterozygous and non-mutant embryos were processed alongside the homozygous mutants to be used as controls. The embryos were then embedded in 1% low melting point agarose. A pulled glass needle was dipped into a saturated solution of either DiI in ethanol or DiO in chloroform (approximately 50mg per ml). After allowing the dye to crystallise onto the needle, the DiO needle was inserted into the temporal extent of the retina of one eye for 20 seconds using manual manipulation under stereomicroscopic observation. This was then repeated for DiI into the nasal extent of the retina of the same eye. The embryos were then immersed in PBS and incubated overnight at 37°C, allowing the dye sufficient time to diffuse along the axonal membrane. Labelling of the retina thusly results in DiO labelled anterior tectum and DiI labelled posterior tectum so revealing any gross errors of pathfinding or the retinotopic map. After incubation the contralateral eye was removed and the embryos whole mounted, injected side down. Using the empty socket as a window, the optic projection was imaged using a laser scanning confocal microscope (LSM510, Zeiss). Approximately 60 optical sections of 2µm step size were scanned per embryo to capture the entire projection from nerve head to tectum. Other *foxi1*$^{-hi3747}$ mutant embryos were traced with DiI only in one eye and DiO only in the other eye, processed as above and then mounted dorsally, to reveal any potential midline crossing defects.

3.3.7 Quantitative PCR

Retinal quadrants were isolated from 7dpl wild type (WIK) adults and RNA was extracted, as previously described. RNA concentration and purity were assessed using the Nanodrop and the Agilent 2100 Bioanalyzer platform, respectively, as described above. RNA samples were then pooled (intra-quadrant pooling) and cDNA production was performed as above. cDNA concentrations and purity were assessed using the Nanodrop. Any samples of low concentration and purity could be discarded at this stage, but all were found to fall within a suitable range. cDNA samples were then pooled (intra-quadrant pooling) and aliquoted. This gave a large volume of sample for each quadrant which minimised experimental variation and biological variation. Fold changes in cDNA levels were calculated using the delta-delta-Ct method, using *gapdh* and *L24* expression as housekeeping genes (Livak and Schmittgen, 2001). qPCR was performed on a Corbett RotorGene 2000 real time cycler using Roche SYBR Green master mix kit.

Reaction assembly, as modified from manufacturer's recommendations:

12.5 µl SYBR Green Master Mix

7 µl H_2O

3 µl Primer pair (10 µM)

(Volumes are for 1 single reaction)

A master mix was made of these three components which was thoroughly mixed by pipetting. 22.5 µl of the mix was aliquoted into 200 µl micro eppendorf tubes, to which 2.5 µl cDNA was added. The dilution of the cDNA was 1/40 of the stock, as determined by running a dilution series of 1/5 to 1/80 to establish amplification efficiency. An efficiency value of greater than 0.6 was considered acceptable as efficiency was adjusted for using the qBase application v1.3.5 (BioGazelle) to calculate fold change based on two housekeeping genes for increased validity.

The program used was as follows:

Initial denaturation   95°C   10 minutes

Denaturation   95°C   15 seconds

Annealing   58.5°C 20 seconds

Elongation   72°C   20 seconds

Final elongation   72°C rising to 95°C over 10 minutes

with stepwise denaturation

Primers for qPCR were designed using Primer3 (http://frodo.wi.mit.edu/primer3/) and Roche ProbeFinder for the Zebrafish Universal ProbeLibrary (http://www.universalprobelibrary.com). They were synthesized by VHBio (VHBio.co.uk). Primers were designed to amplify a sequence of 100 to 150 bases in length. In some cases the length had to be greater than 150 bases to allow for optimum primer binding. Primers were designed to span an intron when possible to minimise the risk of amplification of contaminant genomic DNA. All PCR reactions gave amplicons of the expected size and all minus reverse transcription controls were negative (until 45 cycles). *Gapdh* and *L24* were selected as housekeeping genes as they are generally accepted as good housekeeping genes (Veldman et al., 2007).

Primer sequences of housekeeping genes:

GAPDH, 5'-ATGACCCCTCCAGCATGA-3' and 5'-GGCGGTGTAGGCATGAAC-3'.
L24, 5'-TGAGGAGGTGTCGAAGAAGC-3' and 5'-GCACTTCAGGCTTCTGGTTC-3'.

Primer sequences of genes of interest:

FOXD1L, 5'- AAAGCCTATGGCACTGGTGA -3' and 5'- CGAACAGATGCGGGAGAG -3'.
FOXG1A, 5'- CCACTTCTAGGGCAAAGCTG -3' and 5'- GATGGTGAAGCGAGAGGAAC -3'.
SOHO, 5'- AGCAAAAGAACAACGGCAAG -3' and 5'- GGTAAGCTGCAAGGAGTTCG -3'.

3.4 Results

3.4.1 Microarray validity

Processing and quality control of the RNA samples was carried out by Miltenyi Biotec using the Agilent 2100 Bioanalyzer (Fig. 3.4). The RNA samples were found to have RIN values between 8.8 and 9.3, with anything greater than 6 being considered as sufficient quality for gene expression profiling experiments (Fleige et al, 2006). cRNA yields and dye incorporation rates of each sample were measured by Miltenyi Biotec using the ND-1000 Spectrophotometer (Nanodrop Technologies) and found to be in a comparable range (Table 3.2). Following hybridisation and scanning of the array, the data was analysed by Miltenyi Biotec and then visualised in scatter plots of signal intensities for each sample comparison (Fig. 3.5). The percentage of probes tested that showed signal intensities that were statistically increased or decreased between samples (p<0.01) was as high as 38% for one of the comparisons, with an average of 28% for all comparisons. This p-value refers to the technical replicates within the microarray and therefore is not a direct indication of biological significance as only a single microarray was performed in technical duplicate. With that caveat, following lesion a similar number of genes are upregulated as are downregulated. This is true for both the nasal (Fig3.5B) and temporal (Fig3.5C) extents of the retina. Temporal retina has more regulated genes (up and down) than nasal (8209 out of 21410 versus 5805 out of 21410). For fold difference (spatial regulation) before lesion we see a similar trend of numbers of up and down regulated genes being quite similar (Fig3.5A). For fold difference following lesion (Fig3.5D), there is an increase in the total number of regulated genes, from 3193 without lesion to 6561 following lesion, with the increase being skewed more to downregulation than upregulation, to give a total downregulation of 3568 versus an upregulation of 2903.
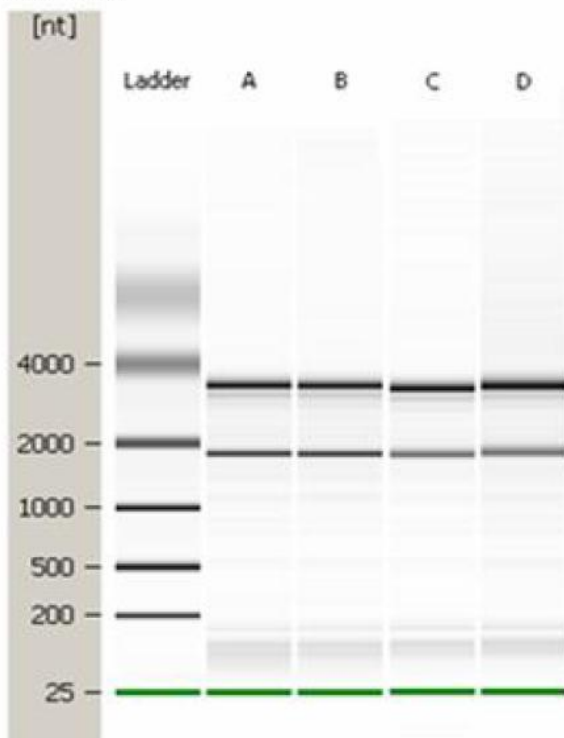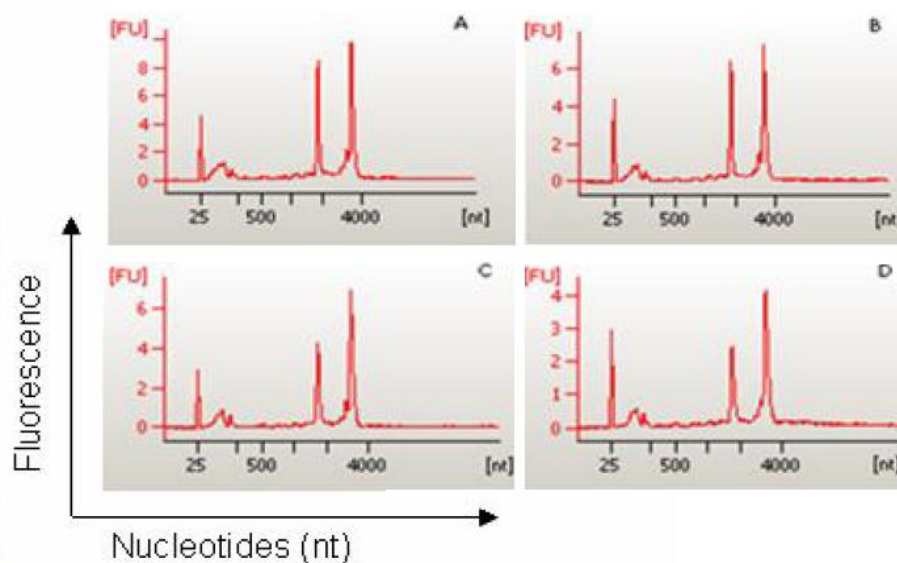
Fig. 3.4. Gel image (A) and electropherogram (B) of total RNA samples. As a reference, the RNA molecular weight ladder (in nucleotides, nt) is shown in the first lane. The lowest migrating green band represents an internal standard. The two prominent peaks within the electropherograms represent ribosomal RNA: left 18S RNA, right 28S RNA. Scaling of the y-axis is done automatically, relative to the strongest signal within a single run. All samples were found to have a RIN greater than 8 and so were satisfactory for microarray processing. Modified from data and images generated by Miltenyi Biotec.

Sample	Labeling	cRNA (ng/µL)	Volume (µL)	Cy3 (pmoL/µL)	Incorporation rate (fmoL/ng)
A	Cy3	262.69	55	3.3	13
B	Cy3	266.61	55	3.78	14
C	Cy3	336.76	55	5.39	16
D	Cy3	239.21	55	3.08	13

Table 3.2. cRNA yield and dye incorporation rates for each sample.
Dye incorporation rates, as measured using the ND-1000 Spectrophotometer
(NanoDrop Technologies), were comparable between the different samples.
Modified from data and images generated by Miltenyi Biotec.

104
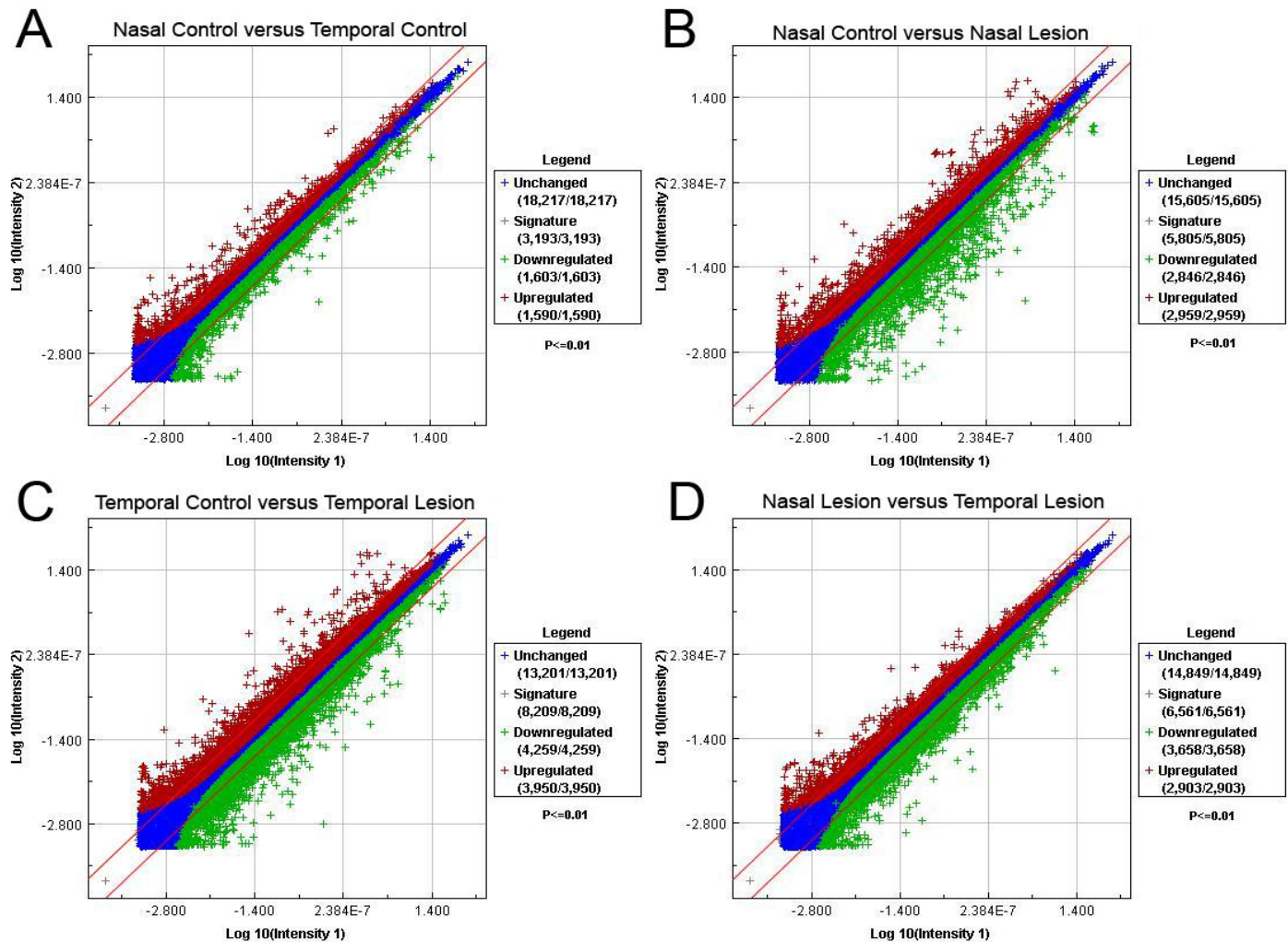
Fig. 3.5. Scatter plot of signal intensities of all spots for all comparisons.

The signal intensities of each feature represented by a dot is shown in double logarithmic scale. X-axis: control-log signal intensity; y-axis: sample-log signal intensity. Red diagonal lines define the areas of 2-fold differential signal intensities.

Blue cross: genes which are not significantly regulated.

Red cross: significantly upregulated genes (technical replicate p-value <0.01).

Green cross: significantly downregulated genes (technical replicate p-value <0.01).

Grey cross in legend: total of significantly up- and downregulated signatures.

A. Nasal Control versus Temporal Control – Spatial fold difference without lesion

B. Nasal Control versus Nasal Lesion – Fold change in the nasal extent of the retina

C. Temporal Control versus Temporal Lesion – Fold change in the temporal extent of the retina

D. Nasal Lesion versus Temporal Lesion – Spatial fold difference with lesion

Following lesion, a similar number of genes are upregulated as are downregulated. This is true for both the nasal (Fig3.5B) and temporal (Fig3.5C) extents of the retina. Temporal retina has more regulated genes (up and down)

105

than nasal (8209 out of 21410 versus 5805 out of 21410). For fold difference (spatial regulation) before lesion we see a similar trend of numbers of up and down regulated genes being quite similar (Fig3.5A). For fold difference following lesion (Fig3.5D), there is an increase in the total number of regulated genes, from 3193 without lesion to 6561 following lesion, with the increase being skewed more to downregulation than upregulation, to give a total downregulation of 3568 versus an upregulation of 2903.

Modified from data and images generated by Miltenyi Biotec.

3.4.1.1 Gene lists

From the raw array data and subsequent analysis, lists of genes were produced which provide varying levels of detail and can be used to follow the process of elimination to arrive at the final candidate genes. These lists are attached as computer files as they contain many hundreds of pages of data. For each list detailed below there are four versions; one for each sample pair comparison.

Single-experiment raw data list

The basic output data from the Agilent Feature Extraction software includes gene lists with the complete raw data sets, referred to as single-experiment raw data list. These are complete gene lists with all raw data.

Single-experiment normalized data list

Signal intensities from the single-experiment raw data lists were normalized by dividing the intensity values by their median. These normalized signal intensities were provided as a common table of single-experiment normalized data list which includes data on whether the signal intensity is positive or negative and if the signal is significantly above background.

Gene ratio list

Using the Resolver software gene ratio lists were generated for all genes compared between sample pairs which includes information on all normalized sample/control log10 ratios and fold changes, sequence descriptions and technical p-values.

Pre-selected candidate gene list

From the gene ratio lists putative candidate genes with a technical p-value <0.01 were pre-selected and summarised in the pre-selected candidate gene list. For each sample pair the preselected candidate list contains approximately 7000 genes, selected from the original 21410 on the array.

3.4.1.2 Indicator genes

Once candidate genes were selected, indicator genes were selected to gauge the biological validity of the array data. Several indicator genes known to have certain patterns of regulation from the literature were compared to the array results for these genes. These analyses largely focused on upregulation following lesion (fold change) as there are many more genes with confirmed upregulation following lesion than those with a confirmed spatial regulation within the retina. Known upregulated genes included *L1.1*, *beta thymosin*, *gap43*, *bmp2b*, *sox11a* and *sox11b* which were all confirmed with an upregulation greater than 2 fold following lesion. *Beta thymosin*, *gap43* and *L1.1* were amongst the most highly regulated genes on the array with 55, 24 and 10 fold change, respectively. To put this in context, only 40 out of 21410 genes had a fold difference greater than 10. However not all indicator genes matched expectations, as *nrp1a* had a fold change of less than two, which is the cut off point recommended by Miltenyi. Widely accepted housekeeping genes (Veldman et al, 2007; McCurley and Callard, 2008) were also used for indicators to detect false positives. *β-actin*, *gapdh*, *L24*, *tbp*, *b2m* and *elfa* all had ratios of less than two fold, indicating lack of regulation. The ratios for these comparisons are what would be expected based on the literature and are therefore in line with the microarray's data being valid.

3.4.2 Candidate genes

The partially annotated data obtained from Miltenyi Biotec, contained comparisons of gene expression between pairs of samples. Depending on which samples were being compared, this gave us a list of fold difference (Nasal versus Temporal retina) or fold change (Control versus Lesion). From these lists of several thousand probes each, a shortlist of candidate genes was selected for further investigation. To arrive at this shortlist we first defined our criteria for selection as follows: It can be expected that many genes involved in regeneration would be

upregulated during regeneration. This information can be obtained from the comparisons of the Nasal Control and the Nasal Lesion samples and the comparison of the Temporal Control and Temporal Lesion samples. However it can also be expected that many of the upregulated genes will be downstream of the genes which initiate and guide regeneration and will have more fundamental, basic roles in growth and repair e.g. producing actin. To narrow the search for more relevant upstream signals, we focussed on cell surface receptors and transcription factors. Interestingly, transcription factors account for up to 20% of the most highly spatially regulated genes on the array, when, in the human genome, transcription factors make up less than 10% of the total genes (Kasowski et al., 2010). Once candidate genes had been selected, their properties were analysed in all four of our sample pair comparisons, but to initially select these genes our main focus was on the spatial regulation following lesion (fold difference of Nasal Lesion versus Temporal Lesion). Spatial regulation of gene expression would indicate a gradient across the retina. If the microarray data indicates more probe binding in Nasal Lesion than Temporal Lesion sample, this indicates higher gene expression in the nasal retina compared to the temporal retina following lesion and we would expect a gradient to exist across the RGC layer of the retina going from nasal high to temporal low. Genes which show spatial regulation following lesion may be involved in axon pathfinding and map formation. Regenerating axons may be repelled or attracted by the molecule which constitutes the gradient and so either turn away from the gradient or grow against the gradient towards higher concentrations. Axon behaviour may be dependent on specific concentration ranges so the low end of a gradient may attract an axon until the concentration increases to the point where it switches to inhibition, thus mapping the axon to a point on the concentration gradient. By focusing on the Nasal Lesion versus Temporal Lesion sample pair we aimed to select genes involved in anterior / posterior mapping onto the tectum. This also increased our chances of finding novel genes or novel functions for genes as this aspect, in comparison to regeneration, has been less studied in microarray studies. From the pre-selected candidate gene list of 7092 probes, we first manually annotated the 100 probes with the greatest positive fold difference (temporal retina expression higher than nasal retina expression) and the 100 probes with the greatest negative fold difference (nasal retina expression higher than temporal retina expression). Each probe was annotated to varying extents, some already had their associated gene name, while others had accession numbers or expressed sequence tag designations which could be searched for in NCBI. Other probes were coded based on third party

databases such as the TIGR Gene Index database (http://compbio.dfci.harvard.edu/tgi/cgi-bin/tgi/gireport.pl?gudb=zfish). A sequence was obtained from these databases which could be BLASTed against the NCBI database to obtain the gene or predicted gene that the probe represents. The final category of annotation was that of Agilent's own probe identifiers. These identifiers correspond to a database of 60mers. These 60mers could then be BLASTed. Once the gene or predicted gene was identified, key properties of the gene were researched, such as possible roles in signal transduction. We sought help from bioinformaticians to automate this process and allow for the use of gene ontology software, but the disparate nature of the existing annotation made the task complex. After 100 genes from the top and 100 genes from the bottom of the list were manually annotated, the next 100 from the top and the next 100 from the bottom were assessed, but not fully annotated. 32 genes were chosen from this short list for further investigation using in situ hybridisation, along with additional genes which are homologues or paralogues of candidate genes but were not selected directly from the array data.

3.4.3 Embryo in situ hybridisation

Of the 34 genes selected for in situ hybridisation, 17 gave distinct mRNA expression patterns in embryos (Table 3.3). These patterns are described in figures 3.6 and 3.7. Four of the candidate genes (*foxi1*, *foxd1-like*, *foxg1a* and *epha4b*) showed expression gradients in the developing retina. These gradients possessed the same polarity as the adult gradients indicated by the array.

Gene	Fold difference	P value	Description	Embryonic expression pattern
FOXI1	22.70273	7.19E-40	Transcription factor	Temporodorsal retina, Otic vesicle, Rostral spinal cord
FGA	20.06361	4.53E-17	Protein bridging	Discrete areas of yolk sac surface
FOXDI-Like	19.5379	6.17E-41	Predicted transcription factor	Temporal retina, Midbrain/chiasm
PLXDC2-Like	19.35315	1.62E-16	Predicted transmembrane protein	Notochord, Midbrain/hindbrain boundary
DLX2A	6.73358	1.77E-09	Transcription factor	Caudal telencephalon, Dorsal diencephalon
HOXC5A	6.47784	0.00001	Transcription factor	Caudal embryo, Spinal cord
HOXB1A	3.92032	0.00005	Transcription factor	Rhombomere
HOXA3A	3.45594	0.00839	Transcription factor	Rhombomere, Gradient in spinal cord rostral high to caudal low
RGMB	1.65077	1.86E-06	NEO1 ligand	Lens, Forebrain
FOXD1	Not significant	Not significant	Transcription factor	Diencephalon/chiasm, Sclerotome (Not in retina)
RGMA	-2.12432	0.00003	NEO1 ligand	Forebrain, Lateral line primordium, Tip of tail, Some cranial ganglia, Differentiated neurones
FGF3	-3.8893	8.38E-08	FGFR ligand	Midbrain/hindbrain boundary, Tip of tail
FGF4	-4.34497	0.00055	Growth factor	Midbrain/hindbrain, Gut, Tip of tail
PDX1	-4.35575	4.87E-12	Transcription factor	Pancreas
HSF2	-4.62179	4.50E-08	Transcription factor	Rostral embryo
FOXG1A	-46.23848	1.95E-43	Transcription factor	Telencephalon, Nasal retina, Cranial ganglia
EPHA4B	Not known on array	Not known on array	Eph receptor	Temporal retina

Table 3.3. Candidate genes which gave distinct expression patterns in 24hpf embryo in situ hybridisation, in order of fold difference.

Contents of the table: The fold difference between nasal lesioned retina and temporal lesioned retina (positive number indicates temporal has higher expression, negative number indicates nasal has higher expression); The p-value of the fold difference indicates that all of the selected genes are technically statistically significant (but does not provide information on biological significance); A basic description of the gene product's molecular function as it relates to our study; A description of the mRNA expression patterns of whole mount 24hpf embryos. Epha4b lacks

associated values as a probe for it is not known to be on the array i.e. array probes may exist for this gene but they are not annotated as such. Epha4b and the genes with fold differences of less than two were studied as they are paralogues or homologues of genes of interest from the array. Genes in red are those that exhibited an expression gradient in the retina and therefore are of interest for their role / potential role in axon guidance during development.

Four of the seventeen genes were expressed as a gradient in the developing retina which is consistent with a role in retinotopic mapping during development; *foxi1*, *foxd1-like*, *foxg1a* and *epha4b*. For the three genes which have microarray data, the direction of the gradient is in agreement. *Foxi1* and *foxd1-like* exhibit temporal high gradients in the in situ hybridisations on embryos and in the adult retina based array data. The same is true for *foxg1a*, with a nasal high gradient. Based on embryo mRNA expression patterns and the array data, *foxd1* lacks a detectable gradient in both embryonic and adult retina. The graded retinal expression pattern of *foxd1-like*, but not *foxd1*, in zebrafish development and regeneration is similar to that of *foxd1* in chick development (Takahashi et al., 2009). Based on the array data, the graded retinal expression pattern of *epha4a* in zebrafish regeneration is similar to that of *epha4* in goldfish regeneration (Rodger et al., 2004). However during the period of development when the optic projection is formed, *epha4b* exhibits a gradient in the retina while *epha4a* does not (Komisarczuk et al., 2008).

A **FOXI1**

B **FGA**

C **FOXD1L** Ch

D **PLXDC2 like**

E **DLX2A** D T

F **HOXC5A**

G **HOXB1** Rh

H **HOXA3A** Rh

I **RGMB** Fb

J **FOXD1** E E

K **RGMA** T M H

L **FGF3**

M **FGF4**

N **PDX1**

O **HSF2**

P **FOXG1A** T

Q **EPHA4B**

R **NEO1**

112

Fig. 3.6. 24 hours post fertilisation whole mount embryos incubated with anti-sense probes show expression patterns of the candidate genes. In order of fold difference.

A. *Foxi1* expression in temporodorsal retina (arrow) and otic vesicle (arrowhead). **B.** *Fga* expression in discrete areas on the surface of the yolk sac (arrows). **C.** *Foxd1-like* expression in temporal retina (arrows) and optic chiasm and surrounding midbrain. **D.** *Plxdc2-like* expression in notochord and midbrain / hindbrain boundary (arrowhead). **E.** *Dlx2a* expression in caudal telencephalon (T) and dorsal diencephalon (D). **F.** *Hoxc5a* expression in the spinal cord (arrow) and caudal embryo. **G.** *Hoxb1* expression in the rhombomere (Rh). **H.** *Hoxa3a* expression in the rhombomere (Rh) and a gradient in spinal cord rostral high (arrow) to caudal low. **I.** *Rgmb* expression in the lens (arrows) and the forebrain (Fb). **J.** *Foxd1* expression in the diencephalon (arrow). **K.** *Rgma* expression in the telencephalon (T), midbrain (M) and hindbrain (H). **L.** *Fgf3* expression in the midbrain/hindbrain boundary (arrow), otic vesicle (arrowhead) and the tip of tail. **M.** *Fgf4* expression in the midbrain/hindbrain boundary (arrow) and the tip of the tail. **N.** *Pdx1* expression in the pancreas. **O.** *Hsf2* expression throughout the rostral embryo. **P.** *Foxg1a* expression in the nasal retina(arrows), telencephalon (T), and cranial ganglia (arrowheads). **Q.** *Epha4b* expression in the temporal retina (arrows). **R.** *Neo1* weak constitutive expression / background labelling only.

Scale bar in G is 200μm. Scale bar in J is 100μm. Scale bar in P for A, K and P is 100μm. Scale bar in N for images D, L, M and N is 200μm. Scale bar in O for images A, B, F, H and O is 200μm. Scale bar in Q for C, E, I and Q is 100μm. Scale bar in R is 100μm.

A, B, D, F- H and L-O: Rostral is left, dorsal is up, viewed from lateral surface.

C, E, I-K and P-R: Rostral is left, viewed from dorsal surface.

E Eye, Tel Telencephalon, Fb Forebrain, M Midbrain, H Hindbrain, Ch Optic Chiasm, Rh Rhombomere.
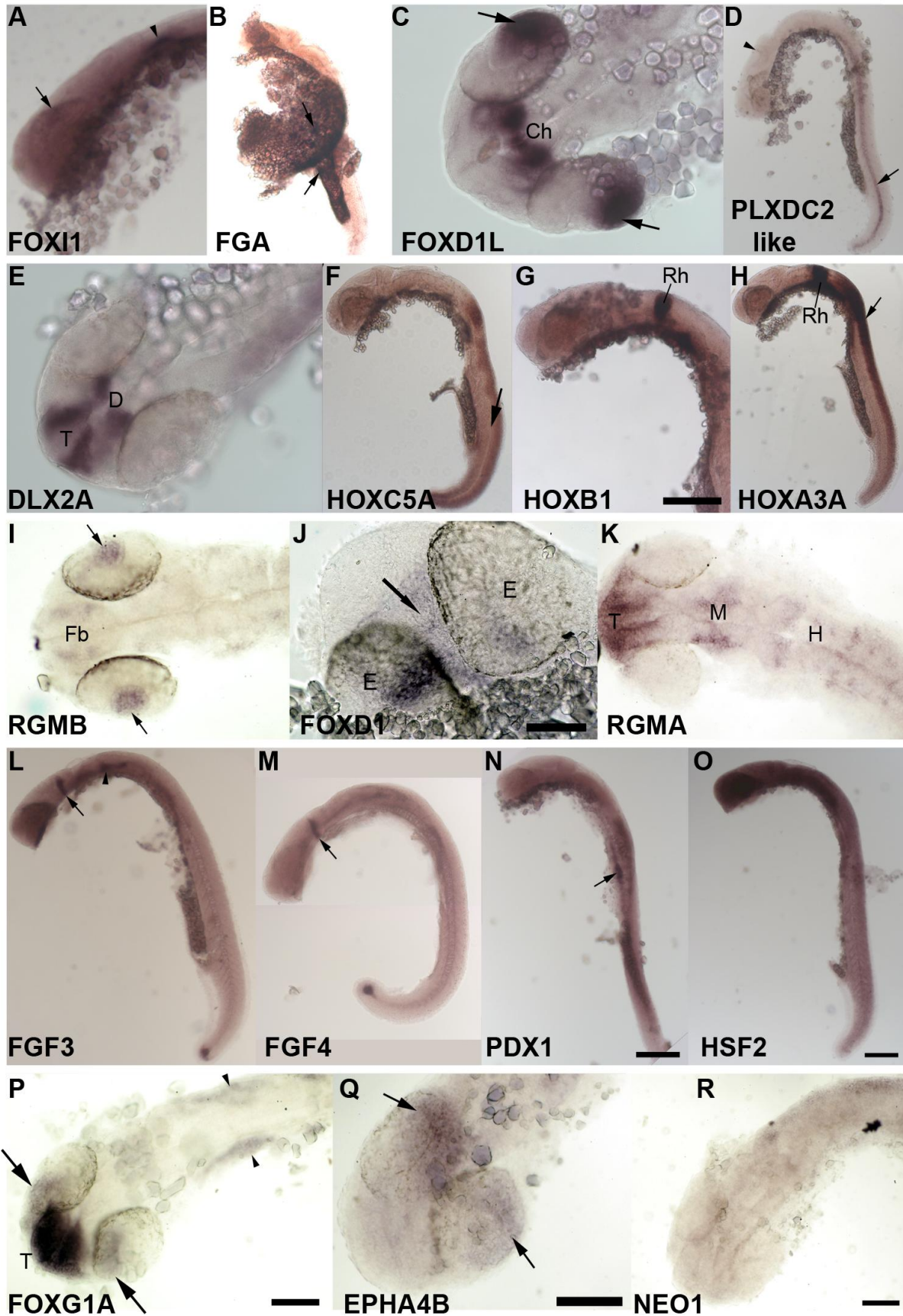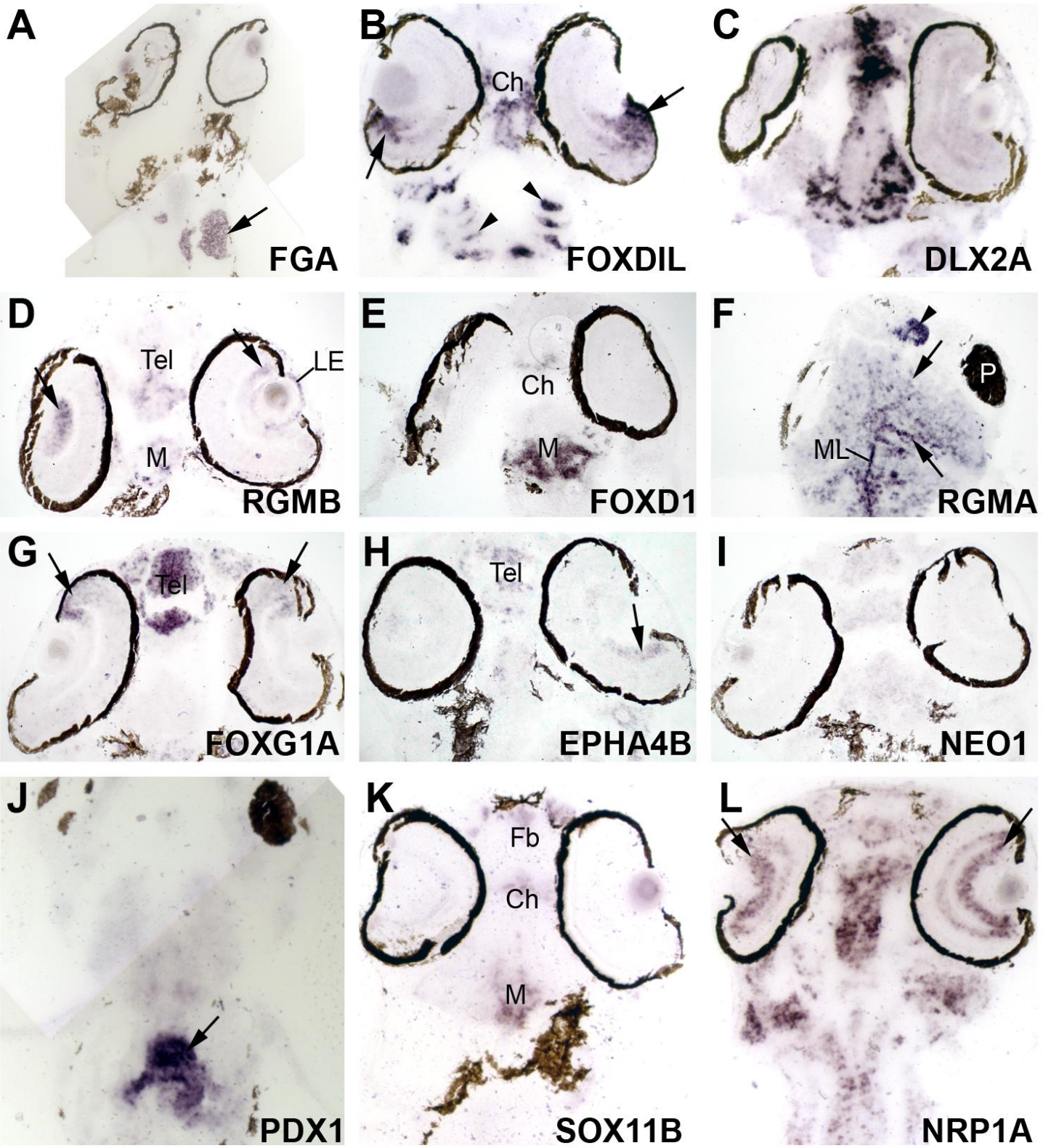
Fig. 3.7. Horizontal cryosections of 3 days post fertilisation embryos incubated with anti-sense probes show expression patterns of the 6 candidate genes and positive controls. These sections were developed on the same slides as the adult retina sections to act as controls for the tissue type. **A.** *Fga* expression in the liver (arrow). **B.** *Foxd1*-like expression in the temporal retina growth zone (arrows), chiasm (Ch) and gill arches (arrowheads). **C.** *Dlx2a* expression in the brain. **D.** *Rgmb* expression in the retinal growth zone ventral to the lens (left arrow) and at the level of the lens (right arrow), the telencephalon (Tel), the midbrain (M) and the lens epithelium (LE). **E.** *Foxd1* expression in the optic chiasm (Ch) and midbrain (M). **F.** *Rgma* graded expression in the tectum, from caudal high (lower arrow) to rostral low (upper arrow). Intense expression in the olfactory epithelium (arrowhead) and the midline of the hindbrain (ML). P is the pigment layer of the eye and is not due to labelling. G. *Foxg1a* graded expression in the nasal retina (arrows) and expression in the telencephalon (Tel) H. *Epha4b* graded expression in the temporal retina (arrow) and expression in the telencephalon (Tel). I. *Neo1* weak constitutive expression / background labelling throughout the brain. J. *Pdx1* expression in the pancreas (arrow). K. *Sox11b* positive control expression in chiasm (Ch), forebrain (Fb) and midbrain (M), particularly along midline. L. *Nrp1a* positive control expression throughout the CNS and particularly in the RGC layer of the retina (arrows).

Horizontal sections. Rostral is up.

T Telencephalon, Fb Forebrain, M Midbrain, H Hindbrain, Ch Optic Chiasm, P Pigment layer of the eye

3.4.4 Adult in situ hybridisation

3.4.4.1 Retina

The embryo analyses indicated which genes have expression patterns which may support a role in axon guidance during development. We next looked at the expression patterns of these genes in adult regeneration to elaborate on the array findings and confirm if these genes are common to both processes or only one. Of the 17 probes which gave distinct mRNA expression patterns in embryos, none were found to give detectable expression patterns in adult retina cryosections. The in situ hybridisations on adult retina cryosections were rigorously controlled. Multiple positive controls were successfully used, examples of which can be seen in Figure 3.8. The controls, *nrp1a*, *sox11a* and *sox11b* show upregulation in the RGC layer of retinas from fish with optic nerve lesions as expected. Cryosections of 3dpf embryos (Fig. 3.7) were processed and developed alongside the adult sections on the same slide, giving clear expression patterns. Based on this evidence, which is discussed below, it is likely that the in situ hybridisation is not sufficiently sensitive to detect the expression patterns of the candidate genes in adult retina cryosections.

3.4.4.2 Brain

In situ hybridisation was performed on cryosections of adult brain for candidate genes which could potentially be expressed in the tectum i.e ligands of receptors expressed by the RGC axons. *Rgma* exhibited an expression gradient in the tectum from caudoventral high to rostrodorsal low, with increased labelling intensity of the ependymal layer (Figure 3.9). *Rgma* was the only gene tested to show a clear expression pattern in the adult tectum.

CONTROL   LESION

SOX11B

A   B

SOX11A

C   D

NRP1A

E   F

FGF3

G   H
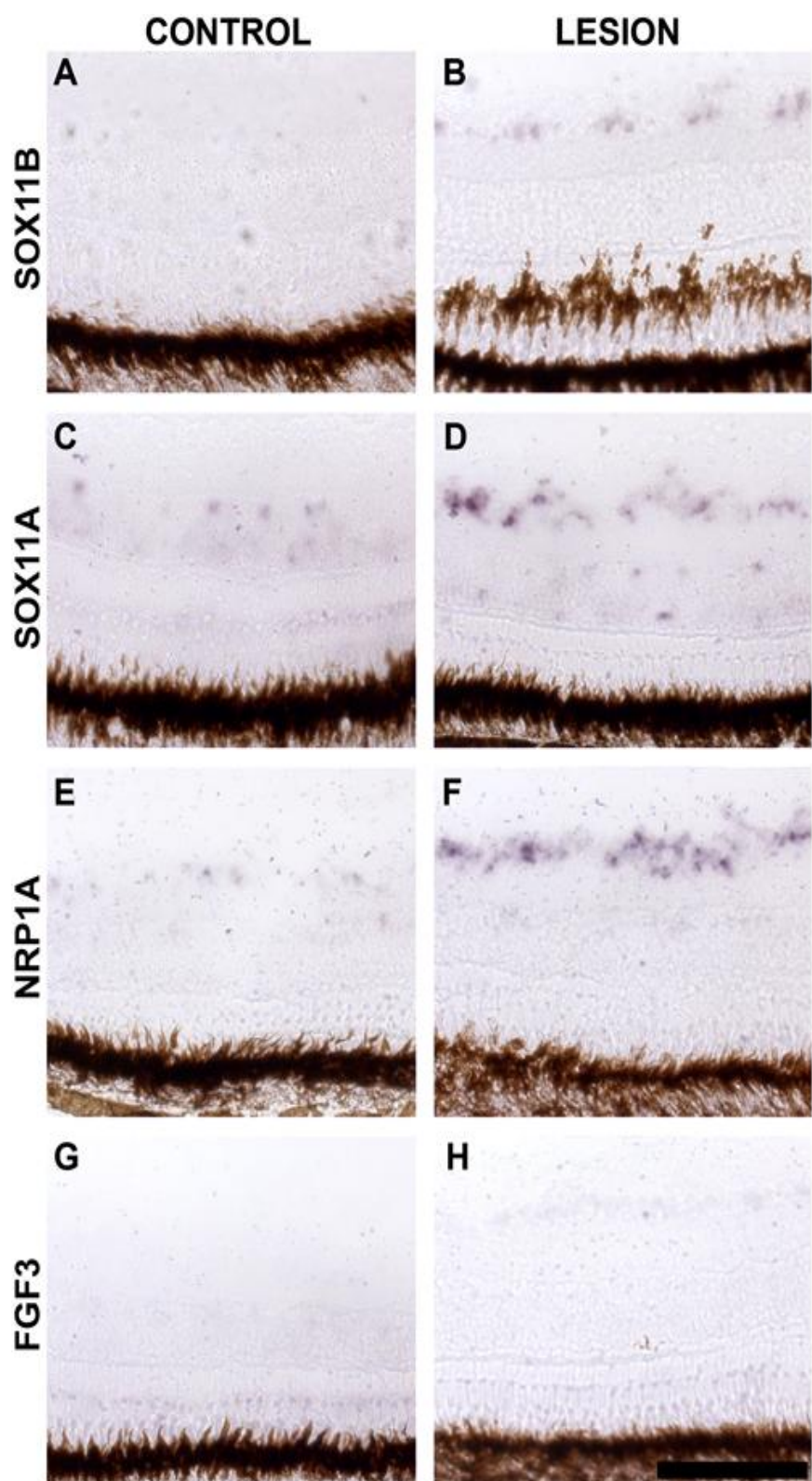
Fig. 3.8. In situ hybridisation on adult retina cryosections. Sections in the lesioned column are from retinas which are 7 days post optic nerve crush. Sections from the control column are from the contralateral eye which did not receive an optic nerve lesion. *Nrp1a*, *sox11a* and *sox11b* are positive controls which have been used previously in the lab. *Nrp1a* and *sox11a* show expression in the RGC layer without lesion. *Nrp1a*, *sox11a* and *sox11b* show clear increases in expression in the RGC layer following lesion. *Fgf3*, one of the candidate genes, shows no clear expression in either situation. *Fgf3* is representative of all the candidate genes.

Scale bar is 100µm.
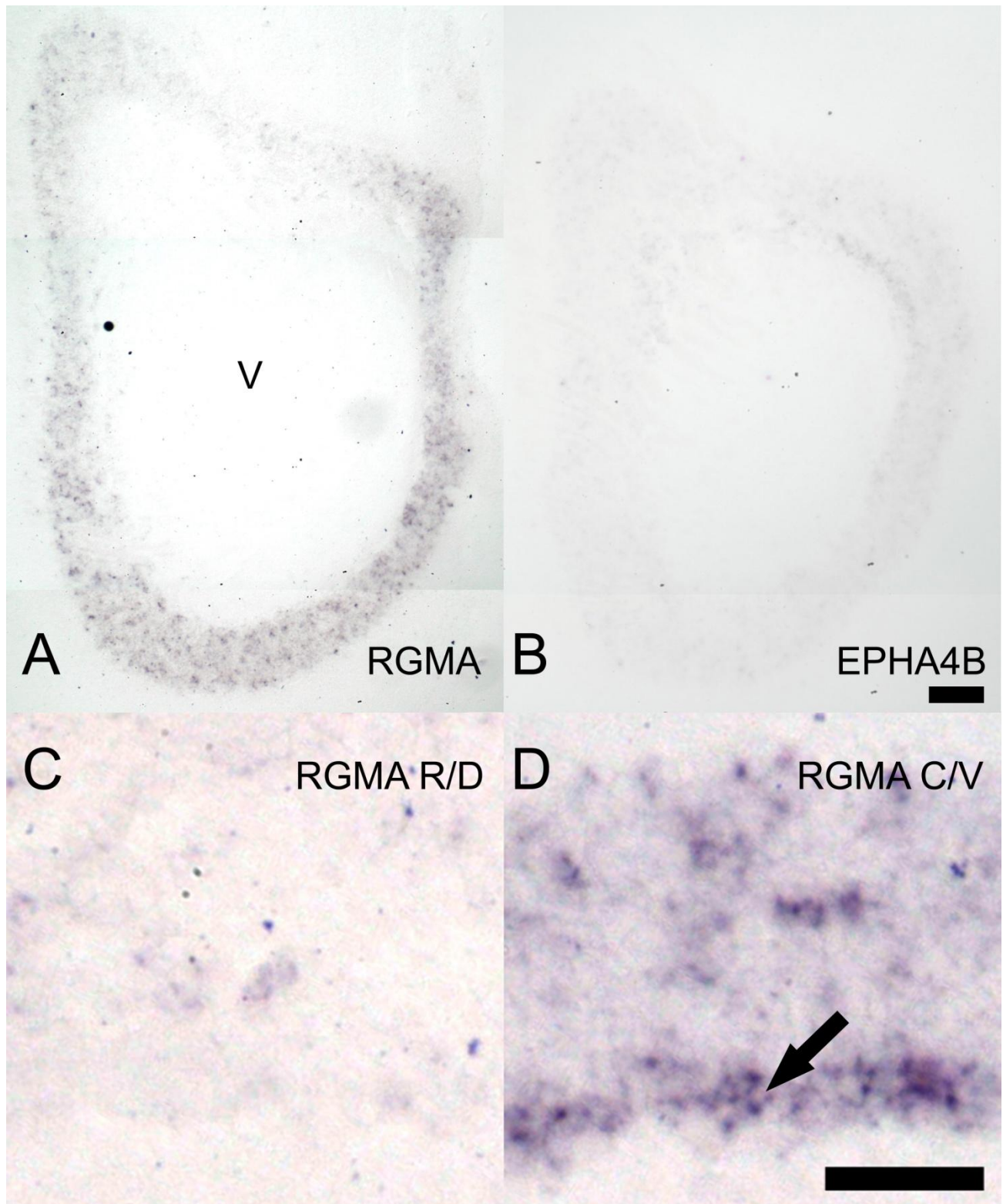
Fig. 3.9. Parasagittal cryosections of the tectum 5 days post left optic nerve crush lesion, incubated with anti-sense probes show graded expression pattern of *rgma*. A. *Rgma* graded expression in the tectum from caudoventral high to rostrodorsal low. V is the tectal ventricle. Caudal is down, dorsal is left. **B.** *Epha4b*,

representative of the candidate genes other than *Rgma*, shows only background staining and is presented as a negative control. **C.** Weak *rgma* expression in the rostrodorsal tectum. Ventricle is down. Caudal is down. **D.** Strong *rgma* expression in the caudoventral tectum showing increased labelling of the ependymal layer (arrow). Ventricle is down. Caudal is up. Scale bar for A and B = 100μm. Scale bar for C and D = 50μm.

3.4.5 qPCR

qPCR was carried out for 12 candidate genes and 2 housekeeping genes, *gapdh* and *L24*. Both of these genes are generally accepted housekeeping genes (Veldman et al., 2007) which have near constant expression in all cells due to their ubiquitous functions. Gapdh is an enzyme that catalyzes the sixth step of glycolysis and L24 is a ribosomal subunit protein. Primers which gave theoretically perfect amplification would result in doubling of amplicon with every cycle and give an efficiency value of 1. An efficiency value of greater than 0.6 was considered acceptable as efficiency was adjusted for using the qBase application to calculate fold change based on 2 housekeeping genes for increased validity. Each gene was run in triplicate for each sample for the concentration optimisation run and then in triplicate within a single test run per gene. The Ct value is the cycle number at which the signal strength, i.e. the amount of amplicon, exceeds a defined threshold. The more template copies present in the sample and the more efficient the amplification, the lower the Ct value. Of the 12 candidate genes chosen for qPCR, 3 gave suitably reproducible results with Cts of replicates within a single cycle of each other (Table 3.4 and Figure 3.10). The others showed very weak or inefficient amplification, resulting in a high Ct value which did not meet stringency cut offs for processing. The delta-delta-Ct method for relative qPCR, whereby product levels for an individual primer pair are compared between samples, produced values for the relative abundance of each gene transcript, normalised against *gapdh* target levels. *Foxg1a* showed higher levels of the target in cDNA derived from the nasal retina, *foxd1-like* showed higher levels of the target in cDNA derived from the temporal retina and *soho* showed no statistically significant differences between samples. Based on the relative abundance values from qPCR, the fold differences and fold changes for these genes between samples were calculated and compared to the values from the microarray (Table 3.5). qPCR confirms the direction and proportion of fold difference found by the array for these 3 candidate genes for all available comparisons. Proportions, rather than levels, are compared as both

methods use relative comparisons between samples, rather than absolute quantitation of target sequence. In the array and qPCR data, *foxg1a* has a high fold difference for Nasal Lesion retina sample (NL) versus Temporal Lesion retina sample (TL) and a high but slightly lower one for Nasal Control retina sample (NC) and Temporal Control retina sample (TC). In the array and qPCR data, *foxd1-like* shows a NL versus TL fold difference which is approximately double that of NC versus TC. *Soho* shows insignificant differences between samples for both the array and qPCR data. Not all conditions can be compared as some genes are not listed for every sample pairing on the array. This is most likely due to a non-significant p-value which may have been contributed to by a low fold difference, as the same probe set was tested for all samples. Miltenyi advised that we should disregard fold differences of less than two due to potential variation introduced in sampling and amplification.

The qPCR was based on cDNA generated from separate biological samples, using different kits and experimenter than the cDNA generated for the array (which was generated by Miltenyi). Despite these differences, and the main difference of a different method (qPCR versus microarray), the results are very similar. When the proportions of the fold differences are compared within each method, it can be seen they are broadly proportional between methods e.g. Based on the qPCR data for *foxg1a* the NL / TL fold difference is 1.2 times the NC / TC fold difference. For the microarray data this relationship is 1.1. Due to the different processes used to arrive at these results it can be expected that they will not match exactly. Given the disparate methods of measuring the same biological property, such broad similarities in the results are a good confirmation that both methods have been successful. However the confirmation of the array as a whole based on the qPCR data should not be overstated, as it based on only 3 genes as only 3 genes investigated for qPCR were found to be suitably reproducible.
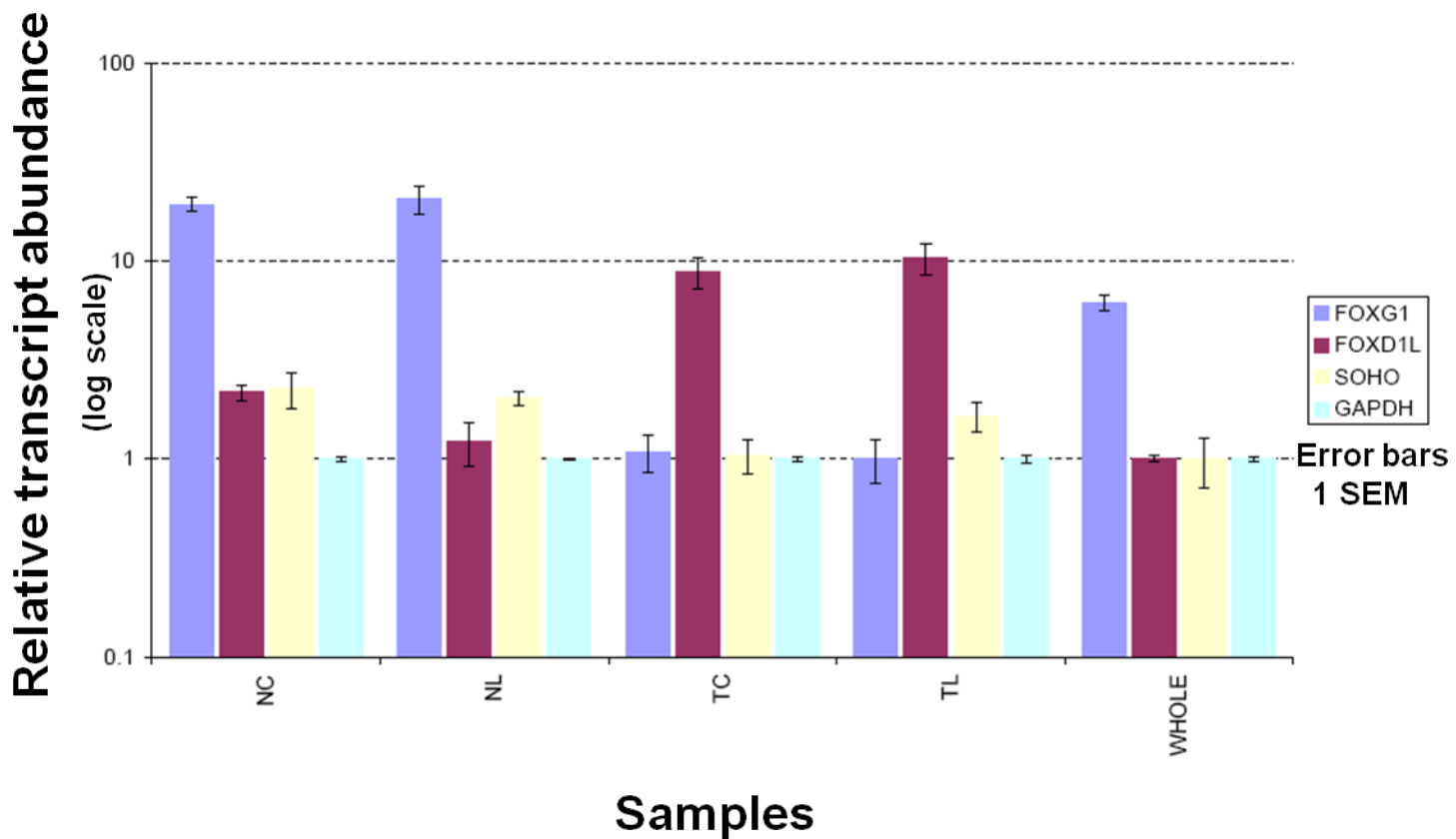
Fig. 3.10. qPCR data for relative abundance of each gene transcript for all samples, normalised against GAPDH.

Foxg1a showed higher levels of the target in cDNA derived from the nasal retina, *foxd1-like* showed higher levels of the target in cDNA derived from the temporal retina and *soho* showed no statistically significant differences between samples.

Each bar represents 3 replicates from within a single run per gene.

NC - Nasal Control, NL – Nasal Lesion, TC – Temporal Control, TL –Temporal Lesion

	FOXG1A		FOXD1L		SOHO	
Sample	qPCR	Microarray	qPCR	Microarray	qPCR	Microarray
NC V TC	-17.5	-41.8	4.1	10.6	-2.3	
NL V TL	-20.5	-46.2	8.7	19.5	-1.2	<±2
NC V NL	1.1		-1.8		-1.2	<±2
TC V TL	-1.1		1.2	<±2	1.7	<±2

Table 3.5. Comparison of measures of fold difference and fold change between samples, derived from qPCR and from microarray. The blank cells are due to no data being present on the array for these comparisons. Microarray data which shows a ratio of less than ±2 is considered as insignificant.

qPCR confirms the direction and proportion of fold difference found by the array for these 3 candidate genes for all available comparisons. In the array and qPCR data, *foxg1a* has a high fold difference for NL versus TL and a high but slightly lower one for NC and TC. In the array and qPCR data, *foxd1-like* shows a NL versus TL fold difference which is approximately double that of NC versus TC. *Soho* shows insignificant differences between samples for both the array and qPCR data.

3.4.6 *Foxi* knockout does not alter retinotectal phenotype in embryos

Of the four genes found to be expressed in the developing retina, *foxi1* was the most interesting. The transcription factor *foxi1* has the highest fold difference for the Nasal Lesion versus Temporal Lesion comparison at 22.7 fold. Contrast this to the Nasal Control versus Temporal Control array where *foxi1* has an impressive but significantly lower fold difference of 9.3. This indicates that *foxi1* is expressed in a gradient in the unlesioned adult retina and the gradient becomes more pronounced following lesion. Moreover, it is a transcription factor, it is in the same family as *foxg1a* and *foxd1* which have also been selected as genes of interest, it has been shown to be expressed in a highly specific spatial pattern in the embryonic zebrafish retina (Fig. 3.11) and has a knockout mutant available. Given the highly localized expression pattern seen in the *foxi1* embryonic in situ hybridisations it could be expected that *foxi1* plays a role in retinotectal mapping. *Foxi1* is known to play an important role in the formation of the otic system (Hans et al., 2007) but there are no publications linking it to mapping in the retinotectal system. We obtained preserved 3dpf *foxi1*$^{-hi3747}$ embryos courtesy of Judy Peirce and Dr. Bernardo Blanco of the Westerfield laboratory. The embryos were sorted based on homozygotes

possessing the "chinless" phenotype due to a reduced hyomandibular and reduced third and fourth branchial arches (Fig3.12).

From our tracing of 19 chinless and 13 non-chinless siblings, we could discern no gross abnormalities of the optic tract or retinotopic mapping (Fig. 3.13). This was in addition to 23 unsorted, traced *foxi1* mutant embryos which also exhibited no obvious retintotectal phenotype.
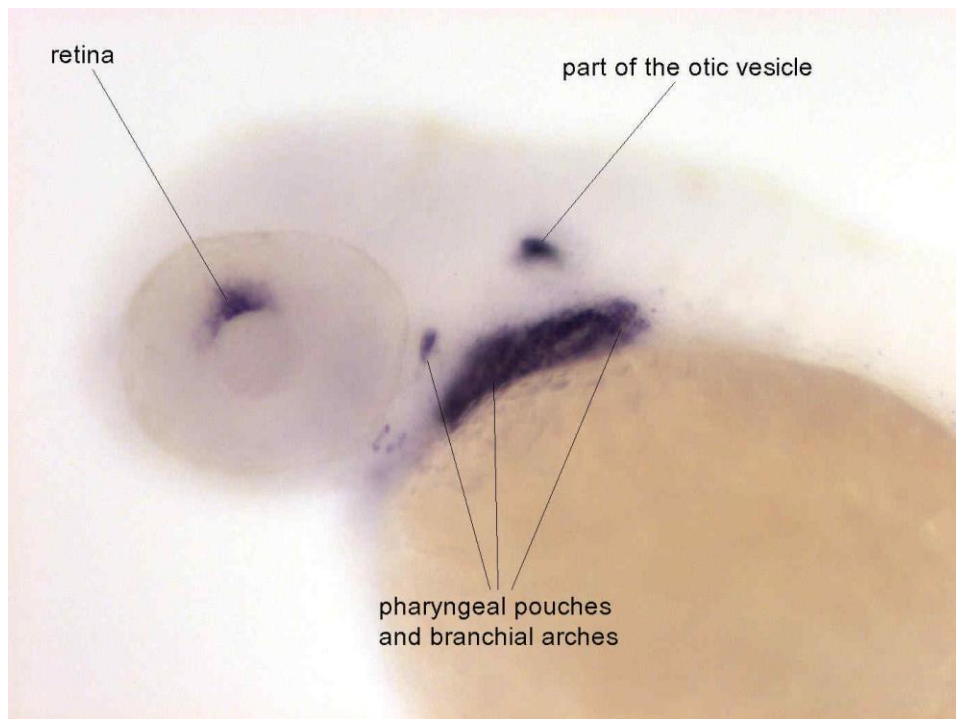
Fig. 3.11. Foxi1 expression in 36hpf Zebrafish embryo.
Indicating expression in the dorsal retina, which shifts temporodorsally during development. Expression is also indicated in the otic vesicle and the branchial arches, both of these tissues have an altered phenotype in the mutant (Fig3.12).
Rostral is left, dorsal is up.
Image modified from Thisse et al., 2001.
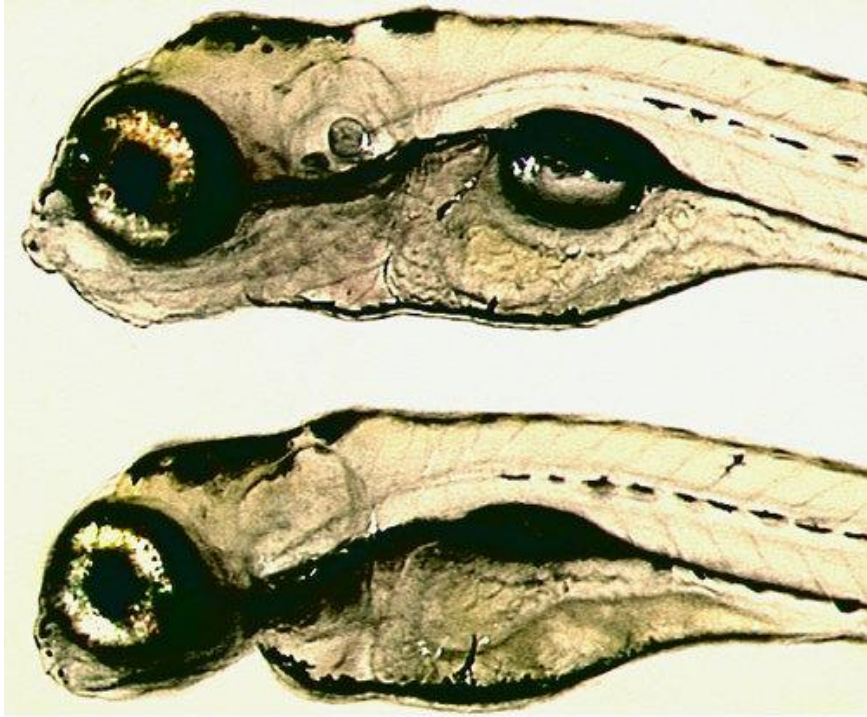
Fig. 3.12. Wild type (upper) and homozygous foxi1 mutant (lower) 5dpf embryos.

Homozygous mutant has a cleft due to a reduced hyomandibular and reduced third and fourth branchial arches. Wild types and heterozygous mutants lack this cleft therefore homozygous mutants can be isolated based on their "chinless" phenotype. The phenotype is evident from 2 to 6 dpf, when the mutant embryos die.

Modified from direct ZFIN submission ZFIN ID: ZDB-FIG-070117-810.
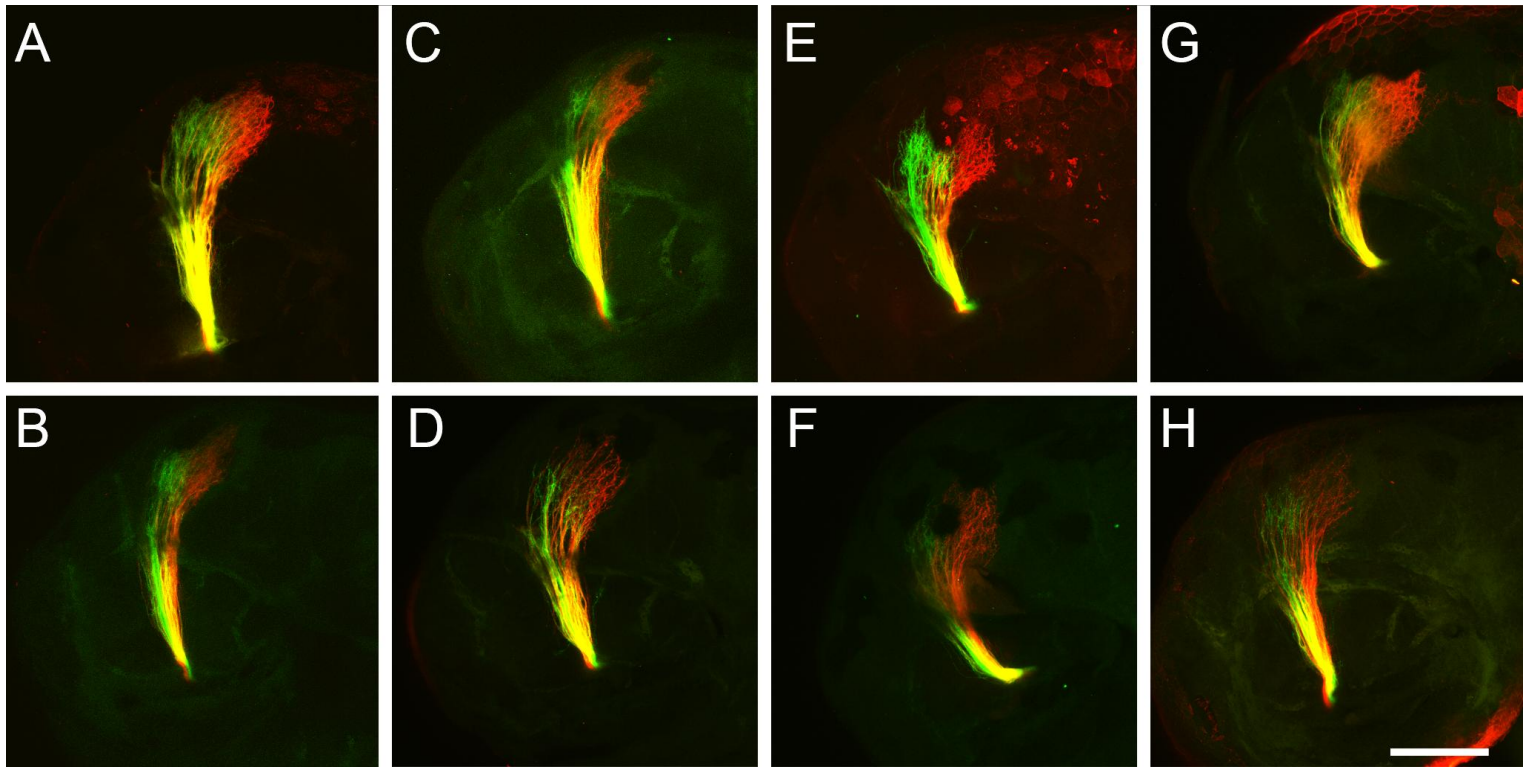
Fig. 3.13. Lack of gross abnormalities in *foxi1^-hi3747* **mutant optic tract or retinotopic mapping revealed by DiI and DiO tracing in the 3dpf embryo. A-D.** Controls which lack the chinless phenotype (wild type and heterozygotes). These controls are indistinguishable from standard WIK controls (See Fig. 4.5C and D). **E-H.** Homozygous mutants possessing the chinless phenotype exhibit no noticeable aberrations in these scans of the retinotectal projection.

Dorsal is up and rostral is left. Scale bar is 100μm.

3.5 Discussion

Informed by microarray data for RGC gene regulation following lesion, differential expression patterns for 17 candidate genes were demonstrated during development when the optic system is being established. None demonstrated expression patterns in the adult regenerating retina, most likely due to insufficient sensitivity of the method. The candidate gene *foxi1* exhibited a spatially restricted expression pattern in the developing retina but knockout of *foxi1* did not induce a detectable phenotype in the optic projection.

3.5.1 Zebrafish orthologues of known guidance cues in other species

Of the 17 genes which were found to be expressed during development, 4 were expressed as a gradient in the developing retina which is consistent with a role in retinotopic mapping during development; *foxi1*, *foxd1-like*, *foxg1a* and *epha4b* (Table 3.3 and Fig. 3.6 and 3.7). For the 3 genes which have microarray data, the direction of the gradient is in agreement between the two methods. *Foxi1* and *foxd1-like* exhibit temporal high gradients in the in situ hybridisations on embryos and in the adult retina based array data. The same is true for *foxg1a*, with a nasal high gradient. In addition to *foxg1a*, there are a further two zebrafish *foxg1* paralogues; *foxg1b* and *foxg1c*. *Foxg1b* has a dorsonasal expression pattern in the developing retina, whereas *foxg1c* is expressed only transitorily in the retina early in development (Zhao et al., 2009). Based on embryo mRNA expression patterns and the array data, *foxd1* lacks a detectable gradient in both embryonic and adult retina. The graded retinal expression pattern of *foxd1-like*, but not *foxd1*, in zebrafish development and regeneration is similar to that of *foxd1* in chick development. (Takahashi et al., 2009). This may indicate that *foxd1-like*, rather than *foxd1*, is the functionally equivalent orthologue of chick *foxd1*. As 3 of the 4 genes which are expressed in a gradient in the developing retina are from the *fox* family, it is likely that this family of genes is highly important in retinotectal development.

   Based on the array data, the graded retinal expression pattern of *epha4a*, but not *epha4b*, in zebrafish regeneration is similar to that of *epha4* in goldfish regeneration. (Rodger et al., 2004). However during the period of development when the optic projection is formed, *epha4b* exhibits a gradient in the retina while *epha4a* does not (Komisarczuk et al., 2008). This could indicate that the *epha4a* is the functional equivalent of goldfish *epha4* during regeneration but that *epha4b* is more likely to play a role in development than *epha4a*.

We found that *rgma* is upregulated in the adult tectum during regeneration (Fig. 3.9) and is expressed throughout the brain during development (Fig. 3.6K), with the expression patterns being compatible with optic axon guidance during development and regeneration. However we did not detect its main known receptor, *neo1*, in the embryonic or adult retina. Other studies have also failed to detect *neo* in the developing retina (Thisse et al., 2001). It is possible that *rgma* has another receptor in zebrafish, such as a paralogue of *neo1*.

3.5.2 To what extent is regeneration a partial recapitulation of development?

Of the 17 genes which gave distinct expression patterns in the embryo, 4 exhibited gradients in the retina (Table 3.3). According to the microarray data 14 of these 17 genes are expressed in a gradient in adult retina following optic nerve lesion. Taken at face value, this indicates that for our candidate genes, 10 of the 14 genes which are expressed as a gradient during regeneration are not expressed as a gradient during development of the retinotectal system. However, as the in situ hybridisations on adult retina cryosections appear to lack the sensitivity required to confirm the array results (discussed below), it may be that gradients in the embryonic retina are also going undetected by in situ hybridisation. In order to resolve this situation an equivalent method must be used on both the adult and embryonic tissue, such as qPCR (discussed in further methods below).

3.5.3 Lack of candidate gene signal in adult retina in situ hybridisation

Due to the qPCR findings concurring with the array data, the statistical confirmation of the technical aspect of the array data and the general agreement of indicator gene patterns from the literature, it is reasonable to assume that the array data is at least partially correct and therefore the negative results from the adult in situ hybridisations require explanation. The overall quality of the cryosection in situ hybridisations was generally good, as indicated by low levels of background staining and robust labelling of multiple positive controls (Fig. 3.8). All 17 probes were confirmed by in situ hybridisation on 24hpf embryos (Fig. 3.6), the majority of which also exhibited expression on 3dpf embryos which were developed on the same slides as the adult cryosections to give each slide a control (Fig. 3.7). These observations argue that neither the probes, tissue or the method can be wholly responsible for the lack of clear signal in the adult sections. This points to a property of the candidate genes themselves being a factor. The most likely explanation is that the method is not sensitive enough to detect certain genes which may be expressed at low levels. Evidence for this is discussed here. The microarray data gives no indication of the absolute levels of gene expression as measured by mRNA levels. However PCR and qPCR can give an indirect, relative indication of mRNA levels. The late amplification of the candidate genes in qPCR, compared to the lower Cts of the housekeeping genes, may be due to less target available for amplification, indicating low expression levels. The relative difficulty in amplifying many of the candidate genes by RT-PCR for probe making, in comparison to amplifying unrelated genes for other projects, could also be explained by low levels of target sequence in the mRNA and hence the cDNA. The candidate genes were found, in general, to be more readily amplified from cDNA based on template embryonic mRNA rather than adult derived mRNA, which may indicate that the embryo derived cDNA has relatively higher levels of the target sequence. Generally, embryonic tissue yielded greater concentrations of cDNA than adult retina samples but this was equilibrated before use. Furthermore, in situ hybridisation on cryosections is generally a less sensitive method than in situ hybridisation on whole tissue due to the additional processing and freeze-thaw of tissue, which can damage mRNA, required for cryosection processing.

Could a bias have been introduced in gene selection to favour genes with low abundance mRNA? Candidate genes were selected for two main criteria; the gene being classed as a transcription factor and having a high fold difference. A majority of the candidate genes (20 of

34) are transcription factors. Transcription factors can take part in a signal transduction cascade activating other genes, possibly other transcription factors, thus leading to an amplification of the signal. Depending on the specific transcription factor, where in the cascade it functions will determine its abundance. It can be expected that those nearer the beginning of the cascade will be found in lower abundance. However the information to support or deny this supposition is not readily available. Furthermore, of the 20 genes which reached the probe stage, 8 are non-transcription factor genes. For the 14 genes which did not successfully reach the probe stage, 6 are non-transcription factor genes. These proportions are not statistically significantly different indicating that transcription factor candidate genes could be amplified by PCR as successfully as non-transcription factor candidate genes. A second potential source of bias is that the candidate genes were selected for having high fold differences on the array. This is a measure of relative abundance of the target sequence between two samples and gives no information on the absolute abundance of the targets. It is possible that genes with low expression levels are more likely to have high fold differences on the array as an equivalent absolute change in the number of mRNAs present for a specific gene would have a more pronounced effect on relative levels if the number of mRNAs for that gene was low to begin with. However, the 17 genes which have probes successfully confirmed in embryos, present a mix of fold differences from the very highest (*foxg1a*, -46.2) to genes which are regarded as having no fold change as they are below the two fold cut off (*rgmb*, 1.7). Thus it seems unlikely that a bias was introduced by our selection methods.

3.5.4 Further methods

Performing immunohistochemistry against the candidate genes is a method which could be used to confirm the array results, via the detection of the end product of the gene regulation rather than the mRNA. Unfortunately the availability of antibodies for use in zebrafish is still relatively poor. We did attempt immunohistochemistry using a Foxg1a antibody known to work in mice but untested in zebrafish. The results were negative, which is not surprising as mammalian and zebrafish proteins tend to share around 50% homology, which is generally insufficient for antibody cross-reactivity.

Performing in situ hybridisation on vibratome sections of retina may enhance any weak signal. This method can be more sensitive than cryosectioning as it avoids freeze-thaw of the tissue and uses the same protocol as the in situ hybridisation on whole embryos. However, due to the soft and fragile nature of the unfrozen eye, vibratome sectioning is more challenging and less efficient than cryosectioning.

As this was a single-channel microarray, data can be compared between different arrays using the same probes. Therefore performing additional arrays, with the same probes, would allow a statistical comparison, confirming the results of the original array. Also performing additional microarrays in triplicate, rather than the microarray in technical duplicate, would allow for more rigorous and informative statistics which would also direct candidate gene selection. Constant improvements in the microarrays available and annotations for microarrays of the zebrafish genome will allow for greater use of automated expression profiling programs such as the EBI Expression Profiler (http://www.ebi.ac.uk/expressionprofiler/index.html).

For any future arrays, sample enrichment for RGCs would allow for increased certainty that the regulated genes being detected are from RGCs. Fluorescence activated cell sorting (FACS) is a relatively quick and large scale method for the isolation of fluorescently tagged cells. This is usually performed in a transgenic line which expresses GFP in the cells of interest. FACS could be applied to the *shh:GFP* and *pou4f3:GFP* lines which express GFP in the RGCs. Following surgical separation of the eye into thirds, the opposing extents of the retina would be homogenised in separate samples and then FAC sorted. FACS can give purities of the target cell which approach 100%. Another method to enrich samples for RGCs, which we trialled, was to use laser capture microdissection (LCM). This technique works by the binding of selected areas of a cryosection onto a plastic slide, such as the Capsure extraction kit (Arcturus), by using a

laser pulse to melt the plastic onto the section. This captures the selected area of cells, which would be the RGC layer. mRNA can then be extracted from these cells and used for a microarray. The downside of this method is the limited amount of mRNA that can be extracted from each section, so requiring many retina sections to achieve a sufficient concentration of mRNA. These methods can also be used to enrich mRNA samples for other methods such as qPCR.

Given that the microarray results are based on end point measurements, albeit from an array performed in technical duplicate, whereas the qPCR ratios are based on a series of measurements performed for each cycle on samples in triplicate, it is likely that the qPCR results are the more accurate of the two sets. However relative qPCR only indicates the relative abundance of the target when compared between samples. Absolute quantification qPCR using multiple primer sets against each gene would be one method of triangulating the number of target transcripts for genes of interest. Despite the difficulty of amplifying less abundant sequences, qPCR remains one of the best ways of confirming microarray data. A higher success rate could be expected with the use of the most appropriate methods, such as Taqman probes, which are more resistant to late cycle contamination, ever-expanding Universal Probe Libraries and specialised kits for the amplification of rare transcripts. qPCR could be applied to embryonic retina mRNA samples. mRNA samples can be generated from opposing extents of the embryonic retina in similar ways to that of the adult, through surgical separation which can optionally be enhanced by LCM or FACS. By performing qPCR on both adult and embryonic retina samples, the problems of inter-method variation would be eliminated which currently exist with the comparison of embryonic in situ hybridisation results versus adult microarray data.

3.5.4.1 Adult manipulations

The genes which are indicated to be expressed as gradients in the adult retina by the array data could be investigated further through manipulation of their expression. In addition to gene knockdown during development, morpholinos can also be used to knockdown gene expression during adult optic nerve regeneration. Morpholino knockdown in RGCs during regeneration can be achieved by implanting a foam pledget soaked in morpholino at the site of optic nerve transection. The morpholino is retrogradely transported to the RGC cell body (Veldman et al., 2007; unpublished observations). Newer vivo-morpholinos (Morcos et al., 2008) may provide the opportunity to apply repeat doses of morpholino during regeneration for as long as is

required, by introducing morpholino into the vitreous humour thus allowing it to pass into the RGCs which are adjacent to this space. The heatshock inducible GAL4/UAS system also offers the potential to perturb putative guidance molecules during adult regeneration (see Fig. 2.7).

3.5.4.2 *Foxi1* knockout does not grossly affect retinotopic mapping

Given the highly localized retinal expression pattern seen in the *foxi1* embryonic in situ hybridisations it could be expected that *foxi1* plays a role in retinotectal mapping. *Foxi1* is known to play an important role in the formation of another sensory system; the otic system (Hans et al., 2007). It is clear that *foxi1* has important functions for development; without *foxi1* the embryo develops mandibular abnormalities, otic vesicle abnormalities and the swim bladder fails to inflate leading to death at 6dpf. However, despite the expression of the gene at the appropriate time and place to affect retinotopic mapping tracing of the optic projection in the mutant shows no indication of altered phenotype in the retinotectal system.

One possible explanation is that the mutant may not be truly null and the effects seen in other organs can be accounted for by toxic effects of the mutant protein or the mutant protein retaining domains sufficient for its putative role in the retinotectal system but not other tissues. This however is unlikely as the mutant protein, which has a proviral integration towards 5', is truncated before the DNA-binding domain which is conserved between species and is therefore likely to be essential for the function of the gene (Nissen et al., 2003). Of the four *foxi1* mutants originally generated, *foxi1*$^{-hi3747}$ had the integration site furthest towards 5' and the most consistent phenotype. The lack of in situ hybridisation signal for *foxi1* expression in the mutants also suggests a destabilised mRNA due to the mutation (Nissen et al., 2003). However the precise sequence of the probe is not given so it may be that the probe targeted a sequence which had insufficient overlap with the mutant sequence. Additionally, the *foxi1* mutant phenotype was phenocopied through the use of morpholinos. This phenocopy was acheived in only 50% of morphants, which is to be expected when comparing a knockdown to a knockout. While unlikely, it cannot be conclusively ruled out from this evidence that part of the enhanced effect of the mutation compared to the morpholino knockdown is due to activity of the truncated mutant protein.

With that caveat, given the lack of altered phenotype in the retinotectal system, it can be concluded that *foxi1* is not necessary for the correct formation of the retinotectal system.

It is possible that *foxi1* does not play an important role in retinotopic mapping but this would seem unlikely due to the very precise and specific expression pattern found in the embryonic retina. It is more likely that the role of the knocked out *foxi1* is being compensated for by one or more other genes. Due to the teleost genome duplication it is possible that *foxi1* has a paralogue. The *foxi1* paralogue has not yet been identified in the zebrafish and it could be that this potential paralogue has assumed the function of *foxi1* in mapping, or both paralogues could be functional, requiring both to be knocked down to induce a phenotype. Alternatively, the lack of *foxi1* could be masked by other genes in the *fox* family such as *foxd1-like*, *foxg1a* or the paralogue *foxg1b* which is expressed in the developing dorsonasal retina (Zhao et al., 2009). As has been shown, knocking down only one of the *ephrin-A* genes is insufficient to disrupt visual mapping in mice, with a triple *ephrin* knockout required to achieve a strong phenotype (Pfeiffenberger et al., 2005; Cang et al., 2008). As we have shown the presence of other *fox* family genes expressed as gradients in the developing retina (Fig3.6C and P), it may be that these and perhaps other *fox* genes are sufficient to compensate for the lack of *foxi1*. Injections of morpholinos against *foxd1-like*, *foxg1a* or *foxg1b* in the *foxi1* mutant line, individually or together, may elicit phenotypes not observed with only a single *fox* knockdown.

3.6 Conclusion

Based on the array and mRNA expression pattern in embryos, less than half of the genes which are expressed in a gradient in the adult eye during regeneration are detected as a gradient in the developing retina. This may hint that the two fundamentally similar processes rely on diverged molecular cues. However given the caveat of failure to reveal these adult gradients with in situ hybridisation and that adult and embryo data derive from two different methods, further work with qPCR, additional microarrays or more sensitive in situ hybridisation methods would be necessary to confirm and expand on these findings. However based on these findings we can confirm the lack of a gross retinotopic phenotype in a *foxi1* mutant and the presence of other *fox* family genes, *foxg1a* and *foxd1-like*, in the developing retina. This suggests these *fox* family genes as potential targets for coordinated manipulation of expression during development.

3.7 Bibliography

Amores A, Suzuki T, Yan YL, Pomeroy J, Singer A, Amemiya C, Postlethwait JH. Developmental roles of pufferfish Hox clusters and genome evolution in ray-fin fish. Genome Res. 2004 Jan;14(1):1-10. PubMed PMID: 14707165; PubMed Central PMCID: PMC314266.

Baraban SC, Dinday MT, Castro PA, Chege S, Guyenet S, Taylor MR. A large-scale mutagenesis screen to identify seizure-resistant zebrafish. Epilepsia. 2007 Jun;48(6):1151-7. Epub 2007 May 23. PubMed PMID: 17521353; PubMed Central PMCID: PMC2211740.

Becker CG, Lieberoth BC, Morellini F, Feldner J, Becker T, Schachner M. L1.1 is involved in spinal cord regeneration in adult zebrafish. J Neurosci. 2004 Sep 8;24(36):7837-42. PubMed PMID: 15356195.

Bonilla IE, Tanabe K, Strittmatter SM. Small proline-rich repeat protein 1A is expressed by axotomized neurons and promotes axonal outgrowth. J Neurosci. 2002 Feb 15;22(4):1303-15. PubMed PMID: 11850458.
Cameron DA, Gentile KL, Middleton FA, Yurco P. Gene expression profiles of intact and regenerating zebrafish retina. Mol Vis. 2005 Sep 20;11:775-91. PubMed PMID: 16205622.

Cang J, Niell CM, Liu X, Pfeiffenberger C, Feldheim DA, Stryker MP. Selective disruption of one Cartesian axis of cortical maps and receptive fields by deficiency in ephrin-As and structured activity. Neuron. 2008 Feb 28;57(4):511-23. PubMed PMID: 18304481; PubMed Central PMCID: PMC2413327.

Carmel JB, Galante A, Soteropoulos P, Tolias P, Recce M, Young W, Hart RP. Gene expression profiling of acute spinal cord injury reveals spreading inflammatory signals and neuron loss. Physiol Genomics. 2001 Dec 21;7(2):201-13. PubMed PMID: 11773606.

Chen WJ, Ortí G, Meyer A. Novel evolutionary relationship among four fish model systems. Trends Genet. 2004 Sep;20(9):424-31. Review. PubMed PMID: 15313551.

Chomczynski P, Sacchi N. Single-step method of RNA isolation by acid guanidinium thiocyanate-phenol-chloroform extraction. Anal Biochem. 1987 Apr;162(1):156-9. PubMed PMID: 2440339.

Costigan M, Befort K, Karchewski L, Griffin RS, D'Urso D, Allchorne A, Sitarski J, Mannion JW, Pratt RE, Woolf CJ. Replicate high-density rat genome oligonucleotide microarrays reveal hundreds of regulated genes in the dorsal root ganglion after peripheral nerve injury. BMC Neurosci. 2002 Oct 25;3:16. Epub 2002 Oct 25. PubMed PMID: 12401135; PubMed Central PMCID: PMC139981.

De Biase A, Knoblach SM, Di Giovanni S, Fan C, Molon A, Hoffman EP, Faden AI. Gene expression profiling of experimental traumatic spinal cord injury as a function of distance from

impact site and injury severity. Physiol Genomics. 2005 Aug 11;22(3):368-81. Epub 2005 Jun 7. PubMed PMID: 15942019.

Driever W, Solnica-Krezel L, Schier AF, Neuhauss SC, Malicki J, Stemple DL, Stainier DY, Zwartkruis F, Abdelilah S, Rangini Z, Belak J, Boggs C. A genetic screen for mutations affecting embryogenesis in zebrafish. Development. 1996 Dec;123:37-46. PubMed PMID: 9007227.

Fleige S, Walf V, Huch S, Prgomet C, Sehm J, Pfaffl MW. Comparison of relative mRNA quantification models and the impact of RNA integrity in quantitative real-time RT-PCR. Biotechnol Lett. 2006 Oct;28(19):1601-13. Epub 2006 Aug 10. PubMed PMID: 16900335.

Gulati-Leekha A, Goldman D. A reporter-assisted mutagenesis screen using alpha 1-tubulin-GFP transgenic zebrafish uncovers missteps during neuronal development and axonogenesis. Dev Biol. 2006 Aug 1;296(1):29-47. Epub 2006 Jun 19. PubMed PMID: 16784739.

Guo Y, Ma L, Cristofanilli M, Hart RP, Hao A, Schachner M. Transcription factor Sox11b is involved in spinal cord regeneration in adult zebrafish. Neuroscience. 2010 Oct 15. [Epub ahead of print] PubMed PMID: 20951776.

Hans S, Christison J, Liu D, Westerfield M. Fgf-dependent otic induction requires competence provided by Foxi1 and Dlx3b. BMC Dev Biol. 2007 Jan 19;7:5. PubMed PMID: 17239227; PubMed Central PMCID: PMC1794237.

Kasowski M, Grubert F, Heffelfinger C, Hariharan M, Asabere A, Waszak SM, Habegger L, Rozowsky J, Shi M, Urban AE, Hong MY, Karczewski KJ, Huber W, Weissman SM, Gerstein MB, Korbel JO, Snyder M. Variation in transcription factor binding among humans. Science. 2010 Apr 9;328(5975):232-5. Epub 2010 Mar 18. PubMed PMID: 20299548; PubMed Central PMCID: PMC2938768.

Komisarczuk AZ, Topp S, Stigloher C, Kapsimali M, Bally-Cuif L, Becker TS. Enhancer detection and developmental expression of zebrafish sprouty1, a member of the fgf8 synexpression group. Dev Dyn. 2008 Sep;237(9):2594-603. PubMed PMID: 18729221.

Livak KJ, Schmittgen TD. Analysis of relative gene expression data using real-time quantitative PCR and the 2(-Delta Delta C(T)) Method. Methods. 2001 Dec;25(4):402-8. PubMed PMID: 11846609.

Liu Q, Londraville RL. Using the adult zebrafish visual system to study cadherin-2 expression during central nervous system regeneration. Methods Cell Sci. 2003;25(1-2):71-8. PubMed PMID: 14739590.

McCurley AT, Callard GV. Characterization of housekeeping genes in zebrafish: male-female differences and effects of tissue type, developmental stage and chemical treatment. BMC Mol Biol. 2008 Nov 12;9:102. PubMed PMID: 19014500; PubMed Central PMCID: PMC2588455.

Morcos PA, Li Y, Jiang S. Vivo-Morpholinos: a non-peptide transporter delivers Morpholinos into a wide array of mouse tissues. Biotechniques. 2008 Dec;45(6):613-4, 616, 618 passim. PubMed PMID: 19238792.

Mueller O, Hahnenberger K, Dittmann M, Yee H, Dubrow R, Nagle R, Ilsley D. A microfluidic system for high-speed reproducible DNA sizing and quantitation. Electrophoresis. 2000 Jan;21(1):128-34. PubMed PMID: 10634479.

Mullins MC, Hammerschmidt M, Haffter P, Nüsslein-Volhard C. Large-scale mutagenesis in the zebrafish: in search of genes controlling development in a vertebrate. Curr Biol. 1994 Mar 1;4(3):189-202. PubMed PMID: 7922324.

Muto A, Orger MB, Wehman AM, Smear MC, Kay JN, Page-McCaw PS, Gahtan E, Xiao T, Nevin LM, Gosse NJ, Staub W, Finger-Baier K, Baier H. Forward genetic analysis of visual behavior in zebrafish. PLoS Genet. 2005 Nov;1(5):e66. Epub 2005 Nov 25. PubMed PMID: 16311625; PubMed Central PMCID: PMC1287954.

Nilsson A, Moller K, Dahlin L, Lundborg G, Kanje M. Early changes in gene expression in the dorsal root ganglia after transection of the sciatic nerve; effects of amphiregulin and PAI-1 on regeneration. Brain Res Mol Brain Res. 2005 May 20;136(1-2):65-74. Epub 2005 Mar 5. PubMed PMID: 15893588.

Nissen RM, Yan J, Amsterdam A, Hopkins N, Burgess SM. Zebrafish foxi one modulates cellular responses to Fgf signaling required for the integrity of ear and jaw patterning. Development. 2003 Jun;130(11):2543-54. PubMed PMID: 12702667

Pfeiffenberger C, Cutforth T, Woods G, Yamada J, Rentería RC, Copenhagen DR, Flanagan JG, Feldheim DA. Ephrin-As and neural activity are required for eye-specific patterning during retinogeniculate mapping. Nat Neurosci. 2005 Aug;8(8):1022-7. Epub 2005 Jul 17. PubMed PMID: 16025107; PubMed Central PMCID: PMC1352169.

Rodger J, Vitale PN, Tee LB, King CE, Bartlett CA, Fall A, Brennan C, O'Shea JE, Dunlop SA, Beazley LD. EphA/ephrin-A interactions during optic nerve regeneration: restoration of topography and regulation of ephrin-A2 expression. Mol Cell Neurosci. 2004 Jan;25(1):56-68. PubMed PMID: 14962740.

Takahashi H, Sakuta H, Shintani T, Noda M. Functional mode of FoxD1/CBF2 for the establishment of temporal retinal specificity in the developing chick retina. Dev Biol. 2009 Jul 15;331(2):300-10. Epub 2009 May 18. PubMed PMID: 19450575.

Thisse, B., Pflumio, S., Fürthauer, M., Loppin, B., Heyer, V., Degrave, A., Woehl, R., Lux, A., Steffan, T., Charbonnier, X.Q. and Thisse, C. (2001) Expression of the zebrafish genome during embryogenesis (NIH R01 RR15402). ZFIN Direct Data Submission

Veldman MB, Bemben MA, Thompson RC, Goldman D. Gene expression analysis of zebrafish retinal ganglion cells during optic nerve regeneration identifies KLF6a and KLF7a as important regulators of axon regeneration. Dev Biol. 2007 Dec 15;312(2):596-612. Epub 2007 Sep 22. PubMed PMID: 17949705.

Westerfield M (1989) The zebrafish book: a guide for the laboratory use of zebrafish (Brachydanio rerio). Eugene: University of Oregon Press.

Xiao T, Roeser T, Staub W, Baier H. A GFP-based genetic screen reveals mutations that disrupt the architecture of the zebrafish retinotectal projection. Development. 2005 Jul;132(13):2955-67. Epub 2005 Jun 1. PubMed PMID: 15930106.

Zhao XF, Suh CS, Prat CR, Ellingsen S, Fjose A. Distinct expression of two foxg1 paralogues in zebrafish. Gene Expr Patterns. 2009 Jun;9(5):266-72. Epub 2009 Apr 18. PubMed PMID: 19379839.

4. Manipulation of *crmp2* expression during development reduces RGC axon arbor complexity

4.1 Introduction

Our microarray results highlighted gene families of interest which are implicated in axon guidance in the CNS. One such family was the *collapsin response mediator proteins* (*crmps*). Crmps are phosphoproteins which are highly expressed in the nervous system and involved in the signal transduction cascade of inhibitory guidance cues during axon growth (Liu and Strittmatter, 2001). They exist in both a cytosolic form and a form which is tightly associated with membrane proteins intracellularly but is not a transmembrane protein itself (Minturn et al., 1995a). There are five known CRMPs in mammals (CRMP1 to 5) and six in zebrafish (*crmp1* to *4*, *crmp5a* and *crmp5b*). The two zebrafish *crmp5* paralogues probably arose during the teleost genome duplication event (Amores et al., 2004; Chen et al., 2004). Zebrafish *crmps* exhibit reasonably high intra-family homology (43-75%, amino acid BLAST) and high homology with human orthologues (67-90%, amino acid BLAST) (Schweitzer et al., 2005). This holds true amongst other species as rat *crmp2* shares 98% of its amino acid sequence with chick *crmp2* and 89% with that of *Xenopus* (Quinn et al., 1999). This high level of evolutionary conservation highlights the functional importance of the *crmps*. The cross-species homology includes a conserved dihydropyriminidase domain which is common to all *crmps* but is non-functional as the *crmps* have not been shown to exhibit DHPase activity (Goshima et al., 1995; Wang and Strittmatter, 1997; Hamajima et al., 1996).

4.1.1 Nomenclature

The *crmps*, particularly *crmp2*, have been studied widely in many organisms indicating their cross species interest and resulting in a variety of names.

The orthologues of zebrafish *crmp2* are:

CRMP-2 in human, rat, *Xenopus* and bovine

CRMP-62 in chick

Ulip-2 in Mouse and human

DRP-2 in human

TOAD-64 in rat

UNC-33 in *C.elegans*

Adding additional complication, the *crmp* family was abortively renamed as *dihydropyrimidinase-like* (*dpysl*) in some organisms but the majority of new literature retains the use of the *crmp* nomenclature. For simplicity, henceforth "*crmp2*" shall refer to all orthologs of *crmp2*, with species noted when relevant.

4.2 Expression patterns of the *crmp* family

In the zebrafish embryo, all six members of the *crmp* family are highly expressed in regions of neuronal differentiation and axiogenesis. Each *crmp* has a specific spatial and temporal pattern of expression, with none being observed outside of the nervous system (Schweitzer et al., 2005). As the cell types which express *crmps* do not change during early neurogenesis, the expression pattern of *crmps* mirrors the changes in morphology during development of the nervous system. Thus as the embryo develops and new neuronal populations appear, the regions expressing *crmps* increase in volume and complexity (Chitnis and Kuwada, 1990; Wilson et al., 1990; Ross et al., 1992; Schweitzer et al., 2005). *Crmp2* expression has been detected in the developing zebrafish brain until at least 97hpf (Christie et al., 2006). In the developing zebrafish retina all *crmps*, with the exception of *crmp1*, can be detected until at least 5dpf (unpublished observations). The *crmps* may have many roles in the developing nervous system as they are similarly widely expressed in the developing brains of the other main model vertebrates, with expression also found throughout the CNS and PNS; in rats (Wang and Strittmatter, 1996) and in mouse (Byk et al., 1998). *Crmp* expression patterns are similar to those of genes associated with neuronal and axonal differentiation, including cell recognition molecules L1.1, L1.2 (Tongiorgi et al., 1995), TAG-1 (Warren et al., 1999) and *contactin* (Gimnopoulos et al., 2002). The *crmps* and their orthologues, are strongly implicated in growth cone signalling as they reach their peak expression levels during periods of rapid axonal growth and are then downregulated after growth. They are expressed in neuronal cell bodies, neurites and growth cones with their expression most concentrated in the distal portion of axons where the actions of the growth cone must take place (Quinn et al., 1999). This is similar to observations in the rat where Crmp2 is one of the earliest expressed proteins known in postmitotic neurons. It is highly enriched in the nervous system, is present in growth cones and is downregulated to almost undetectable levels in the rat cortex during postnatal week two, which is the end of the period of major axon growth (Minturn et al., 1995b).

In the developing mouse retina, differentiating retinal ganglion cells (RGCs), but not the neighbouring mitotic precursor cells, exhibit *crmp* expression (Kamata et al., 1998b). The *crmps*, while expressed in the cortical plate are not expressed in the ventricular zone, indicating that they are expressed in differentiated neurons but not their progenitors. *Crmp2* is the exception to this as it is expressed in the ventricular zone in the rat (Wang and Strittmatter, 1996) and the newly formed neural plate in *Xenopus* (Kamata et al., 1998a) and the mouse (Kamata et al., 1998b).

4.3 *Crmp2*

Of the *crmp* family, *crmp2* may be the most widely studied (Goshima et al., 1995; Wang and Strittmatter, 1996; Inatome et al., 2000). Much of the interest in *crmp2* came from the observation that a *crmp2* mutant in *C.elegans* had severely uncoordinated movement which when investigated further was found to be due to abnormal axon guidance and outgrowth including premature axon termination, abnormal branching, aberrant pathfinding and a superabundance of microtubules in neurons (Hedgecock et al., 1985; Desai et al., 1988; Siddiqui and Culotti, 1991; Li et al., 1992). The expression pattern of *crmp2* in the embryonic brain is consistent across different vertebrate classes, indicating its functional importance; mouse (Byk et al., 1996), cat (Cnops et al., 2004), zebrafish (Schweitzer et al., 2005; Christie et al., 2006), Xenopus (Kamata et al., 1998a) and chick (Goshima et al., 1995). The expression of *crmp2* in zebrafish embryonic RGCs is also consistent with expression of *crmp2* in chick (Goshima et al., 1995; Christie et al., 2006). The mutant *C.elegans* phenotype and the conserved expression patterns across species, suggest a role for *crmp2* in neurite outgrowth as well as axon guidance.

4.3.1 *Crmp2* function

4.3.1.1 Axon formation and growth cone collapse via microtubule assembly regulation

Growth cones are a sensor for guidance molecules during development which localize at the tips of axons and dynamically change their morphology in response to attractive and repulsive guidance cues, thus determining the direction of growth (Dent and Gertler, 2003). They house the receptors and cellular machinery necessary to detect and respond to molecular cues in the environment that guide them to their targets. These cues can be mostly positive / attractant such as the *neurotrophins* or mostly inhibitory / repellent such as the *semaphorins*. In the rat, Crmp2

protein is localised to growth cones, specifically lamellipodia and filopodia at the advancing edge of growth cones, where it is ideally placed to be part of the axon guidance signaling pathway (Minturn et al., 1995a).

It is known that microtubule dynamics and endocytosis regulate growth cone morphology (Goshima et al., 1997; Diefenbach et al., 1999; Fournier et al., 2000; Mack et al., 2000; Kamiguchi and Lemmon, 2000; Buck and Zheng, 2002). Crmp2 binds to the tubulin dimer and enhances the formation of microtubules by acting as a carrier of tubulin heterodimers, delivering them to the assembly sites of growing microtubules (Fukata et al., 2002). Without this enhancement of microtubule assembly, growth cone dynamics would be altered in favour of retraction (Figure 4.1 illustrates a possible pathway connecting Crmp2 and cytoskeletal rearrangement). It has been shown in vitro that Crmp2 mediated microtubule assembly is essential for axonal growth and branching and induces neurite formation (Fukata et al., 2002). In the chick it has been shown that Crmp2 enhances the advance of growth cones by regulating microtubule assembly and Numb-mediated endocytosis (Arimura et al., 2005). In vitro, overexpression of *crmp2* enhances the rate of axon growth, while a mutant form of Crmp2, lacking specific activity of the microtubule assembly, reduces axon growth. Given this and the fact that Crmp2 is enriched in growing axons, it can be inferred that the Crmp2-tubulin complex, which is concentrated in the distal extent of axons, promotes microtubule assembly and so axon formation (Fukata et al., 2002).

4.3.1.2 Numb-mediated endocytosis

Crmp2 also contributes to axon elongation by other mechanisms. Crmp2 binds to Numb and is localised in axonal growth cones. Numb is a membrane bound protein which is involved in clathrin-dependent endocytosis at the plasma membrane (Santolini et al., 2000) and has been implicated in maintaining neural progenitor cells during embryonic neurogenesis (Rasin et al., 2007). Crmp2 facilitated Numb-mediated endocytosis of the cell adhesion molecule L1 in the growth cone leads to axon elongation (Nishimura et al., 2003). Numb mediated L1 endocytosis is necessary for axon growth (Kamiguchi and Lemmon, 2000). It has been inferred that Sema3A and Ephrin-A5 induced growth cone collapse acts via increased phosphorylation of Crmp2 leading to inhibition of Numb-mediated endocytosis and so growth cone collapse (Goshima et al, 1995; Arimura et al., 2005) (Fig 4.1). Contrary to this hypothesis, it has been shown in some

cases that endocytosis is enhanced during Sema3A and Ephrin induced growth cone collapse (Fournier et al, 2000; Jurney et al., 2002), indicating that there may be other factors at work, perhaps to selectively regulate endocytosis depending on the growth state of the axon.

4.3.1.3 Isoforms

In mammalian *crmps*, alternative splicing of exon1 has been described (Quinn et al., 2003, Yuasa-Kawada et al., 2003). Of the two Crmp2 isoforms in mammals, full length Crmp2, which is restricted to the cytoplasm, promotes neurite elongation in vitro (Rogemond et al., 2010). Whereas the short isoform, produced by cleavage, can undergo nuclear translocation leading to suppression of axonal growth and neurite outgrowth inhibition in vitro. This signalling is dependent on nuclear localisation of the short isoform as mutation of the nuclear localisation signal sequence restores neurite elongation activity of the molecule (Rogemond et al., 2008). A possible function of nuclear proteins is that of regulating genes that are involved with control of cell differentiation and proliferation, which is consistent with the expression of Crmp2 in progenitor cells and in tissues prior to neural differentiation (Wang and Strittmatter, 1996; Kamata et al., 1998a; Kamata et al., 1998b). It is likely that the nuclear localised isoform of Crmp2 may regulate transcription factors leading to the inhibition of neurite outgrowth. Therefore rather than simply the total expression level of Crmp2, the balance of the long and short Crmp2 isoforms, with their opposing downstream effects, is an important factor in the effects of Crmp2 on the nervous system. However, isoforms of Crmp2 have not yet been identified in zebrafish.

4.3.1.4 Phosphorylation state dependent activity

The phosphorylation state of Crmp2 is a key factor determining its activity. The microtubule formation enhancing properties of Crmp2 can be suppressed by phosphorylation of Crmp2 by Rho kinase, during growth cone collapse. Following phosphorylation by Rho kinase, Crmp2 has a reduced ability to associate with microtubules, tubulin heterodimers and certain other proteins, including Numb (Arimura et al., 2005). However the actin binding property of Crmp2, distinct from its tubulin binding property, remains following phosphorylation. A similar effect on Crmp2 function results from phosphorylation whether by Rho kinase, Cdk5 or GSK-3ß (Arimura et al.,

2005). The importance of phosphorylation for the functioning of Crmp2 is highlighted by the conserved protein kinase consensus sites found in all orthologues of Crmp2 (Byk et al., 1996).

The phosphorylation state of Crmp2 plays an important role in Crmp2 mediated growth cone collapse. Growth cone collapse is downstream of Crmp2 phosphorylation which can be accomplished by multiple different kinases in different pathways. In vitro work has shown that Crmp2 is phosphorylated when PlexinA1 and Fes protein tyrosine kinase are activated in Sema3A induced growth cone collapse (Mitsui et al., 2002) and that phosphorylation of Crmp2 is required for Sema3A induced growth cone collapse to occur (Brown et al., 2004). The kinase Fes, which is regulated by class A Plexins, phosphorylates PlexinA1 and a Crmp2 / Crmp-associated molecule (CRAM) complex (Mitsui et al., 2002). Fes kinase activity is necessary for the collapse of DRG neuron growth cones (Mitsui et al., 2002). The association of Fes and PlexinA1 is enhanced by the application of Sema3A. As Crmp2 plays a role in microtubule dynamics, it is plausible that the *plexinA1/fes/crmp* pathway might be involved in microtubule destabilisation. Another example is that of growth cone collapse induced by lysophosphatidic acid (LPA), during which Crmp2 is phosphorylated by Rho associated protein kinase (Arimura et al., 2000). It is known that Rho-kinase mediates Ephrin-A5 induced growth cone collapse in RGCs (Wahl et al., 2000; Cheng et al., 2003). While Rho kinases can phosphorylate Crmp2, Crmp2 hetero-oligomers can act upon Rho kinases to alter Rho activity in response to different guidance signals (Leung et al., 2002). The levels of these proteins are influenced by *neurotrophins* (Byk et al., 1998; Ozdinler and Erzurumlu, 2001), so creating a complex interaction surrounding Crmp2 with feedback from Crmp2 itself. How this system performs when *crmp2* is knocked out has yet to be elucidated as viable *crmp2* mutant lines are not yet available in vertebrates. The growth factors BDNF and NT-3, which prevent growth cone collapse following exposure to repulsive guidance cues (Tuttle and O'Leary, 1998; Dontchev and Letourneau, 2002), inhibit phosphorylation of Crmp2 (Yoshimura et al., 2005). Retinoic acid (Gaetano et al., 1997) and NGF (Byk et al., 1998; Leung et al., 2002) can induce changes in the expression patterns and phosphorylation of the Crmps. As NGFs/*neurotrophins* (Byk et al., 1998), *ephrins* and *semaphorins* (Arimura et al., 2005) can all induce changes in phosporylation of Crmps which influences growth cone collapse and the Crmps are expressed in neuronal cells that do not respond to Semaphorins (Takahashi et al., 1999), the *crmps* may modulate the

signalling of multiple guidance cues. This would make the Crmps key molecules in the growth and guidance of sensory axons during development and regeneration.

4.3.2 Axon growth and guidance signalling molecules upstream of *crmp2*

The severity of the *C.elegans* phenotype arising from a single mutation was the first indication that *crmp2* may be involved in the signal cascades of multiple axon guidance and growth molecules. Further studies have linked several guidance and growth molecules with *crmp2*. *Crmp2* appears to be a nexus point for multiple pathways which induce growth cone collapse, including those initiated by Sema3A, LPA and Ephrin-A5 (Arimura et al., 2000; Christie et al., 2006). Some of the most studied are described below.

4.3.2.1 Semaphorins

Crmp2 was initially identified as a signal transducing molecule for the growth cone collapsing activity of *semaphorins* (Goshima et al., 1995). *Semaphorins* are repulsive axon guidance cues which are found in various developing nervous systems including the zebrafish brain (Wolman et al., 2007) and optic system (Liu et al 2004; Callander et al., 2007). The functional receptors for class 3 Semaphorins are a complex consisting of Plexin and Neuropilin (Takahashi et al., 1999). In chick, Crmp2 is one of the intracellular components of the pathway leading to Semaphorin-3A induced growth cone collapse (Goshima et al., 1995). Growth cone collapse induced by Semaphorin-3A/Collapsin-1 in dorsal root ganglion (DRG) neurons can be inhibited by blocking the action of Crmp2 (Goshima et al., 1995), demonstrating that Crmp2 is required for this process. Although *crmp2* and the other *crmps* are mostly associated with Semaphorin-3A response, the *crmps* are also expressed in sympathetic neurons that respond to Semaphorin-3C but not Semaphorin-3A (Koppel et al., 1997). This indicates that the Crmps respond differentially to members of the Semaphorin family and the response to a single member can vary between cell types.

The overlap in specific expression areas in the rat central nervous system of Crmp2 and PlexinA4, a Semaphorin receptor important for sensory axon branching, further implicates *crmp2* in axon formation (Miyashita et al., 2004; Christie et al., 2006). However as there is only a partial overlapping of expression patterns, this may indicate that other *crmps* or *plexins* may be involved in other cell types. This widespread expression of the *crmps* in central and peripheral

neurons also suggests that they may participate in the transduction of other guidance cues in addition to Collapsin-1/Sema3a and play a central role in the transduction of extracellular cues to their effects on axon growth. Furthermore, *crmp2* is expressed in developing chick RGCs which do not express any known Collapsin/Semaphorin receptors and do not respond to Semaphorin-3A, Semaphorin-3B, or Semaphorin-3C (Takagi et al., 1995; Takahashi et al., 1999).

4.3.2.2 Neuropilins

As mentioned, *crmp* activity is not limited to the Semaphorin pathways as Crmps are expressed in RGCs in chick which do not respond to Sema3A or Sema3C and do not express Semaphorin receptors (Takahashi et al., 1999; Quach et al., 2004). While chick RGCs do not express Neuropilin, it is expressed transiently in the retina by amacrine cells (Takagi et al., 1995). However chick appears to be an exception as the RGCs of other vertebrates, such as *Xenopus* (Fujisawa et al., 1990), mouse (Kawakami et al., 1996) and zebrafish (Liu et al., 2004), express Neuropilin.

It has been shown that zebrafish RGCs are guided by Sema3D and three of their four known *neuropilins* are expressed in RGCs; *nrp1a*, *nrp1b* and *nrp2a* (Liu et al., 2004). *Nrp1a* and *nrp1b* are expressed at a time and in a spatially restricted pattern in the retina which is consistent with a role in axon guidance of developing RGC axons (Liu et al., 2004). While *Nrp2b* is expressed in the inner nuclear layer of the retina, it is not expressed in the RGC layer. It is likely that the role for these genes in axon guidance is restricted to gross pathfinding as they are uniformly expressed throughout the retina by 48hpf when axons are reaching the tectum and the map is being established so a role in retinotectal map formation is questionable (Liu et al., 2004).

4.3.2.3 Neurotrophins

Crmps play a role in neurite extension controlled by *neurotrophins*. The Neurotrophin family of signalling molecules (NGF, BDNF, NT3, NT4) play roles in neurite extension, axon arborisation, axon sprouting during regeneration, differentiation and neuron survival (Huang and Reichard, 2001; Mendell and Arvanian, 2002). In the developing zebrafish the *neurotrophins* are expressed in the optic system, including the retina (Hashimoto and Heinrich, 1997; Dethleffsen et al., 2003). NGF is an attractive guidance cue in vitro, inducing axon elongation and branching (Gundersen and Barrett, 1979; Gallo and Letourneau, 1998) and has been shown to reduce the

growth cone collapse induced by Sema3A (Dontchev and Letourneau, 2002). It has been shown in cultured rat DRG cells that expression of a dominant negative form of Crmp2 or specific anti-Crmp2 antibodies that block Crmp2 function during NGF induced neuritogenesis, increases the length of the neurites and the number of neurite bearing cells, but the number of neurites per cell remains unchanged (Quach et al., 2004). The response of cultured DRG cells is in contrast to that of hippocampal cells in vitro, where reducing Crmp2 activity through expression of a dominant negative Crmp2 mutant reduces axon formation and overexpression of Crmp2 leads to the formation of supernumerary axons (Inagaki et al., 2001), indicating cell specific responses to Crmp2. It is clear that the precise role of *crmp2* varies between specific cell types, thus complicating mapping of the pathway.

4.3.2.4 Crmp2-independent axon guidance

As has been demonstrated above, Crmp2 is an important, central molecule in various axon guidance related pathways. However this is not to say that Crmp2 is the sole transducer of axon guidance. Sema3 induced growth cone collapse is mediated by Rac1, a member of the Rho family (Hall, 1998), in addition to Crmp2. Other Crmp2 independent pathways are also active in growth cone collapse as mutants of Crmp2 which act as permanently phosphorylated Crmp2 could not occlude Ephrin-A5 induced growth cone collapse as another downstream molecule of Ephrin-A5, Rho-kinase, phosphorylates multiple targets including MLC and MAPs (Arimura et al., 2005).

While the available evidence indicates the importance of *crmp2* for axon growth and guidance, the other *crmps* should not be overlooked. *Crmp1, 3, 4* and *5* have been shown to have limited influence over neurite extension, branching and growth cone formation (Quinn et al, 2003; Hotta et al., 2005; Schmidt and Strittmatter, 2007). The coexpression of *crmp2* in cells with other *crmps*, along with the fact that Crmps form heterotetramers, may indicate that Crmp activity is influenced by the combination of *crmps* expressed together in a cell (Wang and Strittmatter, 1997; Schmidt and Strittmatter, 2007).

4.4 Other processes involving *crmps*

In addition to the *crmps* involvement in axon growth and guidance, they have been implicated in several other processes such as neuronal polarity, apoptosis and cell migration in the nervous system (Quinn et al., 1999, Liu and Strittmatter, 2001, Charrier et al., 2003 and Arimura et al., 2004). *Crmp2* has been shown to play a role in axon guidance of regenerating axons in the embryonic zebrafish as knockdown of *crmp2* affects the ability of regenerating trigeminal sensory axons to successfully avoid reentering former territories (O'Brien et al., 2009). In vitro, it has been shown that *crmp2* plays a role in determining neural polarity of dorsal root ganglion neurons by regulating axon formation. (Inagaki et al., 2001). While expression of *crmps* is greatly reduced in the adult nervous system, it remains most prominent in areas which undergo neurogenesis in adult life (Quinn et al., 1999). Seizure induced neurogenesis in the adult dentate gyrus is associated with increased expression of *crmp4* in rat (Parent et al.,1997; Scott et al., 1998). *Crmp2* and *crmp4* are reexpressed in the adult rat following sciatic nerve lesion (Minturn et al., 1995a) and there is evidence that overexpression of *crmp2* can promote regeneration of the cranial nerve axons in rats (Suzuki et al., 2003). Finally, an increase in highly phosphorylated Crmp2 can be detected in association with neurofibrillary tangles in Alzheimer's disease models (Yoshida et al., 1998; Gu et al., 2000).
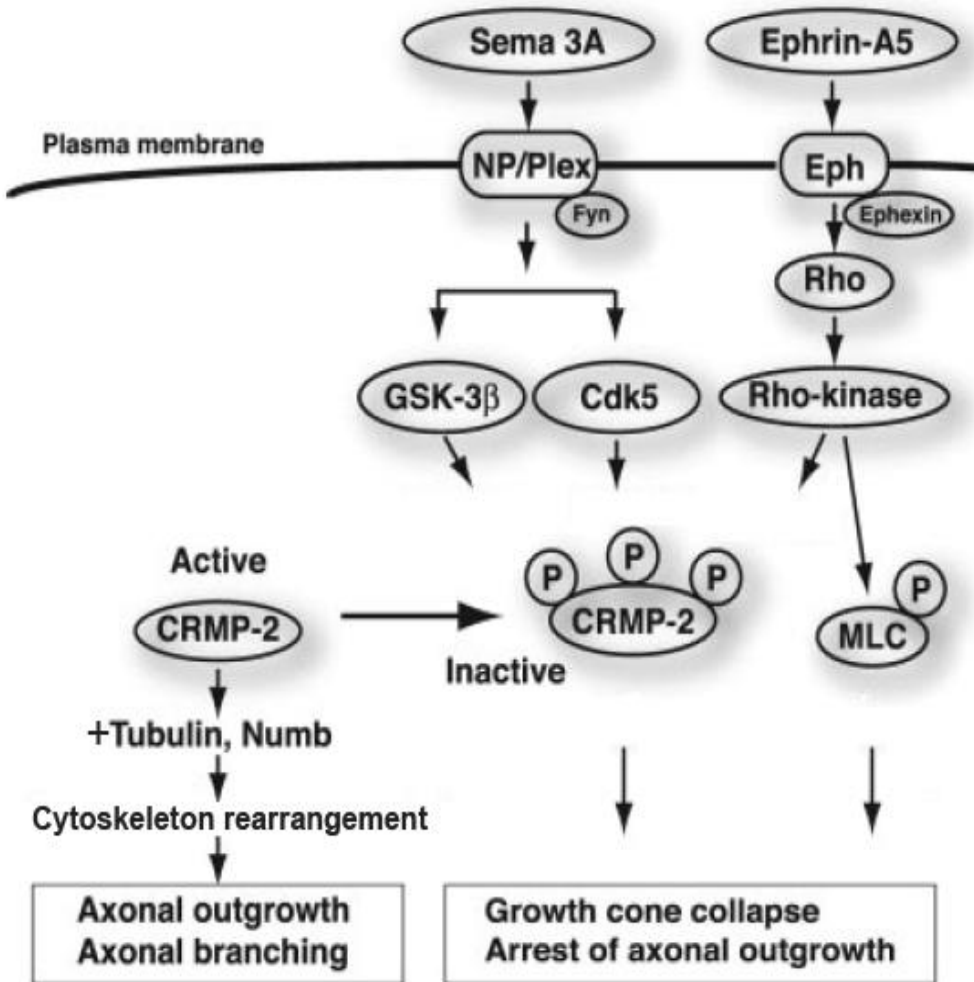
Fig. 4.1. Pathway of *crmp2* activity leading to cytoskeletal rearrangement and axon growth.
This is a possible interpretation of the Crmp2 pathway, largely based on chick DRG data, with a detailed focus on phosphorylation. Sema3A activation of Cdk5 and GSK3 leads to phosphorylations of Crmp2. Ephrin-A5 activates the Rho/Rho kinase pathway leading to Crmp2 phosphorylation. This decreases Crmp2's tubulin binding activity, leading to a reduction in microtubule assembly and Numb-mediated endocytosis which arrests axon growth and causes growth cone collapse. However the Crmp2 pathway is clearly complex and the precise role of Crmp2 differs between cell types and species.
Adapted from Arimura et al., 2005.

4.5 Summary

Crmps are expressed in the nervous system of developing zebrafish, and other model organisms, in specific temporal and spatial patterns which coincide with regions of neuronal differentiation and axonogenesis. *Crmp2* is expressed in the retina during development and in the PNS during regeneration in the adult. Our microarray (chapter 3) results indicate an upregulation of *crmp2* in the retina following an optic nerve crush lesion in the adult zebrafish. In summary, Crmp2 is implicated in multiple signaling pathways which result in growth cone collapse, including those initiated by Sema3A, LPA and Ephrin-A5. However, *crmp2* has a complex role in the nervous system as it is involved in both negative and positive modification of axon growth including growth cone collapse and neurite extension. Taken together this may indicate a role for *crmp2* as a central transducer or nexus in growth cone response to external guidance cues. From this data it can be hypothesised that manipulation of *crmp2* during development will affect axon extension. Thus we manipulated levels of *crmp* gene expression in the developing zebrafish and observed the effects on the retinotectal system, with particular focus on *crmp2*.

We found that knockdown of *crmp2* with two independent morpholinos resulted in an axon phenotype which could be observed in whole tract tracing in the form of sparser, less branched innervation of the tectum by RGC axons. Plasmid construct-induced expression of GFP in individual RGCs in *crmp2* morphant embryos revealed a trend towards less complex arbors with shorter branches and reduced overall axon length. Expression of a Crmp2 dominant negative construct, along with GFP, in individual RGCs resulted in a significantly reduced main branch length. These results indicate that Crmp2 plays a role in RGC axon growth in the developing zebrafish as reducing Crmp2 activity may reduce axon growth.

4.6 Materials and methods

4.6.1 Animals

All fish are kept and bred in our laboratory fish facility according to standard methods (Westerfield, 1989) and all experiments have been approved by the British Home Office.

4.6.2 cDNA

For PCR analysis of aberrant splicing, RNA was extracted from pooled tissue of 15 larvae per time point and treated using the RNeasy Mini Kit (Quiagen, UK). Reverse transcription, using random primers (Promega, Madison, WI, USA), was performed with the SuperScript III kit (Invitrogen, UK). Nanodrop ND-1000 Spectrophotometer (Nanodrop Technologies) was used to check concentrations and give an approximation of quality. The following primers were used to amplify the appropriately and aberrantly spliced sequence in PCR: crmp2ex2 forward (GGGGCTAAGATTGTGAACGATGAT); crmp2ex5 reverse (TAGGCCAGGTAGACGAGGAAAGAG).

4.6.3 Whole retinotectal projection methods

4.6.3.1 Morpholinos

Morpholino oligonucleotides against members of the *crmp* family were purchased from GeneTools (Corvallis, OR). The morpholino target, designated name, type and their sequences are detailed in Table 4.1. Morpholinos are oligonucleotides which have standard nucleic acid bases bound to morpholine rings. Morpholinos exist as two main types with differing modes of action; translation blocking and splice blocking. Start codon directed morpholinos prevent translation of mRNA by interfering with the progression of the ribsomal initiation complex in the region of the start codon. Splice site directed morpholinos act by steric blocking of target pre-mRNA preventing normal processing by spliceosomes. Splice site directed morpholinos were used preferentially as these have a distinct advantage over start codon morpholinos in terms of verifying the efficacy of gene knockdown and the action of the morpholino. Splice blocking morpholinos result in a proportion of the target mRNA being aberrantly spliced. Amplification by RT-PCR of the region which includes the splice site target results in amplicons of varying lengths. The difference between the length of the aberrant amplicon and the wild type amplicon

indicates the length of sequence spliced out, or in some cases in, by the action of the morpholino. The relative intensities of the wild type and aberrant bands when run on a gel give an indication of the relative proportions of wild type mRNA and aberrantly spliced mRNA in the embryo.

The control morpholino was a 5 base mismatch morpholino inactive control used previously in the laboratory (Becker et al., 2004). Morpholinos were introduced by standard zygote injections. Morpholinos were diluted to 0.5, 1, 2 and 4mM in Danieau solution (58 mM NaCl, 0.7 mM KCl, 0.4 mM MgSO$_4$, 0.6 mM Ca (NO$_3$)$_2$, 5 mM HEPES, pH 7.6) (Nasevicius and Ekker, 2000). Glass capillaries (0.8µm internal and 1.0µm external diameter) were pulled to produce injection needles. A micromanipulator in concert with a microinjector (Microinjector Narishige, UK) was used to inject 1nl of morpholino solution into the yolk of a fertilised egg at the 1 to 4 cell stage. Fertilised eggs were of either wild type strain (WIK) or Tg(*pou4f3:gap43-GFP*)^{s356t}. Morpholinos were injected either singly or as a mix containing two morpholinos to investigate possible synergistic action.

Target gene	Morpholino name	Type	Sequence
crmp1	crmp1 Start	Translation blocking	5'-TGG TTA GTT GTC GGT GGA TGC AGC T-3'
crmp2	crmp2 Start Mo1	Translation blocking	5'-CTT GCC CTG ATA GCC AGA CAT CTT C-3'
	crmp2 Start Mo2	Translation blocking	5'-ATG CTC TTA TTG CCT TTG ATG AAC C-3'
	crmp2 IE Mo1	Splice blocking	5'-GAG TTT CAC ACA TAC CGA TCA TGG T-3'
	crmp2 IE Mo2	Splice blocking	5'-CAC TCT GGA AAC ACA GAT AAA CAC A-3'
crmp3	crmp3 IE	Splice blocking	5'-TTT CAC AAA TAG ACT GAC CTC TTG C-3'
crmp4	crmp4 IE Mo1	Splice blocking	5'-TGG TTA GTT GTC GGT GGA TGC AGC T-3'
	crmp4 Start Mo2	Translation blocking	5'-GGT CCA GGC GTC TGC CCT CAG CCA T-3'

Table 4.1. Morpholinos for knockdown of *crmps* during development. The morpholino target, designated name, type and their sequences are given.

4.6.3.2 Tracing

Lipophilic tracers, DiI (1,1'-dioctadecyl-3,3,3',3'-tetramethylindocarbocyanine perchlorate, Invitrogen) and DiO (3,3'-dioctadecyloxacarbocyanine perchlorate, Invitrogen), were used to visualise the optic projection of WIK *crmp* morphants of 2 to 5dpf, as described (Becker et al., 2003). Less than 10% of injected embryos exhibited developmental defects (oedema of the heart, curved tail or spherical yolk) which is not stastistically different from control or uninjected embryos. All embryos exhibiting such defects were excluded from analysis. The embryos were anaesthetised with MS222 and fixed in 4% paraformaldehyde overnight at room temperature. The embryos were then embedded in 1% low melting point agarose. A pulled glass needle was dipped into a saturated solution of either DiI in ethanol or DiO in chloroform (approximately 50mg per ml). After allowing the dye to crystallise onto the needle, the DiO needle was inserted into the temporal extent of the retina of one eye for 20 seconds using manual manipulation under stereomicroscopic observation. This was then repeated for DiI into the nasal extent of the retina of the same eye. The embryos were then immersed in PBS and incubated overnight at 37°C, allowing the dye sufficient time to diffuse along the axonal membranes. Labelling of the retina thusly results in DiO labelled anterior tectum and DiI labelled posterior tectum so revealing any gross errors of pathfinding or the retinotopic map. After incubation the contralateral eye was removed and the embryos whole mounted, injected side down. Using the empty socket as a window, the optic projection was imaged using a laser scanning confocal microscope (LSM510, Zeiss). Approximately 60 optical sections of 2μm step size were scanned per embryo to capture

the entire projection from nerve head to tectum. Other morphant embryos were traced with DiI only in one eye and DiO only in the other eye, processed as above and then mounted dorsally, to reveal any potential midline crossing. A subpopulation of RGCs in the pou4f3 line express GFP, allowing observation of the fluorescent optic tract without the need for tracing, thus providing an additional assessment method, independent of dye tracing. Confocal scans were examined for any aberrations in axon phenotype using LSM Image Browser (Zeiss) by a blinded observer, side by side with scans of controls.

4.6.3.3 PTU treatment

Overlying surface pigment in the melanophores can obscure the optic tract from laser scanning and reduced the number of axons that could be successfully scanned per batch. In order to improve signal detection embryos were treated with 1-phenyl 2-thiourea (PTU). PTU inhibits melanogenesis by blocking all tyrosinase-dependent steps in the melanin pathway. At 24hpf the embryos were transferred to methylene blue fish water containing PTU (75µM) as per standard protocol (Karlsson et al., 2001). The embryos were kept in PTU fish water until 3dpf when they were sorted and scanned. PTU treatment was discontinued following the initial tracing experiments in wild types as there was evidence that it had toxic effects when combined with other manipulations.

4.6.4 Single axon labelling

Tracing of the whole tract is unsuitable for revealing phenotypes of individual axons due to overlapping axons. Therefore, plasmid constructs were used to visualise individual axons under the effect of knockdown or dominant negative expression. The plasmids were obtained dried on filter paper and amplified using standard methods.

4.6.4.1 Plasmid transformation into bacteria

XL blue cells were transformed with plasmids obtained from colleagues' laboratories. The POU4F3:GAL4;UAS:GAP43-GFP (BGUG, formerly BRN3C:GAL4;UAS:GAP43-GFP) insert plasmid and the POU4F3:GAL4 (BG, formerly BRN3C:GAL4) insert plasmid, kindly supplied by the Baier laboratory and the UAS:GFP-UAS:DNCRMP2 (DNcrmp2) insert plasmid, kindly supplied by the Sagasti lab. 3µl of ligation mixture was added to 200µl of frozen XL blue

suspension. After 30 minutes on ice, the mixture was heated to 42°C for precisely 30 seconds to induce uptake of the plasmid. After a further 5 minutes on ice, 250µl of LB medium was added to the bacteria suspension which was then shaken for 1 hour at 37°C. The bacteria were spread onto 0.1% ampicillin agar plates and incubated overnight at 37°C. Bacteria which did not contain vectors with an insert would lack ampicillin resistance and fail to multiply.

4.6.4.2 Colony PCR

To ascertain if any colonies which did develop overnight contained the correct insert, colony PCR was used. This involved RT-PCR (as above) with the exception that a colony picked from a plate was used as the template in place of cDNA. The colony was briefly dipped into the PCR mix and then wiped into a grid square on a fresh 0.1% ampicillin agar plate. Each square of the grid corresponded to a separate PCR tube. Primers against GFP, *crmp2* or the vector sequence flanking the multiple insertion sites were used, with sequences as follows:

Primer	Direction	Sequence
EGFP Outer	Forward	5'- CAT GGT CCT GCT GGA GTT CGT G -3'
EGFP Outer	Reverse	5'- CGT CGC CGT CCA GCT CGA CCA G -3'
EGFP Inner	Forward	5'- GCC ACA AGT TCA GCG TGT CC -3'
EGFP Inner	Reverse	5'- GAT GCC CTT CAG CTC GAT GC -3'
Crmp2	Forward	5'- ACG AAG ATG TCT GGC TAT CAG -3'
Crmp2	Reverse	5'- GGT GAA GTC ATC TTT ACC AAC -3'
T7	Forward	5'- TAA TAC GACTCA CTA TAG GG -3'
SP6	Reverse	5'- ATT TAG GTG ACA CTA TAG AA -3'
T3	Reverse	5'- ATT AAC CCT CAC TAA AGG GA -3'

Table 4.2. Primers used in colony PCR to confirm transformed bacteria contained the intended plasmid with the correct insert.

The reaction product was ran on an agar / ethidium bromide gel to determine if the amplicon was of the expected size before proceeding to create a midi preparation from colonies of the corresponding grid square. 1 colony was selected and incubated overnight at 37°C in 50ml of LB medium (0.1% ampicillin) whilst shaking. The midi preparation was then purified using the HiSpeed Plamsid Midi kit (Qiagen). After checking the concentration of the purified plasmid

was in a suitable range (200 to 600 ng/μl), a sample was sequenced by DNASeq (Dundee). If a midi purification was found to have a concentration lower than 200ng/μl it was usually an indication of reduced quality and so advisable to repeat the midi step.

4.6.4.3 Plasmid microinjections

To visualise individual axons in a *crmp2* morphant embryo, the BGUG plasmid was coinjected into the cell of fertilised WIK eggs at the 1 cell stage (14ng/ μl in a 1nl injection per cell) with morpholinos against specific *crmps* (see Table 4.1). Injection into the cell is necessary as plasmids are not as readily transported from the yolk across the cell membrane as morpholinos. The concentration of plasmid had to be carefully titrated as the combined morpholino and plasmid coinjection had a combinatorial toxic effect on embryo development which was greater than either injected individually. Less than 10% of injected embryos exhibited developmental defects at 3dpf (oedema of the heart, curved tail or spherical yolk) which is not stastistically different from controls. All embryos exhibiting such defects were excluded from analysis. Controls were injected with BGUG and 5mismatch control morpholino. The BGUG plasmid contains the pou4f3 promoter, a GAL4:UAS amplification cassette and membrane targeted GFP. This resulted in expression of GFP in a random minority of cells which have an active Pou4f3 promoter. 5% of embryos exhibited one or more GFP expressing RGC axons when observed under the fluorescent stereomicroscope. Approximately 50% of embryos exhibited sporadic GFP expression in a minority of non-RGC cells, particularly skeletal muscle, but this did not interfere with imaging of the RGC axons. Embryos were dechorionated with watchmaker´s forceps in tank water containing MS222 in a small petri dish and sorted for presence of GFP expressing RGCs under fluorescent stereomicroscope observation. GFP expressing RGCs could be most readily viewed through the lens of the eye. After sorting, anaesthetised embryos were fixed overnight at room temperature in 4% paraformaldehyde before confocal imaging as above. A similar procedure was carried out for the BG and DNcrmp2 plasmids to visualise individual axons, expressing dominant negative Crmp2 in an otherwise wild type embryo. These plasmids were coinjected as the BG plasmid contained the promoter and first half the amplification system and the DNcrmp2 plasmid has the second half of the amplification system coupled to GFP and a dominant negative form of Crmp2. This results in a minority of individual axons expressing GFP and DNcrmp2, while the non-GFP axons do not express DNcrmp2 and remain wild type. These

plasmids were injected at a combined concentration of 60ng / µl in a 1nl injection per cell. Increased concentration of plasmid relative to the BGUG injections was necessary as expression from these plasmids had a lower penetrance and generally weaker expression of GFP. Due to the weaker signal, immunohistochemistry was used to enhance the signal. Controls were injected with BGUG (60ng / µl in a 1nl injection per cell).

4.6.4.4 Immunohistochemical signal enhancement

Following anaesthetisation, dechorionation and sorting, the yolk sac was opened with an insect pin. This results in most of the yolk, which is broadly immunoreactive, disassociating during the protocol. All subsequent steps were performed on a shaker at room temperature unless otherwise stated. The embryos were washed for 5 minutes in PBS twice, followed by 45 minutes in 4% paraformaldehyde with 1% DMSO in PBS. The embryos were then washed in PBS for 5 minutes, 3 times. Embryos were transferred from petri dishes to well plates and incubated with collagenase (Sigma C-9891), 500µl per well. Length of incubation and concentration was titrated for optimum results at different embryo ages to balance penetration of the antibody with preservation of tissue. Treatment with 2mg/ml collagenase for 20 minutes for 3dpf embryos and 2mg/ml collagenase for 25 minutes for 4dpf embryos was found to work well. The embryos were washed in PBS for 5 minutes, 3 times. Then the embryos were incubated with blocking buffer (1% DMSO, 1% normal serum, 1% BSA, 0.7% triton-X 100) for 30 min, 500µl per well. Followed by overnight incubation with primary antibody (anti-GFP, rabbit, A11122, Invitrogen) in blocking buffer at 4 ^{O}C, 300µl per well. The embryos were returned to room temperature and washed in PBS for 5 minutes, 3 times. Followed by overnight incubation with fluorescently labelled secondary antibody (anti-rabbit, donkey, 711-165-152, Invitrogen) in blocking buffer at 4 ^{O}C, 300µl per well. The embryos were returned to room temperature and washed in PBS for 5 minutes, 3 times. The embryos were then mounted and confocal imaged as above.

4.6.5 Analysis

4.6.5.1 Embryo development

Embryo body length and eye width (nasotemporal) were measured using an eyepiece micrometer on a Zeiss Stemi2000 stereomicroscope.

4.6.5.2 Whole retinotectal projection

For traced embryos, phenotype analysis was carried out only on adequately traced embryos, with axons labelled along their full length. Pou4f3:GFP transgenic embryos were used to confirm that what appeared as inadequate labelling was itself not a phenotype of severely stunted axons. Qualitative assessment was carried out by observing compressed image stacks, exported from Zeiss LSM Image Browser software, for axons straying from the tectum, axons changing direction sharply and anything which is not typical of wild type axons. To assess phenotype quantitatively, a dorsoventral cross section was taken of the greyscale collapsed image stack, exported from Zeiss LSM Image Browser software, at the widest point. From the collapsed confocal stacks, a rectangular selection was cropped across the widest part of the tectum, with the rejection of any that had pigment overlying the area chosen for the histogram selection.This was then analysed using the Histogram function of ImageJ to give the standard deviation (SD) of pixel intensity across the selection. This effectively quantifies how coarse and pronounced the bands of colour across the image are. It could be expected that many finely branched axons would show as a diffuse, homogenous distribution of pixels resulting in low SD whereas few, coarse axons would show as distinct bands resulting in a high SD. SDs were then compared using a one way ANOVA with a post hoc Tukey test. The histogram method was employed for the morphants embryos traced with lipophillic tracers but gave no significant results, most likely as a consequence of varying intensities of background labelling and axon specific labelling.

4.6.5.3 Individual axon labelling

To identify the phenotype at the level of the individual axon we used individual axon labelling. Uncollapsed confocal stacks of GFP expressing axons were traced using the ImageJ plugin Simple Neurite Tracer (developed by Mark Longair at Edinburgh University as part of the EPSRC / MRC life sciences interface programme). The individual axons were traced in three

dimensions through the confocal stacks, from the optic nerve head to the branch tips under blinded conditions. Multiple properties of the axons were assessed when comparing *crmp2* morphant and control embryos, injected with BGUG. These included total axon length, number of branch points (total number of times an axon branches) and maximum branch order (number of branch points on a single path from nerve head to termination). Axons with overlapping arbors which could not be reliably separated from their neighbours were rejected from the analysis. Results for each property were compared using a one way ANOVA with a post hoc Tukey test.
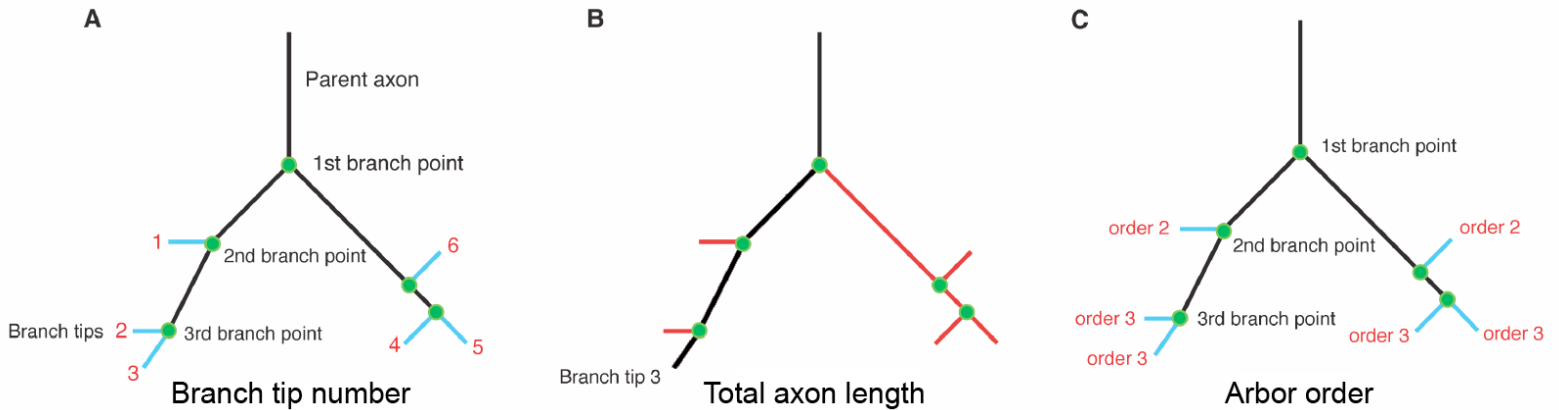
Fig. 4.2. Quantitation of RGC arbor parameters.

A. The number of branch tips longer than 10µm are totalled (light blue branch tips) for branch tip number.

B. The main branch is the longest single path from optic nerve head to termination (black). The total axon length is the sum of all branch tip lengths and internodal distances (red) plus the main branch (black).

C. The order of an arbor is the mean number of branch points counted from the optic nerve head to the highest order branch point of the arbor.

The green dots are branch points. Dorsal view, anterior is up.

Modified from Campbell et al., 2007.

4.7 Results

The *collapsin response mediator proteins* (*crmps*) were flagged as a gene family of interest in our microarray screen. Our array included probes for all 6 *crmps* and the data indicated that *crmp2*, *3*, *4* and *5a* were upregulated following a lesion, with *crmp2* showing the highest fold change of the *crmps* with a fold change of 6 (Table 4.3). *Crmp2* also had the highest fold difference between nasal and temporal, but these fold differences were very modest in comparison to the fold changes following lesion. Previous work in the laboratory elucidated the expression patterns of the *crmps* during development and in the adult, with and without lesion (Table 4.3, right-hand column). In situ hybridisations against the *crmp* family in the adult retina following optic nerve lesion were carried out by previous PhD student, Anselm Ebert. The mRNA expression patterns confirm the array findings that (1) there are no *crmp* spatial gradients in the RGC layer, either before or after lesion of the optic nerve and (2) *crmp2*, *3*, *4* and *5a* are upregulated in the RGC layer following optic nerve lesion. In the nasal control versus nasal lesion comparison, *crmp4* regulation is below the 2 fold cut off but is very close with 1.905 fold change. *Crmp1* and *crmp5b* showed no detectable upregulation during regeneration in either method. Thus, it is unlikely that *crmp1* and *crmp5b* play a role in influencing adult regeneration, while the other *crmps* are expressed in the relevant tissue at the appropriate time to influence regeneration. Furthermore, as the previous findings indicate that *crmp1* is the only *crmp* to not be expressed in the retina during development of the retinotectal system, it is unlikely that *crmp1* influences this process, while the other *crmps* are expressed in the relevant tissue at the appropriate time to influence axon pathfinding and mapping in the retinotectal system. Pilot experiments with low numbers of embryos had been carried out to investigate any gross qualitative effects on the retinotopic projection caused by morpholino knockdown of *crmps* during development. No effects were uncovered for the morpholinos crmp2 Start Mo1, crmp2 IE Mo1, crmp3 IE, crmp4 IE Mo1 and crmp4 Start Mo2. Crmp1 Start morpholino was used as a negative control as in situ hybridisations found it to not be expressed in the developing retina and had no effect on phenotype as expected. Morpholino crmp2 IE Mo2 was tentatively assessed to give an effect which may have been synergistic when combined with crmp4 Start Mo2.

Sample pair	Gene	Fold Difference (Spatial gradient)	mRNA expression pattern
Nasal	crmp1	No	No gradient
Control	crmp2	No	No gradient
versus	crmp3	No	No gradient
Temporal	crmp4	No	No gradient
Control	crmp5a	No	No gradient
	crmp5b	No	No gradient
Nasal	crmp1	No	No gradient
Lesion	crmp2	No	No gradient
versus	crmp3	No	No gradient
Temporal	crmp4	No	No gradient
Lesion	crmp5a	No	No gradient
	crmp5b	No	No gradient

Sample pair	Gene	Fold Change (Upregulation following lesion)	mRNA expression pattern
Nasal	crmp1	No	Not upregulated
Control	crmp2	4.029	Upregulated
versus	crmp3	3.781	Upregulated
Nasal	crmp4	No (1.905)	Upregulated
Lesion	crmp5a	3.171	Upregulated
	crmp5b	No	Not upregulated
Temporal	crmp1	No	Not upregulated
Control	crmp2	6.066	Upregulated
versus	crmp3	3.946	Upregulated
Temporal	crmp4	2.623	Upregulated
Lesion	crmp5a	3.874	Upregulated
	crmp5b	No	Not upregulated

Table 4.3. Specific *crmps* show upregulation in the retina following lesion of the adult optic nerve in the microarray screen and in situ hybridisation. Probe ratios between samples pairs on the array are listed under fold difference for nasal versus temporal retina sample comparisons and fold changes for control versus lesion sample comparisons. Probe ratios on the array of less than 2 fold were disregarded. The microarray findings for the *crmps* are supported by in situ hybridisations performed on adult retina by another PhD student in our group, Anselm Ebert (summarised in the right hand column). The in situ hybridisation results confirm the array findings that (1) there are no Crmp spatial gradients in the RGC layer, either before or after lesion of the optic nerve and (2) *crmp2*, *3*, *4* and *5a* are upregulated in the RGC layer following optic nerve lesion. In the nasal control versus nasal lesion comparison, *crmp4* regulation is below the 2 fold cut off but is very close with 1.905 fold change. The data for these genes can be found in the array supplementary files under the following probe names: *crmp1* - gb_DPYSL1, *crmp2* - gb_DPYSL2, *crmp3* - gb_DPYSL4, *crmp4* - gb_DPYSL3, *crmp5a* - gb_DPYSL5A and *crmp5b* - gb_DPYSL5B.

4.7.1 Crmp2 IE Mo2 activity induces aberrant mRNA splicing

The crmp IE Mo2 splice blocking morpholino had been designed to skip all of exon3. This would have resulted in an aberrant amplicon of 265 bases in length, compared to the 449 bases of the wild type (Fig. 4.3). However, application of crmp2 IE Mo2 lead to the appearance of two mispliced forms of *crmp2* mRNA. Due to a cryptic splice site in exon3, an intermediate amplicon was also produced which contained a portion of exon3. Thus crmp2 IE Mo2 was found to reduce the expression of wild type mRNA and lead to the appearance of two additional mispliced forms of *crmp2* mRNA in 24hpf morphants. At 3dpf the mispliced forms could not be detected and there was no reduction in wild type mRNA expression, which may indicate a relatively brief period of action for this morpholino. However the morphant optic projection phenotype could still be observed in embryos at 3dpf (discussed below).
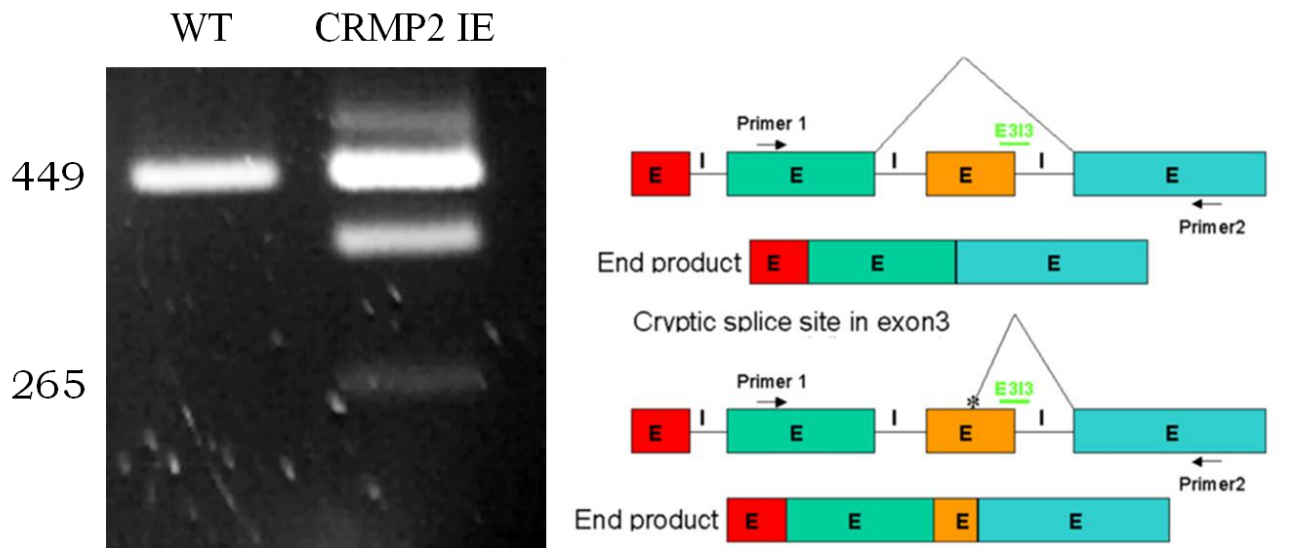

Fig. 4.3. Crmp2 IE Mo2 was found to reduce the expression of wild type mRNA and lead to the appearance of two additional mispliced forms of *crmp2* mRNA.

Aberrant splicing can be detected as a change in amplicon length by PCR. The upper band on the gel is the wild type amplicon, the lower band is the expected aberrantly spliced amplicon and the middle band is an additional aberrantly spliced amplicon. The topmost smeared band is most likely from inappropriate annealing as the primers had to be designed to bind to very specific regions of the mRNA, at the expense of other design considerations. The figure on the right illustrates the splicing which would result in the observed bands.

This figure was kindly contributed by Dr. Eugen Kludt, Göttingen.

4.7.2 Whole tract labelling reveals sparser innervation of the tectum

The first method used to attempt to elucidate any possible optic projection phenotype resulting from a knockdown of *crmp2*, was whole labelling of the optic projection with lipophillic tracers in *crmp2* morphant embryos. Before searching for morphant phentoypes, the range of the baseline phenotype had to be observed by tracing uninjected embryos. The focus was on 3dpf embryos, as the retinotectal system is well established at this timepoint. 103 uninjected wild type embryos were traced to establish a robust baseline to define wild type phenotype and the possible variations which it can include. A time course of earlier timepoints was also studied, to allow comparisons of any potential specific or non-specific retardations of optic system development due to manipulations.

Crmp2 IE Mo2 was injected at concentrations of 0.25mM (n=10), 0.5mM (n=51) and 1mM (n=43). Confocal scans of the morphants at 3dpf, as assessed by a blinded observer alongside control scans, revealed a more sparsley innervated tectum with axons that appear coarser and less branched when compared to controls (Fig. 4.5). The phenotype was most pronounced at the highest concentration and not detectable at the lowest concentration. At 1mM an additional possible phenotype of axons straying from the posterior tectum was observed in 1mM morphants (3 of 43) and was never seen in controls (0 of 103). The RGC axons appeared to reach the posterior tectum as indicated by bisbenzide staining, which may indicate that axon length is not reduced. Axon length was quantified in single axon labelling experiments (see section 4.7.6.2). At 4dpf, morphants were indistinguishable from uninjected controls. This may indicate a retardation of development of the optic system due to the morpholino or may be an effect of the morpholino becoming too dilute to have a significant effect on gene expression as the embryo develops. Furthermore, the 3dpf (72hpf) morphant phenotype (Fig. 4.5A and B) bears a strong resemblance to the 60hpf uninjected embryo (Fig. 4.4C). The possibility of general developmental retardation of the embryo is investigated below (section 4.7.6.1.1). Thus we conclude that knockdown of *crmp2* during development, confirmed by PCR, leads to a qualitative phenotype which appears as a more sparsley innervated tectum with coarser axons which reach the posterior tectum.
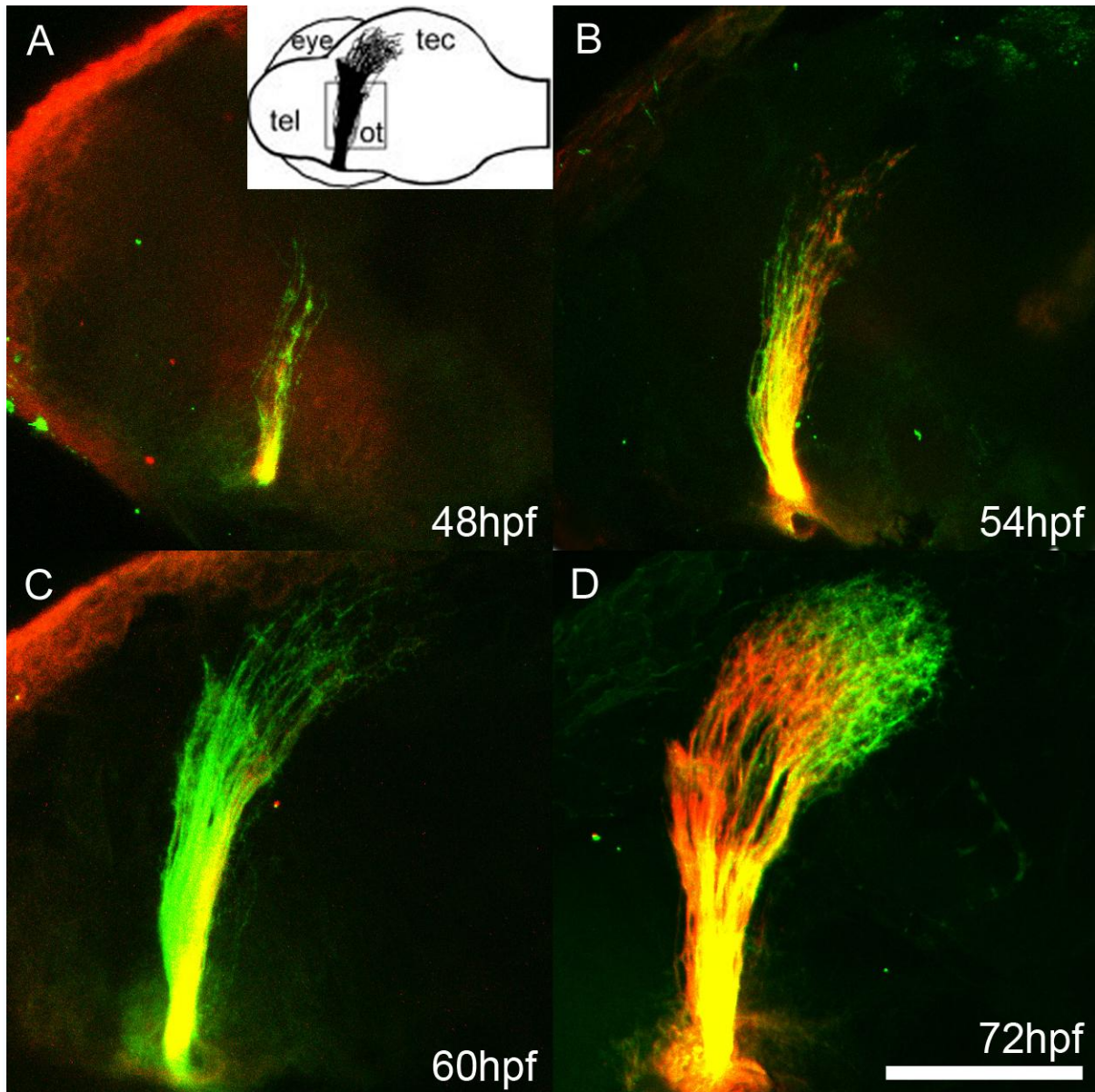
Fig. 4.4. Time course of wild type optic projection development. Lateral views of confocal image stacks of the optic tract in whole-mounted embryos at different time points in development, after labelling of the temporal retina with DiO and nasal retina with DiI (A-C) and labelling of the temporal retina with DiI and the nasal retina with DiO (D). **A.** 48hpf time point showing few, unbranched axons not reaching the tectum. The inset gives the orientation of the brain with the labelled optic projection indicated in black (tel, telencephalon; ot, optic tract; tec, tectum; eye, contralateral eye; the ipsilateral eye was removed before mounting); dorsal is up, and rostral is left. **B.** 54hpf time point showing more numerous axons developing a curve towards the tectum. **C.** 60hpf time point where numerous, fine, branched axons have reached the tectum. **D.** 3dpf time point with dense, fine, branched axons terminating on the tectum showing its distinct shape. Scale bar in D = 100μm.

164

4.7.3 Knockdown of multiple *crmps*

Possibly synergy of multiple *crmp* knockdown was investigated. Crmp2 IE Mo2 was coinjected with crmp4 Start Mo2 at the maximum concentration of morpholino that did not give toxic effects (0.5mM crmp2 IE Mo2 with 0.25mM crmp4 Mo2, n=40). No enhancement of phenotype was seen over control morphants injected with 0.75mM crmp2 IE Mo2 (n=17).

4.7.4 Labelling variability

In morphants, moreso than uninjected embryos, dye transport failed with a well labelled tract fading out as it approached the tectum which made the results unclear as to whether the tract itself was degrading or whether the dye was not being transported. As the dye is passively transported along the cell membrane this could indicate disruption of the membrane. Blebbing (dots of dye along the axon) was increased in morphants which can be an indication of degenerating axons or labelling artefacts. Such examples were rejected from further analysis but by rejecting all those with any imperfection of labelling we may have introduced a bias which rejected all embryos with the most severe phenotypes. For these reasons we sought an alternative, dye independent method to confirm the *crmp2* morphant results.
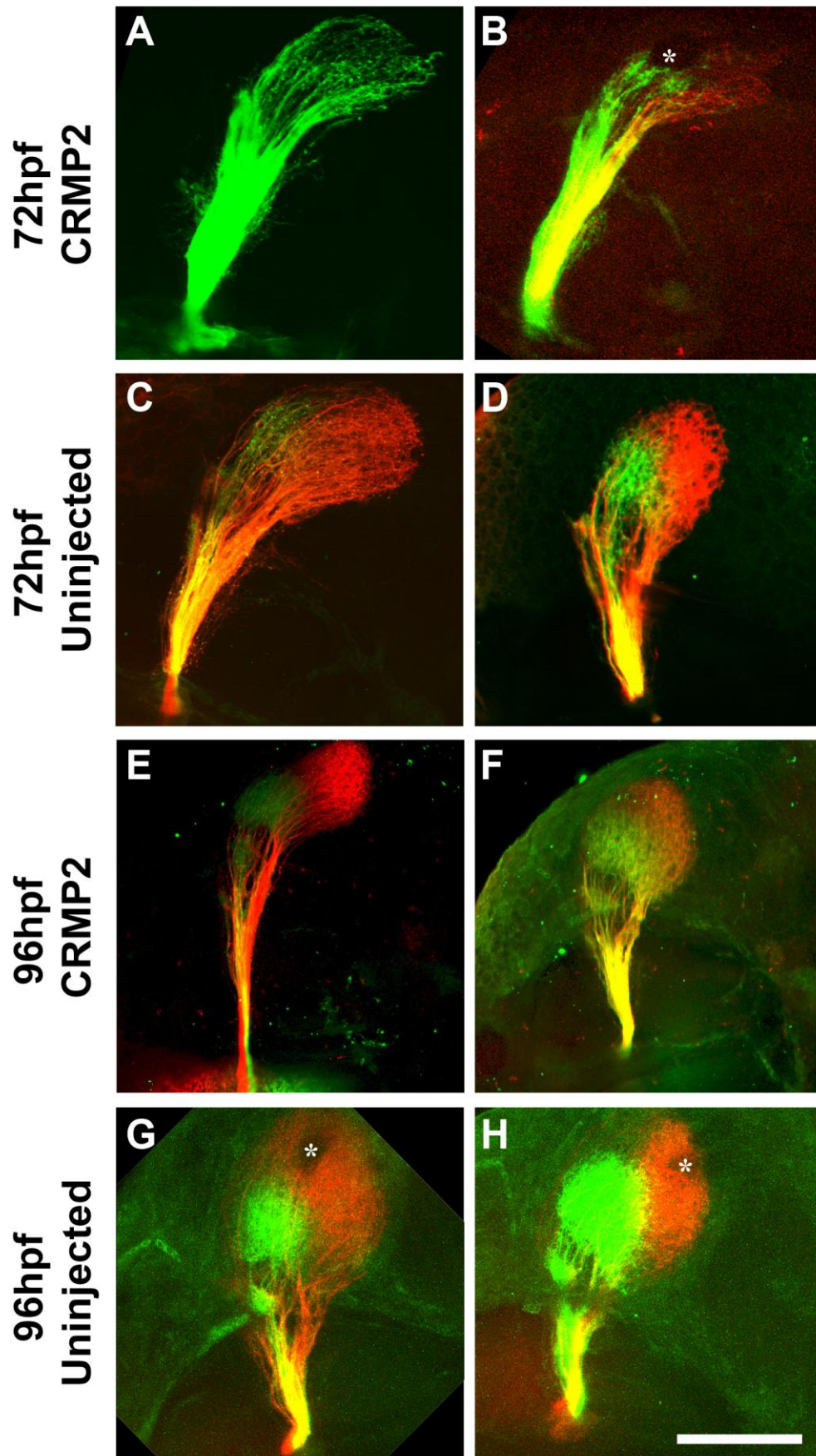
Fig. 4.5. Crmp2 IE Mo2 morphants show sparse innervation of the tectum at 72hpf but are indistiguishable from controls at 96hpf. Lateral views of confocal image stacks of the optic tract in whole-mounted wild type embryos, following labelling of the temporal retina with DiO and nasal retina with DiI.

A, B. 72hpf *crmp2* morphants (injected with 0.5mM crmp2 IE Mo2 at the 1-4 cell stage) exhibit axons that appear sparser, coarser and less branched than untreated 72hpf embryos (C, D). This phenotype is similar to the 60hpf time point (Fig. 4.4C).

C, D. 72hpf controls showing finely branched axons which form a distinctive club shape on the tectum.

E, F. 96hpf *crmp2* morphants (injected with 1mM splice site directed morpholino crmp2 IE Mo2 at the 1-4 cell stage) showing a phenotype of finely branched axons which is indistinguishable from controls (**G, H).**

Asterisks in B, G and H indicate overlying melanophores which impede laser penetration.

Dorsal is up, rostral is left. Scale bar = 100μm.

4.7.5 *Crmp2* morphant phenotype confirmed in the *pou4f3:GFP* line

To independently confirm the morphant phenotypes observed after tracing, we generated morphants in the *pou4f3:GFP* line which expresses GFP in the majority of RGCs.

This phenotype observed in pou4f3 crmp2 IE Mo2 morphants (Fig. 4.6) closely resembles that seen in wild type crmp2 IE Mo2 morphants (Fig. 4.5). That is, more sparsley innervated tectum with axons that appear coarser and less branched when compared to controls. Thus providing a strain and tracer independent confirmation of phenotype. Crmp2 IE Mo2 was injected at concentrations of 0.5mM (n=25), 0.75mM (n=9) and 1mM (n=9). As with the wild types, the phenotype was most pronounced at the highest concentration. These phenotypes were judged against the baseline phenotypes of 1mM control morpholino injected pou4f3 embryos (n=18). The optic projection in control morpholino injected pou4f3:GFP embryos was indistinguishable from that in uninjected embryos (n=30), indicating that morpholino injections do not have nonspecific effects on the branching pattern of RGC axons. The reduced variability in the fluorescence of RGCs due to the expression of transgenic GFP and lack of background labelling, compared to lipophillic tracers, allows for detailed quantitative analysis. This *crmp2* knockdown phenotype was partially phenocopied with a second, independent morpholino against *crmp2*. Crmp2 Start Mo2 elicited an RGC axon phentoype which is qualitatively comparable but less pronounced than that elicited by crmp2 IE Mo2. With injection of 2mM crmp2 Start Mo2 (n=23) the phenotype is that of a more sparsley innervated tectum with axons that appear coarser and less branched when compared to embryos treated with 2mM control morpholino (n=19) (Fig. 4.7). No phenotype was observable at lower concentrations. Efficacy of individual morpholinos varies. As crmp2 Start Mo2 is a start directed morpholino it's efficicacy cannot be readily measured for comparison with that of crmp2 IE Mo2 (Fig. 4.3).

Additional *crmp2* morpholinos were investigated at 2mM but failed to elicit a phenotype; crmp2 Start Mo1 (n=9) and crmp2 IE Mo1 (n=6).
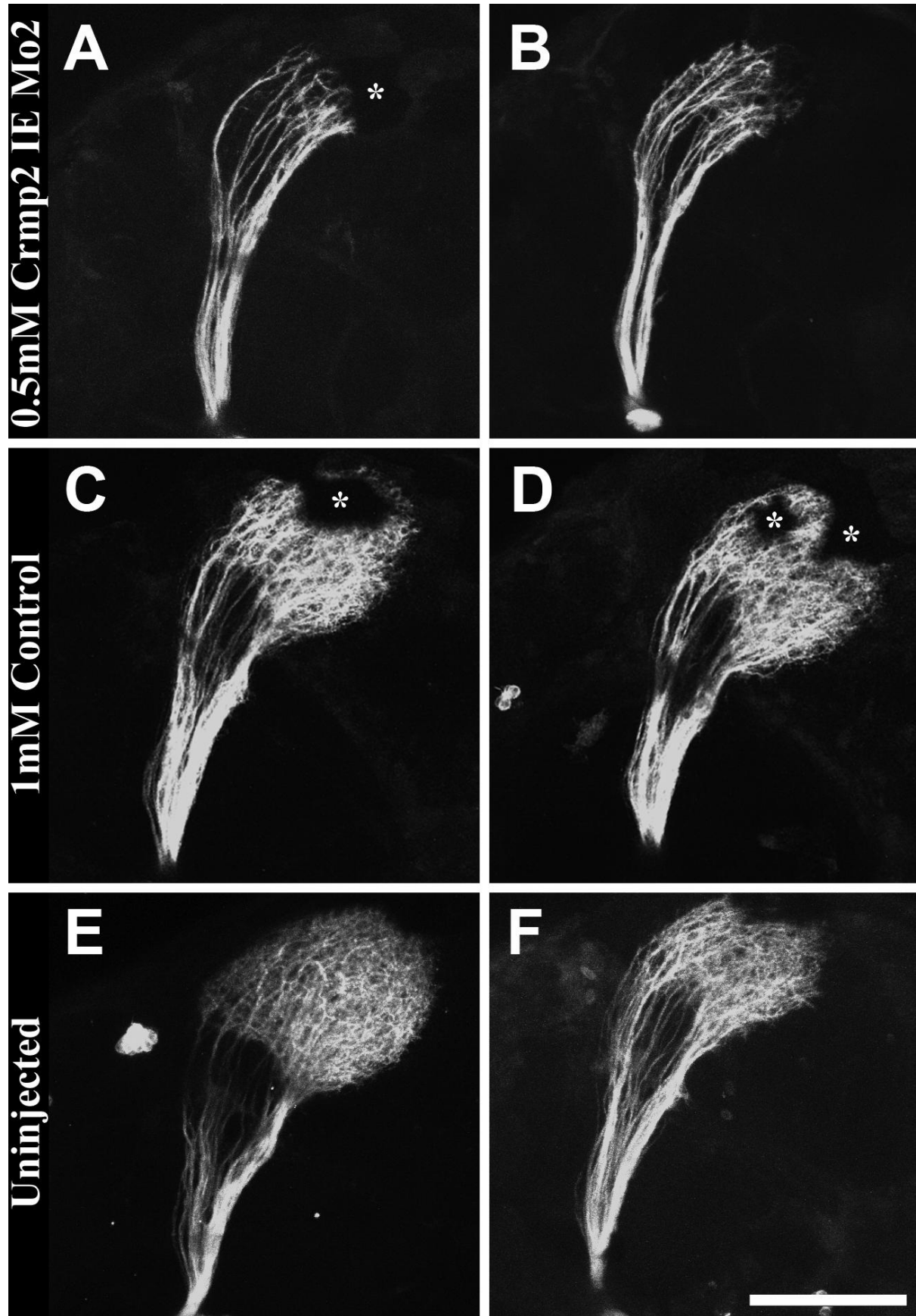
Fig. 4.6. Crmp2 IE Mo2 morphants generated in the Tg(pou4f3:gap43-GFP)^{s356t} line show sparse innervation of the tectum at 72hpf. Lateral views of confocal image stacks of the optic tract in whole-mounted Tg(pou4f3:gap43-GFP)^{s356t} embryos which have GFP expressing RGCs.

A, B. 72hpf *crmp2* morphants (injected with 0.5mM crmp2 IE Mo2 at the 1-4 cell stage) show RGC axons that appear sparser, coarser and less branched than control 72hpf embryos (C, D). This phenotype closely resembles that seen in *crmp2* morphants generated in the wild type strain (Fig. 4.5A and B).

C, D. 72hpf controls showing finely branched axons which form a distinctive club shape on the tectum. This phenotype closely resembles that seen in uninjected Tg(pou4f3:gap43-GFP)^{s356t} embryos (E, F) and wild type embryos (Fig. 4.5C and D).

E, F. 72hpf uninjected embryos showing finely branched axons which form a distinctive club shape on the tectum. Asterisks in A, C and D indicate overlying melanophores which impede laser penetration.

Dorsal is up, rostral is left. Scale bar = 100μm.
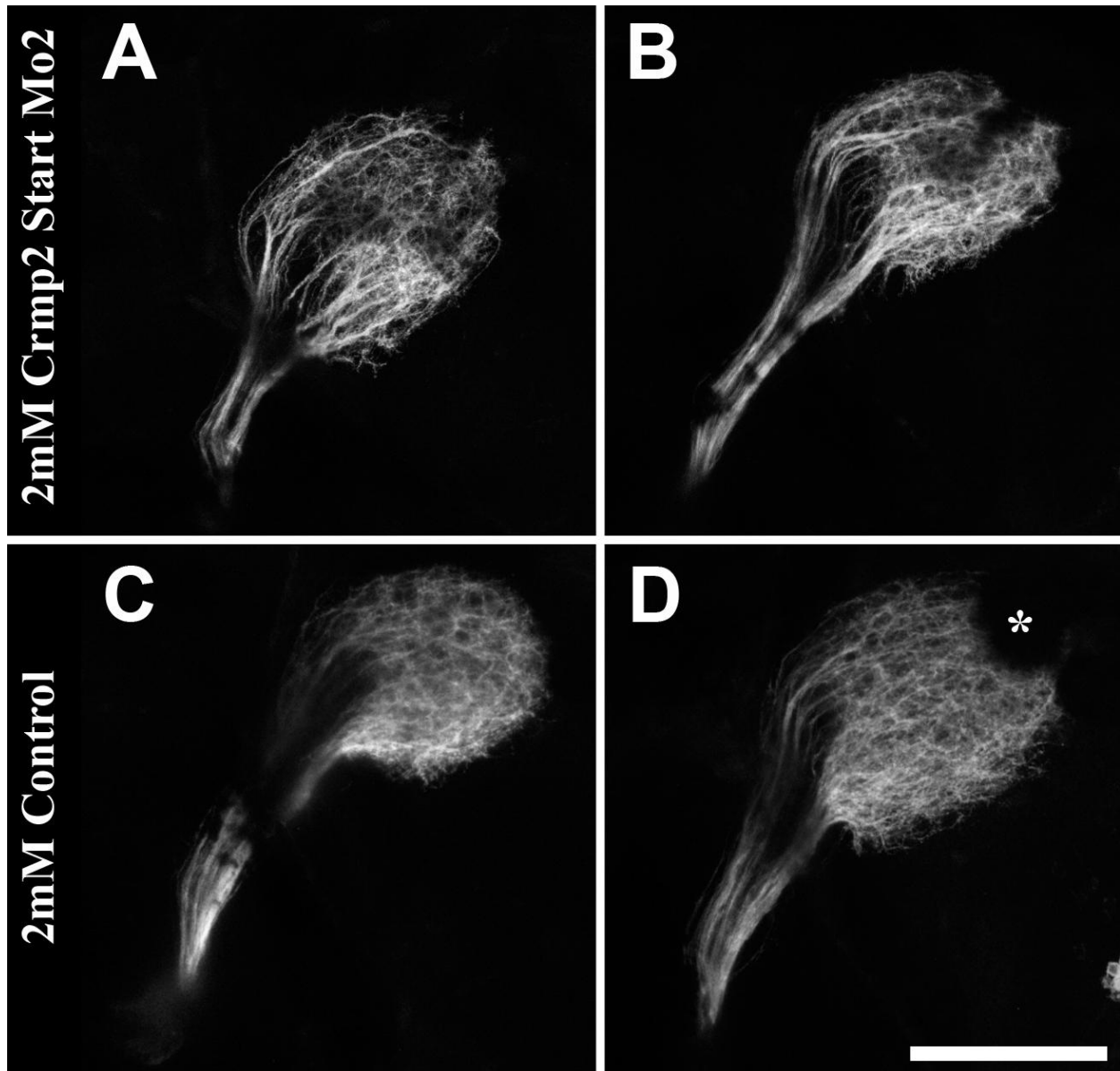
Fig. 4.7. Crmp2 morphants generated in the Tg(pou4f3:gap43-GFP)^{s356t} line show sparse innervation of the tectum at 72hpf. Lateral views of confocal image stacks of the optic tract in whole-mounted Tg(pou4f3:gap43-GFP)^{s356t} embryos which have GFP expressing RGCs.

A, B. 72hpf *crmp2* morphants (injected with 2mM crmp2 Start Mo2 at the 1-4 cell stage) show RGC axons that appear sparser, coarser and less branched than control 72hpf embryos (C, D). This phenotype resembles a less pronounced phenocopy of that seen in crmp2 IE Mo2 morphants (Fig. 4.6A and B).

C, D. 72hpf controls showing finely branched axons which form a distinctive club shape on the tectum. This phenotype closely resembles that seen in wild type embryos (Fig. 4.5C and D).

Asterisk in D indicates overlying melanophores which impede laser penetration.

Dorsal is up, rostral is left. Scale bar = 100μm.

### 4.7.6 Quantitation of RGC axon phenotype on the tectum

4.7.6.1 Morpholinos against *crmp2* have stastistically significant effects on the phenotype of RGC axons on the tectum

The histogram method effectively quantifies how coarse and pronounced the axon fascicles across the tectum are. Many finely branched axons would present a diffuse, homogenous distribution of pixels resulting in low SD of average pixel brightness whereas few, coarse axons would present distinct bright lines with dark pixels in the intervening spaces, resulting in a high SD. The pou4f3:GFP embryos treated with crmp2 IE Mo2 (0.5mM, n=24 and 0.75mM, n=9) had SDs which were stastistically significantly higher than the control morphants (n=18) with $p<0.05$ and $p<0.0001$, respectively (Fig. 4.8). There is no significant difference (NS) between uninjected (n=30) and control morpholino treated embryos. The less pronounced phenocopy elicited by 2mM crmp2 Start Mo2 (n=23), is also statistically signficant compared to 2mM control morpholino treated embryos (n=18) with $p<0.05$ (Fig.4.9).

The single morpholinos and morpholino combinations which did not yield a qualitative phenotype were analysed using the histogram method. All comparisons are non significant, in agreement with observer visual assessment (Fig. 4.10). Crmp2 Start Mo1 was injected at 2mM and still remained qualitatively and quantitatively non-significant (Fig. 4.9). This indicates that this assessment method does not produce false positives for the morpholinos we have analysed, even at higher concentrations of morpholino. However, any morpholino will produce toxic effects at sufficient concentrations. While 2mM control morpholino injections did not lead to an observable phenotype similar to that of the morpholinos against *crmp2*, it did have an effect on the quantified standard deviation. A decrease in pixel intensity SD ($p<0.05$) when compared to controls was observed (Fig. 4.9). Nonetheless, this is in contrast to the standard deviation increases witnessed with both *crmp2* morpholinos which elicit a phenotype (crmp2 IE Mo2, Fig. 4.8 and crmp2 Start Mo2, Fig. 4.9).
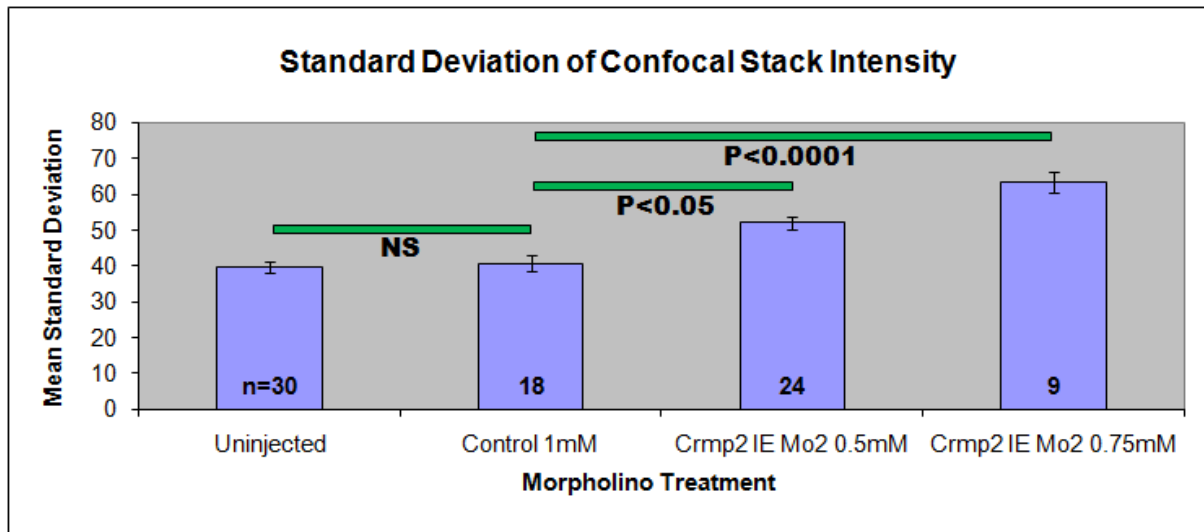
Fig.4.8. Crmp2 IE Mo2 has statistically significant effects on the phenotype of RGC axons on the tectum.
Cross sections of collapsed confocal stacks from 72hpf Tg(pou4f3:gap43-GFP)[s356t] larvae were analysed using the ImageJ histogram function. The mean standard deviations for each condition were then compared using an ANOVA with Tukey post hoc test. There is no significant difference (NS) between uninjected and control morpholino treated embryos, thus ruling out morpholino toxicity. There is a statistically significant difference between the SD of controls and the SD of crmp2 IE Mo2 morphants at 0.5mM ($p<0.05$) and 0.75mM ($p<0.0001$).

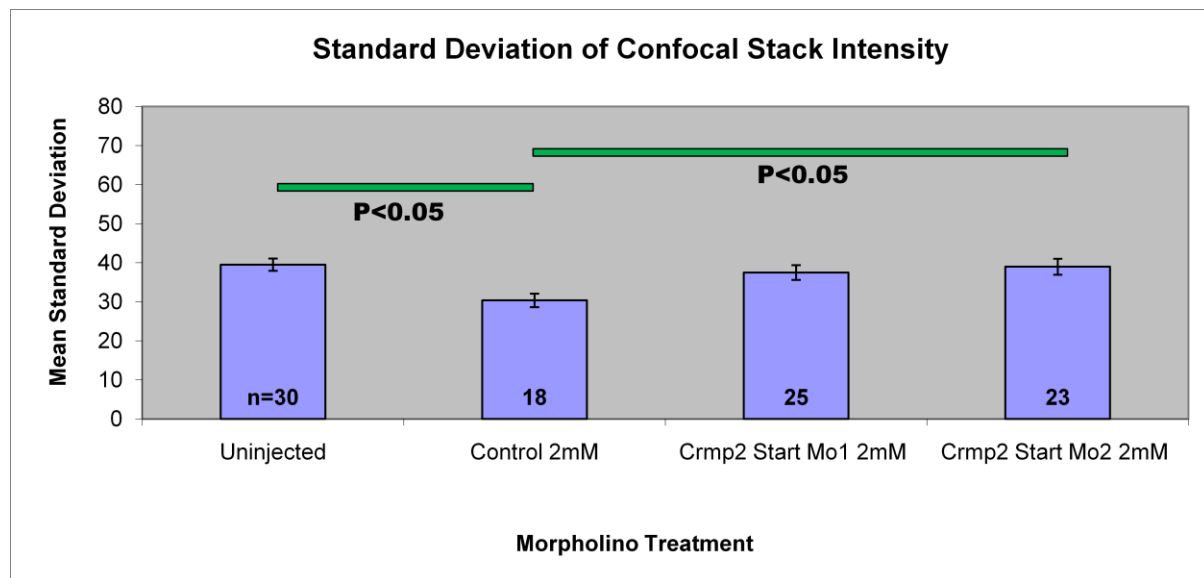**Fig. 4.9. A second *crmp2* morpholino, crmp2 Start Mo2, has statistically significant effects on the phenotype of RGC axons on the tectum.**
There is a statistically significant difference between the SD of control and SD of the crmp2 Start Mo2 morphants at 2mM ($p<0.05$) but not crmp2 Start Mo1. However, at 2mM concentration control morpholino SD is reduced compared to uninjected SD ($p>0.05$).
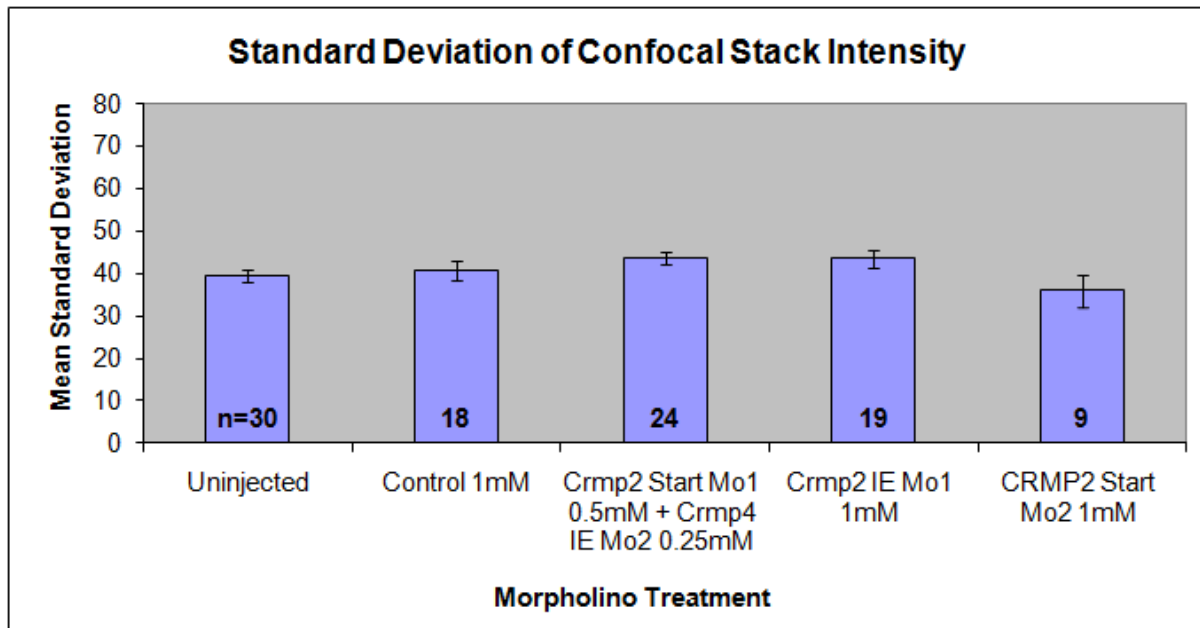
Fig. 4.10. Other *crmp* morpholinos had no stastically significant effect on the phenotype of RGC axon on the tectum.

All comparisons are non-significant. This is in agreement with qualitative methods of observation, indicating a lack of false positives with this method of analysis.

4.7.6.1.1 General embryo development

Two readily accessible and relevant measures of embryo development are the overall embryo length and the width of the eye. A reduction in either of these could indicate a general retardation of development by morpholino treatment. A sparser tectal innervation could then be due to the retarded developmental state of the embryo rather than specific effects on tectal innervation. Crmp2 IE Mo2 morphants exhibit a statistically significant quantitative whole projection phenotype at 0.5mM (Fig. 4.8). At 0.5mM neither body length (Fig. 4.11) or nasotemporal eye width (Fig. 4.12) is statistically significantly reduced. This indicates that the RGC axon phenotype observed in embryos treated with 0.5mM crmp2 IE Mo2 cannot be attributed to general developmental retardation, based on these measures.

174

Fig. 4.11. Crmp2 IE Mo2 does not reduce embryo body length at 0.5mM in 3dpf embryos. Embryo body length is not significantly reduced by these treatments. Thus the RGC axon phenotype observed is not due to retardation of embryo development.

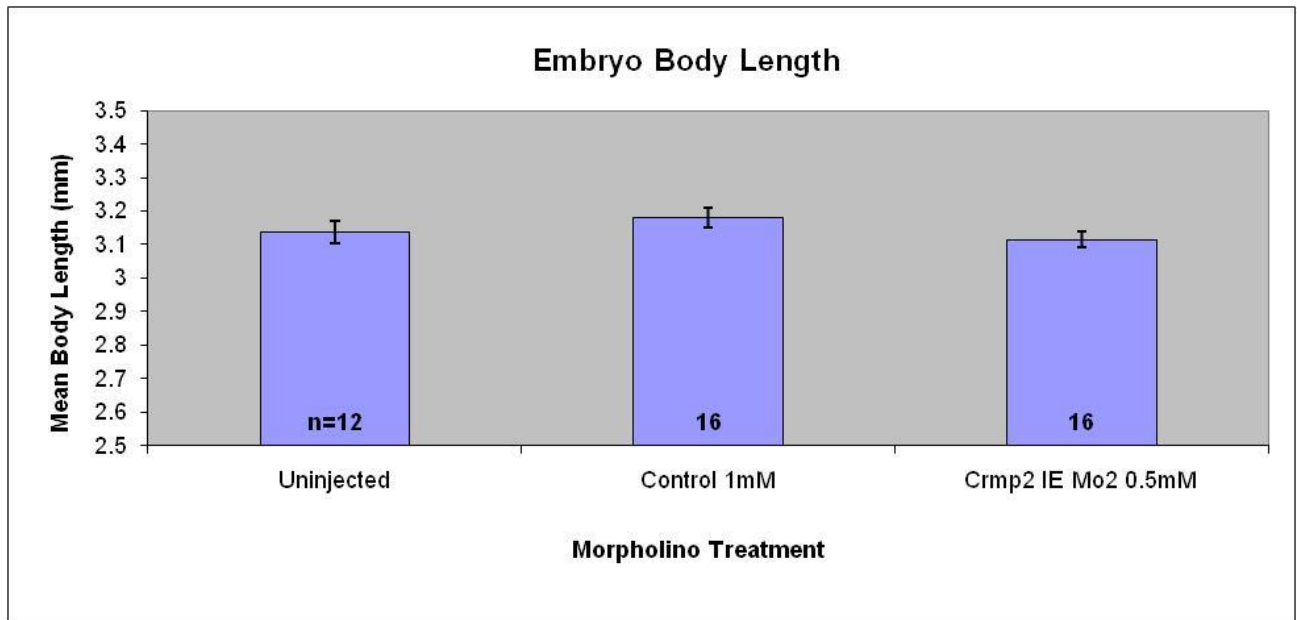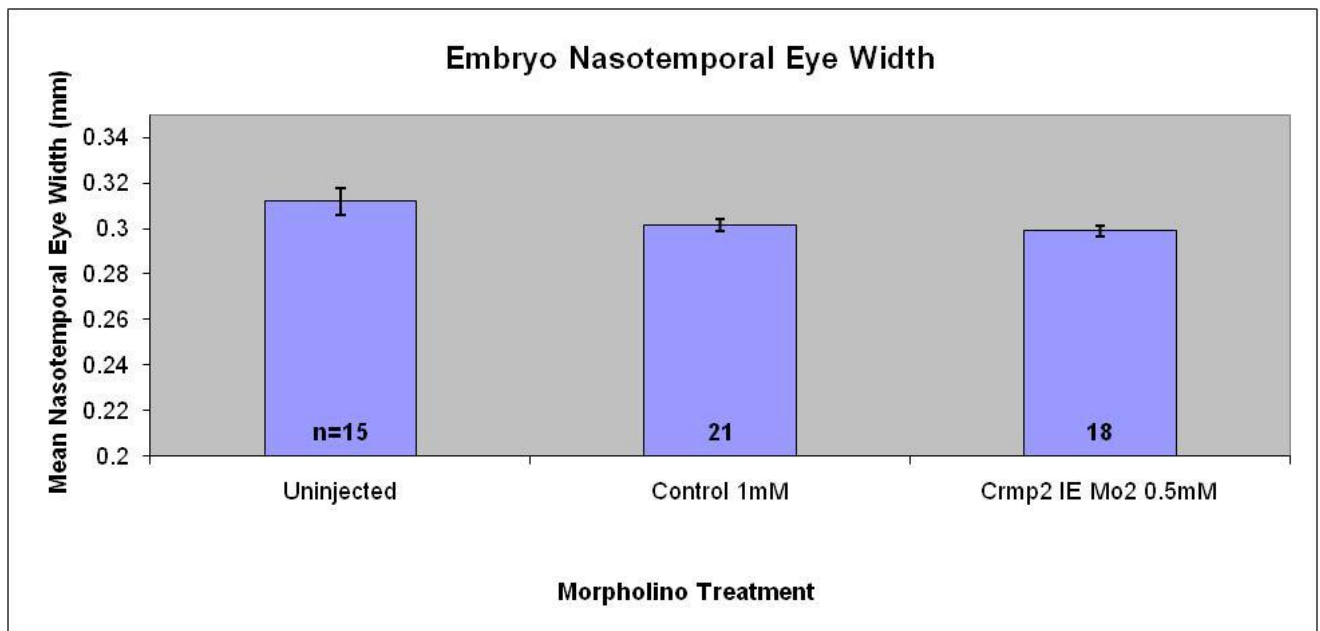**Fig.4.12. Crmp2 IE Mo2 does not reduce eye width at 0.5mM in 3dpf embryos.** Nasotemporal eye width is not significantly reduced by these treatments. Thus the RGC axon phenotype observed is not due to retardation of general eye development.

4.7.6.1.2 Effect on embryo size with increasing morpholino concentration

Crmp2 Start Mo2 morphants exhibit a statistically significant tectal phenotype at 2mM (Fig. 4.9). The body length of crmp2 Start Mo2 morphants is not altered relative to uninjected (Fig. 4.13). However it is increased relative to 2mM control morphants (p<0.01, Fig. 4.13). Whereas nasotemporal eye width is reduced relative to uninjected (p<0.01) and 2mM control morphants (p<0.05, Fig. 4.14). Control morpholino treatment at 2mM reduces nasotemporal eye width relative to uninjected also (p<0.01, Fig. 4.14). The reduction of eye size by both active and control morpholinos at 2mM most likely indicates retardation of development induced by toxic effects. Whereas the increase in body length induced by active but not control morpholino is unexpected and cannot be readily explained by effects of retardation. This may indicate that the phenotype observed in the optic projection in 2mM crmp2 Start Mo2 morphants may in part be caused by non-specific effects of the treatment.
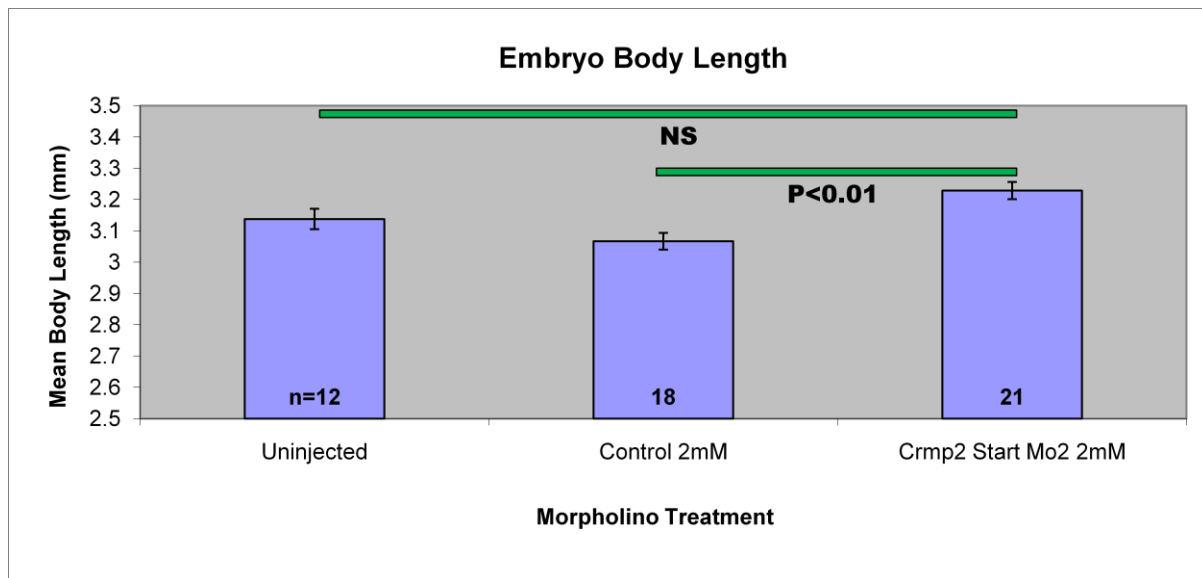
Fig. 4.13. Crmp2 Start Mo2 increases embryo body length relative to controls but not uninjected at 2mM in 3dpf embryos. While control morpholino reduces embryo body length relative to controls it is non-significant, as may be expected from mild toxicity due to the high morpholino concentration. However crmp2 start Mo2 stastically significantly increases embryo body length relative to controls (p<0.01) but not uninjected (non-significant), which cannot be readily explained by general retardation due to morpholino toxicity.
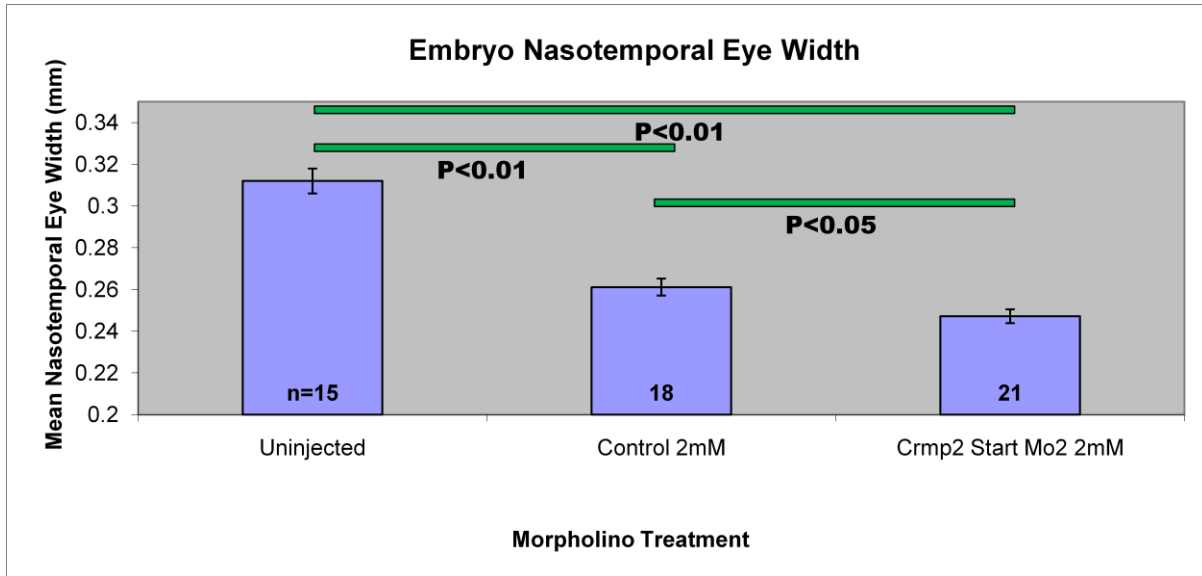
Fig.4.14. Crmp2 Start Mo2 and control morpholino treatment induces reduced eye width at 2mM in 3dpf embryos. As control morpholino treatment also leads to nasotemporal eye width reduction, this may be an indication of developmental retardation of the eye due to morpholino toxicity.

4.7.6.2 Individual axon labelling
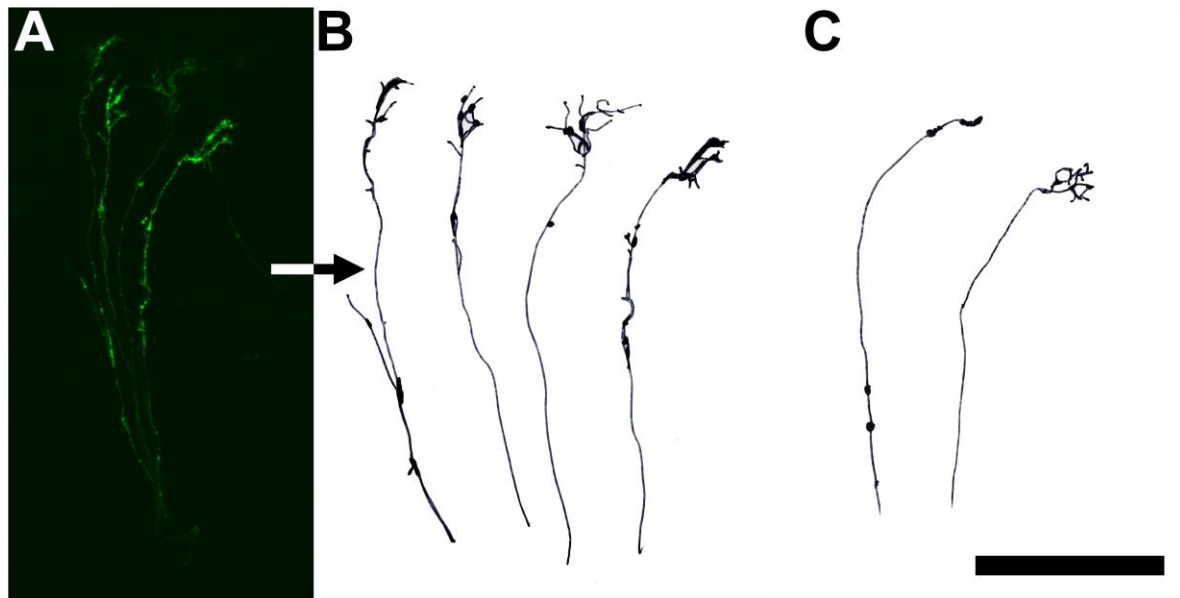
Fig. 4.15. Tracing individual axons for analysis. Injection of the Pou4f3:GAL4;UAS:GAP43-GFP construct results in mosaic expression of GFP in a random minority of retinal ganglion cells. The construct has been co-injected with crmp2 IE Mo2 morpholino allowing individual morphant arbors to be studied using software traces (B) made from compressed confocal stacks (A). Both control morphants and *crmp2* morphants show a wide range of arbor phenotypes in terms of branch number and branch length (C). These examples are from *crmp2* morphants. Dorsal is up, rostral is left. Scale bar = 100μm

4.7.6.2.1 BGUG plasmid coinjected with morpholino

To study the phenotype of individual morphant axons, morpholino was coinjected with the BGUG plasmid which results in a minority of RGCs expressing GFP. The two groups were 0.5mM crmp2 IE Mo2 plus BGUG plasmid, n = 28 axons from 18 embryos and 0.5mM control morpholino plus BGUG plasmid, n =13 axons from 6 embryos. Using SimpleNeuriteTracer, multiple properties of the axons were quantified and assessed with a Mann-Whitney test. Both controls and *crmp2* morphants show a wide range of arbor phenotypes in terms of branch number and branch length which overlap between the two treatments (Fig. 4.15C).

Total axon length

The total length of a traced axon from the optic nerve head to the terminations, including the main branch and all collaterals: *Crmp2* morphants 370.1 ± 19.0 μm, Controls 391.7 ± 21.2 μm, p = 0.2743.

Length of main branch

The length of only the longest continuous branch from optic nerve head to termination, excluding any collaterals: *Crmp2* morphants 301.5 ± 11.4 μm, Controls 328.6 ± 12.9 μm, p = 0.0934.

Mean length of collateral branches

The mean length of the collateral branches, excluding the main branch: *Crmp2* morphants 10.34 ± 0.97 μm, Controls 12.01 ± 1.39 μm, p = 0.0985.

Branch tip number

The total number of branch tips: *Crmp2* morphants 3.536 ± 0.470, Controls 4.385 ± 0.646, p = 0.1112.

Branch order

The maximum number of branches that can be counted along a continuous route from the optic nerve head to a termination: *Crmp2* morphants 2.107 ± 0.342, Controls 3.000 ± 0.494, p = 0.0764.

For all measures the *crmp2* morphants tend to reduced numbers. This trend may indicate a shift towards a stunted, less complex arbor phenotype with fewer, shorter branches. However with current assessed axon numbers there is a lack of statistical significance for all single axon measures.

4.7.6.2.1.1 General embryo development

Embryo body length (Fig. 4.16) and nasotemporal eye width (Fig. 4.17) were not significantly statistically reduced by either plasmid injection with or without crmp2 IE Mo2 application. This indicates that general embryo development and eye development were not retarded by the treatments and so reduces the possibility that the effect observed on individual axons was due to non-specific or toxic effects of the treatment.

Fig.4.16. Combined plasmid and morpholino treatments do not reduce embryo body length in 3dpf embryos.
Embryo body length is not significantly reduced by plasmid treatment, whether in conjunction with control or crmp2 IE Mo2 morpholino. Thus the RGC axon phenotype observed is not due to retardation of embryo development.
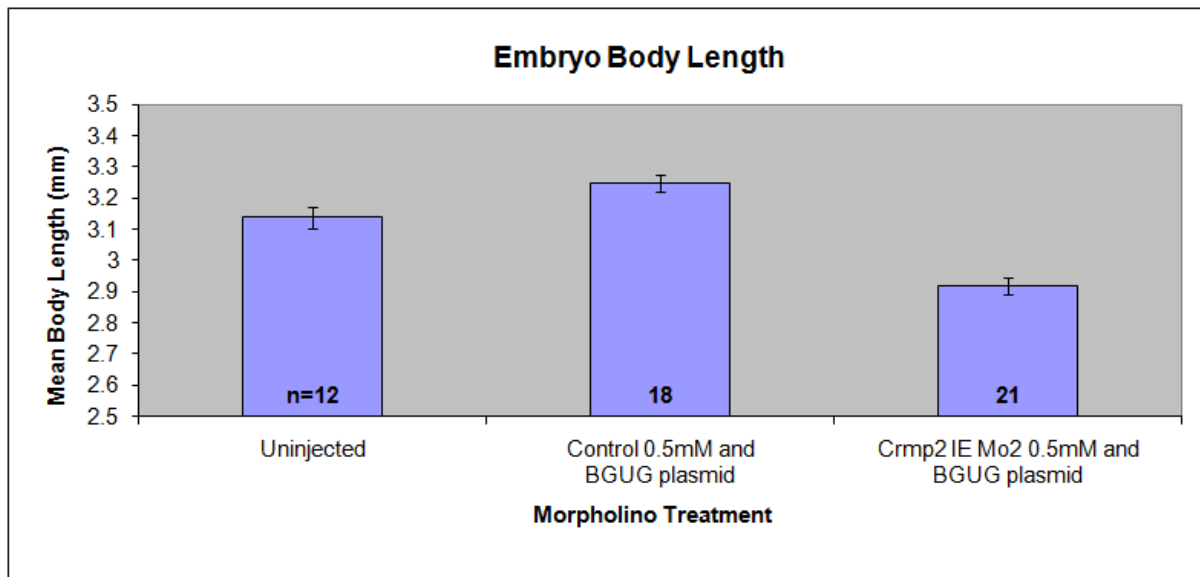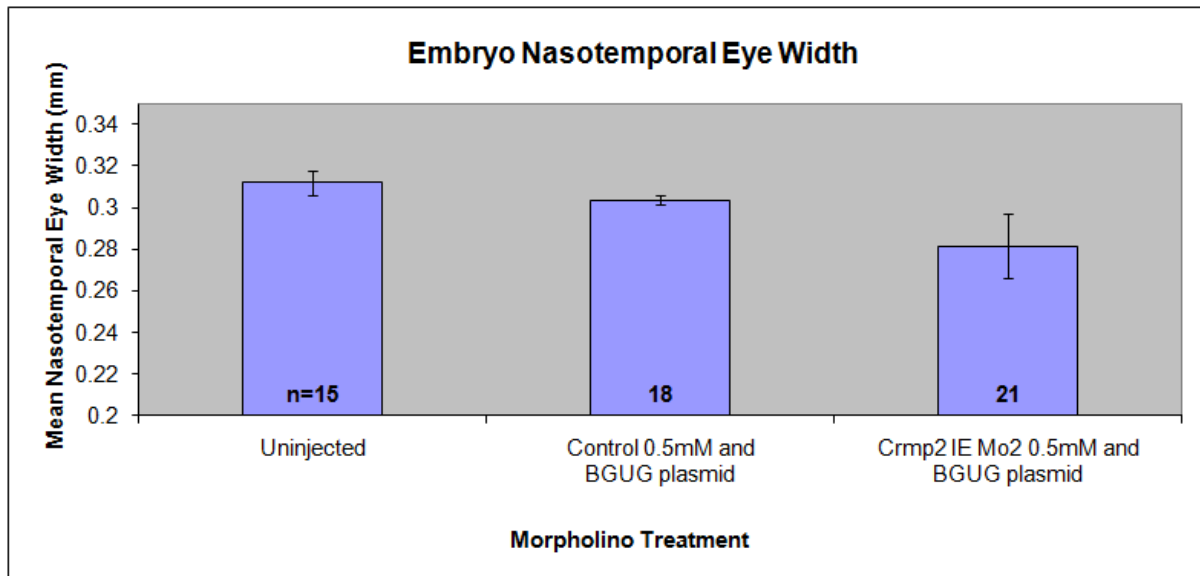
Fig.4.17. Combined plasmid and morpholino treatments do not reduce embryo body length in 3dpf embryos.
Nasotemporal eye width is not significantly reduced by plasmid treatment, whether in conjunction with control or crmp2 IE Mo2 morpholino. Thus the RGC axon phenotype observed is not due to retardation of general eye development.

4.7.6.2.2 Crmp2 dominant negative construct

We analysed the effects of a Crmp2 dominant negative over-expression construct as an alternative approach to morpholinos to reduce Crmp2 activity. The two treatments were DNcrmp2 and BG plasmid, n = 38 axons from 20 embryos and BGUG plasmid, n =21 axons from 13 embryos. The BG plasmid contains the upstream promoter elements which are activated in cells, such as RGCs, which express pou4f3. It is coinjected with the DNcrmp2 plasmid which contains the downstream components which lead to dominant negative Crmp2 and GFP expression when the pou4f3 promoter is active. The control for this experiment is the BGUG plasmid which has the same upstream promoter as the BG which leads to GFP expression only, without dominant negative Crmp2 expression. Using SimpleNeuriteTracer, multiple properties of the axons were quantified and assessed with a Mann-Whitney test.

Total axon length

The total length of a traced axon from the optic nerve head to the terminations, including the main branch and all collaterals: DNcrmp2 444.8 ± 14.3µm, Control 488.5 ± 28.7 µm, p=0.1151.

Length of main branch

The length of only the longest continuous branch from optic nerve head to termination, excluding any collaterals: DNcrmp2 337.8 ± 7.7µm, Control 372.8 ± 16.1µm, p=0.0107.

Mean length of collateral branches

The mean length of the collateral branches, excluding the main branch: DNcrmp2 15.03± 1.20, Control 15.23 ± 1.42, p=0.4761.

Branch tip number

The total number of branch tips: DNcrmp2 4.658 ±0.448, Control 5.238 ± 0.73, p=0.3156.

Branch order

The maximum number of branches that can be counted along a continuous route from the optic nerve head to a termination: DNcrmp2 2.737 ± 0.269, Control 3.619 ± 0.575, p=0.1492.

As with the individual axon measurements from morphants, all measures for the Crmp2 dominant negative expressing axons tend to reduced numbers. This trend may indicate a shift towards a stunted, less complex arbor phenotype with fewer, shorter branches. However with current assessed axon numbers only the length of the main branch is statistically significantly reduced (p=0.0107).

4.7.7 Phenotype screens

We entered into collaborations with Dr. Tom Pratt (Edinburgh) and Dr. Sally Stringer (Manchester) to screen for optic system phenotypes induced in zebrafish embryos by treatment with morpholinos against heparan sulfate 6-O-sulfotransferase 1 (HS6ST1) and various sulfatases, respectively.

4.7.7.1 Heparan sulfate proteoglycans

Heparan sulfate proteoglycans (HSPGs) are expressed extensively in the developing brain and are involved in RGC axon navigation. HSPGs are important for growth cone navigation (Lee and Chien, 2004) and, in mice, a lack of HSPGs has been shown to increase retinoretinal projection of RGCs (Inatani et al., 2003). HSPGs are extracellular matrix molecules with varied fine structure alterations, which contribute to protein interaction, due to the action of modifying enzymes. (Esko and Selleck, 2002). These modifications of the sugar residues of the HSPGs include epimerization, de-acetylation and sulfation. Sulfation is carried out by heparan sulfate transferases (HST) which add sulfate groups to specific sugar residue positions of the heparan sulfate sugars (Lee and Chien, 2004). HS6ST1 sulfates the 6-O position of glucosamine and has been shown to affect retinal axon guidance in the chiasm of mice (Pratt et al., 2006). The investigation of HS6ST1 knockdown is at the preliminary stage. A phenotype of axons straying from the tract or tectum may have been identified but will require further scans to verify. During normal development axons navigate to 10 different arborization fields, which are precursors of retinorecipient nuclei (Burrill and Easter, 1994). Arborization field 3 (AF3) is located caudal to the tract and in controls axons can often be seen leaving the tract and growing towards AF3. In 12 of 99 controls excessive or meandering outgrowth at the level of AF3 can be observed. Treatment with a morpholino against HS6ST1 at 0.5mM increases the frequency of such errors with 7 of 18 embryos showing the tentative phenotype. Axon outgrowth from the tectum has only been observed in 2 of 103 controls and never from the posterior extent of the tectum.
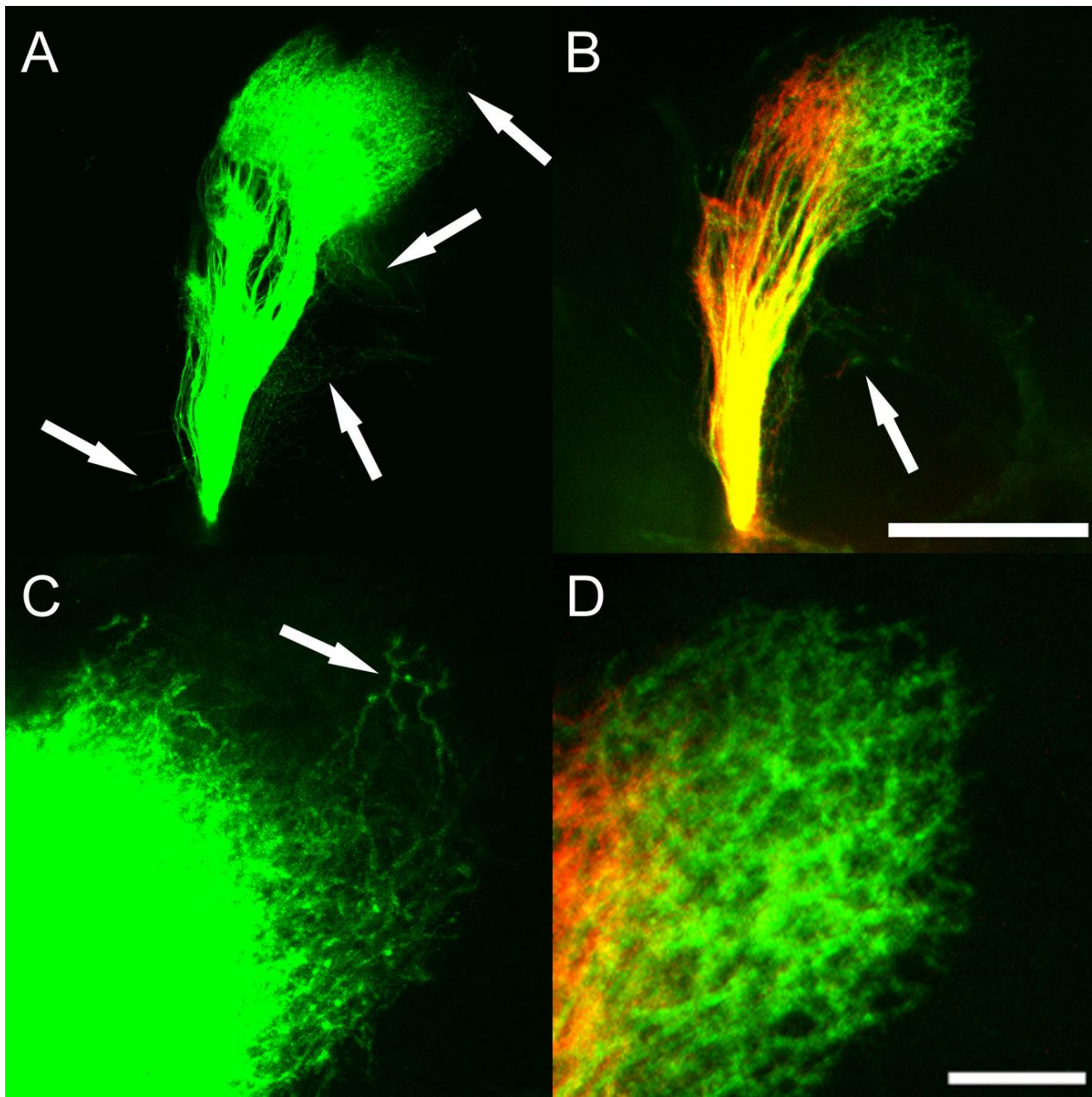
Fig. 4.18. HS6ST1 morphants exhibit axons with an increased tendency to stray from the tract and exit the tectum. Lateral views of confocal image stacks of the optic tract in a 4dpf whole-mounted HS6ST1 morphant and 3dpf uninjected embryo, after labelling of the nasal retina with DiO and temporal retina with DiI. Dorsal is up and rostral is left. **A.** 4dpf HS6ST1 morphant (injected with 0.5mM HS6ST1 morpholino at the 1-4 cell stage) with axon outgrowth from the tract and tectum. Bottom left arrow indicates outgrowth from lower tract which is uncommon in controls. Bottom right arrow indicates outgrowth towards arborization field 3 similar to that seen in controls (Arrow in B). Middle arrow indicates outgrowth from caudal tectum which is very rare in controls. Top arrow indicates outgrowth posterior from tectum which is not seen in controls. **B.** 3dpf uninjected control with outgrowth from tract towards arborization field 3 (arrow) but no outgrowth from tectum. **C.** Enlarged section from (A) showing axons exiting the posterior tectum and growing posteriorly (arrow). **D.** Enlarged section from (B) exhibiting no axon outgrowth from tectum. Scale bar for A and B = 100μm. Scale bar for C and D = 25μm.

4.7.7.2 Sulfatases

Sulfatases (sulfs) remove sulfate groups from specific sugar residues of HSPGs. Sulf1 and Sulf2 are secreted 6-O-endosulfatases involved in the processing of the 6-O position of glucosamine of HSPGs. They have an opposing activity to HS6ST1 which adds sulfate groups to the same target residue. The roles of Sulf1 and Sulf2 during normal development are not well understood but it has been shown in the mouse that they have overlapping yet essential functions (Holst et al., 2007). Six sulf targeted morpholinos are currently under investigation in collaboration with Sally Stringer's goup (Manchester); three splice blockers against Sulf1Csb, Sulf2sb and Sulf2Bsb and three start blockers against Sulf1Ca, Sulf2b and Sulf2Ba. Confocal stacks have been assembled for each of these morpholinos and they have been assessed for any abnormalities of the optic projection (as above) but no phenotype has emerged.

4.8 Discussion

We found that knockdown of Crmp2 with two independent morpholinos resulted in an axon phenotype which could be observed in whole tract tracing in the form of sparser, less branched innervation of the tectum by RGC axons. Individual axon phenotypes induced by morpholino or dominant negative Crmp2 expression tended towards less complex arbors with shorter axons overall.

It is known that microtubule dynamics and endocytosis regulate growth cone morphology (Goshima et al., 1997; Diefenbach et al., 1999; Fournier et al., 2000; Mack et al., 2000; Kamiguchi and Lemmon, 2000; Buck and Zheng, 2002) and that Crmp2 influences both of these processes, through interactions with tubulin heterodimers and Numb, leading to increased axon elongation and branching (Fukata et al., 2002; Nishimura et al., 2003; Arimura et al., 2005). Without the enhancement of microtubule assembly due to Crmp2 acting as a carrier of tubulin heterodimers, growth cone dynamics would be altered in favour of retraction. The trend towards less complex arbors and shorter axons when Crmp2 activity is reduced through dominant negative expression or morpholino application, is consistent with the role of Crmp2 in axonogenesis and neurite extension and as a transducer of known axon guidance cues such as the Sempahorins which are implicated in axon branching (Miyashita et al., 2004). Furthermore, Crmp2 facilitated Numb-mediated endocytosis has been shown to enhance axon elongation (Nishimura et al., 2003). Therefore shorter axons are consistent with reduced Crmp2. Thus reducing Crmp2 reduces axon growth by affecting multiple pathways which each reduce axon growth in their specific manner.

If the various effects of reducing Crmp2 activity are additive we may expect to see a phenotype which is less subtle than the one we have induced. One technical consideration is that we have not quantified the extent of Crmp2 knockdown or the efficacy of the dominant negative. However, it is known that these treatments are effective in the trigeminal nerves of developing zebrafish, given the effects induced by this morpholino and the dominant negative protein by our collaborators (O'Brien et al., 2009). Assuming the subtle effect is not simply due to the incompleteness of knockdown, it may be that it is a result of competing effects of Crmp2. In rat hippocampal cells in vitro, knocking down Crmp2 activity through the expression of a dominant negative Crmp2 mutant reduces axon formation (Inagaki et al., 2001). While this is in accordance with our results, we cannot extrapolate too far from these models as altering Crmp2

187

levels has different effects in different types of cell and may depend on which upstream molecule is the dominant influence at any particular time. In contrast to the results from cultured rat hippocampal cells, in vitro experiments in the rat DRG have shown that Sema3A induced growth cone collapse can be inhibited by blocking the action of Crmp2 (Goshima et al., 1995). Therefore in the rat DRG model reducing Crmp2 activity should lead to an increase in axon growth. Similarly, in vitro experiments in chick DRG have shown that NGF induced neuritogenesis can be enhanced by blocking the action of Crmp2 (Quach et al., 2004). Contradictory results have also been obtained from studies of Crmp2 facilitated Numb-mediated endocytosis which has been shown to be necessary for axon growth (Kamiguchi and Lemmon, 2000; Nishimura et al., 2003). While some studies have found that Sema3A and Ephrin-A5 induced growth cone collapse acts via increased phosphorylation of Crmp2 leading to inhibition of Numb-mediated endocytosis and so growth cone collapse (Goshima et al, 1995; Arimura et al., 2005) (Fig 4.1), others have shown that endocytosis is enhanced during Sema3A and Ephrin induced growth cone collapse (Fournier et al, 2000; Jurney et al., 2002). A possible explanation for individual in vitro experiments having contradictory findings may be due to the model being a skewed or over-simplified version of the role of Crmp2. Given the high concentrations of molecules used in in vitro experiments it is questionable if axons in vivo would ever be presented with such a monolithic influence, rather than multiple, more subtle guidance cues. During the formation of the retinotectal system in zebrafish, many guidance cues are expressed simultaneously and in partially overlapping patterns. The Semaphorins (Liu et al 2004; Wolman et al., 2007; Callander et al., 2007), Neurotrophins (Hashimoto and Heinrich, 1997; Dethleffsen et al., 2003) and Ephrins (Brennan et al., 1997; Picker et al., 1999) have all been implicated as signalling molecules upstream of Crmp2 and are all expressed in the retinotectal system during development. Crmp2 is a nexus for many types of cues ranging from mostly positive/attractant cues (Neurotrophins) to mostly inhibitory/repellent cues (Semaphorins). The Crmp2 pathway is complex and not well elucidated, so it is likely that there are other guidance and growth molecules which influence the pathway. Therefore the effect of reducing Crmp2 on growing RGC axons may be dependent on spatial and temporal expression of a variety of other molecules and to what extent they contribute to the response.

This convergence of multiple pathways and the fact that Crmp2 can act upon some of the kinases that act upon Crmp2 in a feedback loop (Leung et al., 2002) may give this pathway a

robustness that diminishes the effects of Crmp2 manipulation in the in vivo situation. Such robustness would not be unexpected in a system so essential for survival as the retinotectal system. Therefore the subtle phenotype obtained by our experiments may be an indication not of the lack of importance of Crmp2 in the developing zebrafish retinotectal system, but rather the result of complex interactions and compensatory mechanisms.

4.8.1 Manipulations of other molecules in the Crmp2 pathway in the zebrafish retinotectal system

By comparing how perturbations of molecules in the Crmp2 pathway affect the retinotectal phenotype in developing zebrafish we could draw more conclusions regarding the mechanisms underlying our observed phenotype. Unfortunately this information is largely not available as some key genes such as the relevant *semaphorins* (*sema3aa*, *sema3ab*) do not have known mutants in the zebrafish and although morpholino knockdown studies of these molecules have been carried out, they focused on areas other than the retinotectal system e.g. angiogenesis studies. The same is true for NGF, LPA and Rho-kinase (Rock1). Other genes of interest such as *nrp1a* and *nrp1b* do have mutants available but there are no citations associated with these mutants as they were identified by TILLING (Targeting Induced Local Lesions in Genomes) rather than phenotype screening so once again, there is no data on their effect on the retinotectal system. While the effects of Crmp2 knockdown, by the morpholino and by the dominant negative plasmid construct used in this study, have been investigated in the developing zebrafish regenerating trigeminal sensory axons (O'Brien et al., 2009), no comparisons can be drawn regarding axon extension as no data was provided regarding the complexity or length of the axons.

Mutants which have been studied in the retinotectal system and give a comparable phenotype to the *crmp2* morphants, are *tarde demais* (*tard*) and *late bloomer* (*late*) (See Figure 5 of Xiao et al., 2005). These mutants are described as having delayed tectal ingrowth. Both mutants exhibit sparser innervation of the tectum which is similar to that seen in *crmp2* morphants at 3dpf. However the axons appear to be shorter than those of the *crmp2* morphants as they do not reach the posterior tectum. The similarities in phenotype may provide further evidence that the *crmp2* morphant phenotype is not simply due to toxic effects but is due to a specific retardation of retinotectal development, as it is with *tard* and *late* mutants. Beyond their

affect on tectal innervation, little is known regarding these genes which were identified in a retinotectal phenotype screen and have not been sequenced.

4.8.2 Whole projection labelling but not individual axons show a statistically significant phenotype

From our results it can be seen that for crmp2 IE Mo2 morphants a clear qualitative phenotype was observed in whole projection labelling (Fig. 4.5) which was confirmed in a strain and method independent manner (Fig 4.6) and found to be statistically significant (Fig4.8) and specific (Fig 4.11 and Fig. 4.12). Treatment with crmp2 Start Mo2 provided a less pronounced phenocopy (Fig. 4.7). The tendencies of the individual axon measurements are consistent with the bulk labelling phenotypes of apparent sparser innervation of the tectum and less branching of axons but remain non-significant, with the exception of reduced main branch length in the dominant negative expressing axons. This may be due to a relatively subtle phenotype on the level of individual axons as the whole projection scans assess approximately four thousand labelled RGC axons at the 3dpf time point (personal communication, Dr. Chi-Bin Chien). Thus assessment of further individual axons may lead to the other measures also reaching significance. Alternatively there may be fewer RGC axons reaching the tectum in treated embryos due to cell death, which can be assessed in future experiments, or due to failure of neurogenesis as *crmp2* may play a role in neurogenesis (Quinn et al., 1999). There may be a systematic bias introduced as elaborate arbors are more likely to be rejected than compact arbors due to overlap with other axons making them difficult to trace. Significantly more control axons were discarded than *crmp2* morphant axons (in controls 11 axons were traced and 45 rejected, while in *crmp2* morphants 25 axons were traced and 17 rejected, p=0.0384).

4.8.3 Future direction

It is clear from these results that knocking down *crmp2* affects the normal development of the retinotectal system but the phenotype of individual axons appears to be quite subtle when observed from a single time point. As *crmp2* is implicated in growth cone response, knockdown may affect growth cone dynamics which would not be evident from a static datapoint. Time lapse confocal microscopy of transgenic axons in vivo would reveal any abnormal growth dynamics not captured with a single time point. Use of additional splice site directed morpholinos against *crmp* family members other than *crmp2*, the effects of which on mRNA can be quantified, would help to assess if the lack of phenotype when knocking down the other *crmp* family members is due to inefficient knockdown or that knocking down the target gene does not lead to a phenotype. The partial knockdown caused by crmp2 IE Mo2 could only be shown up to 24hpf by RT-PCR and the phenotype of the morphant present at 3dpf was restored to wild type by 4dpf. It is possible that *crmp2* expression is recovering by 3dpf and the phenotype witnessed at 3dpf is already partially recovered. For this reason a knockout mutant would further elucidate the role of *crmp2*. With continuing advances in genetics, such as zinc finger nucleases, creating mutant lines as required is becoming more feasible. However the lack of a vertebrate knockout line for *crmp2*, when lines exist for *crmp1* (Su et al., 2007) and *crmp3* (Quach et al., 2008) may indicate that a level of *crmp2* expression may be required for survival. A *crmp2* knockout RGC cell line would also allow the study of axon density in vitro, which is more readily measurable in culture, and is a possible explanation for why the tectal innervations appears sparser while the overall length of axons is not reduced. However, it is possible that even complete knockout of *crmp2* will not yield a severe phenotype as there are five members of the *crmp* family expressed in the developing retina which are sufficiently homologous to suggest they may share some activity and be able to partially compensate for the loss of one. This has been shown with other regeneration linked genes in zebrafish such as KLF6a and KLF7a which show no effect on axon growth when knocked down individually but have a clear phenotype when simultaneously knocked down (Veldman et al., 2007). While the literature indicates *crmp2* is the family member most integral to growth cone function and it has the most pronounced fold change during regeneration, it may be that a double or triple *crmp* knockdown or knockout would yield an enhanced phenotype. It is possible that the complexity of the pathways leading to Crmp2 and the feedback loop involving Crmp2, have a compensatory effect for altered Crmp2 levels.

Investigating the many upstream signalling molecules implicated in the Crmp2 pathway may provide results that are more readily interpreted. Some of these upstream molecules, such as *nrp1a* and *nrp1b*, already have available mutants which have not yet been studied in the retinotectal system. To fully understand the role of Crmp2 will require the dissection of the various inputs of the pathway to understand their contributions to Crmp2 mediated axon extension. Detailed temporal, in addition to spatial, expression patterns for the upstream guidance and growth molecules will also help to inform the balance of inputs to the pathway as the RGC axon navigates the retinotectal system.

Once the pathway is better elucidated and if a robust *crmp* phenotype can be established in development, a next step would be to investigate *crmp* manipulation in adult regeneration as four of the six *crmps* are upregulated during optic nerve regeneration. Interestingly, while injured rat cranial nerves show increased expression of CRMP1, 2 and 5, but not CRMP3 and 4 (Suzuki et al., 2003), zebrafish RGCs upregulate *crmp2*, *3*, *4* and *5a* following lesion but not *crmp1* and *5b* (Table 4.3). The differing responses of *crmp* family members may contribute to the differing regenerative potentials of these organisms. Manipulation during regeneration could be achieved by application of morpholinos to the transected nerve (Veldman et al., 2007) or by generation of an inducible overexpression line (Fig. 2.7), so determining any effect of *crmp2* overexpression during regeneration. As *crmp2* overexpression enhances rat cranial nerve regeneration (Suzuki et al., 2003), it would be of interest to study if *crmp2* overexpression has similar effects on the CNS of zebrafish. Comparison of the roles of the *crmps* in development and regeneration would contribute to the question of to what extent regeneration is a recapitulation of development. As the phosphorylation state of Crmp2 is a key factor determining its growth cone collapsing activity, the proportion of one state in comparison to the other may be a key factor and by reducing Crmp2 overall it may reduce Crmp2 on each side of the balance resulting in little net effect. Experiments which block or enhance the phosphorylation of Crmp2 may show effects not elicited by a flat reduction of Crmp2. A related approach would be the overexpression of specific forms of phosphorylation insensitive or dephosphorylation insensitive Crmp2 (Arimura et al., 2005). A similar situation may be presented by the relative abundance of the isoforms of Crmp2 in mammals, as the long form promotes neurite extension while the short form inhibits (Rogemond et al., 2010). This balance could be manipulated with the overexpression of one of the forms. Isoforms of Crmp2 have not yet been identified in zebrafish. However, in the latest

revision to the published zebrafish genome *crmp2*/*dpysl2* has been renamed *dpysl2b* and an entry has been created for *dpysl2a*. As yet dpysl2a has very little information associated with it other than a predicted 361bp sequence and has not been included in a scientific publication.

4.9 Conclusion

We have shown that *crmp2* plays a role in development of the retinotectal system in zebrafish. A modest reduction in *crmp2* expression leads to sparser, less branched innervation of the tectum by RGC axons. Individual axons in *crmp2* morphants and axons expressing dominant negative Crmp2, have similar phenotypes which tend towards less complex arbors with shorter branches and reduced overall axon length. This is consistent with the role of *crmp2* as a transducer of axon guidance signals and its role in axonogenesis. Reducing levels of Crmp2 further and for longer may reveal other aspects to this phenotype, as may coordinated knockdown of multiple *crmps* and other genes in the Crmp2 pathway.

4.10 Bibliography

Amores A, Suzuki T, Yan YL, Pomeroy J, Singer A, Amemiya C, Postlethwait JH. Developmental roles of pufferfish Hox clusters and genome evolution in ray-fin fish. Genome Res. 2004 Jan;14(1):1-10. PubMed PMID: 14707165; PubMed Central PMCID: PMC314266.

Arimura N, Inagaki N, Chihara K, Ménager C, Nakamura N, Amano M, Iwamatsu A, Goshima Y, Kaibuchi K. Phosphorylation of collapsin response mediator protein-2 by Rho-kinase. Evidence for two separate signaling pathways for growth cone collapse. J Biol Chem. 2000 Aug 4;275(31):23973-80. PubMed PMID: 10818093.

Arimura N, Menager C, Fukata Y, Kaibuchi K. Role of CRMP-2 in neuronal polarity. J Neurobiol. 2004 Jan;58(1):34-47. Review. PubMed PMID: 14598368.

Arimura N, Ménager C, Kawano Y, Yoshimura T, Kawabata S, Hattori A, Fukata Y, Amano M, Goshima Y, Inagaki M, Morone N, Usukura J, Kaibuchi K. Phosphorylation by Rho kinase regulates CRMP-2 activity in growth cones. Mol Cell Biol. 2005 Nov;25(22):9973-84. PubMed PMID: 16260611; PubMed Central PMCID: PMC1280267.

Brennan C, Monschau B, Lindberg R, Guthrie B, Drescher U, Bonhoeffer F, Holder N. Two Eph receptor tyrosine kinase ligands control axon growth and may be involved in the creation of the retinotectal map in the zebrafish. Development. 1997 Feb;124(3):655-64. PubMed PMID: 9043080.

Brown M, Jacobs T, Eickholt B, Ferrari G, Teo M, Monfries C, Qi RZ, Leung T, Lim L, Hall C.Alpha2-chimaerin, cyclin-dependent Kinase 5/p35, and its target collapsin response mediator protein-2 are essential components in semaphorin 3A-induced growth-cone collapse. J Neurosci. 2004 Oct 13;24(41):8994-9004. PubMed PMID: 15483118.

Buck KB, Zheng JQ. Growth cone turning induced by direct local modification of microtubule dynamics. J Neurosci. 2002 Nov 1;22(21):9358-67. PubMed PMID: 12417661.

Byk T, Dobransky T, Cifuentes-Diaz C, Sobel A. Identification and molecular characterization of Unc-33-like phosphoprotein (Ulip), a putative mammalian homolog of the axonal guidance-associated unc-33 gene product. J Neurosci. 1996 Jan 15;16(2):688-701. PubMed PMID: 8551352.

Byk T, Ozon S, Sobel A. The Ulip family phosphoproteins--common and specific properties. Eur J Biochem. 1998 May 15;254(1):14-24. PubMed PMID: 9652388.

Callander DC, Lamont RE, Childs SJ, McFarlane S. Expression of multiple class three semaphorins in the retina and along the path of zebrafish retinal axons. Dev Dyn. 2007 Oct;236(10):2918-24. Erratum in: Dev Dyn. 2008 Mar;237(3):860. PubMed PMID: 17879313.

Campbell DS, Stringham SA, Timm A, Xiao T, Law MY, Baier H, Nonet ML, Chien CB. Slit1a inhibits retinal ganglion cell arborization and synaptogenesis via Robo2-dependent and - independent pathways. Neuron. 2007 Jul 19;55(2):231-45. PubMed PMID: 17640525.

Charrier E, Reibel S, Rogemond V, Aguera M, Thomasset N, Honnorat J. Collapsin response mediator proteins (CRMPs): involvement in nervous system development and adult neurodegenerative disorders.Mol Neurobiol. 2003 Aug;28(1):51-64. Review. PubMed PMID: 14514985.

Chen WJ, Ortí G, Meyer A. Novel evolutionary relationship among four fish model systems. Trends Genet. 2004 Sep;20(9):424-31. Review. PubMed PMID: 15313551.

Cheng Q, Sasaki Y, Shoji M, Sugiyama Y, Tanaka H, Nakayama T, Mizuki N, Nakamura F, Takei K, Goshima Y. Cdk5/p35 and Rho-kinase mediate ephrin-A5-induced signaling in retinal ganglion cells. Mol Cell Neurosci. 2003 Nov;24(3):632-45. PubMed PMID: 14664814.

Chitnis AB, Kuwada JY. Axonogenesis in the brain of zebrafish embryos. J Neurosci. 1990 Jun;10(6):1892-905. PubMed PMID: 2355256.

Christie TL, Starovic-Subota O, Childs S. Zebrafish collapsin response mediator protein (CRMP)-2 is expressed in developing neurons. Gene Expr Patterns. 2006 Jan;6(2):193-200. Epub 2005 Sep 15. PubMed PMID: 16168718.

Cnops L, Van de Plas B, Arckens L. Age-dependent expression of collapsin response mediator proteins (CRMPs) in cat visual cortex. Eur J Neurosci. 2004 Apr;19(8):2345-51. PubMed PMID: 15090061.

Diefenbach TJ, Guthrie PB, Stier H, Billups B, Kater SB. Membrane recycling in the neuronal growth cone revealed by FM1-43 labeling. J Neurosci. 1999 Nov 1;19(21):9436-44. PubMed PMID: 10531447.

Dent EW, Gertler FB. Cytoskeletal dynamics and transport in growth cone motility and axon guidance. Neuron. 2003 Oct 9;40(2):209-27. Review. PubMed PMID: 14556705.

Desai C, Garriga G, McIntire SL, Horvitz HR. A genetic pathway for the development of the Caenorhabditis elegans HSN motor neurons. Nature. 1988 Dec 15;336(6200):638-46. PubMed PMID: 3200316.

Dethleffsen K, Heinrich G, Lauth M, Knapik EW, Meyer M. Insert-containing neurotrophins in teleost fish and their relationship to nerve growth factor. Mol Cell Neurosci. 2003 Oct;24(2):380-94. PubMed PMID: 14572460.

Dontchev VD, Letourneau PC. Nerve growth factor and semaphorin 3A signaling pathways interact in regulating sensory neuronal growth cone motility. J Neurosci. 2002 Aug 1;22(15):6659-69. PubMed PMID: 12151545.

Fournier AE, Nakamura F, Kawamoto S, Goshima Y, Kalb RG, Strittmatter SM. Semaphorin3A enhances endocytosis at sites of receptor-F-actin colocalization during growth cone collapse. J Cell Biol. 2000 Apr 17;149(2):411-22. PubMed PMID: 10769032; PubMed Central PMCID: PMC2175148.

Fujisawa H, Takagi S, Hirata T. Cell surface molecule A5: a putative involvement in retinal central connection. Neurosci Res Suppl. 1990;13:S11-7. PubMed PMID: 2259479.

Fukata Y, Itoh TJ, Kimura T, Ménager C, Nishimura T, Shiromizu T, Watanabe H, Inagaki N, Iwamatsu A, Hotani H, Kaibuchi K. CRMP-2 binds to tubulin heterodimers to promote microtubule assembly. Nat Cell Biol. 2002 Aug;4(8):583-91. PubMed PMID: 12134159.

Gaetano C, Matsuo T, Thiele CJ. Identification and characterization of a retinoic acid-regulated human homologue of the unc-33-like phosphoprotein gene (hUlip) from neuroblastoma cells. J Biol Chem. 1997 May 2;272(18):12195-201. PubMed PMID: 9115293.

Gallo G, Letourneau PC. Localized sources of neurotrophins initiate axon collateral sprouting. J Neurosci. 1998 Jul 15;18(14):5403-14. PubMed PMID: 9651222.

Gimnopoulos D, Becker CG, Ostendorff HP, Bach I, Schachner M, Becker T. Expression of the zebrafish recognition molecule F3/F11/contactin in a subset of differentiating neurons is regulated by cofactors associated with LIM domains. Gene Expr Patterns. 2002 Nov;2(1-2):137-43. PubMed PMID: 12617852.

Goshima Y, Kawakami T, Hori H, Sugiyama Y, Takasawa S, Hashimoto Y, Kagoshima-Maezono M, Takenaka T, Misu Y, Strittmatter SM. A novel action of collapsin: collapsin-1 increases antero- and retrograde axoplasmic transport independently of growth cone collapse. J Neurobiol. 1997 Sep;33(3):316-28. PubMed PMID: 9298768.

Goshima Y, Nakamura F, Strittmatter P, Strittmatter SM. Collapsin-induced growth cone collapse mediated by an intracellular protein related to UNC-33. Nature. 1995 Aug 10;376(6540):509-14. PubMed PMID: 7637782.

Gu Y, Hamajima N, Ihara Y. Neurofibrillary tangle-associated collapsin response mediator protein-2 (CRMP-2) is highly phosphorylated on Thr-509, Ser-518, and Ser-522. Biochemistry. 2000 Apr 18;39(15):4267-75. PubMed PMID: 10757975.

Gundersen RW, Barrett JN. Neuronal chemotaxis: chick dorsal-root axons turn toward high concentrations of nerve growth factor. Science. 1979 Nov 30;206(4422):1079-80. PubMed PMID: 493992.

Hall A. Rho GTPases and the actin cytoskeleton. Science. 1998 Jan 23;279(5350):509-14. Review. PubMed PMID: 9438836.

Hamajima N, Matsuda K, Sakata S, Tamaki N, Sasaki M, Nonaka M. A novel gene family defined by human dihydropyrimidinase and three related proteins with differential tissue distribution. Gene. 1996 Nov 21;180(1-2):157-63. PubMed PMID: 8973361.

Hashimoto M, Heinrich G. Brain-derived neurotrophic factor gene expression in the developing zebrafish. Int J Dev Neurosci. 1997 Dec;15(8):983-97. PubMed PMID: 9641529.

Hedgecock EM, Culotti JG, Thomson JN, Perkins LA. Axonal guidance mutants of Caenorhabditis elegans identified by filling sensory neurons with fluorescein dyes. Dev Biol. 1985 Sep;111(1):158-70. PubMed PMID: 3928418.

Hotta A, Inatome R, Yuasa-Kawada J, Qin Q, Yamamura H, Yanagi S. Critical role of collapsin response mediator protein-associated molecule CRAM for filopodia and growth cone development in neurons. Mol Biol Cell. 2005 Jan;16(1):32-9. Epub 2004 Oct 27. PubMed PMID: 15509652; PubMed Central PMCID: PMC539149.

Huang EJ, Reichardt LF. Neurotrophins: roles in neuronal development and function. Annu Rev Neurosci. 2001;24:677-736. Review. PubMed PMID: 11520916; PubMed Central PMCID: PMC2758233.

Inagaki N, Chihara K, Arimura N, Ménager C, Kawano Y, Matsuo N, Nishimura T, Amano M, Kaibuchi K. CRMP-2 induces axons in cultured hippocampal neurons. Nat Neurosci. 2001 Aug;4(8):781-2. PubMed PMID: 11477421.

Inatome R, Tsujimura T, Hitomi T, Mitsui N, Hermann P, Kuroda S, Yamamura H, Yanagi S. Identification of CRAM, a novel unc-33 gene family protein that associates with CRMP3 and protein-tyrosine kinase(s) in the developing rat brain. J Biol Chem. 2000 Sep 1;275(35):27291-302. PubMed PMID: 10851247.

Jurney WM, Gallo G, Letourneau PC, McLoon SC. Rac1-mediated endocytosis during ephrin-A2- and semaphorin 3A-induced growth cone collapse. J Neurosci. 2002 Jul 15;22(14):6019-28. PubMed PMID: 12122063.

Kamata T, Daar IO, Subleski M, Copeland T, Kung HF, Xu RH. Xenopus CRMP-2 is an early response gene to neural induction. Brain Res Mol Brain Res. 1998a Jun 15;57(2):201-10. PubMed PMID: 9675418.

Kamata T, Subleski M, Hara Y, Yuhki N, Kung H, Copeland NG, Jenkins NA, Yoshimura T, Modi W, Copeland TD. Isolation and characterization of a bovine neural specific protein (CRMP-2) cDNA homologous to unc-33, a C. elegans gene implicated in axonal outgrowth and guidance. Brain Res Mol Brain Res. 1998b Mar 1;54(2):219-36. PubMed PMID: 9555025.

Kamiguchi H, Lemmon V. Recycling of the cell adhesion molecule L1 in axonal growth cones. J Neurosci. 2000 May 15;20(10):3676-86. PubMed PMID: 10804209; PubMed Central PMCID: PMC1237010.

Karlsson J, von Hofsten J, Olsson PE. Generating transparent zebrafish: a refined method to improve detection of gene expression during embryonic development. Mar Biotechnol (NY). 2001 Nov;3(6):522-7. PubMed PMID: 14961324.

Kawakami A, Kitsukawa T, Takagi S, Fujisawa H. Developmentally regulated expression of a cell surface protein, neuropilin, in the mouse nervous system. J Neurobiol. 1996 Jan;29(1):1-17. PubMed PMID: 8748368.

Koppel AM, Feiner L, Kobayashi H, Raper JA. A 70 amino acid region within the semaphorin domain activates specific cellular response of semaphorin family members. Neuron. 1997 Sep;19(3):531-7. PubMed PMID: 9331346.

Leung T, Ng Y, Cheong A, Ng CH, Tan I, Hall C and Lim L. p8O ROK alpha binding protein is a novel splice variant of CRMP-1 which associates with CRMP-2 and modulates RhoA-induced neuronal morphology. FEBS LETT. 2002 532(3):445-449.

Li W, Herman RK, Shaw JE. Analysis of the Caenorhabditis elegans axonal guidance and outgrowth gene unc-33. Genetics. 1992 Nov;132(3):675-89. PubMed PMID: 1468626; PubMed Central PMCID: PMC1205206.

Liu BP, Strittmatter SM. Semaphorin-mediated axonal guidance via Rho-related G proteins. Curr Opin Cell Biol. 2001 Oct;13(5):619-26. Review. PubMed PMID: 11544032.

Liu Y, Berndt J, Su F, Tawarayama H, Shoji W, Kuwada JY, Halloran MC. Semaphorin3D guides retinal axons along the dorsoventral axis of the tectum. J Neurosci. 2004 Jan 14;24(2):310-8. PubMed PMID: 14724229.

Mack TG, Koester MP, Pollerberg GE. The microtubule-associated protein MAP1B is involved in local stabilization of turning growth cones. Mol Cell Neurosci. 2000 Jan;15(1):51-65. PubMed PMID: 10662505.

Mendell LM, Arvanian VL. Diversity of neurotrophin action in the postnatal spinal cord. Brain Res Brain Res Rev. 2002 Oct;40(1-3):230-9. Review. PubMed PMID: 12589921.

Minturn JE, Fryer HJ, Geschwind DH, Hockfield S. TOAD-64, a gene expressed early in neuronal differentiation in the rat, is related to unc-33, a C. elegans gene involved in axon outgrowth. J Neurosci. 1995a Oct;15(10):6757-66. PubMed PMID: 7472434.

Minturn JE, Geschwind DH, Fryer HJ, Hockfield S. Early postmitotic neurons transiently express TOAD-64, a neural specific protein. J Comp Neurol. 1995b May 8;355(3):369-79. PubMed PMID: 7636019.

Mitsui N, Inatome R, Takahashi S, Goshima Y, Yamamura H, Yanagi S. Involvement of Fes/Fps tyrosine kinase in semaphorin3A signaling. EMBO J. 2002 Jul 1;21(13):3274-85. PubMed PMID: 12093729; PubMed Central PMCID: PMC125392.

Miyashita T, Yeo SY, Hirate Y, Segawa H, Wada H, Little MH, Yamada T, Takahashi N, Okamoto H. PlexinA4 is necessary as a downstream target of Islet2 to mediate Slit signaling for promotion of sensory axon branching. Development. 2004 Aug;131(15):3705-15. Epub 2004 Jun 30. PubMed PMID: 15229183.

Nishimura T, Fukata Y, Kato K, Yamaguchi T, Matsuura Y, Kamiguchi H, Kaibuchi K. CRMP-2 regulates polarized Numb-mediated endocytosis for axon growth. Nat Cell Biol. 2003 Sep;5(9):819-26. Epub 2003 Aug 24. PubMed PMID: 12942088.

O'Brien GS, Martin SM, Söllner C, Wright GJ, Becker CG, Portera-Cailliau C, Sagasti A.Developmentally regulated impediments to skin reinnervation by injured peripheral sensory axon terminals. Curr Biol. 2009 Dec 29;19(24):2086-90. Epub 2009 Dec 3. PubMed PMID: 19962310; PubMed Central PMCID: PMC2805760.

Ozdinler PH, Erzurumlu RS. Regulation of neurotrophin-induced axonal responses via Rho GTPases. J Comp Neurol. 2001 Oct 1;438(4):377-87. PubMed PMID: 11559894.

Parent JM, Yu TW, Leibowitz RT, Geschwind DH, Sloviter RS, Lowenstein DH. Dentate granule cell neurogenesis is increased by seizures and contributes to aberrant network reorganization in the adult rat hippocampus. J Neurosci. 1997 May 15;17(10):3727-38. PubMed PMID: 9133393.

Picker A, Brennan C, Reifers F, Clarke JD, Holder N, Brand M. Requirement for the zebrafish mid-hindbrain boundary in midbrain polarisation, mapping and confinement of the retinotectal projection. Development. 1999 Jul;126(13):2967-78. PubMed PMID: 10357940.

Quach TT, Duchemin AM, Rogemond V, Aguera M, Honnorat J, Belin MF, Kolattukudy PE.Involvement of collapsin response mediator proteins in the neurite extension induced by neurotrophins in dorsal root ganglion neurons. Mol Cell Neurosci. 2004 Mar;25(3):433-43. PubMed PMID: 15033171.

Quach TT, Massicotte G, Belin MF, Honnorat J, Glasper ER, Devries AC, Jakeman LB, Baudry M, Duchemin AM, Kolattukudy PE. CRMP3 is required for hippocampal CA1 dendritic organization and plasticity. FASEB J. 2008 Feb;22(2):401-9. Epub 2007 Sep 4. PubMed PMID: 17785607; PubMed Central PMCID: PMC2268618.

Quinn CC, Chen E, Kinjo TG, Kelly G, Bell AW, Elliott RC, McPherson PS, Hockfield S. TUC-4b, a novel TUC family variant, regulates neurite outgrowth and associates with vesicles in the growth cone. J Neurosci. 2003 Apr 1;23(7):2815-23. PubMed PMID: 12684468.

Quinn CC, Gray GE, Hockfield S. A family of proteins implicated in axon guidance and outgrowth. J Neurobiol. 1999 Oct;41(1):158-64. Review. PubMed PMID: 10504203.

Rasin MR, Gazula VR, Breunig JJ, Kwan KY, Johnson MB, Liu-Chen S, Li HS, Jan LY, Jan YN, Rakic P, Sestan N. Numb and Numbl are required for maintenance of cadherin-based adhesion and polarity of neural progenitors. Nat Neurosci. 2007 Jul;10(7):819-27. Epub 2007 Jun 24. PubMed PMID: 17589506.

Rogemond V, Auger C, Giraudon P, Becchi M, Auvergnon N, Belin MF, Honnorat J, Moradi-Améli M. Processing and nuclear localization of CRMP2 during brain development induce neurite outgrowth inhibition. J Biol Chem. 2008 May 23;283(21):14751-61. Epub 2008 Mar 10. PubMed PMID: 18332147.

Ross LS, Parrett T, Easter SS Jr. Axonogenesis and morphogenesis in the embryonic zebrafish brain. J Neurosci. 1992 Feb;12(2):467-82. PubMed PMID: 1371313.

Santolini E, Puri C, Salcini AE, Gagliani MC, Pelicci PG, Tacchetti C, Di Fiore PP. Numb is an endocytic protein. J Cell Biol. 2000 Dec 11;151(6):1345-52. PubMed PMID: 11121447; PubMed Central PMCID: PMC2190585.

Schmidt EF, Strittmatter SM. The CRMP family of proteins and their role in Sema3A signaling. Adv Exp Med Biol. 2007;600:1-11. Review. PubMed PMID: 17607942; PubMed Central PMCID: PMC2853248.

Schweitzer J, Becker CG, Schachner M, Becker T. Expression of collapsin response mediator proteins in the nervous system of embryonic zebrafish. Gene Expr Patterns. 2005 Aug;5(6):809-16. PubMed PMID: 15922676.

Scott BW, Wang S, Burnham WM, De Boni U, Wojtowicz JM. Kindling-induced neurogenesis in the dentate gyrus of the rat. Neurosci Lett. 1998 May 29;248(2):73-6. PubMed PMID: 9654345.

Siddiqui SS, Culotti JG. Examination of neurons in wild type and mutants of Caenorhabditis elegans using antibodies to horseradish peroxidase. J Neurogenet. 1991;7(4):193-211. PubMed PMID: 1886035.

Su KY, Chien WL, Fu WM, Yu IS, Huang HP, Huang PH, Lin SR, Shih JY, Lin YL, Hsueh YP, Yang PC, Lin SW. Mice deficient in collapsin response mediator protein-1 exhibit impaired long-term potentiation and impaired spatial learning and memory. J Neurosci. 2007 Mar 7;27(10):2513-24. PubMed PMID: 17344389.

Suzuki Y, Nakagomi S, Namikawa K, Kiryu-Seo S, Inagaki N, Kaibuchi K, Aizawa H, Kikuchi K, Kiyama H. Collapsin response mediator protein-2 accelerates axon regeneration of nerve-injured motor neurons of rat. J Neurochem. 2003 Aug;86(4):1042-50. PubMed PMID: 12887701.

Takagi S, Kasuya Y, Shimizu M, Matsuura T, Tsuboi M, Kawakami A, Fujisawa H. Expression of a cell adhesion molecule, neuropilin, in the developing chick nervous system. Dev Biol. 1995 Jul;170(1):207-22. PubMed PMID: 7601310.

Takahashi T, Fournier A, Nakamura F, Wang LH, Murakami Y, Kalb RG, Fujisawa H, Strittmatter SM. Plexin-neuropilin-1 complexes form functional semaphorin-3A receptors. Cell. 1999 Oct 1;99(1):59-69. PubMed PMID: 10520994.

Tongiorgi E, Bernhardt RR, Schachner M. Zebrafish neurons express two L1-related molecules during early axonogenesis. J Neurosci Res. 1995 Nov 1;42(4):547-61. PubMed PMID: 8568941.

Tuttle R, O'Leary DD. Neurotrophins rapidly modulate growth cone response to the axon guidance molecule, collapsin-1. Mol Cell Neurosci. 1998 May;11(1-2):1-8. PubMed PMID: 9608528.

Veldman MB, Bemben MA, Thompson RC, Goldman D. Gene expression analysis of zebrafish retinal ganglion cells during optic nerve regeneration identifies KLF6a and KLF7a as important regulators of axon regeneration. Dev Biol. 2007 Dec 15;312(2):596-612. Epub 2007 Sep 22. PubMed PMID: 17949705.

Wahl S, Barth H, Ciossek T, Aktories K, Mueller BK. Ephrin-A5 induces collapse of growth cones by activating Rho and Rho kinase. J Cell Biol. 2000 Apr 17;149(2):263-70. PubMed PMID: 10769020; PubMed Central PMCID: PMC2175154.

Wang LH, Strittmatter SM. A family of rat CRMP genes is differentially expressed in the nervous system. J Neurosci. 1996 Oct 1;16(19):6197-207. PubMed PMID: 8815901.

Wang LH, Strittmatter SM. Brain CRMP forms heterotetramers similar to liver dihydropyrimidinase. J Neurochem. 1997 Dec;69(6):2261-9. PubMed PMID: 9375656.

Warren JT Jr, Chandrasekhar A, Kanki JP, Rangarajan R, Furley AJ, Kuwada JY. Molecular cloning and developmental expression of a zebrafish axonal glycoprotein similar to TAG-1. Mech Dev. 1999 Feb;80(2):197-201. PubMed PMID: 10072788.

Westerfield M (1989) The zebrafish book: a guide for the laboratory use of zebrafish (Brachydanio rerio). Eugene: University of Oregon Press.

Wilson SW, Ross LS, Parrett T, Easter SS Jr. The development of a simple scaffold of axon tracts in the brain of the embryonic zebrafish, Brachydanio rerio. Development. 1990 Jan;108(1):121-45. PubMed PMID: 2351059.

Wolman MA, Regnery AM, Becker T, Becker CG, Halloran MC. Semaphorin3D regulates axon axon interactions by modulating levels of L1 cell adhesion molecule. J Neurosci. 2007 Sep 5;27(36):9653-63. PubMed PMID: 17804626.

Xiao T, Roeser T, Staub W, Baier H. A GFP-based genetic screen reveals mutations that disrupt the architecture of the zebrafish retinotectal projection. Development. 2005 Jul;132(13):2955-67. Epub 2005 Jun 1. PubMed PMID: 15930106.

Yoshida H, Watanabe A, Ihara Y. Collapsin response mediator protein-2 is associated with neurofibrillary tangles in Alzheimer's disease. J Biol Chem. 1998 Apr 17;273(16):9761-8. PubMed PMID: 9545313.

Yoshimura T, Kawano Y, Arimura N, Kawabata S, Kikuchi A, Kaibuchi K. GSK-3beta regulates phosphorylation of CRMP-2 and neuronal polarity. Cell. 2005 Jan 14;120(1):137-49. PubMed PMID: 15652488.

Yuasa-Kawada J, Suzuki R, Kano F, Ohkawara T, Murata M, Noda M. Axonal morphogenesis controlled by antagonistic roles of two CRMP subtypes in microtubule organization. Eur J Neurosci. 2003 Jun;17(11):2329-43. PubMed PMID: 12814366.

5. Final thoughts

5.1 The zebrafish is an ideal model for CNS regeneration studies

The zebrafish CNS is capable of a high degree of spontaneous CNS regeneration and possesses an environment rich in growth promoting molecules and low in inhibitory molecules. The retinotectal system provides an anatomically discrete and highly accessible extension of the CNS in which over 80% of the RGC axons regenerate following optic nerve lesion, leading to full functional recovery. Zebrafish readily regenerate from crush injuries which are a realistic simulation of the majority of human CNS injuries. In vertebrate models, the regenerative capabilities of the zebrafish can only be matched by other teleost fish and a select few amphibians, such as the salamander. While more primitive fish, such as the jawless fish, are also highly regenerative they are a less appropriate model for higher vertebrates due to their relatively simple nervous system, lack of myelin, lack of limbs and technically primitive genetics (i.e. little changed from the first vertebrates) (Bullock et al., 1984; Kuratani and Ota, 2008; Kuratani, 2008). Compared to many amphibians and other teleost models, such as the goldfish, zebrafish develop and regenerate rapidly, allowing for more efficient experiments and rapid collection of results (Bernhardt, 1999). The ease of raising zebrafish and their breeding habits allows for robust numbers of embryos to be rapidly generated on demand. The use of zebrafish as a research model also sidesteps many ethics concerns which are becoming increasingly central research issues, particularly in the UK. The extent to which fish can perceive pain is still in question (Sneddon, 2009) and the concept of research being carried out on fish is less offensive to the general public than more relatable mammals. A disadvantage of the zebrafish as a newer model organism, was the lack of support infrastructure in the form of tools and mutants. However the zebrafish is gaining on the mouse with rapid mutagenesis screens generating libraries of mutant lines, especially in the optic system due to the ease of automation for detection of mutants which affect vision (Muto et al., 2005; Xiao et al., 2005; Gulati-Leekha and Goldman, 2006). With the annotation of the zebrafish genome nearing completion and new advances in genetic manipulation such as zinc finger nucleases, the availability of custom designed lines will explode. While many may harbour concerns over how well insights gained from fish CNS regeneration would translate to the ultimate goal of human CNS regeneration, it is worth noting that the zebrafish has a complex nervous system and highly developed senses,

particularly vision. The adult zebrafish retina contains 100,000 RGCs (Mangrum et al., 2002), in comparison to the mouse retina which contains around 80,000 once mature (Danius et al., 2003; Nakazawa et al., 2006). Furthermore it cannot be overstated that while the zebrafish provides an easily accessible, manipulable regeneration model, currently mammals provide models for lack of regeneration only.

5.2 Zebrafish studies inform mammalian CNS regeneration studies

CNS regeneration in the zebrafish provides a "how to guide" for regeneration of the injured vertebrate CNS, which can be more widely applied by identification of conserved components of the regeneration machinery in other species, with much still to be elucidated. With our current understanding of neuroscience and state of the art techniques, the *robo2* project (chapter 2) would have been impossible in any model which lacks intrinsic CNS regeneration. At present, much of the work concerned with regeneration in non-regenerating models focuses on determining the gene activity and set of guidance molecules that are required for axon growth during development and how to apply these findings to the adult situation. While these avenues of research will undoubtedly advance our understanding of neurogenesis, axonogenesis and axon guidance, which are vital to regeneration, it still remains unproven to what extent regeneration is a recapitulation of development. The overlap may not be sufficient to allow experimentally reexpressed developmental programs to induce regeneration in the adult. The zebrafish can directly inform us of regeneration linked cues and in doing so informs us as to what extent regeneration is a recapitulation of development for better direction of studies in higher vertebrates and humans. Our work with *robo2* (chapter 2), and hinted by the array data (chapter 3), suggests that these two processes are distinct but share expression of some genes, such as *robo2*, although the relative importance of expression of the gene differs between the two processes. Similarly, the expression of *crmps* varies between developing and adult regenerating CNS (chapter 4). Other work comparing development and regeneration in the zebrafish optic projection has revealed that, of the genes studied, while two thirds of the genes were expressed during both development and regeneration, a third were unique to regeneration (Veldman et al, 2007). Given that there are genes specific to regeneration and the genes common to both processes may have altered importance and roles, working from knowledge of developmental growth and guidance cues alone may prove an insurmountable task without a blueprint from an

existing regenerating system to work towards. The zebrafish is an ideal model to supply this guide.

5.3 Future direction

It is clear that there are complex interactions between regeneration linked genes, such as *crmp2* and multiple guidance pathways, and that the function of any one particular gene may be masked by any number of others. In zebrafish RGC explants, individual knockdown of several genes regulated during regeneration failed to elicit a phenotype until a double knockdown unmasked the function of two genes which when knocked down individually had no effect (Veldman et al., 2007). In the developing mouse optic system, individual *ephrin* knockouts have little effect on mapping, while a triple knockout of *ephrin* A2, A5 and the linked β2 subunit of the nicotinic acetylcholine receptor was required to cause a substantial disruption of mapping along the nasotemporal axis (Cang et al., 2008). This is especially true of genes which have close family members with high homology, such as the *crmps* which have both high intra-family and interspecies homology (Schweitzer et al., 2005). Generation of mutants which are knockouts for multiple *crmps* may enhance the *crmp2* phenotype we observed and would be worth further study in the context of regeneration as four of the six family members are upregulated in the RGC layer following optic nerve lesion. Likewise for members of the *fox* family, which are implicated from the microarray and in situ hybridisation findings as regulated in gradients in the retina during development and regeneration. The lack of an optic system phenotype in the *foxi1* mutant was surprising in light of its highly spatially restricted expression in the developing retina. Given the gradients of *foxg1a*, *foxg1b* and *foxd1-like* in the retina during development, knocking down these family members in a *foxi1* mutant may uncover a previously masked function of *foxi1*. As the mutation is lethal, manipulation of adult regeneration could be achieved by morpholino, heatshock inducible or other inducible system such as tetracycline inducible expression (Knopf et al., 2010). The *slits* are also highly homologous within and between species with significant homology between invertebrate and human *slits* (Brose et al., 1999). The functional properties of Slits and Robos are preserved across species as Slit and Robo proteins from different species can successfully interact (Brose et al., 1999). Similarities of expression and high homology of families between species and comparable activity between model organisms are good indications that lessons learned in zebrafish will be applicable to other

models and ultimately humans. Complete knockout of *robo2* had little effect on regeneration, despite its importance during development. At the moment we cannot be certain if this is because lack of *robo2* function is compensated for during regeneration, or if *robo2* only has its main axon guidance properties during development. The upregulation of Robo2 and its ligands during regeneration may indicate the former. Knockout of multiple *robos* and/or *slits* may also unmask phenotypes which would otherwise be compensated for by other family members in a single knockout. In mouse knockouts it has been shown that triple *slit* knockouts exhibit defects in commissural axon guidance that are not present in single or double *slit* knockouts (Long et al., 2004) and double knockouts of *robo1* and *robo2* also reveal aspects of *robo* function not apparent from single knockouts (Jaworski et al., 2010). As we already have the *robo2* knockout line, knocking down additional *robos* in this mutant would be a logical next step with the availability and ease of use of morpholinos in the zebrafish. *Robo4* is the least homologous member of the *robo* family (Park et al., 2003) and Robo3 suppresses the action of Robo1 and 2, while *robo1* knockout has shown to be a weak phenocopy of *robo2* knockout (Long et al., 2004). This would imply that of the possible *robo* combinatorial knockdowns, knockdown of *robo1* and *robo2* may have the greatest effect on axon guidance. However there is some evidence that *slits* may have other receptors apart from *robo* and targeting *slits* may reveal functions of other regeneration linked pathways (Jaworski et al., 2010). Effects of manipulations will elucidate unknown pathways and so provide better targets for future manipulation. In some cases, such as Robo/Slit interactions, the genetic work has outpaced the molecular and structural biology leaving geneticists to inform their own work through manipulation studies. How precisely vertebrate Robos and Slits interact on the structural level is poorly understood and the affinity of one Robo family member for any particular Slit family member is unclear. Whilst all three *Drosophila* Robos bind Slit domains with comparable affinities (Howitt et al., 2004), *Drosophila robo2* and *robo3* are not direct orthologues of vertebrate *robos* having arisen most likely because of independent genome duplication events (Dickson and Gilestro, 2006). Due to this we cannot conclude if our Slit2 overexpression experiments occupied all Robo receptors or if a specific Robo has a low affinity for Slit2 and could still detect other Slit cues. Such information would greatly inform which *slits* or *robos* would make the best targets of study. Molecular and structural biologists will play an important role in elucidating such interactions which will inform selection of the next generation of targets for manipulations. For example, there is

evidence that specific Heparan sulfate proteoglycan (HSPG) (see section 1.3.5.7.5) modifications may be necessary for Robo/Slit interactions to occur (Bülow and Hobert, 2004). Therefore altering the expression of a single, specific heparan sulfate modifying enzyme may be the key to knocking out all Slit/Robo interactions in one fell swoop. However more elucidation of structure is required to deduce which specific HSPG modifications are required, as given the complexity and variety of HSPGs, traditional genetic approaches would be intensive and time consuming. Such smart targeting may also help ease the transition of findings in zebrafish regeneration across to mammals, by identifying the most likely functional orthologues.

To achieve regeneration in the injured human CNS many challenges must be met and overcome. Many techniques may have to be combined to achieve this; activation of endogenous stem cells, introduction of exogenous stem cells, expression of transgenic neurotrophic factors, suppression of inhibitory factors, biological graft transplants, synthetic graft transplants, electrical stimulation, bionics and many more. Whatever methods come to the fore to combat neurodegeneration and nervous system injury, it appears certain that control of axonogenesis and directed axon guidance will play a key role towards this goal. Towards that end, zebrafish, in conjunction with many of the techniques outlined in this thesis, will make important contributions. Functional regeneration in the non-regenerative human CNS is a tall order and it is my hope that this work will contribute in some small part to that end.

5.4 Bibliography

Bernhardt RR. Cellular and molecular bases of axonal regeneration in the fish central nervous system. Exp Neurol. 1999 Jun;157(2):223-40. Review. PubMed PMID: 10364435.

Brose K, Bland KS, Wang KH, Arnott D, Henzel W, Goodman CS, Tessier-Lavigne M, Kidd T.Slit proteins bind Robo receptors and have an evolutionarily conserved role in repulsive axon guidance. Cell. 1999 Mar 19;96(6):795-806. PubMed PMID: 10102268.

Bullock TH, Moore JK, Fields RD. Evolution of myelin sheaths: both lamprey and hagfish lack myelin. Neurosci Lett. 1984 Jul 27;48(2):145-8. PubMed PMID: 6483278.

Bülow HE, Hobert O. Differential sulfations and epimerization define heparan sulfate specificity in nervous system development. Neuron. 2004 Mar 4;41(5):723-36. PubMed PMID: 15003172.

Cang J, Niell CM, Liu X, Pfeiffenberger C, Feldheim DA, Stryker MP. Selective disruption of one Cartesian axis of cortical maps and receptive fields by deficiency in ephrin-As and structured activity. Neuron. 2008 Feb 28;57(4):511-23. PubMed PMID: 18304481; PubMed Central PMCID: PMC2413327.

Danias J, Lee KC, Zamora MF, Chen B, Shen F, Filippopoulos T, Su Y, Goldblum D, Podos SM, Mittag T. Quantitative analysis of retinal ganglion cell (RGC) loss in aging DBA/2NNia glaucomatous mice: comparison with RGC loss in aging C57/BL6 mice. Invest Ophthalmol Vis Sci. 2003 Dec;44(12):5151-62. Erratum in: Invest Ophthalmol Vis Sci. 2004 Mar;45(3):806. PubMed PMID: 14638711.

Dickson BJ, Gilestro GF. Regulation of commissural axon pathfinding by slit and its Robo receptors. Annu Rev Cell Dev Biol. 2006;22:651-75. Review. PubMed PMID: 17029581.

Howitt JA, Clout NJ, Hohenester E. Binding site for Robo receptors revealed by dissection of the leucine-rich repeat region of Slit. EMBO J. 2004 Nov 10;23(22):4406-12. Epub 2004 Oct 21. PubMed PMID: 15496984; PubMed Central PMCID: PMC526463.

Jaworski A, Long H, Tessier-Lavigne M. Collaborative and specialized functions of Robo1 and Robo2 in spinal commissural axon guidance. J Neurosci. 2010 Jul 14;30(28):9445-53. PubMed PMID: 20631173.

Knopf F, Schnabel K, Haase C, Pfeifer K, Anastassiadis K, Weidinger G. Dually inducible TetON systems for tissue-specific conditional gene expression in zebrafish. Proc Natl Acad Sci U S A. 2010 Nov 16;107(46):19933-8. Epub 2010 Nov 1. PubMed PMID: 21041642; PubMed Central PMCID: PMC2993373.

Kuratani S. Evolutionary developmental studies of cyclostomes and the origin of the vertebrate neck. Dev Growth Differ. 2008 Jun;50 Suppl 1:S189-94. Epub 2008 Apr 22. Review. PubMed PMID: 18430164.

Kuratani S, Ota KG. Hagfish (cyclostomata, vertebrata): searching for the ancestral developmental plan of vertebrates. Bioessays. 2008 Feb;30(2):167-72. PubMed PMID: 18197595.

Long H, Sabatier C, Ma L, Plump A, Yuan W, Ornitz DM, Tamada A, Murakami F, Goodman CS, Tessier-Lavigne M. Conserved roles for Slit and Robo proteins in midline commissural axon guidance. Neuron. 2004 Apr 22;42(2):213-23. PubMed PMID: 15091338.

Mangrum WI, Dowling JE, Cohen ED. A morphological classification of ganglion cells in the zebrafish retina. Vis Neurosci. 2002 Nov-Dec;19(6):767-79. PubMed PMID: 12688671.

Nakazawa T, Nakazawa C, Matsubara A, Noda K, Hisatomi T, She H, Michaud N, Hafezi-Moghadam A, Miller JW, Benowitz LI. Tumor necrosis factor-alpha mediates oligodendrocyte death and delayed retinal ganglion cell loss in a mouse model of glaucoma. J Neurosci. 2006 Dec 6;26(49):12633-41. PubMed PMID: 17151265.

Park KW, Morrison CM, Sorensen LK, Jones CA, Rao Y, Chien CB, Wu JY, Urness LD, Li DY.Robo4 is a vascular-specific receptor that inhibits endothelial migration. Dev Biol. 2003 Sep 1;261(1):251-67. PubMed PMID: 12941633.

Schweitzer J, Becker CG, Schachner M, Becker T. Expression of collapsin response mediator proteins in the nervous system of embryonic zebrafish. Gene Expr Patterns. 2005 Aug;5(6):809-16. PubMed PMID: 15922676.

Sneddon LU. Pain perception in fish: indicators and endpoints. ILAR J. 2009;50(4):338-42. PubMed PMID: 19949250.

6. Appendix

6.1 Abbreviations and acronyms

A	adenine
BG	plasmid construct containing brn3c:gal4 sequence
BGUG	plasmid construct containing brn3c:gal4;uas:gap43-gfp sequence
BSA	bovine serum albumine
C	cytosine
cDNA	complementary deoxyribonucleic acid
CMZ	ciliary margin zone
CNS	central nervous system
CPN	central pretectal nucleus
cRNA	complementary ribonucleic acid
Ct	threshold cycle
dATP	desoxyadenosine triphosphate
dCTP	desoxycytosine triphosphate
dGTP	desoxyguanosine triphosphate
DiI	1,1'-dioctadecyl-3,3,3',3'-tetramethylindocarbocyanine perchlorate
DiO	3,3'-dioctadecyloxacarbocyanine perchlorate
dpf	days post fertilisation
DMSO	dimethylsulfoxide
DNA	deoxyribonucleic acid
DNase	desoxyribonuclease
dNTP	2-desoxyribonucleotide-5'-triphosphate
dpf	days post fertilization

dpl	days post-lesion
DRG	dorsal root ganglia
dTTP	deoxyhymidine triphosphate
DTT	dithiothreitol
ECM	extracellular matrix
E. coli	Escherichia coli
EDTA	ethylendiamintetraacetic acid
FACS	fluorescence activated cell sorting
G	guanosine
hpf	hours post fertilisation
LB medium	lysogeny broth medium
LCM	laser capture microdissection
LSM	laser scanning microscope
min	minute
mRNA	messenger ribonucleic acid
MS222	aminobenzoic acid ethylmethylester
n	number of animals
NaOH	sodium hydroxide
NC	nasal control retina derived sample
NL	nasal lesion derived sample
PBS	phosphate buffer saline
PC	posterior commissure
PCR	polymerase chain reaction
PFA	paraformaldehyde
pMN	motor neuron progenitor

PNS   peripheral nervous system

PPd   periventricular pretectal nucleus

qPCR   quantitative polymerase chain reaction

RGCs   retinal ganglion cells

RIN   RNA Integrity Number

RNA   ribonucleic acid

RNase   ribonuclease

RPE   retinal pigment epithelium

RT   room temperature

RT-PCR   reverse transcriptase polymerase chain reaction

SD   standard deviation

SEM   standard error of the mean

SFGS   stratum fibrosum et griseum superficiale

SPV   stratum periventriculare

T   thymine

TC   temporal control retina derived sample

TL   temporal lesion retina derived sample

Tm   melting temperature

VL   ventro-lateral thalamus

v/v   volume per volume

w/v   weight per volume

WIK   wild type strain

wpl   weeks post lesion

6.2 Materials

6.2.1 Reagents and consumables

Acetic acid anhydride 99%	Fisher Scientific, UK
Aminobenzoic acid ethylmethylester (MS222)	Sigma, MO, USA
Ampicillin, Sodium Salt	Fisher Scientific, UK
Anti-Digoxigenin-AP, Fab fragments	Roche, UK
Biocytin	Sigma, UK
Blocking Reagent	Roche Diagnostics, Germany
BSA, Fraction V	Sigma, UK
Chloroform 99%	Fisher, UK
Denhardt´s solution	Sigma, UK
DiI	Invitrogen, UK
DiO	Invitrogen, UK
DNA sample buffer (10x)	Eppendorf, UK
dNTPs	VHBio, UK
DTT	Sigma, UK
EDTA	Fisher Scientific, UK
Ethanol AR Grade	Sigma, UK
Ethidium bromide solution	Fisher, UK
Formamide 99%	Sigma, UK
Glycine >99%	Sigma, UK
Glutaraldehyde (25% solution)	VWR, UK
H_2O (nuclease free)	Fisher, UK
HCl 4M	Sigma, UK
Heparin sodium salt	Sigma, UK
LB Agar Miller Fisher BioReagents	Fisher Scientific, UK
LB medium	Fisher Scientific, UK
NBT/BCIP staining solution	Sigma, UK
Neutral Red	Sigma, UK
PAP-Pen	VWR, UK
Parafilm	Fisher Scientific, UK
Paraformaldehyde (crystalline)	Sigma, UK
Poly A RNA (P 9403)	Sigma, UK
Proteinase K	Roche, UK
Random primers	Promega, UK
Ready-Load 1Kb Plus DNA Ladder	Invitrogen, UK
Restriction endonucleases (various)	New England Biolabs, UK
RNaseOUT recombinant ribonuclease inhibitor	Promega, UK
Superfrost glass slides	VWR, UK

T4 DNA Ligase	New England Biolabs, UK
Taq Polymerase enzyme	New England Biolabs, UK
ThermoPol Buffer	New England Biolabs, UK
TissueTek	Fisher, UK
Triethanolamine	Sigma, UK
Tween-20	Sigma, UK
Yeast tRNA (brewer's)	Sigma, UK

All other chemicals purchased as pro analysis quality from Sigma-Aldrich (UK) or Fisher Scientific (UK).

6.2.2 Kits

ABC-kit	Vectastain, CA, USA
Agilent Low RNA Input Linear Amplification	Agilent Technologies, UK
GFX Micro Plasmid Prep	GE Healthcare, UK
HiSpeed Plasmid Midi	Qiagen, UK
MAXIscript	Ambion, UK
MinElute Gel Extraction	Qiagen, UK
MinElute PCR Purification	Qiagen, UK
pGEM-T Easy	Promega, UK
QIAQuick Gel Extraction	Qiagen, UK
QIAQuick PCR Purification	Qiagen, UK
RNeasy Mini	Qiagen, UK
SuperScript III	Invitrogen, UK
SYBR Green Master Mix	Roche, UK

6.2.3 Antibodies

4C4 antibody	See Becker and Becker, 2001
Anti-GFP (A 11122)	Invitrogen, UK
Anti-Tenascin-R	See Becker et al., 2004
Mab318 (anti-Tyrosine Hydroxylase)	Millipore, UK
S5545 (anti-Serotonin)	Sigma, UK
Secondary antibodies (Cy2 and Cy3 conjugated)	Jackson ImmunoResearch Laboratories, PA, USA

6.2.4 Bacterial strains

XL1 blue competent *E.coli*	Stratagene, UK
NEB Turbo Competent *E. coli* (High Efficiency)	New England Biolabs, UK

6.2.5 Equipment

Agilent 2100 Bioanalyzer	Agilent Technologies, UK
Aquarium system	Aqua Schwarz, Germany
Corbett RotorGene 2000 qPCR cycler	Corbett Life Science, UK
Grant SS40-2 water bath	Grant Instruments, UK
Hotplate stirrer Fisherbrand metal top	Fisher Scientific, UK
Hybridizer UVP HB-1000	Jencons PLS, UK
Incubated shaker MaxQ Mini 4450	Fisher Scientific (UK)
Laser scanning microscope LSM510	Zeiss (Goettingen, D)
Leica CM3050 cryostat	Leica, Germany
LSM510 confocal laser scanning microscope	Zeiss, Germany
MaxQ Mini 4450 benchtop incubated shaker	Fisher Scientific, UK
Microcentrifuge 5415 D	Eppendorf (Hamburg, D)
MJ Mini, Personal thermal cycler	BioRad, UK
Nanodrop ND-1000 Spectrophotometer	Nanodrop Technologies
Narishige Intracel microinjector and manipulator	Intracel, UK
PowerPac Basic electrophoresis power supply	BioRad, UK
Technico Mini microcentrifuge	Fisher, UK
Thermostat 5320 tube heater	Eppendorf, Germany
Sigma 1-13 benchtop centrifuge	Sigma Laborzentrifugen GmbH, Germany
Sigma 3K30C high speed centrifuge	Sigma Laborzentrifugen GmbH, Germany
Uvitec gel documentation system with Spacecom camera (06-12297)	Uvitec, UK
Vibratome Microm	Optech Scientific Instruments, UK
Vortex Genie 2 benchtop vortex	Scientific Industries, NY, USA

This page intentionally left blank. Apart from this bit.